Understanding cluster topology and metal-cluster dynamics of two zinc binding plant metallothionein isoforms

Hasan Tanvir Imam

A thesis submitted in partial fulfilment of the requirements of the degree of

Doctor of Philosophy in Chemistry

Department of Chemistry

The University of Warwick

June 2015

Table of Contents

List of Figures vi
List of Tables x
Acknowledgements xi
Declaration xii
Abstract xiii
List of Abbreviations xv

Chapter 1: Introduction

1.1 Zinc in plants 1
1.2 Metallothioneins: brief history, classification and biological functions 2
1.3 Structure and metal-thiolate clusters in metallothioneins 6
1.4 *In vitro* interactions of MTs with exogenous reagents 11
1.5 Plant metallothioneins 13
1.6 Localization, expression and metal specificity 16
1.7 Metal contents of plant metallothioneins 17
1.8 Type 4 plant metallothioneins 21
1.8.1 Case study of a type 4 MT: Wheat E_C 23
1.8.2 Type 4 MTs from *Arabidopsis thaliana*: The research focus 26
1.9 Aims and objectives 30

Chapter 2: Experimental

2.1 Design and cloning of expression constructs 32
2.2 Transformation of bacterial cells with plasmid DNA 32
2.3 Plasmid extraction and preservation of bacterial overnight culture 33
2.4 Recombinant protein expression 33
2.4.1 Overnight starter culture 33
2.4.2 Unlabelled protein expression 33
2.4.3 Labelled protein expression 34
2.5 Protein purification 34
2.5.1 Cell disruption by Sonication 34
2.5.2 Chemical precipitation 35
2.5.3. Protein purification: Size exclusion chromatography 35
2.6 Protein Identification 36
2.6.1 Sodium Dodecyl-Sulfate-Polyacrylamide Gel Electrophoresis (SDS-PAGE) 36

2.6.2 Native Polyacrylamide Gel Electrophoresis (NPAGE) 36
2.6.3 SDS-PAGE: Treatment with EDTA and DTT 37
2.6.4 Silver Staining 37
2.7 Anion exchange chromatography 38
2.8 Determination of metal-protein stoichiometry: Inductively-Coupled Plasma-Optical Emission Spectroscopy (ICP-OES) 38
2.9 Thiol quantification: Ellman's Test 39
2.10 Desalting and buffer exchange 40
2.11 Mass spectrometry: Electrospray Ionization mass spectrometry (ESI-MS) 40
2.11.1 Sample preparation 40
2.11.2 Acquisition parameters 41
2.12 Nuclear magnetic resonance (NMR) Spectroscopy 41
2.12.1 Sample conditions and instruments 41
2.12.2 1D ^{1}H-NMR spectroscopy 42
2.12.3 2D Homonuclear NMR spectroscopy: TOCSY and NOESY 42
2.12.4 2D Heteronuclear NMR spectroscopy: ^{15}N HSQC and ^{13}C HSQC 43
2.12.5 Zinc coordination to histidines: Extended [^{1}H,^{15}N] HSQC 43
2.12.6 3D heteronuclear NMR spectroscopy: HNCA and HN(CO)CA 44
2.12.7 3D heteronuclear NMR spectroscopy: [^{1}H, ^{1}H, ^{15}N] TOCSY-HSQC and NOESY-HSQC 44
2.13 ^{111}Cd NMR spectroscopy 45
2.13.1 Sample preparation for ^{111}Cd loaded MT4a and MT4b: Filtration 45
2.13.2 Sample preparation for ^{111}Cd loaded MT4a and MT4b: Titration 45
2.13.3 1D ^{111}Cd-NMR spectroscopy 46
2.13.4 2D [^{1}H, ^{111}Cd] HSQC-NMR spectroscopy 46
2.13.5 Cadmium titration of Zn_6MT4b: [^{1}H, ^{15}N] HSQC 46
2.14 Cadmium exchange: UV-Visible spectroscopy and Mass spectrometry 47
2.14.1 Cadmium titration: UV-Visible spectroscopy 47
2.14.2 Cadmium speciation: Mass spectrometry 47
2.15 Zinc release/transfer dynamics: UV-Visible spectroscopy 48
2.15.1 Zinc transfer to PAR: Kinetics 48
2.15.2 EDTA-mediated Zn transfer: Kinetics 48
2.15.3 pH titration: UV-Visible spectroscopy 49
2.16 Metal speciation during metal release/transfer: Mass spectrometry 49
2.16.1 Reaction with PAR: Equilibrium 49

2.16.2 Reaction with EDTA: Kinetics 50
2.16.3 Variation of pH 50
2.17 Dynamic and structural aspects: ^{1}H-NMR spectroscopy 50
2.17.1 Reaction with PAR: Sample preparation and ^{1}H NMR spectroscopy 50
2.17.2 Reaction with EDTA: 1D ^{1}H NMR spectroscopy 51
2.17.3 Reactivity of individual domains: ^{15}N HSQC spectra 51
2.17.4 pH variation: ^{1}H NMR spectroscopy 52
2.18 Effect of phytate on MT4a and MT4b 52
2.18.1 Zinc transfer to PAR in presence and absence of phytate: UV-Visible spectroscopy 52
2.18.2 Effect of phytate on MT4a and MT4b: Mass spectrometry 52
2.18.3 Effect of Phytate on MT4a and MT4b: ^{1}H-NMR Spectroscopy 53
2.19 Effect of redox active reactants on MT4a and MT4b 53
2.19.1 Thiol reactivity of MT4a and MT4b: UV-Visible Spectroscopy 53
2.19.2 Effect of glutathione (GSH) and glutathione disulfide (GSSG): Mass spectrometry experiments 54
2.19.3 Effect of pH and Cd on MT4b-GSSG adducts: Mass spectrometry 54
2.19.4 Effect of glutathione (GSH)/ glutathione disulfide (GSSG) couple 55
2.19.5 Reaction with DTNB: Mass spectrometry 55
2.19.6 Reaction with H_2O_2: Time course 56
2.20 Kinetics and protein folding: ^{1}H-NMR spectroscopy 56
2.20.1 Reaction with GSH/GSSG redox couple: 1D ^{1}H and 2D [^{1}H, ^{1}H] TOCSY spectroscopy 56
2.20.2 Reaction with H_2O_2: 1D ^{1}H and 2D [^{1}H, ^{1}H] TOCSY spectroscopy 56
2.20.3 Reaction with DTNB: 1D ^{1}H and 2D [^{1}H, ^{1}H] TOCSY spectroscopy 57
2.21 Homology models 57

Chapter 3: Expression, purification, identification of MT4a and MT4b

3.1 Introduction 58
3.2 Protein expression 59
3.3 Expression of MT4a and MT4b 60
3.4 Protein purification: Chemical precipitation and chromatography 61

3.5 Characterization 68
3.5.1 Mass spectrometry and ICP-OES 68
3.5.2 Protein folding: 1D ^{1}H and 2D [^{1}H, ^{15}N] HSQC NMR spectroscopy 70

Chapter 4: Towards structure and metal-cluster topology

4.1 Introduction 74
4.2 Sequential assignment of backbone and side chain resonances 75
4.2.1 Side chain and backbone assignment: 2D NMR Spectroscopy 75
4.2.2 Assignment of [^{1}H ^{15}N] HSQC spectrum 78
4.2.3 Side chain and backbone assignment: 3D NMR spectroscopy 80
4.3 Zinc coordination to histidines: Identification of mononuclear zinc binding site 83
4.4 Fully cadmium-exchanged MT4b: Protein folding and metal clusters 87
4.5 Zinc replacement by cadmium: UV-visible spectroscopy and mass spectrometry 90
4.6 Protein folding of mixed metal species: NMR spectroscopy 93
4.7 Effect of cadmium on zinc-binding histidines 97
4.8 Paving the way to metal-ligand connectivities: ^{111}Cd NMR spectroscopy 99
4.9 Studies with MT4a 111
4.9.1 Peaks assignment: [^{1}H ^{15}N] HSQC 111
4.9.2 Involvement of histidines to zinc coordination 112
4.9.3 Fully exchanged cadmium form: Protein folding 113
4.9.4 Exchanged with cadmium: Mixed metal species 114
4.9.5 Mixed metal species: Protein folding and metal-ligand Connectivity 116
4.10 Homology models 119
4.10.1 Model of Domain I 120
4.10.2 Model of domain II 122

Chapter 5: Metal binding dynamics of MT4a and MT4b

5.1 Introduction 126
5.2 Zinc binding dynamics: Effects of pH variation 127
5.3 Zinc transfer to Ethylediaminetetraacetic acid (EDTA) 134
5.4 Zinc transfer to 4-(2-Pyridylazo) resorcinol (PAR) 145
5.5 Zinc release from MT4a and MT4b: Influence of phytate 151

Chapter 6: Metal binding properties of MT4a and MT4b: Effect of redox active reactants

6.1 Introduction 159
6.2 Interaction of MT4b with GSSG, GSH and GSH/GSSG: Mass spectrometry 160
6.3 Zinc release and thiol reactivity: Effect of 5, 5'-dithiobis (2-nitrobenzoic acid (DTNB) 170
6.4 Zinc release and thiol reactivity: Influence of hydrogen peroxide (H_2O_2) 177

Chapter 7: Conclusions: Structure and Properties relationships

7.1 Introduction 184
7.2 MT4a and MT4b bind zinc 185
7.3 Mixed metal species: Towards cluster topology 185
7.3.1 Cluster topology of mixed metal species at 4 equivalents of Cd^{2+} 187
7.4 MT4a and MT4b can transfer or release zinc 188
7.5 MT4a transfers/releases zinc faster than MT4b 190
7.6 MT4a and MT4b transfer or release zinc in domain specific manner 191
7.7 Origins of cluster reactivity 193
7.8 Future work 199

References 201

Appendix 218

List of Figures

Chapter 1: Introduction

Figure 1.1 Examples for MT sequences from class I and class II 3
Figure 1.2 Structural features of MTs 6
Figure 1.3 Metal-thiolate cluster structures in metallothioneins 8
Figure 1.4 Demonstration of 1D ^{111}Cd and 2D [^{1}H, ^{111}Cd] HSQC NMR spectroscopy for metal- ligand connectivity study of bacterial SmtA 11
Figure 1.5 MTs and MT-like proteins distributed in different plant taxa 14
Figure 1.6 Sequence alignments of the 4 families of plant MTs 15
Figure 1.7 3D structure of E_C from wheat 24
Figure 1.8 3D Schematic diagram of proposed 3 metal cluster 26
Figure 1.9 Protein sequence alignment of MT4a and MT4b 27
Figure 1.10 Electronic fluorescent pictograph (eFPs) for *Arabidopsis thaliana* MT4a gene 28

Chapter 3: Expression, purification, identification of MT4a and MT4b

Figure 3.1 Protein expressions as a function of induction time 61
Figure 3.2 Optimization of chemical precipitation for MT4b by silver-stained SDS-PAGE 63
Figure 3.3 Chromatograms and silver-stained SDS-PAGE of MT4a and MT4b 64
Figure 3.4 Native-PAGE and SDS-PAGE of MT4a and MT4b 66
Figure 3.5 Mass spectra of MT4a and MT4b 69
Figure 3.6 1D ^{1}H NMR spectra of MT4a and MT4b 71
Figure 3.7 2D [^{1}H, ^{15}N] HSQC NMR spectra of MT4a and MT4b 72

Chapter 4: Towards structure and metal-cluster topology

Figure 4.1 Protein sequence alignment of MT4a and MT4b 75
Figure 4.2 Overlaid 2D [^{1}H, ^{1}H] TOCSY and 2D [^{1}H, ^{1}H] NOESY spectra for MT4b 77
Figure 4.3 Assignment of [^{1}H, ^{15}N] HSQC spectra of MT4b 79
Figure 4.4 Schematic diagrams of different NMR spectroscopic techniques 81
Figure 4.5 Sequential assignments of 3D spectra of MT4b 82

Figure 4.6 Histidine coordination to zinc in MT4b, as revealed by extended [^{1}H, ^{15}N] HSQC spectra 85
Figure 4.7 Overlaid 2D NOESY and TOCSY spectra of MT4b 86
Figure 4.8 Effect of cadmium on protein folding 88
Figure 4.9 Cadmium replacements to Zn from MT4b monitored by UV-Visible spectroscopy 91
Figure 4.10 Deconvoluted mass spectra of MT4b at different Cd stoichiometry 92
Figure 4.11 Comparison of protein folding 94
Figure 4.12 Overlay of [^{1}H, ^{15}N] HSQC spectra of cadmium titration to zinc form of MT4b 95
Figure 4.13 Chemical shift perturbation of metal coordinating and non-coordinating residues of MT4b as a result of cadmium addition 96
Figure 4.14 Effect of cadmium on histidines resonances 97
Figure 4.15 Possible localization of Zn and Cd in the metal binding sites of MT4b at 2 equiv. mol Cd^{2+} 100
Figure 4.16 Localization of Zn and Cd in the metal binding sites of MT4b at 3 equiv. mol Cd^{2+} 102
Figure 4.17 1D and 2D ^{111}Cd NMR spectra of mixed metal species at 3 equiv. mol $^{111}Cd^{2+}$ 103
Figure 4.18 Possible localization of Zn and Cd in the metal binding sites of MT4b at 4 equiv. mol Cd^{2+} 105
Figure 4.19 1D and 2D ^{111}Cd NMR spectra of mixed metal species at 4 equiv. mol $^{111}Cd^{2+}$ 106
Figure 4.20 Overlaid [^{1}H ^{15}N] HSQC spectra of Zn_6MT4b and 5 equiv. mol of Cd^{2+} MT4b 107
Figure 4.21 Schematic connectivity diagram 110
Figure 4.22 Assignment of MT4a 112
Figure 4.23 Histidine coordination to zinc in MT4a 113
Figure 4.24 Effect of cadmium on protein folding of MT4a 114
Figure 4.25 Cadmium replacements to Zn from of MT4a monitored by UV-Visible spectroscopy 115
Figure 4.26 Deconvoluted mass spectra of MT4a at different Cd stoichiometry 116
Figure 4.27 Comparison of protein folding 117
Figure 4.28 1D and 2D ^{111}Cd NMR spectra of mixed metal species at 4 equiv. mol $^{111}Cd^{2+}$ 118
Figure 4.29 Homology models and cluster structures of Domain I of MT4a and MT4b 121
Figure 4.30 Comparison of homology models with template E_C domain I 122
Figure 4.31 Homology model and cluster structure of Domain II

of MT4a and MT4b 123
Figure 4.32 Comparison of homology models with template E_C domain II 124

Chapter 5: Metal binding dynamics of MT4a and MT4b

Figure 5.1 Influence of pH change on Zn forms of MT4a and MT4b studied by UV-Visible spectroscopy 127
Figure 5.2 Deconvoluted mass spectra of MT4a and MT4b at different pH values 130
Figure 5.3 Stacked plot of 1D ^{1}H-NMR spectra of MT4a and MT4b at various pH 131
Figure 5.4 1D ^{1}H NMR spectra of regenerated MT4a and MT4b 133
Figure 5.5 Reactions of MT4a and MT4b with EDTA 135
Figure 5.6 Reactions of MT4a and MT4b with EDTA studied by mass spectrometry 137
Figure 5.7 1D ^{1}H NMR time course reactions of MT4a and MT4b with EDTA 139
Figure 5.8 Superimposed [^{1}H, ^{15}N] spectra of MT4a in absence and presences of EDTA at various time intervals 141
Figure 5.9 Superimposed [^{1}H, ^{15}N] spectra of MT4b in absence and presences of EDTA at various time intervals 143
Figure 5.10 Zinc transfer reaction from MT4a and MT4b to PAR 145
Figure 5.11 Reactions of MT4a and MT4b with PAR observed by mass spectrometry 147
Figure 5.12 ^{1}H-NMR spectra of amide regions of MT4a and MT4b before and after reaction with PAR 149
Figure 5.13 Chemical structure of phytate 151
Figure 5.14 Reactions of MT4a and MT4b with phytate studied by mass spectrometry 152
Figure 5.15 Reactions of MT4a and MT4b with 1 equivalent of phytate 154
Figure 5.16 pH stability of MT-phytate adducts 155
Figure 5.17 Zinc transfer from MT4a and MT4b to PAR in presence and absence of phytate 156
Figure 5.18 1D ^{1}H NMR spectra of upfield regions of MT4a and MT4b before and after addition of phytate 157

Chapter 6: Metal binding properties of MT4a and MT4b: Effect of redox active reactants

Figure 6.1 Reactions of MT4b with GSSG observed by mass spectrometry 161
Figure 6.2 Reactions of MT4b with the GSSG/GSH redox couple observed by mass spectrometry 162
Figure 6.3 Reactions of MT4b with GSH observed by mass spectrometry 164
Figure 6.4 Collision induced dissociation tandem mass spectra of peak 1532.1 m/z 165
Figure 6.5 Effect of pH and Cd^{2+} on [Zn_6MT4b+nGSSG] complexes 166
Figure 6.6 1D ^{1}H NMR spectra of MT4b treated with 1:30 and 30:1 (GSSG/GSH) at a fixed concentration of 5 mM 167
Figure 6.7 Superimposed [^{1}H, ^{1}H] TOCSY spectra of MT4b in absence and presence of 1:30 and 30:1 GSSG/GSH 168
Figure 6.8 Time courses for the reactions of MT4a and MT4b with DTNB under two different reaction conditions 171
Figure 6.9 Reactions of MT4a with DTNB observed by mass spectrometry 172
Figure 6.10 Reactions of MT4b with DTNB observed by mass spectrometry 175
Figure 6.11 1D ^{1}H NMR spectroscopic time course reactions of MT4a and MT4b with DTNB 176
Figure 6.12 Raw mass spectra showing the 6+ charge states for the time dependent reactions of MT4a and MT4b with H_2O_2 179
Figure 6.13 Superimposed [^{1}H, ^{1}H] TOCSY NMR spectra of MT4a and MT4b in absence and after reaction with H_2O_2 181

Chapter 7: Conclusions: Structure and Properties relationships

Figure 7.1 Chemical structures of metal chelators and oxidants 189
Figure 7.2 Protein sequence alignment of MT4a and MT4b 193
Figure 7.3 Surface plots of domain I 194
Figure 7.4 Surface plots analysis of domain II 196
Figure 7.5 Solvent accessible residues in both domains 197

List of Tables

Chapter 1: Introduction

Table 1.1 Summary of 20 3D structures of 14 metallothioneins published to date 5
Table 1.2 Observed $^{111/113}$Cd chemical shifts for different metal binding sites in MTs 9
Table 1.3: Summary of metal contents of plant metallothioneins 19
Table 1.4 Expression profiles of Type 4 plant MTs 22
Table 1.5 Expression profiles of MT4a and MT4b 27

Chapter 4: Towards structure and metal-cluster topology

Table 4.1 Chemical shift values of histidine ring nitrogens in different states 85
Table 4.2 Chemical shift perturbation data for some metal coordinating and non-coordinating residues of MT4b 97
Table 4.3 1D ^{111}Cd NMR resonances observed in fully exchanged and mixed metal species of MT4b 108
Table 4.4 1D ^{111}Cd NMR resonances observed in fully exchanged and mixed metal species of MT4a 119

Acknowledgements

At first, Thanks to Allah (God), for blessing me and giving me the knowledge and strength to complete this research work.

I would like to show my heartfelt gratitude to my supervisor Dr. Claudia Blindauer for her visionary supervision, enthusiastic encouragement and wise advice throughout the research work. Her motivating and inspiring guidance was the key to make this work success.

Thanks to Professor Peter B. Goldsbrough, Purdue University, USA for providing MT4a and MT4b plasmids.

I am grateful to Dr. Esther Martin for her inspiring suggestion, valuable discussion and assisting with experiments on mass spectrometry. Glad, I have found Esther in the Blindauer group.

Very special thanks to all the present and past members in the Blindauer group for all the help and contribution they made to my research: Dr. Gregory Kowald, Dr. James Bernett, Dr. Maria Tareen, and Amira Ksibe. Thanks should be given to Dr. Oksana Leszczyszyn for all her pioneering work on plant type 4 MTs which many ways guided me in the right direction.

I want to extend my thanks to all the people who gave me training on different instruments. Without their help and support it would have difficult to perform many of my experiments so thanks to Dr. Lijiang song, Dr. Ivan Prokes, Mr. Phil Aston and Mrs. Anne smith.

Very personal thanks to my housemate Dr. Zahir Ahmad and her wife Fatema Zannat for all their supports in the last three years. My warm thanks to Dr. Diluar Khan, Dr. Sourav Sarkar, Mr. Jewel Rana and Jayaharan Dhadchi for their care, inspiration and supports.

Thanks to Chancellor Scholarship and Department of Chemistry, Warwick University for funding.

I would like to express my gratitude to my family members for all their love, inspiration, motivation and supports to my entire life, thanks to my mother, my sister-in-law: Likha, my sister: Merry and my brothers: Tawhid, Tawfiq, Tarique and Taiab.

Finally, I would like to dedicate this thesis in the memory of my father Mr. Abdul Karim.

Declaration

The work presented in this thesis is original and has never been submitted in this university or any other university for any qualification. The work was carried out between October 2011 and December 2014 by the author under the direct supervision of Dr. Claudia Blindauer, Associate professor (Reader), Department of Chemistry, Warwick University.

Plasmids of MT4a and MT4b were gifts from the lab of Professor Peter B. Goldsbrough, Purdue University, USA.

Parts of the research work presented in this thesis have been published in a review article

Leszczyszyn, O.I., Imam, H.T., and Blindauer, C.A. (2013). Diversity and distribution of plant metallothioneins: a review of structure, properties and functions. Metallomics ,5,1146-69.

Hasan Tanvir Imam

June 2015

Abstract

Metallothioneins (MTs) are small metalloproteins, ubiquitously found in every phylum. Type 4 MTs (MT4s) from plants are attracting significant attention because of their frequent occurrence in plant embryos. The proposed function of MT4s is to store and distribute Zn^{2+} ions during seed germination. It is thus plausible that manipulation of MT4s could alleviate Zn^{2+} deficiency in cereal products. A better understanding of structure and metal binding dynamics of MT4s is necessary to use them as a tool to maintain seed Zn^{2+} nutritional value and to improve crop production. The dicotyledonous plant *Arabidopsis thaliana* has two seed-specific MT4s isoforms, MT4a and MT4b. The proteins have been expressed in *E. coli* and purified proteins have been found to bind 6 Zn^{2+} ions, like their homolog from wheat E_C. For wheat E_C, 6 Zn^{2+} ions bind in two domains - domain I binds 2 Zn^{2+} ions to form a binuclear cluster (Zn_2Cys_6); for domain II, a mononuclear ($ZnHis_2Cys_2$) site and a 6 membered ring cluster (Zn_3Cys_9) has been proposed. In Cd^{2+} saturated protein, domain II was unfolded, rendering study of metal-ligand connectivities by means of $^{111/113}$Cd NMR spectroscopy impossible. It has also been shown that the mononuclear site plays a significant role in proper folding of domain II, but only in presence of Zn^{2+} but not Cd^{2+}. The focus of this research is to extend knowledge and understanding of the cluster topology, particularly regarding that of the domain II 3-metal cluster, and metal binding dynamics of MT4a and MT4b, using techniques including UV-Visible spectroscopy, native Electrospray Ionization-Mass Spectrometry (ESI-MS) and solution Nuclear Magnetic Resonance (NMR) spectroscopy.

Like wheat E_C, domain II of MT4a and MT4b was misfolded when Cd^{2+} saturated. A possible solution to the absence of ^{1}H and ^{111}Cd resonances in fully Cd^{2+}-substituted MT4s has been developed, based on mixed Zn/Cd MT4 species, which would contain Zn^{2+} in the isolated His_2Cys_2 site to achieve ordered protein folding, with most of the other sites occupied by NMR-active $^{111}Cd^{2+}$. For mixed metal species (Zn/Cd) at 4 equivalents of Cd^{2+}, a maximal number of metal-to-ligand connectivities was observed, allowing some new insights into the topology of the 3-metal cluster of MT4s. Metal transfer reactions with EDTA suggested that the 3 metals in this cluster were kinetically not equivalent, as one labile metal site within this domain was identified. Combination of connectivities data and metal transfer dynamics results allowed building an alternative 3 metal cluster – a binuclear M_2Cys_6 cluster connected to a single metal ion through one bridging cysteine.

Despite 84% sequence identity, MT4a and MT4b have shown remarkable differences in their metal binding dynamics against metal chelators, oxidants,

protons, and phytate. Although both isoforms have very similar pH of half dissociation values, proton-induced Zn^{2+} release from MT4a was found to be cooperative while from MT4b, it was non-cooperative. MT4a transferred Zn^{2+} faster than MT4b to the metal chelators ethylenediaminetetraacetic acid (EDTA) and 4-(2-pyridylazo)resorcinol (PAR), and released Zn^{2+} faster during oxidation by the disulfide reagent 5,5'-dithiobis(2-nitrobenzoic acid) (DTNB). While MT4b was prone to oxidation by the reactive oxygen species hydrogen peroxide (H_2O_2), MT4a resisted oxidation elicited by H_2O_2. The anti-nutrient phytate alone had very little effect on Zn^{2+} mobilisation from both MT4s but it accelerated Zn^{2+} transfer to PAR from both isoforms; however, the effect was more pronounced for MT4a than for MT4b. Glutathione disulfide (GSSG) and the glutathione redox couple (GSH/GSSG) were found to release Zn^{2+} from MT4b. Moreover, GSSG was found to form a non-covalent adduct with MT4b. Both isoforms exhibited domain-specific dynamics, where domain II was often more prone to metal transfer or release than domain I.

The findings of this research have enhanced the knowledge and understanding of cluster topology and metal-binding dynamics of MT4s, particularly MT4a and MT4b from *Arabidopsis thaliana.*

Abbreviations

1D, 2D, 3D	One-, Two-, Three-dimensional
Å	Angstrom
ABA	Abscisic acid
CID	Collission induced dissociation
DTT	Dithiothreitol
DTNB	5,5′-dithiobis-(2-nitrobenzoic acid) or Ellman's reagent
Da	Dalton
E_C	Early cysteine protein
EDTA	Ethylenediaminetetraacetic acid
ESI-MS	Electrospray ionization mass spectrometry
FPLC	Fast protein liquid chromatography
GSH	Glutathione
GSSG	Glutathione disulfide
HSQC	Heteronuclear single quantum coherence
ICP-OES	Inductively coupled plasma-optical emission spectroscopy
IP6	Myo-inositol-1,2,3,4,5,6-hexakisphosphate
LB	Luria-Bertani
mol. equiv.	Molar equivalent or equivalent molar
MT(s)	Metallothionein(s)
MS	Mass spectrometry
MS/MS	Tandem mass spectrometry
MWCO	Molecular weight cut-off
m/z	mass/charge
NMR	Nuclear magnetic resonance
NOESY	Nuclear overhauser enhancement spectroscopy
PAR	4-(2-Pyridylazo)resorcinol
pI	Isoelectric point
pMTs	Plant metallothioneins
ppm	Parts per million
SDS-PAGE	Sodium dodecyl sulphate-polyacrylamide gel electrophoresis
TOCSY	Total correlation spectroscopy
TOF	Time of flight
UV	Ultraviolet
mM	millimolar
µM	micromolar
µL	microliter
min	Minutes
hr	Hour

Abbreviations

Amino acids

Name	3 Letters code	1 letter code
Alanine	Ala	**A**
Asparagine	Asn	**N**
Aspartic acid	Asp	**D**
Arginine	Arg	**R**
Cysteine	Cys	**C**
Glutamic acid	Glu	**E**
Glutamine	Gln	**Q**
Glycine	Gly	**G**
Histidine	His	**H**
Isoleucine	Ile	**I**
Lysine	Lys	**K**
Leucine	Leu	**L**
Methionine	Met	**M**
Phenyalalanine	Phe	**F**
Proline	Pro	**P**
Serine	Ser	**S**
Threonine	Thr	**T**
Tryptophan	Trp	**W**
Tyrosine	Tyr	**Y**
Valine	Val	**V**

Chapter 1

Introduction

1.1 Zinc in plants

Plants accumulate a number of metal ions from the terrestrial and aquatic environment (Rauser, 1999). Among them six metal ions, also known as micronutrients - copper (Cu), iron (Fe), manganese (Mn), nickel (Ni), molybdenum (Mo) and zinc (Zn) - play a significant role in plant growth and life cycle, but in excess have adverse effects (Palmer and Guerinot, 2009). The roles played by iron and copper for electron transfer reactions, manganese for water oxidation, and magnesium for light harvesting in photosynthesis are well documented, but a lot of information is still to be revealed for zinc (Blindauer and Schmid, 2010). Zinc acts as a cofactor in all six enzyme classes, and around 10 % of genes in eukaryotes encode for zinc-binding proteins. In plants, deficiency of zinc has a negative influence on photosynthesis, fixation of CO_2 and phosphate metabolism. Moreover, necrosis is a result of severe zinc deficiency, and sublethal zinc deficiency causes chlorosis, bronzing, resetting, epinasty, curling leaf, small leaf, delay in flowering and most importantly, reduction in crop yields (Broadley et al., 2007). It is thus obvious that zinc deficiency is an important agricultural issue in terms of nutrition and food security. It is to be noted that half of the cereal crops produced in the world are zinc deficient, resulting in hypozincemia of

billions of people who are consuming cereals as a staple food (Marquès and Oomen, 2011). Although alleviation of zinc deficiency could be achieved by fertilization, this is problematic owing to agronomic and economic factors including topsoil drying, subsoil constraints, disease interaction and cost of fertilizer (Hacisalihoglu and Kochian, 2003). Biofortification achieved by breeding or genetic engineering could be suitable, efficient and sustainable to improve the nutritional value of crops. However, the success of this process largely depends on better understanding of the mechanism of zinc accumulation, housekeeping, sequestration and seed filling in the plant (Blindauer and Schmid, 2010). Plants produce a number of ligands that play a role in metal ion trafficking. These include organic acids, amino acids, phytochelatins and metallothioneins (MTs) (Rauser, 1999). Among them, type 4 MTs are of particular interest. These proteins are expressed in developing seeds, are regulated by the phytohormone abscisic acid, and are thought to store zinc for seed germination. Manipulation of seed zinc content by means of these proteins could play a pivotal role to change the nutritional value of seeds (Cobbett and Goldsbrough, 2002). Knowledge on structure and metal binding properties of this group of MTs, in particular metal specificity, is an important complement to *in vivo* studies

1.2 Metallothioneins: brief history, classification and biological functions

Metallothioneins (MTs) form a heterogeneous superfamily of small cysteine-rich proteins (Kägi and Vallee, 1960). They have generally low molecular weight and are found ubiquitously in almost every phylum, i.e. the animal kingdom,

eukaryotic microorganisms, prokaryotes, and plants (Blindauer and Leszczyszyn, 2010; Capdevila et al., 2011) . They are mostly found in the cytoplasm, but their existence in blood plasma and cerebrospinal fluid of higher organisms is also evident. At the developing stage, mammalian MTs also occur in the nucleus (Blindauer and Leszczyszyn, 2010; Kaegi and Schaeffer, 1988b; Kägi and Kojima, 1987). While studying cadmium binding proteins in horse kidney cortex, Margoshes and Vallee discovered the first MT in 1957 (Margoshes and Vallee, 1957). It was later isolated as a cadmium binding protein (Kägi and Vallee, 1960) with 4.1% sulfur and 2.9% cadmium, hence the name metallothionein. Since then, MTs were isolated from parenchymatous tissues of animals (liver, kidney, pancreas and intestines), fungi (Prinz and Weser, 1975), plants (Rauser and Curvetto, 1980) and from bacteria (Higham et al., 1983). Based on their primary structures, MTs were first classified into three classes (Nordberg and Kojima, 1979). Mammalian MTs and other vertebrate MTs form class I, Class II MTs that are phylogenetically distant from Class I MTs include MTs from plants, fungi and nonvertebrate animals. Class III MTs are enzymatically synthesized and contain γ-glutamylcysteinyl units, and include phytochelatins and cadystines (Cobbett and Goldsbrough, 2002; Kaegi and Schaeffer, 1988a).

Class I: Human MT2

```
MDPNCSCAAGDSCTCAGSCKCKECKCTSCKKSCCSCCPVGCAKCAQGCICKGASDKCSCCA
    CXC      CXC  CXC  CXCXXC    CXXCC    CXXC     CXC       CXCC
```

Class II: E_c (*Triticum aestivum*)

```
MGCDDKCGCAVPCPGGTGCRCTSARSGAAAGEHTTCGCGEHCGCNPCACGREGTPSGRANRRANCSCGAACNCASCGSATA
  C    CXC    C      CXC               CXC    CXC  CXC                CXC    CXCXXC
```

Figure 1.1 Examples for MT sequences from class I and class II. Cysteine patterns in human MT2 and Wheat E_C are also given.

According to sequence similarities and phylogenetic relationships, class I and II MTs are better classified into 15 families (Binz and Kägi, 1999). However, most recently an additional classification has been put forward, in which MTs are classified into two groups, Zn-thioneins and Cu-thioneins, based on metal stoichiometry, spectroscopic and spectrometric properties of the purified recombinant products (Capdevila et al., 2011; Valls et al., 2001).

Although they are differently classified, all MTs have some prominent characteristics in common which define this protein superfamily (i) low molecular weight (<10 kDa), (ii) high metal (usually d^{10}) and cysteine content (15-30%), (iii) inducible by different chemicals and physical stress, (iv) optical features characteristic of metal-sulfur bonds, (v) bridging thiolate ligands and (vi) devoid or deficient of aromatic residues (Blindauer and Leszczyszyn, 2010; Capdevila et al., 2011). *In vivo*, MTs can exist in fully metallated form and partially under-metallated form, thus giving them a unique functional and structural diversity compared to other metalloproteins (Jacob et al., 1998; Krezel et al., 2007).

Moreover, due to their wide occurrence in almost every phylum in nature, it is assumed that MTs play vital biological roles. Some established functions are metal ion homeostasis of essential (Zn^{2+}, Cu^{+}) metal ions, detoxification of toxic (Cd^{2+}, Hg^{2+}) metal ions, and protection against reactive oxygen species. Because of their functional and structural diversity, MTs have become a topic of extensive research. Since their discovery, the best characterized MTs have been the mammalian MTs, although tertiary structures of a few non-mammalian and invertebrate MTs are available (Table 1.1).

Table 1.1 Summary of 20 3D structures of 14 metallothioneins published to date.

MT source and isoform	Method	PDB Code		Metal content	References
		α -domain	β -domain		
Rat MT2	NMR	1 mrt	2mrt	Cd_7MT 2	(Braun et al., 1986)
	X-ray	4 mt2		Cd_5Zn_2MT	(Braun et al., 1992)
Mouse MT1	NMR	1dfs	1dft	Cd_7MT1	(Zangger et al., 1999)
Mouse MT3	NMR	1ji9		Cd_7MT3	(Öz et al., 2001)
Rabbit MT2A	NMR	1mrb	2mrb	Cd_7MT2A	(Arseniev et al., 1988)
Human MT2	NMR	1mhu	2mhu	Cd_7MT2	(Messerle et al., 1992)
Human MT3	NMR	2f5h, 2fj4, 2fj5		Cd_7MT3	(Wang et al., 2006)
Fish MT	NMR	1m0g	1m0j	Cd_7MT	(Capasso et al., 2003)
Sea urchin MTA	NMR	1qjk	1qil	Cd_7MTA	(Riek et al., 1999b)
Blue crab MT1	NMR	1dmc,1dmd	1dme,1dmf	Cd_6MT1	(Narula et al., 1995)
Lobster MT1	NMR		1j5l,1j5m	Cd_6MT1	(Munoz et al., 2002)
Wheat E_c	NMR	2kak		Zn_4E_c	(Peroza et al., 2009)
Wheat E_c	NMR	2l61/2l62		Zn_2E_c	(Loebus et al., 2011a)
Wheat E_C	NMR	2mfp		Zn_2E_C	(Tarasava et al., 2013)
Yeast CuMT (Cup1)	NMR	1aoo,1aqq		Ag_7Cup1	(Peterson et al., 1996)
	NMR	1aqr, 1aqs		Cu_7Cup1	(Peterson et al., 1996)
	NMR	1fmy		Cu_7Cup1	(Bertini et al., 2000)
	X-ray	1rju		Cu_8Cup1	(Calderone et al., 2005)
Fungi MT	NMR	1t2y		Cu_6MT	(Cobine et al., 2004)
Synechococcus PCC 7942 SmtA	NMR	1jid		Zn_4SmtA	(Blindauer et al., 2001)

1.3 Structure and metal-thiolate clusters in metallothioneins

The primary structure of MTs is directly related to the tertiary structure that governs the function and properties of the respective protein. Mammalian and other vertebrate MTs contain 20 conserved cysteines in their 60-68 amino acid sequences. However, the most prominent feature of MTs is the arrangement of their cysteines in the primary structure. The most common characteristic sequence motifs are CXC and CXXC, where X is an amino acid other than cysteine. Apart from this, CC and CCC motifs are also possible in MTs (Freisinger, 2011). Furthermore, the high abundance of Gly and Ala residues provides structural flexibility. Another common feature of MTs primary structures is the absence or lack of aromatic and hydrophobic amino acids such as Tyr, Trp, Phe, Leu and Ile which usually give structural rigidity to other proteins (Blindauer and Leszczyszyn, 2010). In fact, a few mammalian MTs do contain Pro, Phe and Tyr in their amino acid chains, whereas histidine is found in bacterial and some invertebrate and plant MTs (Blindauer, 2008). Lack of secondary structural units was thought to be another feature of MTs as shown in Figure 1.2 (A) for human MT2.

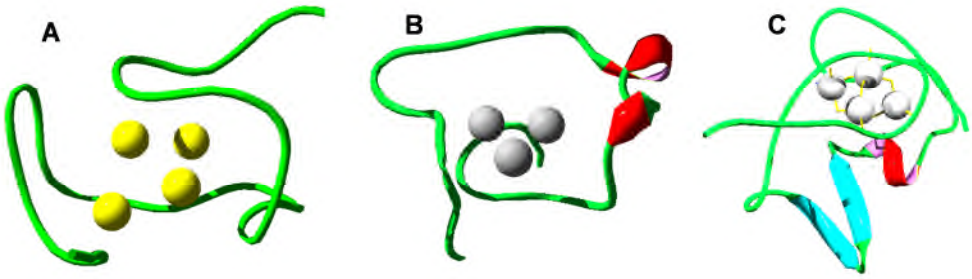

Figure 1.2 Structural features of MTs. (A) α-domain of human MT2 (PDB code 1mhu), (B) α-helix in *C. sapidus* MT-1 (PDB code 1dmc). (C) α-helix and β-sheet in bacterial SmtA (PDB code 1jjd).

However, *C. sapidus* MT1 (Narula et al., 1995) and bacterial MTs (Blindauer et al., 2002) contain some short β-strands and α-helices shown in Figure 1.2 (A and B)

The 3D structures of MTs depend on metal ions and their coordination to the ligands. However, scarcity of aromatic and hydrophobic amino acid residues, high content of glycine and the low complexity of their primary sequences render the tertiary structure determination of MTs difficult. This is evident when searching for MTs in the Protein Data Bank (PDB), as only 35 entries are available (see Table 1.1). Among them, vertebrate MTs represent 15 entries and these exhibit very similar structural patterns within their two domains. Eight entries belong to echinoderm and crustacean MTs, and their structures show resemblance to vertebrate MT structures. The remaining 12 entries refer to 4 proteins from yeast Cup1, another fungus, a cyanobacterium and a plant. Each of these proteins shows distinct structural features (Blindauer and Leszczyszyn, 2010).

In all MTs, metal ions bind to the protein through coordination via sulfur of the cysteine residues forming clusters, containing terminal and bridging metal-thiolate bonds. For divalent metal ions, the basic cluster structures are M_3Cys_9 of the vertebrate MT β-domain, where a six-membered ring is formed by the coordination of three metal ions with three bridging sulfur ligands of cysteine. Each of the three metal ions is bound to two further sulfurs, resulting in six terminal metal-thiolate bonds (Figure 1.3). Vertebrate, crustacean and echinodermata MTs contain this kind of cluster. The α-domains of vertebrate and echinodermata MTs contain M_4Cys_{11} clusters. In this cluster, two metal ions are bound to two bridging and two terminal thiolates, while the remaining two metal

ions are each coordinated to one terminal and three bridging thiolates resulting in two fused six-membered rings. Furthermore, a very similar $M_4Cys_9His_2$ cluster is

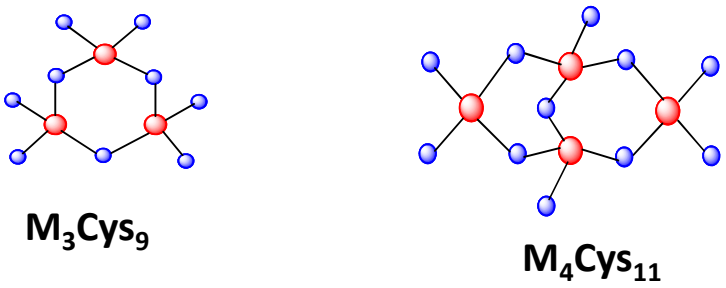

Figure 1.3 Divalent metal-thiolate cluster structures in metallothioneins. N terminal β-domain (M_3Cys_9) and C-terminal α-domain (M_4Cys_{11}). Represents cysteine residues, represents metal ions.

present in bacterial MTs, where two histidines residues take part in metal coordination through their imidazole nitrogens, resulting in an $M_4Cys_9His_2$ arrangement. For monovalent metal ions, a M_8Cys_{10} cluster structure is found in yeast Cup1, a Cu(I)-binding MT (Calderone et al., 2005). Six metal ions of this cluster bind to the sulfurs forming trigonal planar sites and two are coordinated to thiolate ligands with linear or digonal geometry. The striking feature of this cluster is that it is devoid of terminal thiolates, with each thiolate forming two or three bridging bonds with the metal ions.

For zinc (Zn^{2+}) and copper (Cu^{+}) MTs, getting metal-ligand connectivities is problematic because both metals have no or very limited spectroscopic properties. Furthermore, large quadrupole moment makes zinc unsuitable to use as probe for metal cluster studies by NMR spectroscopy. Both zinc and cadmium are in the same group in the periodic table and replacement of zinc by cadmium provides a

means of cluster study as for many zinc proteins, isostructural replacement by Cd^{2+} was observed (Armitage and Otvos, 1982). Cadmium has two NMR active isotopes of ^{111}Cd and ^{113}Cd, both with a spin of I = ½. Both isotopes are suitable for connectivity studies; the only difference is that ^{113}Cd provides slightly better sensitivity while ^{111}Cd has higher natural abundance (Armitage and Otvos, 1982; Vašák, 1998).

Table 1.2 Observed $^{111/113}Cd$ chemical shifts for different metal binding sites in MTs

MTs	$^{111/113}Cd$ Chemical shift (ppm)		References
	Cluster A	Cluster B	
Human MT1	670.5, 629.7, 626.0, 610.5	670.5, 652.0, 654.8	(Boulanger and Armitage, 1982)
Human MT2	669.6, 630.8, 625.4, 611.9	669.6, 646.6	(Zangger et al., 1999)
Rabbit MT1,MT2	670.3, 629.3, 622.0, 611.2	665.1, 647.5, 643.5	(Otvos and Armitage, 1980)
Calf MT1	668.2, 629.2, 624.4, 612.3	This site for Cu^{+}	(Otvos et al., 1985)
Calf MT2	668.0, 629.4, 624.2, 613.1	This site for Cu^{+}	(Otvos et al., 1985)
Crab MT1	659.2, 650.5, 621.4	647.2, 646.3, 631.0	(Otvos et al., 1982)
Crab MT2	660.6, 648, 624.2	661.6, 634.8, 632.7	(Otvos et al., 1982)
Lobster MT	664.0, 645.2, 622.2	649.1, 645.2, 632.5	(Riek et al., 1999a)
SmtA	712, 660, 596, 567		(Blindauer et al., 2001)
Wheat E_C	661, 659 (Domain 1)	NO connectivity observed for Domain 2	(Loebus et al., 2011b)

Therefore, for most of the metal clusters in Table 1.1, the metal-to-ligand connectivities were determined by means of $^{111/113}Cd$ NMR spectroscopy. This method is indispensable in MTs cluster structure determination as use of

crystallography as an alternative method is severely hampered by the difficulties to crystallise MTs due to their high flexibility.

The advantage is that Cd-NMR spectroscopy is sensitive to the number and variations in ligands and coordination environment. For $^{111/113}$Cd nuclei, a decrease in shielding is observed in a series of S>N>O containing ligands (Sadler et al., 1978). Furthermore, for some MTs, cadmium is biologically relevant as it binds to these MTs *in vivo* (Dallinger et al., 2001).

In MTs, sulfur ligands from cysteines are bound to Cd^{2+} in a tetrahedral geometry. However, the chemical shift values (Table 1.2) are higher than for usual Cd-S tetrahedral coordination due to at least one cysteine being bridging (Sadler et al., 1978). In addition to 1D $^{111/113}$Cd NMR spectroscopic experiments, two other NMR spectroscopic methods, namely [Cd, Cd] COSY (correlation spectroscopy) and/or [^{1}H, ^{111}Cd] heteronuclear single-quantum coherence (HSQC) spectroscopy are also important. Homonuclear [Cd, Cd] COSY provides information on Cd-Cd coupling, whereas [^{1}H,^{111}Cd] HSQC spectra provide direct information on 3-bond couplings between Cd and the Hβ protons of cysteines or the Hε1 and Hδ2 protons of histidine residues (Blindauer et al., 2001). Compiling all the information from these techniques provides the cluster topology of the protein. The cluster structure of bacterial SmtA, for which a single 4-metal cluster was determined (Figure 1.4), consists of two Cys_4Cd sites (A and B) and two $HisCys_3Cd$ sites (C and D). SmtA was the first MT containing a cluster involving histidines.

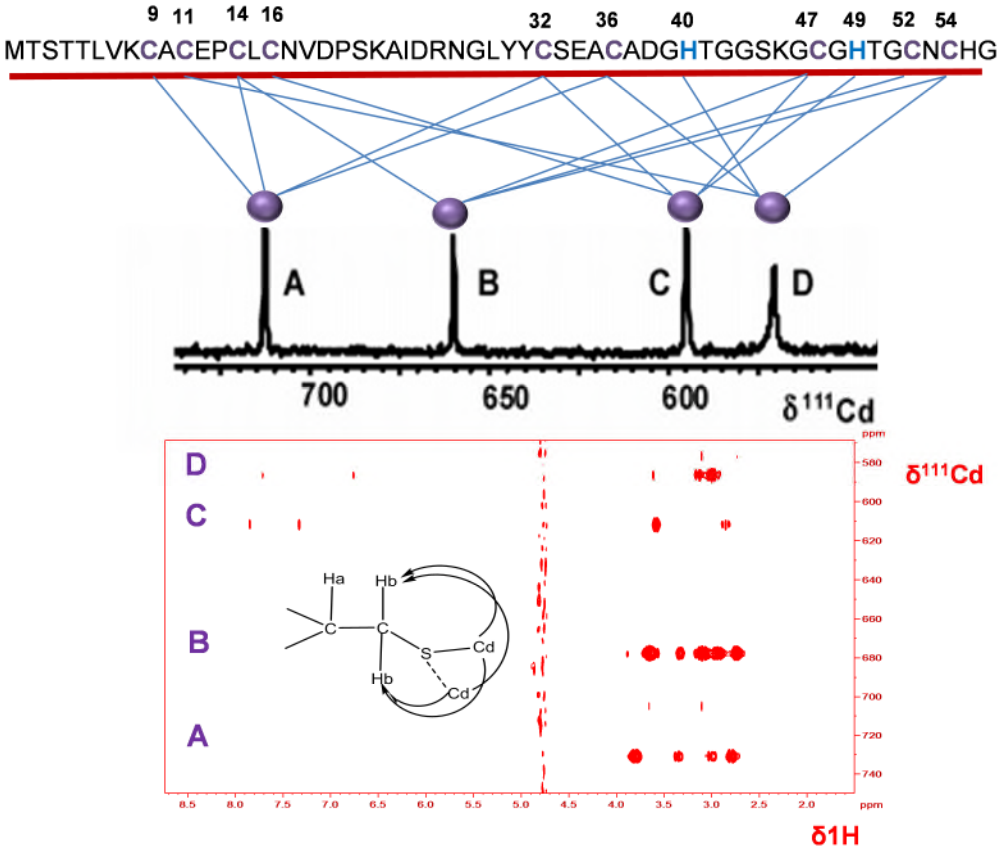

Figure 1.4 Demonstration of 1D ^{111}Cd and 2D [^{1}H,^{111}Cd] HSQC NMR spectroscopy for metal-ligand connectivity study of bacterial SmtA. The top Figure illustrates four Cd binding sites involving cysteines and histidines. In the bottom figure, four sets of crosspeaks, corresponding to sites A, B, C, and D, and resulting from 3-bond ^{111}Cd,^{1}H scalar coupling, are observed in an [^{1}H,^{111}Cd] HSQC spectrum. These crosspeaks directly reflect the metal-ligand connectivities shown in the top Figure.

1.4 *In vitro* interactions of MTs with exogenous reagents

Since their discovery as cadmium binding proteins, roles of MTs in heavy metal detoxification, metal homeostasis or housekeeping were considered. A plethora of exogenous reagents have been used to understand the metal binding dynamics and consequently functional properties. Reaction of apo-MT (thionein) with the Zn and Cd forms of transcription factor IIIA (TFIIIA) suggested a protective role of MT against cadmium (Huang et al., 2004). In a metal transfer reaction, the α

domain of rabbit liver Cd_7MT2 was found to be reactive in metal transfer to Ethylene diaminetetraacetic acid EDTA (Gan et al., 1995). Zinc transfer from mammalian Zn_7MT to EDTA and apo-carbonic anhydrase suggested a zinc transfer role for MTs (Li et al., 1980). Reactions between Zn_7MT with the zinc sensor FluoZin-3 and the cell permeable metal chelator N,N,N',N'-tetrakis (2-pyridinylmethyl)-1,2-ethanediamine (TPEN) were studied to investigate the metal transfer properties and low affinity binding site for zinc (Namdarghanbari et al., 2010; Rana et al., 2008). Similarly, the N-terminal β domain of rabbit liver MT2 was found to transfer zinc to various apo-zinc finger peptides (Hathout et al., 2001). The beta domain of human MT1a was also found to compete for zinc with apo-carbonic anhydrase in a zinc competition reaction (Pinter and Stillman, 2014). Adenosine triphosphate (ATP) and glutathione (GSH) were proposed to bind MTs in a domain-specific manner; it was proposed that while ATP bound to the α domain, GSH bound to the β domain (Brouwer et al., 1993; Jiang et al., 1998a). Moreover, the ATP-MT complex was proposed to play a role in respiration (Maret et al., 2002). Furthermore, MT was found to release metals to apo-sorbitol dihydrogenase in presence of glutathione disulfide GSSG but not GSH (Jiang et al., 1998b); this suggests that the GSH/GSSG redox couple regulates zinc release from MT *in vivo* (Maret, 1994). Recently, the proteins exo84p, 14-3-3 zeta, α and β enolase, aldolase C, malate dehydrogenase, ATP synthase, and pyruvate kinase were found to bind to the beta domain of human MT3 through multiple thiol/disulfide exchange (El Ghazi et al., 2010). The apo-β domain was also found to be more reactive in acquiring zinc from $Zn_2(insulin)_6$, supporting the hypothesis that MT may be involved in the control of blood and liver sugar levels (Zaia et al.,

1998). The β domain of mouse MT1 was found more prone to oxidation induced by nitric oxide (NO), leading to the release of all three metal ions, but leaving the α domain intact (Zangger et al., 2001). Both domains of rabbit liver MT2 were found to release metal ions under the influence of NO and peroxynitrite ($ONOO^-$) in presence of GSSG but not GSH (Khatai et al., 2004). Moreover, the reactions of S-nitrosopenicillamine (SNAP), S-nitrosoglutathione (GSNO), and 2-(N,N-diethylamino)-diazenolate-2-oxide (DEA/NO) with Zn_7MT and Cd_7MT helped to release metals from MTs (Zhu et al., 2010a). The α domain of rabbit liver MT2 was found to be more prone to alkylation by the anticancer drugs Melphalan and Chlorambucil, and a binding site of these drugs on the α domain was proposed (Yu et al., 1995; Zaia et al., 1996). Chlorambucil modulated Zn_7MT transfer more zinc to apo-carbonic anhydrase than from unmodified MTs, suggesting a role for MTs in drug resistance. Cisplatin preferentially bound to the β domain of Cd_7MTs (Lemkuil et al., 1994). Binding of organometallic tricarbonyl technetium and rhenium complexes with four mammalian MT isoforms suggested a potential application of MTs in radiopharmaceuticals (Lecina et al., 2014). Selenium compounds (Jacob et al., 1999), chromate (Krepkiy et al., 2003) and aldehydes (Hao and Maret, 2006) were also found to mobilize zinc from MTs.

1.5 Plant metallothioneins

Plant MTs are a relatively new branch of MTs to be studied. They form the 15^{th} family of MTs and are further divided into four subfamilies - MT1, MT2, MT3 and MT4 or $E_{C,}$ based on the number and arrangement of cysteine residues in the protein sequence. Plant MT sequences have been identified in angiosperms,

gymnosperms, ferns, spike moss, and liverwort (Blindauer and Leszczyszyn, 2010; Leszczyszyn et al., 2013). A recent search for MT nucleotide sequences in the National Centre for Biotechnology Information (NCBI) database revealed 1551 nucleotide sequences deposited for green plants (Figure 1.5). Most of them belong to land plants and a large share of them are seed plants.

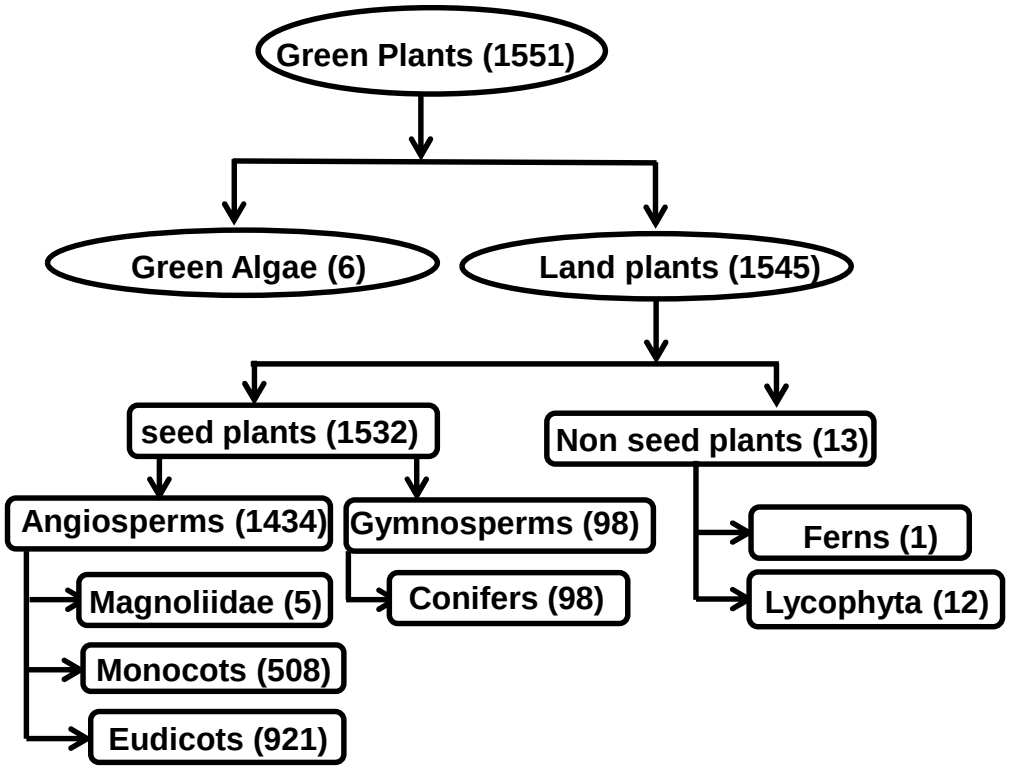

Figure 1.5 MTs and MT-like proteins distributed in different plant taxa. Data were retrieved from National Centre for Biotechnology (NCBI) on 02.02.15. (Figure adapted from (Leszczyszyn et al., 2013).

All four types of MTs are found in seed plants, however, the existence of type 1, 2 and 4 in nonvascular bryophytes suggests a common evolutionary relationship among them before the emergence of seeds (Leszczyszyn et al., 2013). Plants containing genes encoding for all four types of MTs include *Arabidopsis thaliana*, rice, sugarcane and the majority of flowering trees. Plant MT1, MT2 and MT3

contain 12, 14 and 10 cysteines, respectively, in two cysteine-rich regions, separated by a more or less long stretch devoid of Cys residues. The C-terminal region comprises six cysteines and is conserved for all three subfamilies in an arrangement of CxCxxxCxCxxCxC, while the cysteine residues in the N-terminal region differ in number, and are distributed in different arrangements, making this region characteristic for each of the subfamilies. Figure 1.6 shows some examples.

Plant MT1

```
MT1_PEA         MSG--CGCGSSCNCGDSCKCNKRSSGLSYSEMETTETVILGVGPAK---IQFEGAEMSAASEDGGCKCGDNCTCDP-CNCK
MT1A_ARATH      MADSNCGCGSSCKCGDSCSCEKN-----YN----------------------------KECDNCSCGSNCSCGSNCNC-
MT1_MAIZE       MS---CSCGSSCGCGSSCKCGKKYPDLEETSTAAQPTVVLGVAPEKKAAPEFVEAAAESGEAAHGCSCGSGCKCDP-CNC-
```

Plant MT2

```
MT2_MUSAC       MSCSGENCGCGSSCSCGSGCGGCRKLTDLG-EERSSTSQTMIMGVAP-QKGHFEELETAAGSEN-GCKCGSNCTCDPCNCK
MT2_QUESU       MSCCGGNCGCGTGCKCGSGCGGCKMFPDIS-SEK-TTTETLIVGVAP-QKTHFEGSEMGVGAEN-GCKCGSNCTCDPCNCK
MT2A_ARATH      MSCCGGNCGCGSGCKCGNGCGGCKMYPDLGFSGETTTTETFVLGVAPAMKNQYEASGESNNAENDACKCGSDCKCDPCTCK
```

Plant MT3

```
MT3_MUSAC       MS-TCGNCDCVDKSQCVKKGNSYGIDIVETEKSYVDEVIVAAEAAEHDG--KCKCGAACACTDCKCGN-
MT3_HORVU       MADKCGNCDCADKTQCVKKGDSYGIVMVDTEKSHLE----VHETAENDD--KCKCGTSCTCTNCTCGH-
MT3_ARATH       MSSNCGSCDCADKTQCVKKGTSYTFDIVETQESYKEAMIMDVGAEENNANCKCKCGSSCSCVNCTCCPN
```

Plant E_C(MT4)

```
EC1_ARATH       MADTGKGSSVAGCNDSCGCPSPCPGGNSCRCRMR-EASAGDQGHMVCPCGEHCGCNPCNCPKTQTQTSAKG----CTCGEGCTCASCAT---
EC2_ARATH       MADTGKGSASASCNDRCGCPSPCPGGESCRCKMMSEASGGDQEHNTCPCGEHCGCNPCNCPKTQTQTSAKG----CTCGEGCTCATCAA---
EC1_WHEAT       ----------MGCDDKCGCAVPCPGGTGCRCTSARSGAAAG-EHTTCGCGEHCGCNPCACGREGTPSGRANRRANCSCGAACNCASCGSATA
```

Figure 1.6 Sequence alignments of the 4 families of plant MTs. Codes, origin, and UniprotKB accession numbers: Type 1: MT1_PEA (*Pisum sativum*, P20830), MT1_MAIZE (*Zea mays*, P30571), MT1A_ARATH (*Arabidopsis thaliana*, P43392). Type 2: MT2_MUSAC (*Musa acuminata*, AAG44758), MT2_QUESU (*Quercus suber*, Q93X22), MT2A_ARATH (*Arabidopsis thaliana*, P25860). Type 3: MT3_MUSAC (*Musa acuminata*, DN239297), MT3_HORVU (*Hordeum vulgare*, I3QM94), MT3_ARATH (*Arabidopsis thaliana*, O22433). Type 4: EC1_ARATH (*Arabidopsis thaliana*, F4ILY7), EC2_ARATH (*Arabidopsis thaliana*, Q42377), EC1_WHEAT (*Triticum aestivum*, P30569)

MT1s usually contain six cysteines, MT2 eight cysteines and MT3 four cysteines in their N-terminal region. In contrast, 17 cysteine residues in MT4 or E_C proteins are distributed in three well-separated regions, the N-terminal, the central and the C-terminal region. They also contain two histidines in the primary sequence,

which are conserved in MT4 sequences from angiosperms. The central and C-terminal Cys-rich stretches form one C-terminal domain, the so-called βE-domain (Peroza et al., 2009). Moreover, the "linker" regions in MT4 are considerably shorter in comparison to most other plant MTs.

1.6 Localization, expression and metal specificity

Localization of proteins is important for functional studies. Plant MTs transcription are abundant in roots, leaves, flowers, fruits, seeds and stems and is evident by monitoring mRNA (Cobbett and Goldsbrough, 2002; Guo et al., 2003). In general, transcription of MT1 mRNA is higher in leaves than in roots, while MT2 genes tend to be more abundant in roots than in leaves. MT3s are expressed mostly in ripening fruits and/or leaves. However, in *Arabidopsis* mesophyll tissue, transcription of MT3 mRNA was also observed (Murphy et al., 1997). Transcription of MT4 is seed specific in most plants (Cobbett and Goldsbrough, 2002).

Various factors that influence plant MT gene expression include metal ions, hormones, chemical and physical stress such as heat shock, salt, and wounding (Leszczyszyn et al., 2013). Transcription of the Type 1 OsMT1a from rice is up-regulated by dehydration and Zn (Yang et al., 2009). In contrast, expression of HtMT2 in *Helianthus tuberosus* was found to be repressed by Zn (Chang et al., 2004). Zinc exposure had no effect on transcripts level of *Populus alba* PaMT2 (Castiglione et al., 2007). Copper (Cu) exposure enhanced the expression of TcMT1 in the shoots of the hyper-accumulator *Thlaspi caerulescens*, but had no

effect on TcMT2 expression (Roosens et al., 2005). Cadmium (Cd) induction doubled the expression level of *Arabidopsis* AtMT2 (Zhu et al., 2009). Both BcMT1 and BcMT2 from *Brassica campestris* were found to be induced by Cd and over-expression in transgenic *Arabidopsis* led to a higher Cd and Cu tolerance (Lv et al., 2012). When over-expressed in transgenic *Arabidopsis*, higher Cd resistance was also observed for *Brassica rapa*, (BrMT1) (Kim et al., 2007), and for AtMT2a and AtMT3 when over-expressed in yeast and guard cells of *Vicia faba* (Lee et al., 2004). *Brassica juncea* BjMT2 (Zhigang et al., 2006) and *Cajanus cajan* (CcMT1), over-expressed in *E. coli* and *Arabidopsis*, conferred increased Cu and Cd tolerance (Sekhar et al., 2011). *Hevea brasiliensis* (HbMT2) transcription is induced by ethephon and H_2O_2 (Zhu et al., 2010b). In cotton seedlings, GhMT3a was up-regulated by heavy metal ions, high salinity and reactive oxygen species (ROS) (Xue et al., 2009). It is suggested that Buckwheat MT3 expression during leaf development may play a protective role in ROS formation and photo-oxidative stress (Samardžić et al., 2010).

1.7 Metal contents of plant metallothioneins

Metal ion homeostasis within the cell requires the understanding on how the respective metal ions interact with the respective proteins. How cells ensure that metal ions will bind to the right protein is still an enigma, especially metal ions with isostructural properties, such as Zn^{2+} and Cd^{2+}, that have different biological functions and effects (Leszczyszyn et al., 2010). MTs, due to their functional diversity, with different temporal and spatial expression patterns, can bind metal

ions selectively *in vivo* (Guo et al., 2008) and *in vitro* (Bofill et al., 2009). They are therefore believed to be suitable candidates for intracellular trafficking of zinc, cadmium and copper (Maret, 2009). Root specific *Cicer arietinum* (chickpea) MT1 contains 12 cysteines in two regions separated by a 42 amino acid linker, and can coordinate five zinc or cadmium ions in either one- or two-cluster composition depending on metal ion content (Schicht and Freisinger, 2009). MT1 of *Quercus suber* (Qs, cork oak) binds four zinc ions and can coordinate six cadmium ions in cadmium-enriched medium (Domènech et al., 2007). *C. arietinum* MT2 binds five zinc or cadmium ions to form a single cluster (Wan and Freisinger, 2009). In QsMT2, inorganic sulfide (S^{2-}) and histidine residues play a significant role in metal coordination. Four zinc ions were found to bind with QsMT2 to form a hairpin structure with low numbers of sulfide and no involvement of histidine coordination. However, five cadmium ions bound to QsMT2 with histidine coordination (Domenech et al., 2007). For plant MT3, the metal binding ability of *Musa acuminata* (banana) varied from three to four zinc ions. However, the study suggested that the three-metal cluster is preferable to the four-metal cluster, with a single cluster connecting both cysteine-rich domains (Freisinger, 2007). Barley MT3 was reported to bind zinc with a 1:1 ratio, and it was suggested that metal binding stoichiometry of MTs largely depends on metal ion composition and concentration of the cytosol (Hegelund et al., 2012). Type 4 MTs, including wheat E_C, can accommodate six zinc ions. However, cadmium

Table 1.3 Summary of metal contents of plant metallothioneins (Leszczyszyn et al., 2013).

Type	Species	Metal Metal Ion	Stoichiometry	Remarks [a)]	Reference
1	*Pisum sativum* ($PsMT_A$)	Cd(II)	5.6-6.1	No tag	(Kille et al., 1991)
	Pisum sativum ($PsMT_A$-GST)	Zn(II)	6.0±1.8	Uncleaved	(Tommey et al., 1991)
		Cd(II)	4.4±0.4	Uncleaved	
		Cu(I)	3.2±0.3	Uncleaved; impure	
		Cd(II)	5.8	Uncleaved; incubated	
		Cu(I)	6.2	Uncleaved; incubated	
	Vicia faba (MT1a-GST and MT1b-GST)	Zn(II)	2.1-3.8	Uncleaved; Zn only	(Foley et al., 1997)
		Zn(II)	0.1-0.2	Uncleaved; Zn, Cd, Cu, Fe	
		Cd(II)	1.6-2.9		
		Cu(I)	0.3-1.3		
	Arabidopsis thaliana	Cu(I)	8.5	As isolated from plant	(Murphy et al., 1997)
	Triticum durum (TdMT1-GST)	Cd(II)	4	cleaved and uncleaved	(Bilecen et al., 2005)
	Cicer arietinum (CaMT1)	Zn(II)	4.5	Cleaved intein tag fusion	(Schicht and Freisinger, 2009)
		Cd(II)	4.5		
		Cu(I)	6.9		
	Glycine max (GmMT1)	Zn(II)	3.8-5.0	Cleaved	(Pagani et al., 2012b)
		Cd(II)	3.9-8.1		
2	*Vicia faba (VfMT2-GST)*	Zn(II)	3.6-4.3	Zn only medium	(Foley et al., 1997)
		Zn(II)	0.1-0.2	Zn, Cd, Cu, Fe medium	
		Cd(II)	2.0-2.8		
		Cu(I)	0.3-0.5		
	Quercus suber (QsMT2)	Zn(II)	4	Cleaved ; values for major species	(Domènech et al., 2006; Mir et al., 2004)
		Cd(II)	6-7		
		Cu(I)	8		
	Citrullus lamatus	Zn(II)	3.6	Cleaved and reconstituted	(Akashi et al., 2004)
		Cu(I)	5.1		
	Arabidopsis thaliana	Cu(I)	7.0	As isolated from plant	(Murphy et al., 1997)
	Bruguira gymnorrhiza (BgMT2-GST)	Zn(II)	4.7	Uncleaved	(Huang et al., 2011)
		Cd(II)	4.7		
		Cu(I)	3.6		
		Pb(II)	2.5		
	Kandelia candel (KcMT2-GST)	Zn(II)	4.3	Uncleaved	(Huang et al., 2012)
		Cd(II)	4.3		
		Cu(I)	3.2		
		Pb(II)	3.9		
	Cicer arietinum (CaMT2)	Zn(II)	5	Cleaved intein tag fusion; integer values of dominant species	(Wan and Freisinger, 2009)
		Cd(II)	5		
		Cu(I)	8		
	Glycine max (GmMT2)	Zn(II)	4.3-4.4	Cleaved	(Pagani et al., 2012b)
		Cd(II)	5.6-6.7		
	Colocasia esculenta	Zn(II)	5.4 (±0.3)	His- and intein tag	(Kim et al., 2012)
		Cd(II)	6.0 (±1)		(Kim et al., 2011)
	Avicennia marina (AmMT2-GST)	Zn(II)	3.9	Uncleaved	(Huang et al., 2011)
		Cd(II)	3.6		
		Cu(I)	4.7		
		Pb(II)	2.8		
3	*Arabidopsis thaliana*	Cu(I)	5.5	as isolated from plant	(Murphy et al., 1997)
	Elaeis guinensis	Zn(II)	2.2-2.3	Uncleaved	(Abdullah et

	(MT3A-GST)				al., 2002)
	Musa acuminata MaMT3)	Zn(II)	4.0	Intein tag	(Freisinger, 2007)
		Cd(II)	4.0		
	Glycine max (GmMT3)	Zn(II)	3.2	Cleaved GST fusion	(Pagani et al., 2012b)
		Cd(II)	4.2-4.3		
	Hordeum vulgare (HvMT3)	Zn(II)	0.32-0.81	Cleaved GST fusion, cleaved; lower ratios from non-supplemented media	(Hegelund et al., 2012)
		Cd(II)	0.00-0.19		
		Cu(I)	0.01-0.34		
	Noccaea caerulescens (NcMT3)	Zn(II)	4-5	Intein tag fusion	(Fernandez et al., 2012)
	Helianthus annuus(HaMT3)	Zn(II)	3.5	Cleaved GST fusion	(Tomas et al., 2014)
		Cd(II)	4.5		

4	*Sesamum indicum*	Zn(II)	2.0	GST fusion	(Chyan et al., 2005)
		Cu(I)	2.0		
	Triticum aestivum (wheat E_C or E_C-I)	Zn(II)	~5	As isolated from wheat	(Lane et al., 1987)
		Zn(II)	5.8	As isolated from wheat	(Leszczyszyn et al., 2007)
		Zn(II)	5.0-6.0	Cleaved intein tag fusion	(Freisinger, 2008; Peroza and Freisinger, 2007)
		Cd(II)	6.0	Cd-exchanged	
	Glycine max (GmMT4)	Zn(II)	5.6-5.8	GST fusion, cleaved	(Pagani et al., 2012b)
		Cd(II)	6.0-7.4		
	Hordeum vulgare (HvMT4)	Zn(II)	2.6-3.3	GST fusion, cleaved; lower ratios from non-supplemented media	(Hegelund et al., 2012)
	Helianthus annuus(HaMT4)	Zn(II)	6	GST fusion, cleaved	(Tomas et al., 2014)
		Cd(II)	7.7		

can also bind to this protein (Leszczyszyn et al., 2007; Peroza and Freisinger, 2007).

The importance of histidines in MTs has attracted attention because of its pivotal role in metal binding for a number of MTs (Blindauer, 2008), for example from the cyanobacteria *Synechococcus* PCC 7942 and *Anabaena* PCC7120, the nematode *C. elegans*, the plants *M. acuminata* and *Q. suber*, chicken, and the fungus *Magnaporthe grisea* (Leszczyszyn et al., 2010). Bacterial SmtA contains four zinc ions in a single cluster of $Zn_4Cys_9His_2$ (Blindauer et al., 2001). However,

site-directed mutagenesis (Blindauer et al., 2007) studies of this protein revealed that the His residues are essential for stabilising the protein fold and governing metal-exchange properties. Of the four types of plant MTs, a number of MT3 contain C-terminal histidine residues and a few MT1s have histidine in their amino acid sequence. Recently it has been shown that histidines from MT3 take part in metal binding (Tomas et al., 2014). Type 4 MTs contain two well-conserved histidine residues in domain II, and studies on wheat E_C show that they can bind one zinc ion together with two Cys residues to form a mononuclear Cys_2His_2 zinc site (Leszczyszyn et al., 2010).

1.8 Type 4 plant metallothioneins

A type 4 plant MT was first isolated from the monocotyledonous plant wheat (*Tricitum aestivum)* (Lane et al., 1987). A protein with a high content of cysteines was detected in wheat embryos during germination, and was thus called E_C or early cysteine-rich protein. Later, related genes were isolated from developing seeds of maize (White and Rivin, 1995), *A. thaliana* (MT4a and MT4b) (Guo et al., 2003), sesame (Chyan et al., 2005), Douglas fir (Chatthai et al., 1997), and white spruce (Dong and Dunstan, 1996).

The expression of type 4 plant MTs was thought to be restricted to reproductive tissues such as developing seeds, embryogenic microspores and pollen embryoids. Recently, expression of type 4 MT from *Hordeum vulgare* (Barley) (Hegelund et al., 2012) was identified in the seed aleurone layer. Moreover, MT4 homologues have also been identified in the leaf tissue in the resurrection plant *Xerophyta*

humilis and in non-seed producing mosses (Leszczyszyn et al., 2007). Expression is induced by abscisic acid (ABA), a plant hormone, rather than by metal ions such as Zn^{2+} or Cd^{2+}.

Table 1.4 Expression profiles of Type 4 plant MTs. Available information governing the spatial and temporal expression is given (Leszczyszyn et al., 2013)

Species	Location of expression	Developmental Expression	Regulation	Regulator	Reference
Triticum aestivum	Embryo and pollen	embryonic microspores	Up by ABA - seed; Down by light - pollen; Up by Ca – pollen	ABRE	(Hanley-Bowdoin and Lane, 1983)
Oryza sativa	Embryo	Developing seed	Up by ABA		(Zhou et al., 2005)
Hordeum vulgare	Embryo and Aleurone layer	Developing seed		ABRE, ERE	(Hegelund et al., 2012)
Glycine max	Embryo	Developing seed	Not by Cd		(Pagani et al., 2012a)
Xerophyta humilis	Leaf		Up by drought stress		(Collett et al., 2004)
Zea mays	Embryo	embryonic microspores	Up by ABA		(White and Rivin, 1995)
Sesamum indicum	Embryo	Developing seed	Developmental		(Chyan et al., 2005)
Pseudotsuga menziesii	Embryo	Developing seed	Up by metal ions, osmotic stress, ABA		(Chatthai et al., 1997)

ABRE = abscisic acid responsive elements. ERE= Ethylene responsive elements

Involvement of ABA in MT4 expression suggested a role of these proteins in desiccation and embryogenesis (Kawashima et al., 1992). A rapid decline of wheat E_C mRNA within 5 h of imbibition (after uptake of water) was observed. After 24 h, a very low concentration of protein was still detected, proposing a zinc

homeostasis role for E_C. A very similar phenomenon was observed for *Oryza sativa (Zhou et al., 2005),* however, mRNA was also detected in 15-day old seed after pollination, proposing a zinc donation role in germinating pollen. Other MT4s including *Hordeum vulgare* (Hegelund et al., 2012) *and Sesamum indicum* (Chyan et al., 2005) have also given rise to similar observations. Moreover, low Cu and Cd tolerance in yeast complementation assays and tight binding to Zn as observed for *Hordeum vulgare* MT4 proposed a zinc storage function for MT4s (Hegelund et al., 2012). Furthermore, occurrences of MT4s in resurrection plant *Xerophyta humilis (Collett et al., 2004)* was proposed to be related to an antioxidant role of MT4s. Alternatively, a role for MT4s in drought tolerance and rehydration has also been proposed (Leszczyszyn et al., 2013).

1.8.1 Case study of a type 4 MT: Wheat E_C

Among the four subfamilies, type 4 or E_C MTs have become a topic of particular interest due to their functional and structural significance. Wheat E_C contains 79 amino acids in its primary amino acid sequence, and among them 17 cysteines and two histidines are conserved. Wheat E_C is the only plant MT for which 3D structures are available, (Loebus et al., 2011b; Peroza et al., 2009; Tarasava et al., 2013). All 17 cysteines and the two histidines bind six zinc ions in two separate domains which were given the names γ-E_C-1 domain and βE-domain (Loebus et al., 2011b; Peroza et al., 2009). Six cysteines fall into the γ-E_C-1 domain and can accommodate two zinc ions, forming a binuclear cluster with composition of Zn_2Cys_6. This type of cluster is unparalleled in other known MTs but is present in fungal transcription factors of the GAL4 family (Pan and Coleman, 1989).

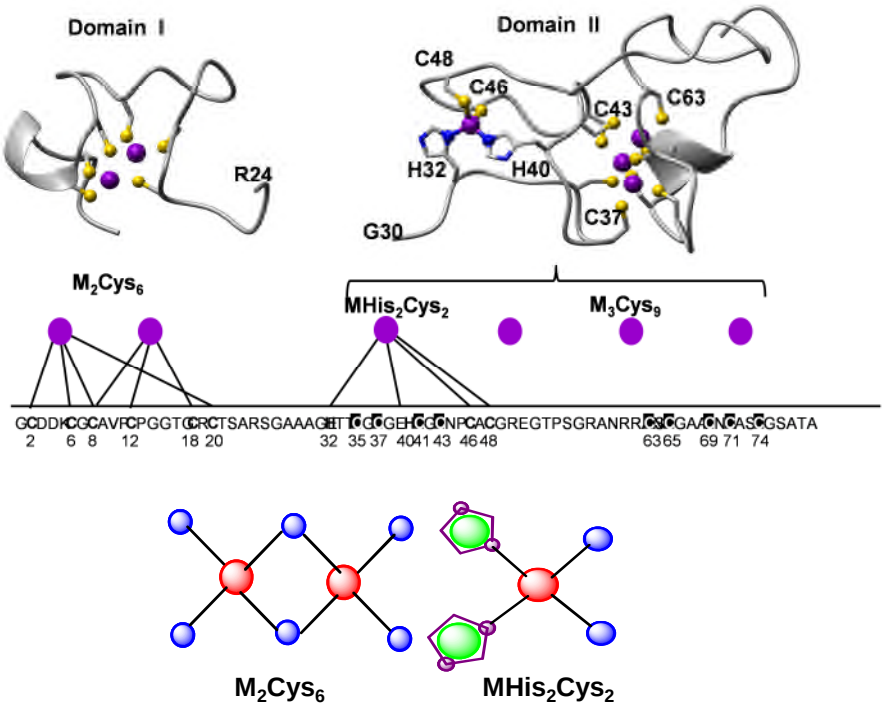

Figure 1.7 3D structure of E_C from wheat. Domain I binds 2 Zn ions in a Zn_2Cys_6 cluster whereas domain II binds 4 Zn ions forming a mononuclear site ($ZnHis_2Cys_2$) and a 3-metal cluster (Zn_3Cys_9). For the Zn_3Cys_9 cluster, no experimental metal-ligand connectivity was determined. (Adapted from (Leszczyszyn et al., 2013)).

In the so-called βE-domain, eleven cysteines and two histidines bind to four zinc ions. In its N-terminal region, a mononuclear $ZnHis_2Cys_2$ site is present. The remaining three zinc ions are bound to nine cysteines, and it was suggested that a cluster similar to those found in the β domains of mammalian MTs was present; hence the name "extended β domain" or βE-domain. Interestingly, for both Zn^{2+} and Cd^{2+} forms of E_C, the γ-E_C-1 domain is well folded, but in the presence of Cd^{2+}, the βE-domain is thought to undergo conformational and configurational changes that result in chemical exchange broadening of both backbone NH

protons and bound Cd nuclei. This chemical exchange broadening behaviour of the Cd form of the βE-domain and mutational studies suggested that the isolated $ZnHis_2Cys_2$ site plays a crucial role for proper folding of the entire βE-domain. This site is only formed in the presence of Zn and this metal-specific folding has been proposed as a means to discriminate between zinc and cadmium (Leszczyszyn et al., 2010). It has been proposed that type 4 MTs can act as a filter to prevent cadmium accumulation in the plant embryo (Leszczyszyn et al., 2013)

The non-isostructural replacement of zinc by cadmium in wheat E_C is the reason why the published structure (Peroza et al., 2009) for the βE-domain, and in particular the M_3Cys_9 cluster, is ambiguous because it was not based on experimentally determined ^{1}H-^{111}Cd connectivities. The structure was initally calculated without the inclusion of metal ion-based restraints using automated Nuclear Overhauser Effect (NOE) assignments. This has shown that His33, His41, Cys47, and Cys49 coordinated to a single metal. Subsequently, 7560 different possible cluster structures for the Zn_3Cys_9 cluster were considered - all assuming the formation of a six-membered ring as shown in Figure 1.3. Among them only the structures producing the lowest target function values which showed consistency with NOE NMR data were considered. A three-metal cluster configuration was put forward where one metal ion coordinated to Cys36, Cys38, Cys67, and Cys71, with Cys36, Cys44, Cys73, and Cys76 coordinating a second metal ion, and a third metal ion binding to Cys42, Cys65, Cys67, and Cys76. The authors noted that several other configurations were almost equally likely.

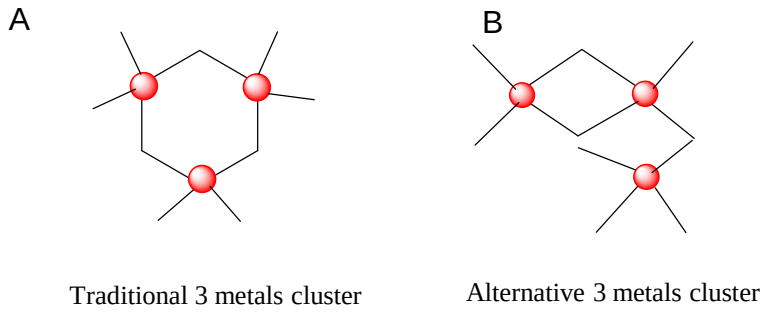

Figure 1.8 3D Schematic diagram of proposed 3 metal cluster. (A) Traditional 3 metal cluster (B) Alternative arrangement of 3 metal cluster.

An alternative cluster structure as shown in Figure 1.8 (B) could also be possible (O. I. Leszczyszyn, PhD thesis, 2008). In the alternative cluster two metal ions will form a binuclear cluster bridging to a single metal and that single metal will be connected to 3 terminal cysteines. Because the three metal cluster structure is not unambiguous and it is not proven yet that the Zn_3Cys_9 cluster does indeed form a 6-membered ring structure like those of the mammalian β domain, a less suggestive name for this domain is preferable. Hence, throughout this thesis, the two domains will be named domain I and domain II.

1.8.2 Type 4 MTs from *Arabidopsis thaliana*: The research focus

Arabidopsis thaliana, a dicotyledenous plant, has two type 4 MT isoforms, MT4a and MT4b. MT4a and MT4b contain 84 and 85 amino acid residues, respectively, in their primary protein sequences with a molecular weight of 8.3 and 8.5 kDa, respectively. They have isoelectric points of 6.65 and 5.49, respectively, with MT4b containing two extra negatively charged residues (at pH 7) compared to

MT4a. Like their E_C homolog from wheat, they have 17 cysteines and 2 conserved histidines and bind 6 zinc ions (Leszczyszyn et al., 2013). The cysteines are found distributed into 3 cysteine-rich regions with 6, 6 and 5 Cys residues, respectively, leaving 2 cysteine-poor regions of 14/15 and 11 residues length (Figure 1.9).

Figure 1.9 Protein sequence alignment of MT4a and MT4b. The numbers refer to cysteine residues in MT4b, with the alanine residue (A) considered as residue No 1.

Despite their 84% sequence identity, marked differences are observed between MT4a and MT4b in terms of functional studies.

In *Arabidopsis*, expression of both isoforms are restricted to developing seeds (Guo et al., 2003). Expression of both isoforms are regulated by a number of factors as presented in Table 1.5. Expression is up-regulated by the phytohormone abscisic acid but down-regulated by gibberelic acid for both isoforms. However, another hormone, auxin, represses MT4b expression.

Table 1.5 Expression profiles of MT4a and MT4b

Species	Location of expression	Developmental Expression	Regulation	Regulator	Reference
Arabidopsis thaliana	embryo	Mature & dry embryo	Up by ABA, MeJa, Man; Down by ZT, GA, cold; Down by IAA - MT4b; Up by NaCl - MT4a	ABRE	(Ren et al., 2011)

ABA – abscisic acid; GA – giberellic acid; IAA – indole-3-acetic acid (auxin); Man - mannitol; MeJA – methyl jasmonate; ZT - zeatin;ABRE = abscisic acid responsive elements.

MT4a expression was up-regulated by NaCl. Moreover, low temperature decreases the expression of both isoforms. Their expression begins during formation of siliques and ends at the stage of mature embryo (Figure 1.10). MT4a is expressed strongly in vascular tissues whereas predominant expression of MT4b was observed almost evenly across the entire embryo (Ren et al., 2011). However, in embryo, MT4b was expressed earlier and to a higher abundance than MT4a, thus it was suggested that MT4b stores metal ions, whilst MT4a distributes metals through the vascular tissue (Ren et al., 2011).

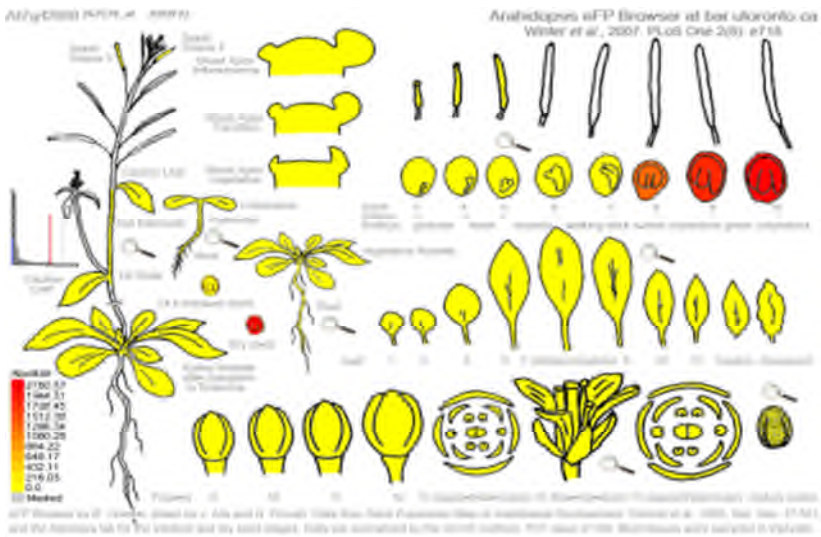

Figure 1.10 Electronic fluorescent pictograph (eFPs) for *Arabidopsis thaliana* MT4a gene (At2g42000) in different plant organs over various developmental stages. High expression levels of MT4a observed in cotyledons of dry seed are indicated by red colour, no expression is reported in yellow (Winter et al., 2007).

MT4a conferred better Zn tolerance than MT4b in mutant yeast. MT4a also provided higher tolerance to Co, but not to Cd (Guo et al., 2008). Interestingly, when expressed in transgenic *A. thaliana* vegetative tissue, MT4a led to an increase in Cu content, whereas that of Zn remained the same (Rodríguez-Llorente et al., 2010).

Gene analysis suggested that both the isoforms contain conserved single introns near the 6th cysteines and are located on chromosome II, however, they are not adjacent. Like their homolog from wheat $E_{C,}$ the promoters of both isoforms possess abscisic acid responsive elements (ABRE). The presence of ABRE, elements responsive to dehydration, suggests that *A. thaliana* MT4s play roles in embryogenesis, seed desiccation and storing Zn required for seedling growth after seed germination (Guo et al., 2003).

Further understanding regarding the *in vivo* function of these two proteins - as demonstrated using overexpressing and knock-down RNAi transgenic plants - was provided by a study of *Ren et. al.* Co-silencing the two MT4a/b genes led to the accumulation of less Zn than in wild-type plants, whilst in overexpressing transgenic plants, increased Zn contents were observed, suggesting a Zn-storing effect of MT4a and MT4b. Moreover, Zn addition was found to restart the seedling growth in seedlings where MT4a/b had been co-silenced. Furthermore, no increased Zn or Cu tolerance was observed when either MT was overexpressed in *E. coli* cells as a GST fusion protein, but Zn or Cu accumulation was observed. Importantly, gene expression of some zinc finger proteins and zinc-requiring enzymes, namely GATA transcription factors, C2H2 type zinc fingers and carbonic anhydrase 1 and 2, was found to decline in the MT4a/b co-silencing seedlings. However, increased expression was observed in the overexpression systems. All these observations suggest that MT4a and MT4b play a significant role in Zn storage and distribution during seed germination and seedling growth.

1.9 Aims and objectives

The aims of this project are twofold – (A) to work towards a complete structure for type 4 plant MTs: determination of cluster topology in mixed-metal species, and (B) to study to metal binding dynamics of two highly similar isoforms: reactivity in metal-release reactions

(A) Towards a complete structure for type 4 plant MTs: determination of cluster topology in mixed-metal species:

It has been hypothesised that type 4 MTs may be able to prevent the accumulation of cadmium in plant embryos. In fact, cadmium is an indispensable tool for MT structural studies to determine metal-thiolate connectivities and thus cluster topology. Hence, UV-Vis and NMR spectroscopies and native Electrospray Ionisation Mass Spectrometry (ESI-MS) will be used to study how MT4a and MT4b interact with increasing quantities of Cd^{2+}. The ultimate objective of this study is to elucidate the structure of at least one of the isoforms with the aid of ^{1}H-NMR, ^{111}Cd-NMR and multinuclear, multidimensional NMR spectroscopy, but the work towards this goal will also provide valuable insights into *in vitro* metal specificity.

(B) Metal binding dynamics of two highly similar isoforms: reactivity in metal-release reactions

It is believed that Type 4 MTs release or transfer zinc to zinc requiring enzymes, peptides or proteins during seed germination, which may perhaps help seedling growth and/or play a pivotal role for seedling

nutrition. However, very little information is available for metal release or transfer reactions from plant MTs in general, and none for the two isoforms under study. Hence, *in vitro* metal exchange and metal transfer to and release from MT4a and MT4b and their consequences on structure will be studied in two different contexts:

a. Zinc transfer to biomimetic ligands: 4-(2-pyridylazo)resorcinol (PAR) and ethylenediaminetetraacetic acid (EDTA) will be used as mimics for biomolecules to study the metal transfer dynamics of MT4a and MT4b. The effect of low pH to their metal binding dynamics will also be explored.
b. Effects of selected exogenous biomolecules on zinc mobilisation: Thermodynamically, metal binding to MT is strong, but kinetically MT-bound metal ions are often labile. Thus it is important to understand what factors influence MTs to release metals. Hence to get further insight into their zinc mobilisation dynamics, the influence of the biological redox couple GSH/GSSG, reactive oxygen species (H_2O_2), and phytate will be studied.

Issues of particular interest include how these type 4 MTs from a dicotyledonous plant behave in comparison to the prototypical type 4 MT E_C from monocotyledonous wheat, but also to be able to compare two very similar isoforms from the same organism. Yeast complementation assays (Guo et al., 2008) and studies in planta (Ren et al., 2011) suggested that the two MTs do not behave the same *in vivo*.

Chapter 2

Experimental

2.1 Design and cloning of expression constructs

Design and cloning of expression plasmids for MT4a and MT4b were performed in Professor Peter Goldsbrough's research lab (Purdue University, USA). The pET-28a (http://richsingiser.com/4402/pET28.pdf) vector was used for cloning both genes without any tags, and kanamycin was used as selective marker. In brief, the MT4a gene was amplified from pGEM:MT4a introducing NcoI and BamHI restriction sites. The amplified fragment was ligated into NcoI and BamHI digested pET-28a vector and the product was transformed into One Shot® TOP10 *E. coli* cells. Insertion was checked by sequencing using a T7 terminator primer. The same procedure was followed for MT4b.

2.2 Transformation of bacterial cells with plasmid DNA

Competent cells were transformed according to the protocol provided by the manufacturer Novagen. In brief, *E. coli* cells (20 μL, Rosetta 2(DE3) pLysS competent cells; Novagen) were taken and plasmid DNA (1 μL) of MT4a (obtained from the lab of Prof. Peter Goldsbrough) was added to the thawed *E. coli* cells. The mixture was then placed on ice for 5 minutes before heat shock at 42 °C for 30 seconds in a water bath and again kept on ice for 2 minutes. Into the cell/DNA mixtures, LB medium (80 μL) was added and the mixture was shaken

in an incubator at 37°C for 45 minutes at 180 rpm. 50 µL cell/DNA mixture was pipetted and spread on antibiotic containing Kanamycin (50 µg/mL) and Chloramphenicol (34 µg/mL) agar plates. The plates were incubated (upside down) at 37 °C for 16-18 hours. The whole process was repeated for a plasmid containing the gene for MT4b.

2.3 Plasmid extraction and preservation of bacterial overnight culture-glycerol stocks

Plasmid was collected following the Qiagen protocol using QIAprep spin miniprep kit. Glycerol (1 mL, 70%) was added to the overnight culture (1 mL) and the mixture was then placed in liquid Nitrogen for 10 minutes. The mixture was stored at −80°C.

2.4 Recombinant protein expression

2.4.1 Overnight starter culture

Sterile LB medium (100 mL) was taken and antibiotics 100 µL Kanamycin (50 µg/mL) and 100 µl Chloramphenicol (34 µg/mL) were added to the medium. An appropriate single bacterial colony was added to the medium with a pipette tip. The culture was placed in the incubator shaker at 37°C for 16 hours at 180 rpm.

2.4.2 Unlabelled protein expression

Overnight culture (6 mL) was added to fresh LB medium (600 mL) along with antibiotics 600 µL Kanamycin (50 µg/mL) and 600 µL Chloramphenicol (34 µg/mL). The mixture was placed in the incubator shaker at 37°C at 180 rpm.

Bacterial cell growth was monitored by measuring optical density (OD) at 600 nm using UV-Visible spectroscopy. When OD_{600} reached 0.65-0.75, protein expression was induced by IPTG (0.5 mM) and at the same time, the medium was supplemented with $ZnSO_4$ (0.5 mM). After 4-5 hours of induction, the cells were harvested by centrifugation at 3000×g for 10 minutes at 4°C. The cell pellets were re-suspended in fresh LB medium in a Falcon tube and centrifuged at 5000×g at 4°C for 10 minutes, the supernatant was discarded and the cell pellet was stored at −20°C.

2.4.3 Labelled protein expression

Starter culture (12-15 mL) was added to the labelled media (M9) and incubated at 37°C for 12 hr, at 20°C for 10 hr, and again at 37°C for 6 hr at 180 rpm. Bacterial cell growth was monitored by measuring OD_{600} using UV-Visible spectroscopy. When OD_{600} reached 1-1.1, protein expression was induced by IPTG (0.5 mM) and supplemented with $ZnSO_4$ (0.5 mM). The cells were then allowed to grow for 14 hr at 20°C at 180 rpm. The cells were harvested (OD_{600}~ 3) by centrifugation at 5000×g for 15 minutes at 4 °C. The cell pellets were re-suspended in fresh M9 medium in a Falcon tube and centrifuged at 5000×g at 4°C for 10 minutes, the supernatant was discarded and the cell pellet was stored at −20°C.

2.5 Protein purification

2.5.1 Cell disruption by Sonication

Sonication buffer (3mL/g cell weight, 50 mM Tris-Cl, 0.1 M KCl, 3 mM DTT, 1% Tween 20, pH 8.5) was added to the thawed cell pellet with addition of $ZnSO_4$

(1 mM). Sonication (1 second pulse, 15 watts, 4 minutes) was carried out until a turbid suspension was achieved. Streptomycin solution (10%, 0.375 mL/gcw) was added to the translucent suspension before centrifuging at 30000×g at 4°C for 50 minutes. The cell lysate was subjected to chemical precipitation prior to gel filtration chromatography.

2.5.2 Chemical precipitation

0.5 volumes of ice cold ethanol:chloroform (100:8) mixture (1 volume equivalent to supernatant volume) was added drop-wise to the supernatant with constant stirring in an ice bath. The protein pellet was collected by centrifugation at 5000×g for 20 minutes at 4°C and was stored at −20°C. Another 3.5 volumes of ethanol: chloroform (100:8) mixture were added to the supernatant and the protein pellet was collected by centrifugation at 5000×g for 20 minutes at 4°C.

2.5.3. Protein purification: Size exclusion chromatography

The protein was purified by FPLC (Pharmacia Akta Purifier) mounted with a size exclusion column (HiLoad 16/60 Superdex 75, Amersham Biosciences). All the buffers were filtered to remove suspended particles and degassed to remove dissolved oxygen by stirring the buffer for 30 minutes prior to use. The protein pellet (3.5 volume fraction) was dissolved in ammonium bicarbonate buffer (20 mM, pH 7.8), filtered through millipore filter (0.2 μm - 0.4 μm, Minisart®) and loaded into a super-loop. Proteins were eluted with ammonium bicarbonate buffer (20 mM, pH 7.8, degassed) at a flow rate of 1 mL/min. The elution of protein fractions (4 mL) was monitored at wavelengths of 220 nm (peptide bond and Zn-S

charge transfer bands) and 280 nm (aromatic residues). Selected FPLC fractions were analysed by Sodium Dodecyl-Sulfate-Polyacrylamide Gel Electrophoresis (SDS-PAGE)

2.6 Protein Identification

2.6.1 Sodium Dodecyl-Sulfate-Polyacrylamide Gel Electrophoresis (SDS-PAGE)

The samples for Sodium Dodecyl-Sulfate-Polyacrylamide Gel Electrophoresis (SDS-PAGE) were prepared by mixing an aliquot of a protein fraction (40 µL) with Laemmli buffer (40 µL, prepared by mixing 950 µL Laemmli sample buffer with 50 µL β-mercaptoethanol). The gel (Mini-PROTEAN® TGXTM, 4-15%, BIO-RAD) was placed in the electrophoresis apparatus and the SDS buffer (100 mL 10xSDS buffer, 900 mL dH_2O) was poured into the electrophoresis tank. The marker (5 µL) was loaded into the first well and the rest of the wells were loaded with selected protein fractions from FPLC. The parameter set for running the electrophoresis was a fixed voltage of 150 V for 45-50 minutes.

2.6.2 Native Polyacrylamide Gel Electrophoresis (NPAGE)

Native PAGE of the protein was performed using native sample buffer (250 mM Tris base, 0.0185% Coomassie R-250, 0.00625% Phenol Red, 10% Glycerol, pH 8.7) and native running buffer (50 mM Tris base, 50 mM MOPS, 0.0375% SDS, pH 7.4). In brief, prior to loading the protein sample into precast PAGE gels, the

precast gel was run only with water at a fixed voltage of 150 V for 30 minutes. The respective protein samples were loaded on to the water-treated precast PAGE gel. Electrophoresis was carried out at a fixed voltage of 80 V for 120 minutes.

2.6.3 SDS-PAGE: Treatment with EDTA and DTT

This experiment was performed similarly as mentioned in 2.6.1, but the protein sample was treated separately with EDTA and DTT. In brief, proteins (35 µM, 50 µL) were incubated with EDTA (9 mM) or DTT (28 mM) for 28 hours. Samples for SDS-PAGE were prepared as mentioned in section 2.6.1.

2.6.4 Silver Staining

The gel was submersed into the fixer solution (60 mL 50% acetone, 1.5 mL 50% trichloroacetic acid, 25 µL formaldehyde) and placed in the rocker for 15 minutes. The gel was then washed with distilled water. The water was discarded and 50:50 acetone:water solution was added for 5 minutes. The solution was discarded and the gel was soaked in sodium thio-sulfate solution (0.1 g , 60 mL water) for one minute and washed with distilled water. The gel was stained with a solution containing 160 mg silver nitrate and 600 µL formaldehyde in 60 mL water, placed in the rocker for 10 minutes and washed with distilled water. Gel developing solution (1.2 g sodium carbonate, 25 µL formaldehyde, 2.5 mg sodium thio-sulfate, 60 mL water) was added until bands were visible and then stopping

solution (1 % acetic acid) was added. The gel was rinsed with water and a photograph was taken.

2.7 Anion exchange chromatography

Selected FPLC protein fractions as identified by SDS-PAGE were combined and if required further purified by anion exchange chromatography. The sample was loaded into a superloop and injected to an anion exchange column (HiTrap Q XL, 5mL, GE Healthcare) connected to an FPLC system (Pharmacia Akta Purifier). Gradient elution (buffer A: 20 mM NH_4HCO_3, pH 7.6, buffer B: 1 M NaCl, 20 mM NH_4HCO_3, pH 7.6) at a flow rate of 2 mL/min with a gradient length of 20 column volumes was employed. In brief, the column was cleaned with 100% of buffer B and then pre-equilibrated with 100% of buffer A. The elution of protein fractions (3 mL) was monitored at an absorbance of 220 nm (peptide bond and Zn-S charge transfer) and 280 nm (aromatic residues). MT4a and MT4b eluted around 28-32% buffer B. Selected protein fractions were analysed by SDS-PAGE as described above.

2.8 Determination of metal-protein stoichiometry: Inductively-Coupled Plasma-Optical Emission Spectroscopy (ICP-OES)

Inductively Coupled Plasma-Optical Emission Spectroscopy (ICP-OES) (Perkin-Elmer Optima 5300 DV, Model S10) was used to determine the S, Zn, Cd and Cu content of the proteins by measuring S at 180.669 and 181.975 nm, Zn at 206.200 and 213.857 nm, Cd at 228.802 and 214.440 nm and Cu at 327.393 and 324.752 nm. Plasma operating conditions were: Argon (Ar) flow rate 13.0 L/min, auxiliary gas flow rate 0.2 L/min, nebuliser flow rate 0.8 L/min and RF power at 1300W.

The samples were prepared by diluting 0.2-1 mL of protein to a final volume of 3-5 mL in 0.1 M ultrapure HNO_3 (prepared from 72% distilled HNO_3) in order to remove possible traces of labile sulfide ions. All samples were analysed using three replicate readings, with a washing time of 60 seconds for each sample. Data were analysed using WinLab 32 software (Perkin-Elmer).

The data in mg/L were divided by dilution factor followed by 1000 to obtain units in μg/L. The result was then divided by the appropriate atomic masses which gives the concentration in μmol/L of the given elements in the sample. To obtain the protein concentration, the sulfur concentration in μmol/L was divided by 19, the number of sulfurs (17 Cys and 2 Met) in the protein. The metal-to-protein ratio was calculated by dividing the metal concentration by the protein concentration.

2.9 Thiol quantification: Ellman's Test

The protein concentration was determined as equivalent free thiols (cysteine) by Ellman's reagent, 5,5'-dithio-bis(2-nitrobenzoic acid) (DTNB). Different concentrations (0, 13.3, 26.7, 40 and 53.3 μM) of cysteine solution were prepared from a cysteine stock (800 μM, 1 mM EDTA) in Tris-Cl buffer (2.6 mL, 0.1 M, pH 7.05) and DTNB (200 μL, 2.5 mM in 50 mM ammonium acetate, pH 5.0, 1 mM EDTA) was added to obtain a total volume of 3 mL using MilliQ water. The absorbances at 412 nm were taken immediately after preparation of these standards (Biomate 3 spectrophotometer, Fisher Scientific). The protein samples (20-100 μL) were prepared in the same way as the standards, but samples were allowed to react with the reagent for 15-20 minutes and absorbance at 412 nm was

recorded. The thiol concentration was determined from the calibration curve obtained from the standard readings. The protein concentration was calculated by dividing the thiol concentration by the number of cysteines in the protein backbone, in this case it was 17 for MT4a and MT4b.

2.10 Desalting and buffer exchange

The protein samples were desalted and buffer exchanged (10 mM ammonium bicarbonate) using PD-10 columns (Sephadex G-25, GE Healthcare) prior to mass spectrometry following the protocol provided by the manufacturer. In brief, the column was pre-equilibrated with the buffer (10 mM ammonium bicarbonate, 25 mL). The protein sample (2.5 mL) was then loaded on to the equilibrated column. Protein sample was collected by elution with buffer (3.2-3.5 mL). The column was again washed with buffer (25 mL) and kept at 4ºC for further use. When necessary, concentrated protein was obtained by centrifugation using Amicon Ultra (3000 MWCO, Millipore) filter devices.

2.11 Mass spectrometry: Electrospray Ionization Mass Spectrometry (ESI-MS)

2.11.1 Sample preparation

Protein sample (90 μL, in 10 mM ammonium bicarbonate buffer, pH 7.8) was mixed with methanol (10 % v/v) and a “native” protein spectrum was taken. The apo form of the protein was generated by addition of formic acid (2% v/v) to the same mixture, and a second mass spectrum was acquired.

2.11.2 Acquisition parameters

Mass spectra were recorded on a Bruker Daltonics MicroTOF fitted with an electrospray ionization source operating in positive mode. The samples were injected into the spectrometer by a syringe pump with a flow rate of 240 μL/hr. Other parameters were fixed as: temperature 195°C, nebulizer 0.6 Bar, dry gas 4.5 l/min, capillary exit 100 V, skimmer1 50 V, skimer2 25.2 V, hexapole1 24.2 V, hexapole2 22.4 V, hexapole RF 450 V, transfer time 81 μs and detector TOF 2300 V.

The data were obtained over 0.4-2 min for the range of 500-5000 m/z. The experimental data were then smoothed and deconvoluted using the data analysis software Bruker compass data analysis v 4 provided by Bruker Daltonics.

2.12 Nuclear magnetic resonance (NMR) Spectroscopy

2.12.1 Sample conditions and instruments

All protein samples (various concentrations) were prepared in a standard buffer, in the following referred to as "NMR buffer" (50 mM Tris-D_{11}, 10 % D_2O, 50 mM NaCl) at different pH values (mentioned in the text). A number of 2D and 3D homonuclear and heteronuclear experiments were carried out for backbone and side-chain elucidation using a Bruker Avance 700 Ultrashield spectrometer mounted with a TCI cryoprobe. Spectra were recorded at an operating frequency of 700.24 MHz for ^{1}H, 70.95 MHz for ^{15}N and 176.08 MHz for ^{13}C. Metal-ligand connectivity experiments were performed on a Bruker DRX500 spectrometer fitted with a broad band observe (BBO) probe at an operating frequency of 106.10

MHz for ^{111}Cd and 500.13 MHz for ^{1}H nuclei. The residual water resonance was used as a reference for ^{1}H chemical shifts (Wishart, Bigam et al. 1995) and $^{15}NH_4Cl$ was used as external reference standard for ^{15}N chemical shifts.

Recorded spectra were processed using Bruker Topspin v. 2.1 software. For 2D and 3D spectra, phase- and baseline-corrected topspin file were transferred to Sparky v3.106 (T. D. Goddard and D. G. Kneller, SPARKY 3, University of California, San Francisco) for analysis.

2.12.2 1D ^{1}H-NMR spectroscopy

1D ^{1}H-NMR spectra of the protein samples as prepared were recorded at 700 MHz (Avance 700 Ultrashield with TCI cryoprobe, Bruker) spectrometer at 25 °C using excitation sculpting with gradients for water suppression. The spectra were recorded with 16k complex data points, 128 scans and a spectral width of 15.9 ppm.

2.12.3 2D Homonuclear NMR spectroscopy: TOCSY and NOESY

2D [^{1}H ,^{1}H] Total Correlation (TOCSY) and Nuclear Overhauser Enhancement (NOESY) spectra were recorded on the same protein samples (1.2 mM, NMR buffer, pH 7.4). Acquisition parameters were selected as 16 scans, 4k data points in F2 and 512 or 400 increments in F1 with a spectral width of 16 ppm centred at the water peak at ~4.7 ppm. TOCSY spectra were recorded using dipsi2esgpph, mlevesgpph, or mlevgppw5 pulse programs with a mixing time of 60-65 ms. Water suppression was done using excitation sculpting with gradient (A J Shaka, 1988). The pulse program used for NOESY was noesyesgpph, using a mixing

time of 60 or 100 ms. A squared sine-bell function was used to apodize the raw data prior to Fourier transformation with 2k×2k data points.

2.12.4 2D Heteronuclear NMR spectroscopy: [^{1}H, ^{15}N] HSQC and [^{1}H, ^{13}C] HSQC

A homogeneously labelled (^{15}N) or (^{13}C and ^{15}N) protein sample (~500µM, NMR buffer, pH 7.43) was used to record 2D [^{1}H,^{15}N] heteronuclear single quantum coherence (HSQC) spectra with 4k data points in F2 (^{1}H) and 128 increments in F1 (^{15}N). The spectrum was acquired with a spectral width of 16 ppm in F2 and 40 ppm in F1 dimensions over 16 scans with $^{1}J_{NH}$ coupling constant of 90 Hz. The raw data were apodized using a squared sine-bell function and Fourier transformed into 2048×256 data points in the F2×F1 dimensions, respectively.

2D [^{1}H ,^{13}C] heteronuclear single quantum coherence (HSQC) spectrum was obtained with 2k data points in F2 (H) and 256 increments on F1 (C). The spectrum was acquired with over 8 scans on a spectral width of 16 ppm in F2 and 165 ppm in F1 dimensions $^{1}J_{NH}$ coupling constant of 145 Hz. A squared sine-bell function was used to apodize the raw data and Fourier transformed with 1k×1k data points.

2.12.5 Zinc coordination to histidines: Extended [^{1}H, ^{15}N] HSQC

Homogeneously labelled ^{15}N protein samples of Zn_6MT4a and Zn_6MT4b (~400 µM, NMR buffer, pH 7.43) were used to record 2D [^{1}H,^{15}N] heteronuclear single quantum coherence (HSQC) spectra in the extended region between 65 and 265

ppm with 4k data points in F2 (^{1}H) and 512 increments in F1 (^{15}N) with a $^{2}J_{NH}$ coupling constant of 30 Hz. The spectrum was acquired with a spectral width of 16 ppm in F2 and 200 ppm in F1 dimensions over 16 scans. The raw data were apodized using a squared sine-bell function and Fourier transformed into 4k×2k data points in the F2×F1 dimensions, respectively.

2.12.6 3D heteronuclear NMR spectroscopy: HNCA and HN(CO)CA

HNCA and HN(CO)CA spectra were obtained with 2048 data points in F3 (^{1}H), 40 increments for F2 (^{15}N) and 64 increments for F1(^{13}C) dimensions with 16 scans. Spectral widths were 14.0 ppm for F3 (^{1}H), 32 ppm for both F2 (^{15}N) and F1 (^{13}C). Pulse programs used were hncagpwg3d and hncocagpwg3d for HNCA and HN(CO)CA, respectively. The raw data were apodized and Fourier transformed into 2048×64×256 data points in the F3×F2×F1 dimensions, respectively.

2.12.7 3D heteronuclear NMR spectroscopy: [^{1}H, ^{1}H, ^{15}N] TOCSY-HSQC and NOESY-HSQC

[^{1}H, ^{1}H, ^{15}N] TOCSY-HSQC spectra were acquired with spectral widths of 14 ppm for F3 (^{1}H), 32 ppm for F2 (^{15}N) and 14 ppm for F1 (^{1}H) with 16 scans. Spectra were acquired with 2048 data points in F3 (^{1}H), 36 increments for F2 (^{15}N) and 128 increments for F1 (^{1}H) with a TOCSY mixing time of 60 ms. A [^{1}H, ^{1}H, ^{15}N] NOESY-HSQC spectrum was obtained with the same spectral

widths and data points as for the [^{1}H, ^{1}H, ^{15}N] TOCSY-HSQC spectrum, with a mixing time of 100 ms. The data were apodized and Fourier transformed in to 2k (F3)×64(F2)×512(F1) data points for [^{1}H, ^{1}H, ^{15}N] TOCSY-HSQC and 2k(F3)×64(F2)×256(F1) data points for [^{1}H, ^{1}H, ^{15}N] NOESY-HSQC.

2.13 ^{111}Cd NMR spectroscopy

2.13.1 Sample preparation for ^{111}Cd loaded MT4a and MT4b: Filtration

Zn_6MT4a or Zn_6MT4b (0.8-1.4 mM, 20 mM NH_4HCO_3 buffer, pH 7.8) was incubated with $^{111}CdCl_2$ (2-7 equivalents) for 18-20 hours. The protein was desalted and buffer exchanged (10 mM NH_4HCO_3 buffer) using a PD-10 column (Sephadex G-25, GE Healthcare) and concentrated (500 µL) using Amicon Ultra-4 (3000 MWCO, Millipore) filter devices. Protein samples were washed with NMR buffer (1 mL, pH 7.42) using the same Amicon filters. The process was repeated for three times and finally the volume was adjusted to 600 µL with NMR buffer to a final concentration of 0.8-1.4 mM. The sample pH was adjusted to 7.40-7.50 by addition of NaOH or HCl from 1 M stock solutions.

2.13.2 Sample preparation for ^{111}Cd loaded MT4a and MT4b: Titration

A solution of Zn_6MT4a or Zn_6MT4b (550 µL, 1-1.8 mM, NMR buffer, pH 7.42) was titrated with incremental volumes of $^{111}CdCl_2$ (1-6 equivalents, 50 or 100 mM stock solution). Samples were used directly, without further equilibration or purification.

2.13.3 1D ^{111}Cd-NMR spectroscopy

The 1D ^{111}Cd NMR spectra of the ^{111}Cd loaded MT4a or MT4b were recorded on a Bruker DRX500 spectrometer with a Broad Band Observe (BBO) probe suitable for observation of ^{111}Cd nuclei at 106.037 MHz. A GARP sequence was applied to achieve inverse-gated decoupling during acquisition. The data were acquired at various temperatures from 0-35°C with 4k complex data points and a number of scans of 65536, with a spectral width of 250 ppm centered at 625 ppm. A repetition rate of 0.5 s and a tip angle of 90° were also applied. The raw spectra were apodized using exponential multiplication with a 30 Hz line broadening factor and Fourier transformed.

2.13.4 2D [^{1}H, ^{111}Cd] HSQC-NMR spectroscopy

2D [^{1}H, ^{111}Cd] HSQC spectra were recorded with a $^{3}J(H_{\beta},Cd)$ coupling constant of 25 and 50 Hz at various temperature of 20 to 35 °C. The experiment was run with 196 scans with 2k complex data points in F2 (^{1}H) and 108 increments in F1 (^{111}Cd). Spectral widths of 13 and 130 ppm were used in F2 and F1, respectively. Raw data were apodized using an exponential function in F1 and sine-bell function in F2 and Fourier transformed with 2k×2k data points in F2 and F1, respectively.

2.13.5 Cadmium titration of Zn_6MT4b: [^{1}H, ^{15}N] HSQC

1-6 equivalents of $CdCl_2$ were added to a homogeneously ^{15}N-labelled sample of Zn_6MT4b (~400 µM, NMR buffer, pH 7.43) and after each addition, a 2D

[^{1}H,^{15}N] heteronuclear single quantum coherence (HSQC) spectrum was recorded as described in section 2.12.4. Spectra for the extended region at 3, 4 and 5 equivalents of cadmium were also recorded and analysed as mentioned in section 2.12.5.

2.14 Cadmium exchange: UV-Visible spectroscopy and mass spectrometry

2.14.1 Cadmium titration: UV-Visible spectroscopy

Cadmium (Cd^{2+}) (1-9 equivalents) was added to a solution of Zn_6MT4a and Zn_6MT4b (2 μM, 0.7 mL, 0.2 M Tris buffer, pH 7.58). Prior to taking a UV-Vis spectrum, samples were incubated for 5 minutes after each addition of cadmium. Spectra were recorded in the range of 200-300 nm at a scan rate of 300 nm/min at room temperature. Dilution effect for addition of cadmium was negligible.

2.14.2 Cadmium speciation: Mass spectrometry

Fully zinc-loaded protein samples of MT4a and MT4b (25 μM, 20 mM NH_4HCO_3 buffer, pH 7.8) were incubated with different 1 to 8 molar equivalents of Cd for 18 h at 4ºC. The protein samples were desalted and buffer exchanged (10 mM NH_4HCO_3 buffer, pH 7.8) using PD-10 columns (Sephadex G15, GE Healthcare), and concentrated (Amicon Ultra (3000 MWCO) filter device, Millipore) to 0.8-1 mL. Mass spectra of protein samples (25 μM, 10 % v/v methanol) were recorded.

2.15 Zinc release/transfer dynamics: UV-Visible spectroscopy

All the UV-Visible experiments were carried out using Cary 50 (Varian) spectrophotometer. Data were analysed in excel and plots were made using Origin pro 9.1 software

2.15.1 Zinc transfer to PAR: Kinetics

Zinc-loaded protein samples of MT4a and MT4b (2 µM, 0.2 M Tris buffer, pH 7.33) were incubated with PAR (200 µM, 0.2 M Tris buffer, pH 7.33) and the absorption change due to $Zn(PAR)_2$ complex formation was monitored at 500 nm for 80 minutes. The blank solution contained an equivalent concentration of PAR in 0.2 M Tris buffer. Acquired data were processed using equation $\ln [(A_\infty - A_t)/(A_\infty - A_0)]$ and plotted against time.

2.15.2 EDTA-mediated Zn transfer: Kinetics

The metal chelator EDTA was used to study the metal transfer dynamics of MT4a and MT4b by UV-Vis spectroscopy. Zn_6MT4a or Zn_6MT4b (5 µM, 0.7 mL, 25 mM Tris buffer, pH 7.33) was reacted with EDTA (0.05 mM, 0.25 mM, 0.5 mM, 25 mM Tris buffer, pH 7.33). The metal release was monitored as a change in absorption at 220 nm. The blank solution contained an equivalent concentration of

EDTA in the same reaction buffer. Changes in absorbance were monitored for 3 hours. Data were plotted as ln ($A_t - A_\alpha$) vs time.

2.15.3 pH titration: UV-Visible spectroscopy

pH titrations of zinc-loaded proteins were carried out in the range of 200-300 nm at a scan rate of 300 nm/min at room temperature. Respective protein samples (1.5 mL, 10 μM, 1 mM Tris buffer, pH 7.92) were titrated with dilute HCl (1-5 μL, 0.01-5 M). The dilution effect due to addition of HCl was negligible. The pH of the samples was measured before and after the UV-spectrum was recorded. The absorbances at 230 nm for Zn forms of MT4a and MT4b were plotted vs. pH for the determination of the pH of half-displacement.

2.16 Metal speciation during metal release/transfer: Mass spectrometry

2.16.1 Reaction with PAR: Equilibrium

Solutions of Zn_6MT4a (60 and 44 μM, 20 mM NH_4HCO_3 buffer, pH 7.8) were incubated with 4-(2-Pyridylazo) resorcinol (PAR) (6 mM (100 times) and 6.6 mM (150 times), 20 mM NH_4HCO_3 buffer, pH 7.8) for 18-20 hours. For MT4b, 51 or 41 μM (20 mM NH_4HCO_3 buffer, pH 7.8) were incubated with 4-(2-Pyridylazo) resorcinol (PAR) (5.1 mM (100 times) or 6.15 mM (150 times), 20 mM NH_4HCO_3 buffer, pH 7.8) for 18-20 hours. The protein fractions (3.5 mL) were collected during the desalting and buffer exchange (10 mM NH_4HCO_3 buffer) using PD-10 columns (Sephadex G-25, GE Healthcare). Protein fractions were concentrated using Amicon Ultra-4 (3000 MWCO, Millipore) filter devices. Mass

spectra of samples (25 µM, 10% v/v CH_3OH, 10 mM NH_4HCO_3 buffer, pH 7.8) were recorded.

2.16.2 Reaction with EDTA: Kinetics

A desalted solution of Zn_6MT4a or Zn_6MT4b (1620 µM with respect to Zn), 10 mM NH_4HCO_3 buffer, pH 7.8) was reacted with EDTA (1620 µM) within a time period of 22 hours. Aliquots at different time intervals were taken and diluted to the required concentration (25 µM, 10% v/v CH_3OH, 10 mM NH_4HCO_3) prior to record mass spectra.

2.16.3 Variation of pH

Desalted aliquots of Zn_6MT4a and Zn_6MT4b (25 µM, 200 µL, 10 mM NH_4HCO_3 buffer, pH 7.8) were incubated with different concentrations of formic acid (0.1-5 M). Mass spectra of the samples (25 µM, 10% v/v CH_3OH, 10 mM NH_4HCO_3 buffer pH 7.8-2.4) were recorded. To avoid salt contamination, incubated samples were separated into two aliquots and pH was measured (Hamilton Biotrode pH electrode) before and after the mass spectra.

2.17 Dynamic and structural aspects: ^{1}H-NMR spectroscopy

2.17.1 Reaction with PAR: Sample preparation and ^{1}H NMR spectroscopy

Zn_6MT4a (71.4 µM, 20 mM NH_4HCO_3 buffer, pH 7.8) was incubated with PAR (7.14 mM, 100 equivalents, 20 mM NH_4HCO_3 buffer) for 18-20 hours. The

protein (2.5 mL) was desalted and buffer exchanged (10 mM NH_4HCO_3 buffer) using a PD-10 column (Sephadex G-25, GE Healthcare) and concentrated to 500 µL using an Amicon Ultra-4 (3000 MWCO, Millipore) filter device. The protein sample was washed with NMR buffer (1 mL, pH 7.42) using the Amicon filter (3000 MWCO, Millipore). The process was repeated for four times and finally the volume was adjusted to 250 µL, giving a final protein concentration of 250 µM. MT4b (68.75 µM, 20 mM NH_4HCO_3 buffer, pH 7.8) was incubated with PAR (6.875 mM, 100 equivalents, 20 mM NH_4HCO_3 buffer) for 18-20 hours, and sample was prepared similar to MT4a. 1D ^{1}H-NMR spectra were recorded.

2.17.2 Reaction with EDTA: 1D ^{1}H NMR spectroscopy

Zn_6MT4a and Zn_6MT4b (277 µM, NMR buffer, pH 7.4) was mixed with EDTA (1:6 w.r.to [protein], NMR buffer, pH 7.4). Immediately after mixing a series of 1D ^{1}H-NMR spectra were recorded.

2.17.3 Reactivity of individual domains: [^{1}H, ^{15}N] HSQC spectra

Homogeneously labelled (^{15}N) samples of Zn_6MT4a or Zn_6MT4b (251 and 267 µM, NMR buffer, pH 7.43) were mixed with EDTA (1:6 with respect to [protein], NMR buffer, pH 7.4). Immediately after mixing, a series of 2D [^{1}H, ^{15}N] HSQC spectra were recorded with 4k data points in F2 (^{1}H) and 128 increments in F1 (^{15}N). The raw data were apodized and Fourier transformed into 2048×256 data points in the F2×F1 dimensions respectively.

2.17.4 pH variation: ^{1}H NMR spectroscopy

Zn_6MT4a or Zn_6MT4b (400 µM, NMR buffer, pH 8.48) was allowed to react with incremental addition of acid (0.1 -1 M, HCl,) for 5-15 minutes and 1D ^{1}H-NMR spectra were recorded. Spectra were apodized and Fourier transformed. Trimethylsilyl propionate (TSP) was used as an internal standard. pH was measured before and after a spectrum was recorded.

2.18 Effect of phytate on MT4a and MT4b

2.18.1 Zinc transfer to PAR in presence and absence of phytate: UV-Visible spectroscopy

Zinc transfer from MT4a and MT4b to the metal chelator PAR was monitored at 500 nm for the formation of the $Zn(PAR)_2$ complex in presence and absence of phytate. Zn_6MT4a and Zn_6MT4b (2 µM, 0.2 M Tris buffer, pH 7.53) was allowed to react with a 100-fold excess of PAR (200 µM, 0.2 M Tris buffer, pH 7.53). Subsequently, under the same experimental conditions, phytate (1 mM, 0.2 M Tris buffer, pH 7.53) was added. The blank solutions contained the equivalent quantities of PAR and phytate, respectively.

2.18.2 Effect of phytate on MT4a and MT4b: Mass spectrometry

Samples of Zn_6MT4a or Zn_6MT4b (30 µM, 20 mM NH_4HCO_3 buffer, pH 7.8) were incubated with different stoichiometric ratios of phytate (1, 6 and 50 with

respect to protein concentration) for 18 hours at 4ºC. The samples were then desalted and buffer-exchanged (10 mM NH_4HCO_3 buffer, pH 7.8) using gel filtration (Sephadex G-25, PD-10, GE Healthcare). Desalted protein was concentrated by ultrafiltration (Amicon filter device, 3000 MWCO, Millipore). Protein samples (25 µM, 10%v/v CH_3OH, 10 mM NH_4HCO_3 buffer, pH 7.8) were prepared for native protein-phytate interaction studies. To study adduct pH stability, protein samples (25 µM, , 10%v/v CH_3OH, 10 mM NH_4HCO_3 buffer, required amount of formic acid, pH 3.5-2.5) were prepared and Mass spectra were recorded.

2.18.3 Effect of Phytate on MT4a and MT4b: ^{1}H-NMR Spectroscopy

Zn_6MT4a or Zn_6MT4b (250 µM, NMR buffer, pH 7.42) was allowed to react with phytate (50 equivalents, NMR buffer, pH 7.4) at different time interval. 1D ^{1}H-NMR spectra at different time points were recorded. All acquired data were processed (apodized, Fourier transformed, phase corrected and baseline corrected).

2.19 Effect of redox active reactants on MT4a and MT4b

2.19.1 Thiol reactivity of MT4a and MT4b: UV-Visible spectroscopy

Reactions of DTNB with MT4a and MT4b were studied under two different experimental conditions where either [Protein Thiol] < [DTNB] or [Protein Thiol] > [DTNB]. In the first condition, Zn_6MT4a or Zn_6MT4b (2.5 µM, 0.2 M Tris

buffer, pH 7.33) was reacted with DTNB (1 mM, 0.2 M Tris buffer, pH 7.33) and in the second case, MT4a or MT4b (5 µM, 0.2 M Tris buffer, pH 7.33) was reacted with DTNB (2 µM, 0.2 M Tris buffer, pH 7.33). In both cases, the reaction was monitored at 412 nm.

2.19.2 Effect of glutathione (GSH) and glutathione disulfide (GSSG): Mass spectrometry experiments

Zn_6MT4a or Zn_6MT4b (30 µM, 20 mM NH_4HCO_3 buffer, pH 7.8) was incubated with GSH and GSSG (2.5 and 5.5 mM, 20 mM NH_4HCO_3 buffer, pH 7.8) for 18-20 hours. The proteins were desalted and buffer exchanged (10 mM NH_4HCO_3 buffer) using PD-10 columns (Sephadex G-25, GE Healthcare). Protein fractions were concentrated using Amicon Ultra-4 (3000 MWCO, Millipore) filter devices. Mass spectra of samples (25 µM, 10% v/v CH_3OH, 10 mM NH_4HCO_3, pH 7.8) were recorded.

2.19.3 Effect of pH and Cd^{2+} on MT4b-GSSG adducts: Mass spectrometry

Zn_6MT4b-GSSG samples prepared as described in section 2.19.2 were incubated with $CdCl_2$ (5 equivalents with respect to protein concentration) for 18-20 hours at 4°C. The proteins were desalted and buffer exchanged (10 mM NH_4HCO_3 buffer, pH 7.8) using PD-10 columns (Sephadex G-25, GE Healthcare). Protein fractions were concentrated using Amicon Ultra-4 (3000 MWCO, Millipore) filter devices. Mass spectra of samples (~25 µM, 10% v/v CH_3OH, 10 mM NH_4HCO_3, pH 7.8) were recorded.

For pH stability, Zn_6MT4b-GSSG samples prepared (section 2.19.2) were subjected to lowering the pH to 3.5 and 2.5 by addition of formic acids to samples of (~25 µM, 10% v/v CH_3OH, 10 mM NH_4HCO_3, required amount of formic acids) and mass spectra were recorded.

2.19.4 Effect of glutathione (GSH)/ glutathione disulfide (GSSG) couple

Zn_6MT4b (36 µM, 20 mM NH_4HCO_3, pH 7.8) was incubated with mixtures of GSH and GSSG (molar ratios of 1:1, 3:1, 30:1 and 100:1, fixed total concentration of 5.5 mM) for 20 hours. The proteins were desalted, buffer-exchanged (10 mM NH_4HCO_3) and concentrated using Amicon Ultra-4 (3000 MWCO, Millipore) filter devices. Mass spectra of samples (25 µM, 10% v/v CH_3OH, 10 mM NH_4HCO_3, pH 7.8) were recorded.

2.19.5 Reaction with DTNB: Mass spectrometry

Solutions of Zn_6MT4a or Zn_6MT4b (25 µM, 20 mM NH_4HCO_3, pH 7.8) were incubated with DTNB (1 and 17 molar equivalents with respect to [protein]) for 2-3 hours. The proteins were desalted and buffer-exchanged (10 mM NH_4HCO_3 buffer) using PD-10 columns (Sephadex G-25, GE Healthcare). Protein fractions were concentrated using Amicon Ultra-4 (3000 MWCO, Millipore) filter devices. Mass spectra of samples (~25 µM, 10% v/v CH_3OH 10 mM NH_4HCO_3 buffer, pH 7.8) were recorded.

2.19.6 Reaction with H_2O_2: Time course

Desalted Zn_6MT4a or Zn_6MT4b (250 µM, 10 mM NH_4HCO_3, pH 7.8) were mixed with H_2O_2 (4.25 mM, 1:1 with respect to [sulfur]). Immediately after mixing, aliquots (10 µL) were removed from the reaction mixture at different time intervals and diluted (25 µM, 10% v/v CH_3OH, 10 mM NH_4HCO_3 buffer, pH 7.7) and mass spectra were acquired.

2.20 Kinetics and protein folding: ^{1}H-NMR spectroscopy

2.20.1 Reaction with GSH/GSSG redox couple: 1D ^{1}H and 2D [^{1}H, ^{1}H] TOCSY spectroscopy

Zn_6MT4b (220 µM, NMR buffer, pH 7.33) was mixed with GSH/GSSG (30:1 and 1:30 ratio, fixed concentration of 5 mM, NMR buffer, pH 7.33). Immediately after mixing, a series of 1D ^{1}H-NMR spectra were recorded. A 2D [^{1}H, ^{1}H] TOCSY spectrum of the same sample was acquired after 7 hours at a mixing time of 65 ms.

2.20.2 Reaction with H_2O_2: 1D ^{1}H and 2D [^{1}H, ^{1}H] TOCSY spectroscopy

Zn_6MT4a or Zn_6MT4b samples (250 µM, NMR buffer, pH 7.3) were mixed with H_2O_2 (4.25 mM, 1:1 with respect to [Sulfur]). 1D ^{1}H NMR spectra were recorded immediately after mixing. Also, after 10 hours, a 2D [^{1}H, ^{1}H] TOCSY spectrum was acquired.

2.20.3 Reaction with DTNB: 1D ^{1}H and 2D [^{1}H, ^{1}H] TOCSY spectroscopy

Zn_6MT4a or Zn_6MT4b (298 µM, NMR buffer, pH 7.33) was mixed with DTNB (5.066 mM, 1:1 with respect to [Sulfur]). 1D ^{1}H NMR spectra were recorded immediately after mixing. Also, after 7 hours, a 2D [^{1}H, ^{1}H] TOCSY spectrum was acquired.

2.21 Homology models

Structural models were generated using MODELLER (Šali, Potterton et al. 1995). Solution structure of wheat E_C (PDB 2L62 and 2KAK) used as templetes. Side chain conformation of MODELLER-generated models were optimised using the program Scwrl4 (Bower, Cohen et al. 1997), however, side chain conformation of metal coordinated residues (Cys and His) were not optimised. Finally, metal ion-Zn was incorporated into the Scwrl4 optimised model using the program MOE. Structure was energy-minimised using AMBER PARM99 force field. Generated models were validated using the WHATIF server (Vriend 1990).

Chapter 3

Expression, purification and identification of MT4a and MT4b

3.1 Introduction

Since their discovery in 1980 (Rauser and Curvetto, 1980), plant MTs have been less well-studied proteins within the MT super-family compared to their mammalian counterparts. Among the 4 types of plant MTs, one representative from the type 4 plant MTs, E_C (early cysteine rich protein) from the monocotyledonous plant wheat, discovered by the group of Byron Lane, has been extensively studied in the Blindauer group and the group of Professor Dr. Eva Freisinger (Zürich University, Switzerland). Hence, for this protein, a partial structure and metal binding dynamics studies are well established. This thesis aims to extend our knowledge towards structure, properties and function of type 4 MTs from a model dicotyledonous plant, *Arabidopsis thaliana.*

Arabidopsis thaliana has two type 4 MT isoforms - MT4a and MT4b. Plasmids containing the genes for MT4a and MT4b were kindly donated by Professor Peter Goldsborough (Purdue University, USA). Throughout this work, proteins that were used for structural and metal binding studies have been recombinantly synthesised in *E. coli* using these two plasmids.

This chapter discusses recombinant protein expression, purification and identification by using biomolecular methods and bioanalytical techniques including SDS-PAGE and chromatography. Initial studies on metal-protein stoichiometry, metal speciation by mass spectrometry and also in brief proteins folding as revealed by NMR spectroscopy are also presented.

3.2 Protein expression

Plasmids containing genes of MT4a or MT4b were recombinantly expressed in *E. coli*. *E. coli* was selected as a host because its ribosomal components suitably act as a catalyst for recombinant protein expression and make protein expression simple (Sørensen and Mortensen, 2005). Moreover, its genetics is well-known and it is inexpensive. Like other host cells, *E. coli* uses an array of 61 codons. Among the codons, those that occur frequently are known as major codons, and those that occur less frequently are called minor or rare codon (Kane, 1995). Codon usage of different species is not the same, thus heterologous genes that have codons which are substantially different from *E. coli*'s codon usage create problems for high quantity protein expression when transformed into *E. coli* (Kurland and Gallant, 1996). Arginine codons AGG and AGA, which are major codons in some eukaryotic organisms, but are rare in *E. coli*, have a profound effect on translation efficiency when cloned into *E. coli* (Rosenberg et al., 1993). Even a single rare codon has a pronounced effect on protein expression (Kane 1995). Methods are available to overcome this codon bias problem – site-directed mutagenesis of the desired gene sequence, use synthetic gene to replaced rare codons with major

codons and co-transformation with genes encoding for tRNAs for rare codons. The latter method is commercially available and is less time-consuming. Therefore in this work, the competent cell strain Rosetta 2(DE3) pLysS (Novagen) was used as a host for protein expression. Rosetta cells contain pRARE plasmids encoding for rare codon tRNAs, and this results in elevated eukaryotic protein expression from genes that are cloned into pET vectors and are inducible by isopropyl β-D-1thiogalactopyranoside (IPTG).

At the time of induction, the cultures were also supplemented with $ZnSO_4$ (0.5 mM) to stabilize nascent MTs and to protect from oxidation and proteolytic digestion (Wang et al., 1994).

3.3 Expression of MT4a and MT4b

Pre and post induction protein expression levels of MT4a and MT4b were checked by silver-stained SDS-PAGE. Expression levels of MT4b are shown in Figure 3.1. It is apparent from Figure 3.1 that new proteins bands appeared at around ~50 kDa and ~ 20kDa after induction. Because the cells are normalised to the same OD_{600}, it is thus obvious that gradual increase in the intensity of specific protein bands corresponds to higher protein quantity. 50 kDa is quite a high molecular weight for both protein isoforms (8.3 and 8.5 kDa, respectively), but erratic migration of MTs is common (Meloni et al., 2005) A similar trend was also observed for earthworm MTs (Kowald, 2012), for which a band at around ~150 kDa was observed. The expression conditions used for MT4a and MT4b were previously successfully employed for other MTs in the Blindauer group.

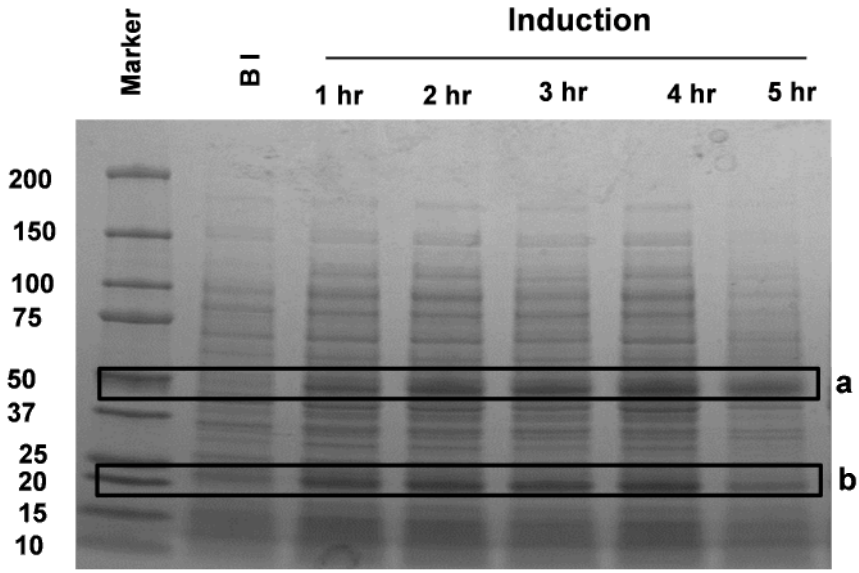

Figure 3.1 Protein expressions as a function of induction time. MT4b were expressed in *E. coli* and induced by IPTG (0.5 mM) and supplemented with $ZnSO_4$ (0.5 mM), 37 °C, 5 hr, 180 rpm). Pre and post induction protein expression is shown in the 12-15% SDS-PAGE. The first lane corresponds to the molecular weight marker, BI = Before induction, 1hr, 2hr, 3hr, 4hr and 5hr = hours post induction. Each sample was normalised to an OD_{600} of 0.2. An increase of protein bands at ~50kD and ~20kDa was observed.

Without further optimisation, the condition was used for MT4a and MT4b expressions as a very similar expression pattern was observed for both the isoforms. However, as at 5 hr the protein band intensities were decreased, the post induction time was maintained at 4 hr for the rest of the expressions throughout this project.

3.4 Protein purification: Chemical precipitation and chromatography

To purify the proteins, harvested cell pellets were sonicated and cell lysates were separated from cell debris by centrifugation. During the sonication 1 mM $ZnSO_4$

was supplemented to the sonication buffer to avoid any zinc loss due to sonication. To get proteins from cell lysates in pure form, two purification procedures have been employed - chemical precipitation followed by chromatographic methods. For chromatographic method two techniques were used, either gel filtration only, or gel filtration followed by anion exchange chromatography.

In the chemical precipitation method, a mixture of ethanol and chloroform (100:8) was used to fractionally precipitate proteins. Addition of the organic mixture to the protein solution essentially reduces the dielectric constant and hence lowers protein solubility (Van Oss, 1989) resulting in protein precipitation. The advantage of this method is not only the removal of other cytosolic components and proteins, but also it helps concentrating the desired protein. Precipitated MT can be readily re-solubilised in aqueous buffer, as shown for many other MTs purified in the Blindauer group, particularly bacterial SmtA, earthworm MTs and wheat E_C. Hence, the chemical precipitation method was optimised for MT4a and MT4b. In brief, initially 0.5 volumes (1 volume = total supernatant (cell lysate) volume; typically 8-10 mL) ethanol: chloroform mixture was used to precipitate a fraction of proteins from cell supernatants, subsequently the mixture was added up to 4 volumes. The precipitated fractions (4 vol) were re-solubilised into ammonium bicarbonate buffer for chromatographic purification. The ammonium bicarbonate buffer was used because this buffer is suitable for further protein biophysical studies using mass spectrometry. Silver-stained SDS-PAGE of the re-solubilised protein fractions of different chemical fractions are shown in Figure 3.2. Most of the proteins were precipitated at 2 vol of ethanol: chloroform mixture

as a very intense band at around 50 kDa was observed. However, lower molecular weight bands were also observed. Thus for further chemical precipitation process, the initial 0.5 vol precipitate was discarded and the remaining proteins pellets were re-solubilised into ammonium bicarbonate buffer (20 mM, pH ~7.8) for MT4a and MT4b. The re-solubilised proteins were purified by chromatography.

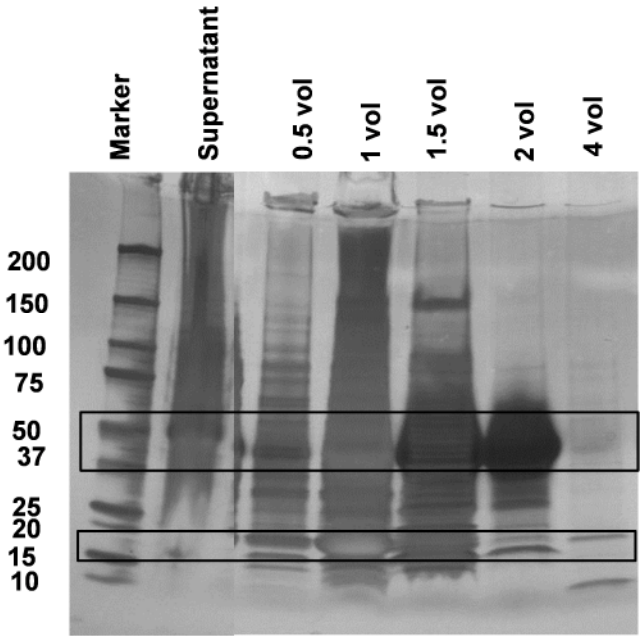

Figure 3.2 Optimization of chemical precipitation for MT4b by silver-stained SDS-PAGE (12-15%). The first lane corresponds to the molecular weight marker, Supernatant = 8 mL, 0.5 vol = 4 mL 100:8 ethanol (E):chloroform (C) mixture. 1 vol = 8 mL (E:C), 1.5 vol = 12 mL (E:C), 2 vol = 16 mL (E:C), 4 vol = 32 mL (E:C). Most of the desired protein was found to precipitate at 2 vol of E:C as a protein band with high intensity was observed at ~50kD, however, ~18kDa was also observed.

Gel filtration chromatography of proteins was performed on a Fast Protein Liquid Chromatography system mounted with a 120 mL bed volume gel filtration column (Superdex: dextran cross linked agarose). The protein elution was achieved using ammonium bicarbonate buffer (20 mM, pH ~7.8).

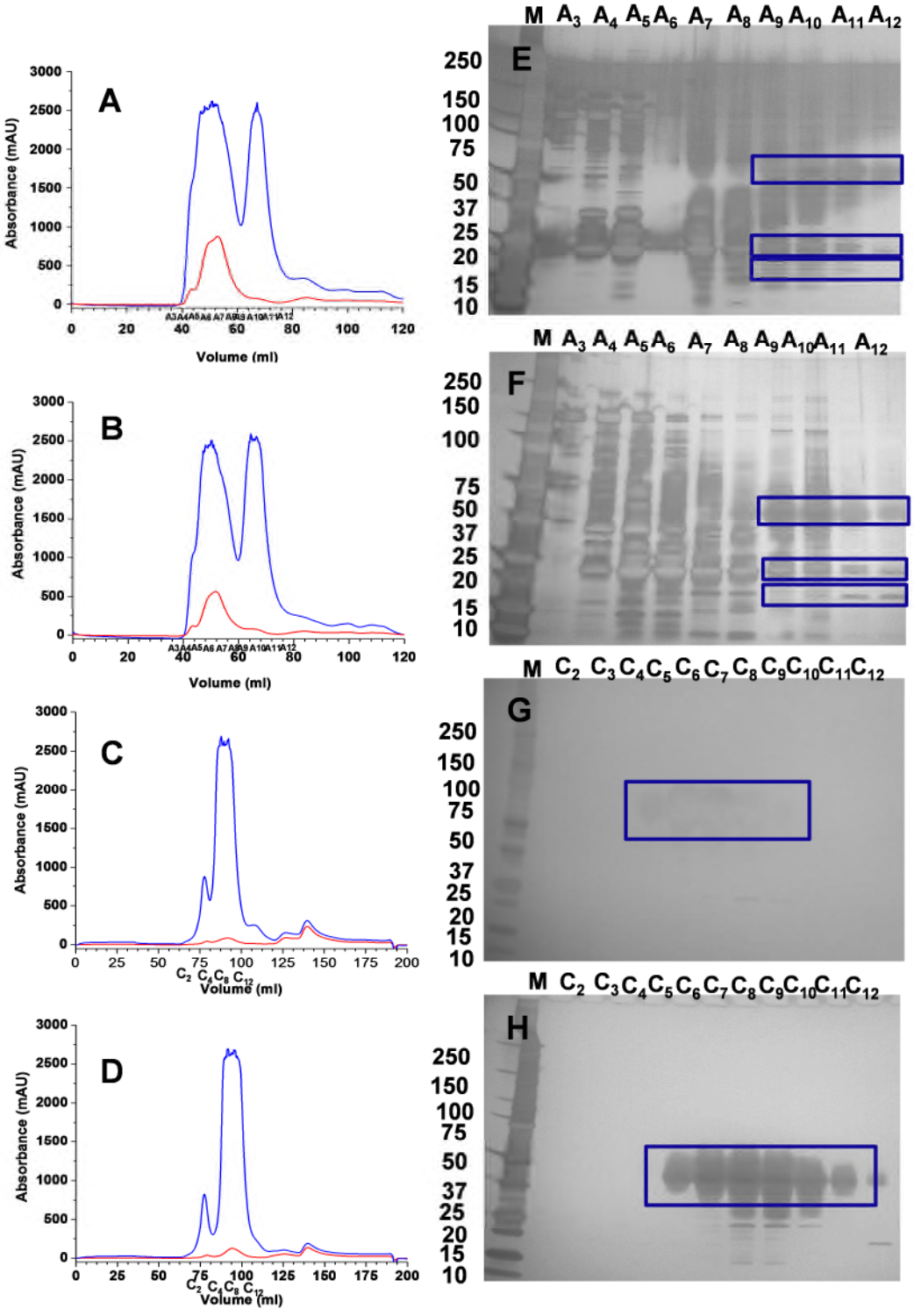

Figure 3.3 Chromatograms and silver-stained SDS-PAGE of MT4a and MT4b. Protein elution was monitored at 220 nm (blue) and 280 nm (red). Gel filtration after chemical precipitation of MT4a (A) and MT4b (B). Anion exchange chromatograms of selected gel filtration fractions of MT4a (C) and MT4b (B). SDS-PAGE gels of selected gel filtration and anion exchange chromatographic fractions from purification of MT4a and MT4b. Gel filtration (E) and anion exchange (G) of MT4a. Gel filtration (F) and anion exchange (H) of MT4b.

This method yielded two relatively well-resolved peaks (A4-A8) and (A9-A12) as shown in Figure 3.3 (A, B) for MT4a and MT4b respectively. Silver-stained SDS-PAGE of selected gel filtration fractions indicated some resemblances of proteins bands for (A9-A12) with previously identified protein bands observed in SDS-PAGE in Figure 3.1 and 3.2, particularly the band at ~50 kDa. However, these fractions (A9-12) also exhibited low absorption at 280 nm suggesting the presence of protein(s) with few aromatic groups. As both MT4a and MT4b have only two aromatic residues (histidines) and as very similar high molecular weight bands along with low molecular weight proteins bands were observed in SDS-PAGE during protein expression, chemical precipitation and also gel filtration fractions (A9-A12), it was thus highly likely that these (A9-A12) fractions contained MT4a and MT4b. Another purification process was achieved by anion exchange chromatography using gradient elution with buffer A (20 mM NH_4HCO_3, pH ~7.60) and buffer B (20 mM NH_4HCO_3, 1 M NaCl, pH ~7.60). The pH of the buffer was selected to be at least one unit higher than the protein's isoelectric point (pI), in case of MT4a and MT4b, the theoretical pI value is 6.65 and 5.49, respectively. Chromatograms and SDS-PAGE of selective anion exchange fractions are shown in Figure 3.3 (C, D, G and H).

In the anion exchange chromatograms, two peaks were observed between 70-120 mL, corresponding to fractions C2 to C12. SDS-PAGE of these fractions suggested pure protein to be present in fractions C5 to C12. Only faint bands were observed for MT4a, perhaps because of too little time allowed during silver stain developments of SDS-PAGE gel. Again, proteins migrated at high molecular weight, as previously observed, suggesting that the high molecular weight bands

correspond to MT4a and MT4b. In Native PAGE, both MT4a and MT4b also migrated at apparent high molecular weight. There could be two possible reasons for this abnormal behaviour, oxidative formation of intermolecular disulfide bonds (Mounaji et al., 2002) and the compact cluster structure (Pitt-Rivers and Impiombato, 1968) which causes lower charge-to-protein mass ratio and reduced protein mobility.

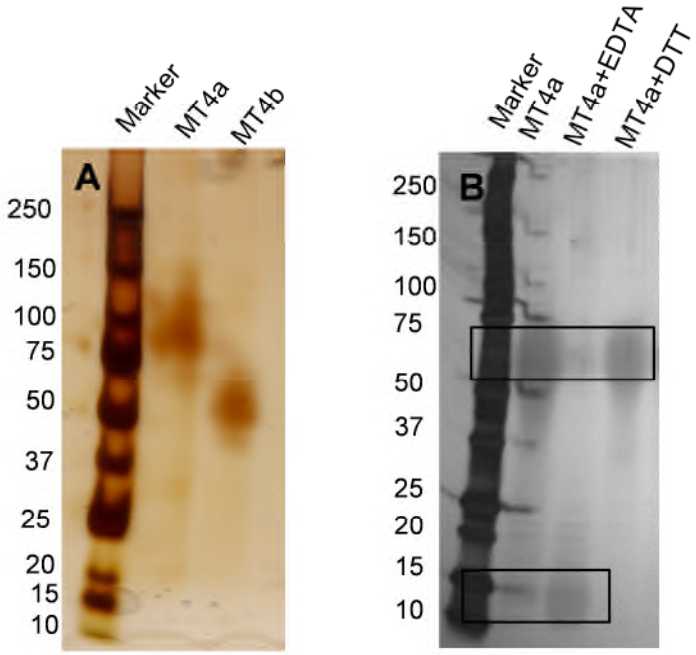

Figure 3.4 Native-PAGE and SDS-PAGE of MT4a and MT4b. (A) Native-PAGE suggesting high molecular weight band for MT4a and MT4b. (B) EDTA and DTT treated MT4a reveals that oxidative polymerization is not the cause, but that rather the resilience of the metal-cluster against conventional SDS-denaturing conditions (LaemmLi buffer and heat) is responsible for the low electrophoretic mobility of MTs.

However, the presence of β-mercaptoethanol in SDS-PAGE makes the persistence of disulfide bonds highly unlikely. To investigate whether the incomplete destruction of the metal-sulfur clusters by the denaturing conditions may account for the slow migration of the MTs, the proteins were treated with either the metal

chelator EDTA or the reducing agent DTT, and then were analysed by SDS-PAGE. EDTA-treated samples displayed a lower molecular weight band at ~12 kDa for MT4a. EDTA is expected to remove the metals from the protein, resulting in the destruction of the metal cluster and protein unfolding/denaturation. A similar result was observed for monobromobimane alkylated wheat E_C (Peroza and Freisinger, 2007). Oxidative polymerization through disulfide bond formation was ruled out as the DTT-treated samples ran very much similar to untreated samples. These experiments support the idea that sample preparation for SDS-PAGE leaves metal-sulfur clusters of MT4a and MT4b mostly intact, preventing their complete unfolding and adequate loading with SDS. This in turn accounts for their reduced mobility in SDS-PAGE,

Protein fractions were concentrated and average protein yields were recorded as 4 mg/l culture for both MT4a and MT4b as measured by Inductively Coupled Plasma-Optical Emission Spectroscopy (ICP-OES) and by Ellman's reagent. For further biophysical studies using UV-visible spectroscopy and mass spectrometry, proteins were collected only from gel filtration fractions A9-A11; those fractions essentially provide desired proteins and also the buffer used for gel filtration was "mass spectrometry-friendly", while further purification by anion exchange leads to unavoidable contamination with sodium to such an extent that even desalting by Sephadex G-25 gel filtration could not remove all salt adducts. For protein NMR studies, anion exchange was performed, as for NMR spectroscopy; the presence of salt is less of an issue.

3.5 Characterization

3.5.1 Mass spectrometry and ICP-OES

Mass spectrometry can be a valuable technique for investigating metalloproteins as it provides direct information about the proteins' identity and the nature and number of metal ions bound to them (Yu et al., 1993). In electrospray ionization mass spectrometry (ESI-MS), analytes in solution transfer into the gaseous state forming ions. Solvent compatibility and presence of other analytes in the solution thus play a significant role for getting a sensitive and well resolved mass spectrum (Iavarone et al., 2004). Taking these ESI-MS phenomena into consideration, purified proteins were desalted and buffer exchanged into 10 mM ammonium bicarbonate buffer when necessary. Desalting is necessary for removing any metal salts present in solution, as even very low concentrations of metal salt could form adducts with the protein, resulting in peak broadening (Loo, 2000). Ammonium bicarbonate buffer was used as its volatile nature helps desolvation and, importantly, it does usually not form adducts with analytes. To enhance sensitivity, 10% methanol was added prior to recording the mass spectra. The primary sequences of MT4a and MT4b as deposited in UniProt (accession code MT4a-F4ILY7 and MT4b-Q42377) consist of 84 and 85 amino acids, respectively, with molecular weights of 8290.2 and 8437.3 Da, respectively. The mass spectra of the apo proteins displayed in Figure 3.5 (G and H) show masses of 8159.0 for apoMT4a and 8306.3 for apoMT4b, which for both is nearly 131.2 Da deficient from the theoretical values. This indicates cleavage of the N-terminal methionine from the proteins. Cleavage of the N-terminal methionine is catalysed by methionyl-aminopeptidase (Bradshaw et al., 1998; Hirel et al., 1989).

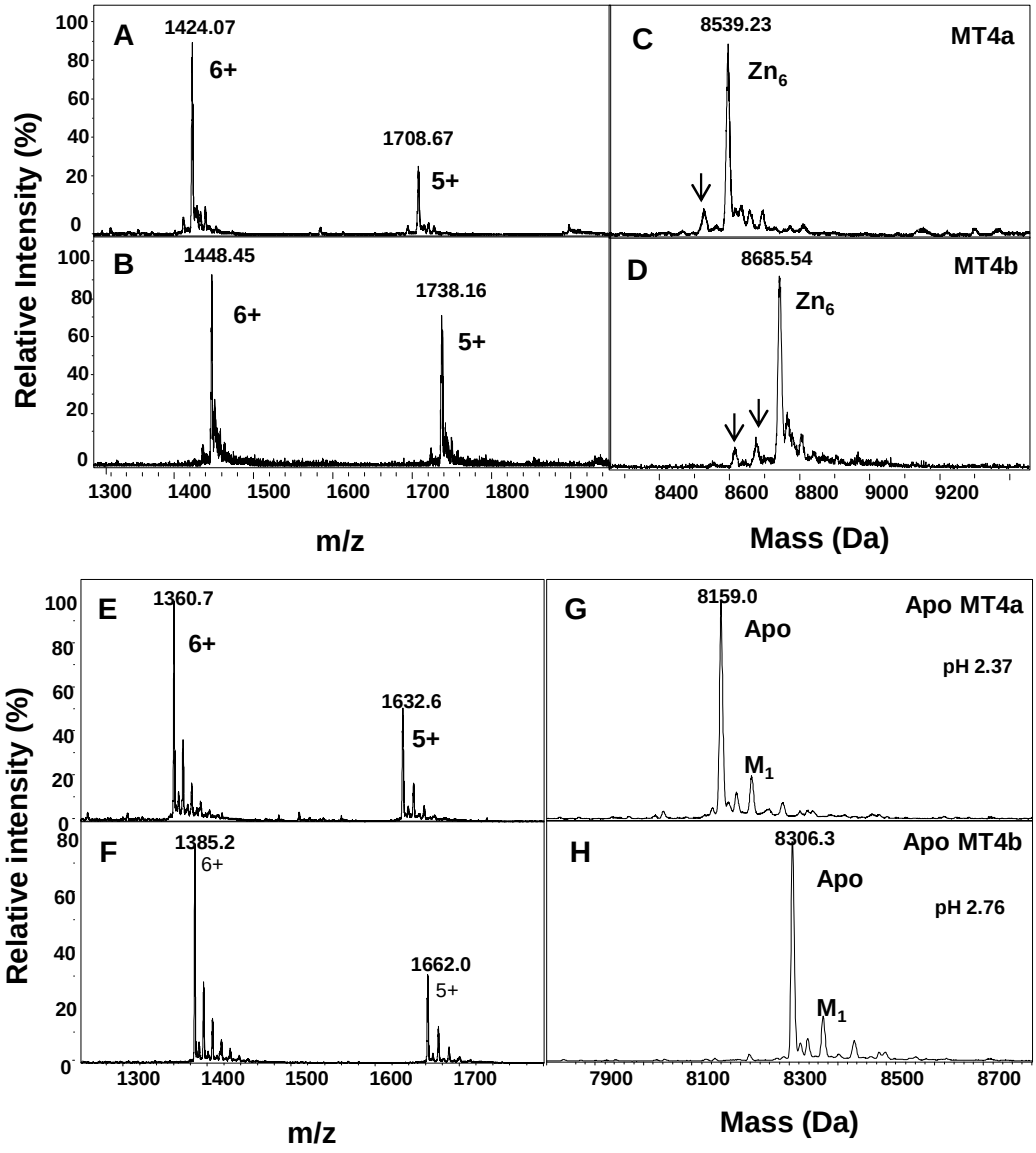

Figure 3.5 Mass spectra of MT4a and MT4b. Raw mass spectra of (A) Zn_6MT4a and (B) Zn_6 MT4b. Deconvoluted mass spectra (C) MT4a and (D) MT4b. Raw mass spectra of (E) apo-MT4a and (F) apo-MT4b. Deconvoluted mass spectra of 6+ charge states of (G) apo-MT4a and (H) apo-MT4b

Its catalytic activity depends on the nature and length of the amino acid following the methionine. If the second amino acid has a side-chain length of less that 4 Å, significant cleavage activity is expected. The smaller the side-chain, the better the reactivity and the highest cleavage activity was observed, hence activity follows the order Gly>Ala>Pro>Ser>Thr>Val>Cys>Asn>Asp>Leu>Ile. Both MT4a and

MT4b have Ala as second amino acids thus mass deficits of 131.2 Da suggests due to cleavage of N-terminal methionine (Met). Cleavage of the N-terminal Met had also been observed for E_C from wheat as isolated from the native host (Leszczyszyn et al., 2007).

The deconvoluted mass spectra of the holo forms of the proteins (Figure 3.5 C and D) reveal that both isoforms bind up to six zinc ions giving rise to mono charged molecular masses of 8539.2 Da for MT4a, very close to its theoretical value of 8539.07 Da and for MT4b 8685.5 Da with a theoretical mass of 8686.07 Da. However, there are also low abundance peaks of under-metallated species observed as shown by arrows in Figure 3.5 (C and D). Elemental analysis by ICP-OES indicated zinc-to-protein stoichiometries of 5.9±0.2 for MT4a and 6.0±0.2 for MT4b. Previously, the existence of under- or partially metallated species in mammalian MTs isolated from native tissues or cells has been demonstrated (Krężel and Maret, 2008; Petering et al., 2006). Recently Blindauer *et al.* hypothesised that the existence of under-metalled species in plant MTs may have a role to play against oxidative stress (Leszczyszyn et al., 2013).

3.5.2 Protein folding: 1D ^{1}H and 2D [^{1}H, ^{15}N] HSQC NMR spectroscopy

The expression and purification procedures developed in this work were suitable to obtain sufficient quantities of the proteins for protein NMR spectroscopic studies.

Like all protein NMR spectra, the 1D ^{1}H spectra displayed in Figure 3.6 have three distinct areas of peaks. One area comprises aliphatic side-chain protons in

the region of 0.3-3.8 ppm, a second set of CHα protons which resonate between chemical shifts of 3.0-4.5 ppm, and a third set includes backbone and side-chain amide (NH and NH_2) and aromatic protons, which resonate in the downfield region with chemical shifts between 6.5 and 10 ppm.

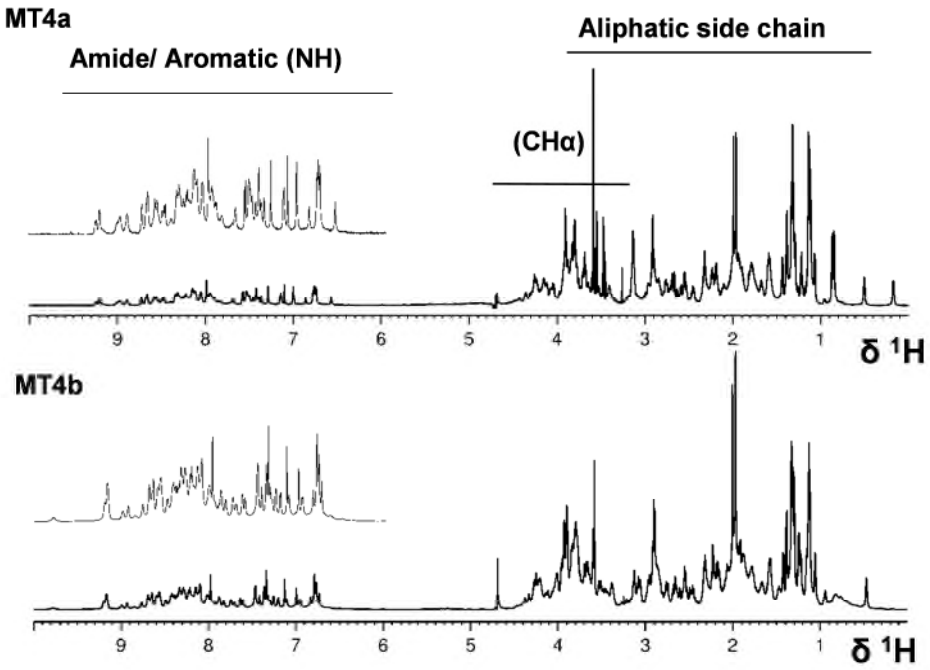

Figure 3.6 1D ^{1}H NMR spectra of MT4a and MT4b. Three distinct set of peaks observed. Inset shows magnifying section of finger print regions.

The 1D ^{1}H spectra are well-dispersed in both amide and aliphatic regions, indicative of well-folded protein structures (Page et al., 2005; Vasak et al., 1980). To establish foldedness and allow counting the number of resolved backbone NH peaks, 2D [^{1}H, ^{15}N] HSQC spectra of MT4a and MT4b were acquired and are displayed in Figure 3.7. Each peak in the spectrum represents the N-H crosspeak from one amino acid residue, with the exception of the side-chain amide crosspeaks from glutamine and asparagine shown in the boxes.

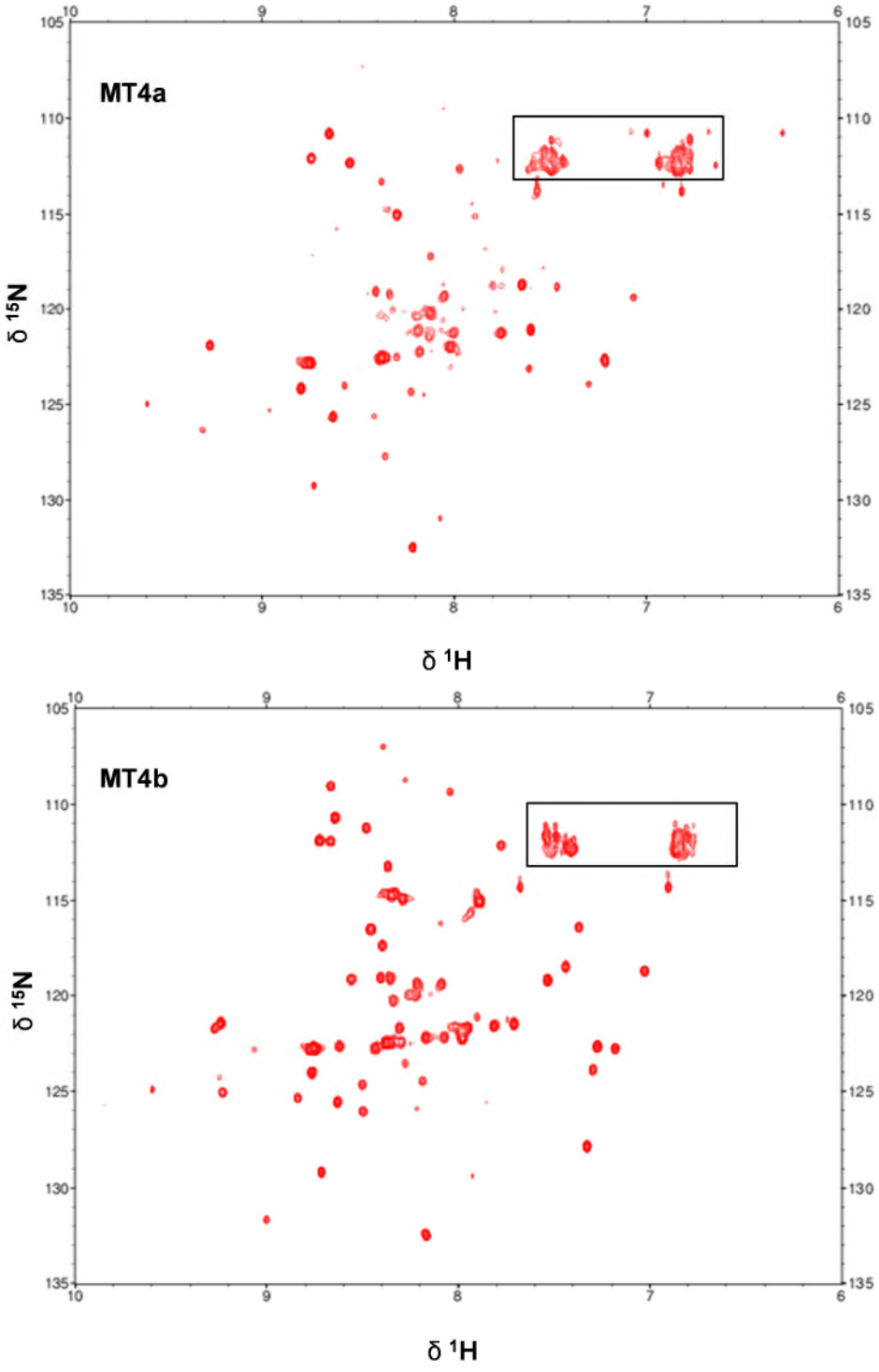

Figure 3.7 2D [^{1}H, ^{15}N] HSQC NMR spectra of MT4a and MT4b. Each peak represents one amino acid. Side chain NH_2 of asparagine and glutamate are shown in boxes. Out of 83 and 84 amino acids 68 and 69 NH crosspeaks were observed. Six prolines residues which have no NH groups did not appear in the spectra. Sample conditions were 251 (MT4a) and 267 (MT4b) µM uniformLy ^{15}N labelled protein, 50 mM Tris-D_{11}, 10 % D_2O, 50 mM NaCl, pH 7.4; spectra were recorded on an NMR spectrometer operating at 700.24 MHz for ^{1}H.

MT4a and MT4b consists of 83 and 84 amino acids residues respectively provided terminal methionine was cleaved from both isoforms. Among the 83 and 84 residues 68 and 69 NH crosspeaks were observed in the spectra. Because proline has no backbone amide proton, Pro residues do not appear in the [^{1}H, ^{15}N] HSQC spectrum. The number of NH crosspeaks and the good dispersion of NH resonances in both ^{15}N and ^{1}H dimensions suggest that the proteins were in well-folded form, and should be amenable to NMR structural studies.

In summary, two type 4 MT isoforms from the dicotyledonous plant *Arabidopsis thaliana* have been recombinantly expressed in *E. coli.* SDS-PAGE revealed that proteins migrated unexpectedly slowly through the gel, giving high molecular weight bands at around ~50 kDa. Native-PAGE also exhibited a very much similar result. A further investigation using a metal chelator and a reducing agent indicated that incomplete destruction of the metal clusters by the SDS sample buffer is responsible for high molecular weight band formation in SDS-PAGE. Both proteins were purified using chemical precipitation and chromatographic methods. Purified proteins were found to lack the N-terminal methionine, and to bind six zinc ions, as confirmed by mass spectrometry and ICP-OES. 1D ^{1}H and 2D [^{1}H, ^{15}N] HSQC NMR spectroscopy revealed well-folded proteins.

Chapter 4

Towards structure and metal-cluster topology

4.1 Introduction

Metallothioneins are able to bind a range of metal ions including divalent Zn^{2+} or Cd^{2+} and monovalent Cu^{+}. However, when they bind metal ions they form clusters. Metal ensembles in metallothioneins provide structural rigidity and ensure proper protein folding. *A. thaliana* MT4a and MT4b each bind six zinc ions. It is important to understand how these six zinc ions are organised within the proteins to create 3D protein folding and to ascertain which role they play in structure-function relationships. To understand the effect of divalent metals (Zn^{2+} and Cd^{2+}) on protein folding and their consequences on metal-cluster topology, data have been acquired using solution NMR spectroscopy. A variety of multinuclear (^{1}H, ^{15}N, ^{13}C) and multidimensional (2D and 3D) NMR spectroscopy experiments have been performed to get information on protein backbone and side chains. Furthermore, 1D and 2D ^{15}N and ^{111}Cd NMR spectroscopy in conjunction with UV-Vis and mass spectrometry has been employed to study the effects of zinc replacement by cadmium on protein folding. The ultimate goal was to determine the metal-cluster topology in the two domains.

4.2 Sequential assignment of backbone and side chain resonances

MT4a and MT4b have 84 and 85 amino acids, respectively, in their primary protein sequences. However, as it was observed from mass spectrometry that the initial methionines from both isoforms were cleaved during protein synthesis, for numbering, the N-terminal alanine was considered as first residue in both cases. The two isoforms share 84% sequence identity and both contain 17 cysteines and 2 histidines with few dissimilarities in amino acids as shown in red in Figure 4.1. Most of the dissimilarities are observed in the cysteine-free spacer regions.

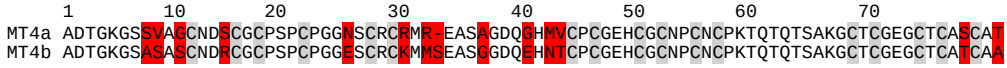

Figure 4.1 Protein sequence alignment of MT4a and MT4b. Red color highlights dissimilarities in amino acids between the sequences. Number considers alanine (A) as position 1, since the terminal methionine is cleaved during purification.

.

The data required for backbone and side-chain assignment were acquired for both isoforms; however, due to the large volume of data required to be analysed for the full assignment of both the isoforms which would have required a large amount of time, focus was given to the assignment of MT4b, in the hope that it would help assignment of MT4a, given the high sequence similarity (84%). Multidimensional (2D, 3D) and multinuclear (^{1}H, ^{15}N, ^{13}C) NMR spectroscopy has been employed to acquire data for backbone and side-chain assignments.

4.2.1 Side chain and backbone assignment: 2D NMR Spectroscopy

Since MT4a and MT4b are small proteins (<10kDa), initially 2D Total Correlation Spectroscopy (TOCSY) and Nuclear Overhauser Effect Spectroscopy

(NOESY) were considered to get information for protein backbone and side chain assignment. For assignment of MT4b, initially, unlabelled 2D TOCSY and NOESY spectra were acquired. The TOCSY spectrum provides information of intra-residue crosspeaks and the NOESY gives through-space connectivity of both intra- and inter-residue proton resonances within 5Å. Thus, overlay of these two spectra eventually helps walking through intra- and inter-residue crosspeaks in a sequential way to get information on backbone and side-chain resonances from one amino acid to the next and so on and so forth. The idea behind this technique relies on defining spin systems of amino acids. Depending on the nature of their crosspeak patterns, all 4 types of spin system (J, U, A/T and G) (Dell et al., 1975) were identified in MT4b. Among 20 types of amino acids, only 14 types constitute the 84 residues of MT4b. Among these 84 residues, 34 are type J (N, D, C, H and S) for which characteristic Hβ resonances are observed between ~2.5-4 ppm. For U-type (K, R, M, Q, P and E), Hβ, Hγ, Hδ and/or Hε resonances appear around ~2.2-1.0 ppm. MT4b has 23 U-type amino acids. 16 amino acids belong to A/T type for which Hβ or Hγ resonances, respectively, are observed at around 2-1 ppm (with threonine having a β resonance around 4-5 ppm); finally, glycines have characteristic patterns for their two α protons between about 3.5 and 4.5 ppm. The TOCSY and NOESY spectra of MT4b were recorded at 25 °C, as temperature dependent 1D ^{1}H NMR spectra suggested well defined peak dispersion at this temperature. A portion of 2D TOCSY and NOESY overlay spectra is shown in Figure 4.2. In the Figure 4.2, a stretch of 4 amino acids are assigned with a pattern of spin systems of TJGU. As this pattern occurs only once in the sequence, the sequence identified for TJGU corresponds to Thr72, Cys73, Gly74 and Glu75. In

this way it was possible to assign many of the backbone and side chain resonances of MT4b but ambiguity remained for assigning peaks of very close ^{1}H chemical shifts due to peak overlap as evident from Figure 4.2, in the region around 8-8.5 ppm for instance.

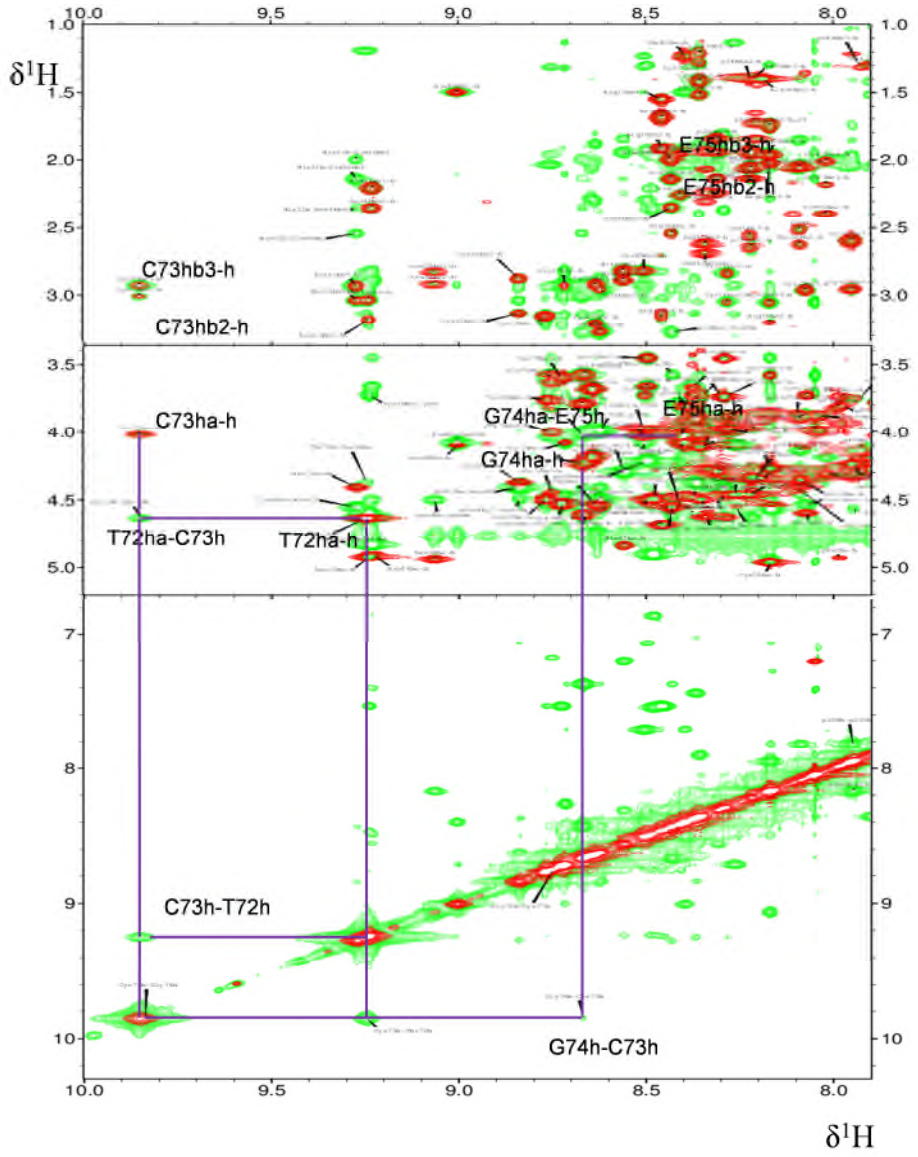

Figure 4.2 Overlaid 2D [^{1}H, ^{1}H] TOCSY (red) and 2D [^{1}H, ^{1}H] NOESY (green) spectra for MT4b. Sequential assignment of a stretch of 4 spin systems with the sequence TJGU, identified as Thr72, Cys73, Gly74 and Glu75, is indicated. Spectra were recorded on the same protein samples (1.2 mM, 50 mM Tris-D_{11}, 10 % D_2O, 50 mM NaCl, pH 7.4) at an operating frequency of 700.24 MHz for ^{1}H using a TCI cryoprobe at 25°C.

To overcome this obstacle, the protein was expressed in isotope (^{15}N, ^{13}C) enriched medium and labelled protein samples were prepared for 3D NMR spectroscopy.

4.2.2 Assignment of [^{1}H, ^{15}N] HSQC spectrum

A [^{1}H, ^{15}N] HSQC spectrum generates crosspeaks for each backbone nitrogen-hydrogen pair, thus helps distinguishing individual amino acids, even with very similar chemical shifts for their amide protons. Moreover, the side-chain amide N-H crosspeaks from Asn and Gln appear on the spectrum. The ^{15}N HSQC spectrum for MT4b has been assigned as shown in Figure 4.3. The number of peaks and their wide dispersion suggested well-folded proteins for both isoforms. Among the 84 (N-terminal methionine cleaved) amino acids, 65 amino acids were assigned for MT4b, which accounted for 75% of sequence coverage. MT4b has 6 prolines, and due to the absence of a backbone amide, they do not appear in the ^{15}N HSQC spectrum. With the help of 2D TOCSY and NOESY and the HNCOCA and HNCA spectra, it was possible to assign all 6 prolines, thus giving a total of 71 assigned amino acids, i.e. 84.5% complete sequential assignment of MT4b was achieved. The first 10 amino acids residues have not been assigned perhaps they are likely to be unstructured and flexible.

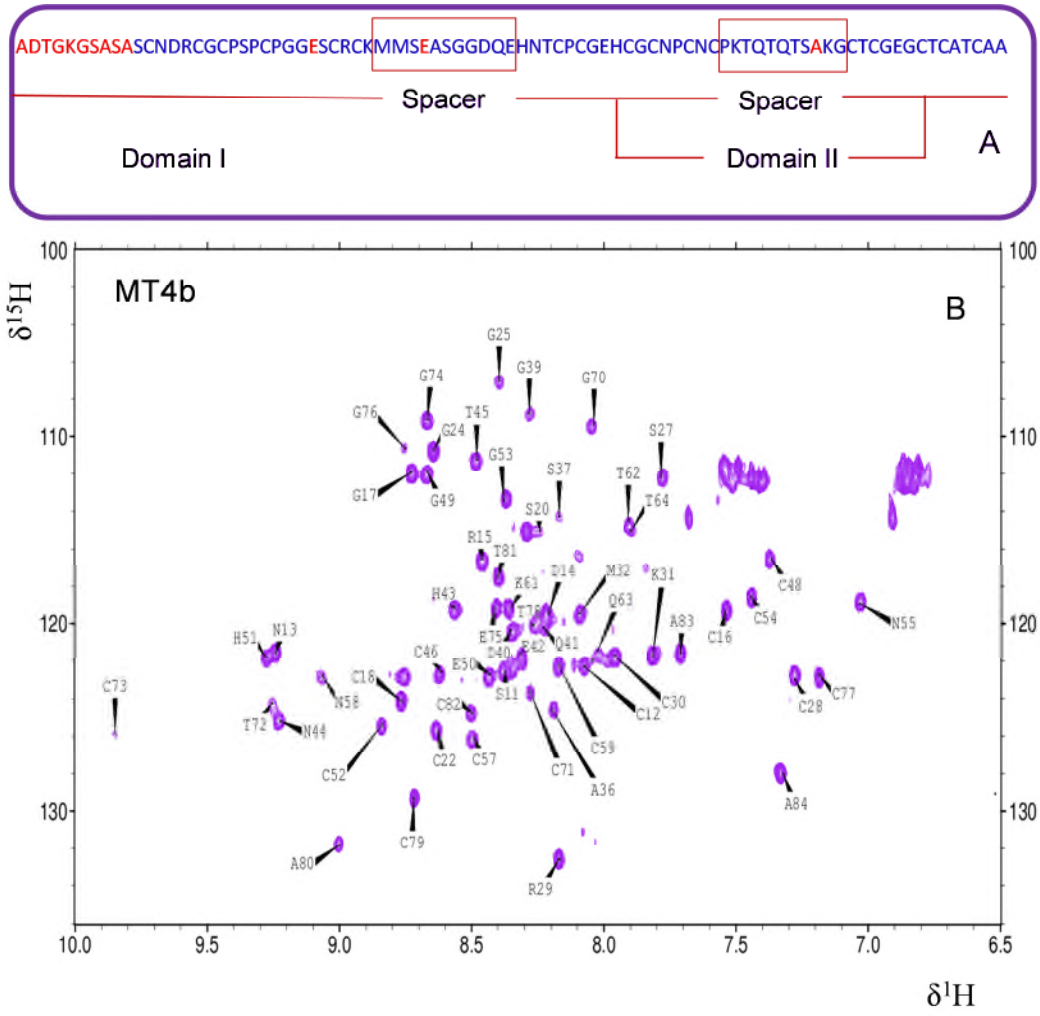

Figure 4.3 Assignment of [^{1}H, ^{15}N] HSQC spectra of MT4b. (A) Schematic sequence coverage diagram (B) [^{1}H, ^{15}N] HSQC spectrum of MT4b. Out of 84 residues, 7 are not expected to be observed in this spectrum (N-terminal A and 6 prolines; no backbone amide). Of the remaining 77, 65 residues were assigned, providing 84.5% complete sequential assignment. Most non-assigned residues are in the Cys-free N-terminal region.

Importantly, however, all the metal binding cysteine and histidine residues were assigned; thus, in principle, this may provide sufficient information to study the metal-ligand connectivities and cluster dynamics (Chapter 5 and 6).

4.2.3 Side chain and backbone assignment: 3D NMR spectroscopy

3D NMR spectroscopy helps getting better resolution and well-defined peak visualization as it introduces the three frequencies to produce three dimensional spectra. As in 3D NMR spectroscopy, resonance from an amino acid occurs in three different frequencies thus helps distinguishing overlapped peaks which would otherwise appear at very close chemical shifts in one frequency. There are number of 3D experiments useful for unambiguous assignment of amino acids backbone and side chains resonances. For backbone assignment, a set of two experiments were performed – HNCA and HN(CO)CA; a schematic diagram is shown in Figure 4.4 (E and F). In an HNCA experiment, magnetization transfer occurs from $^{1}H_{N}$ to ^{15}N and then to vicinal $^{13}C\alpha$ and $^{13}C\alpha$-1, and finally returns to ^{15}N and $^{1}H_{N}$. Thus, an HNCA experiment produces two crosspeaks, where the amide proton is coupled to the intra-residue Cα as well as the preceding Cα-1, whereas in an HN(CO)CA experiment, magnetization is passed through $^{1}H_{N}$ to ^{15}N then through ^{13}CO to $^{13}C\alpha-1$ and finally evolves in $^{1}H_{N}$ and ^{15}N. HN(CO)CA generates only one peak of NH to the inter-residue Cα-1. Thus, an overlay of these two spectra provides a means to go through the backbone from one amino acid to the next one, as shown in Figure 4.5 (A).

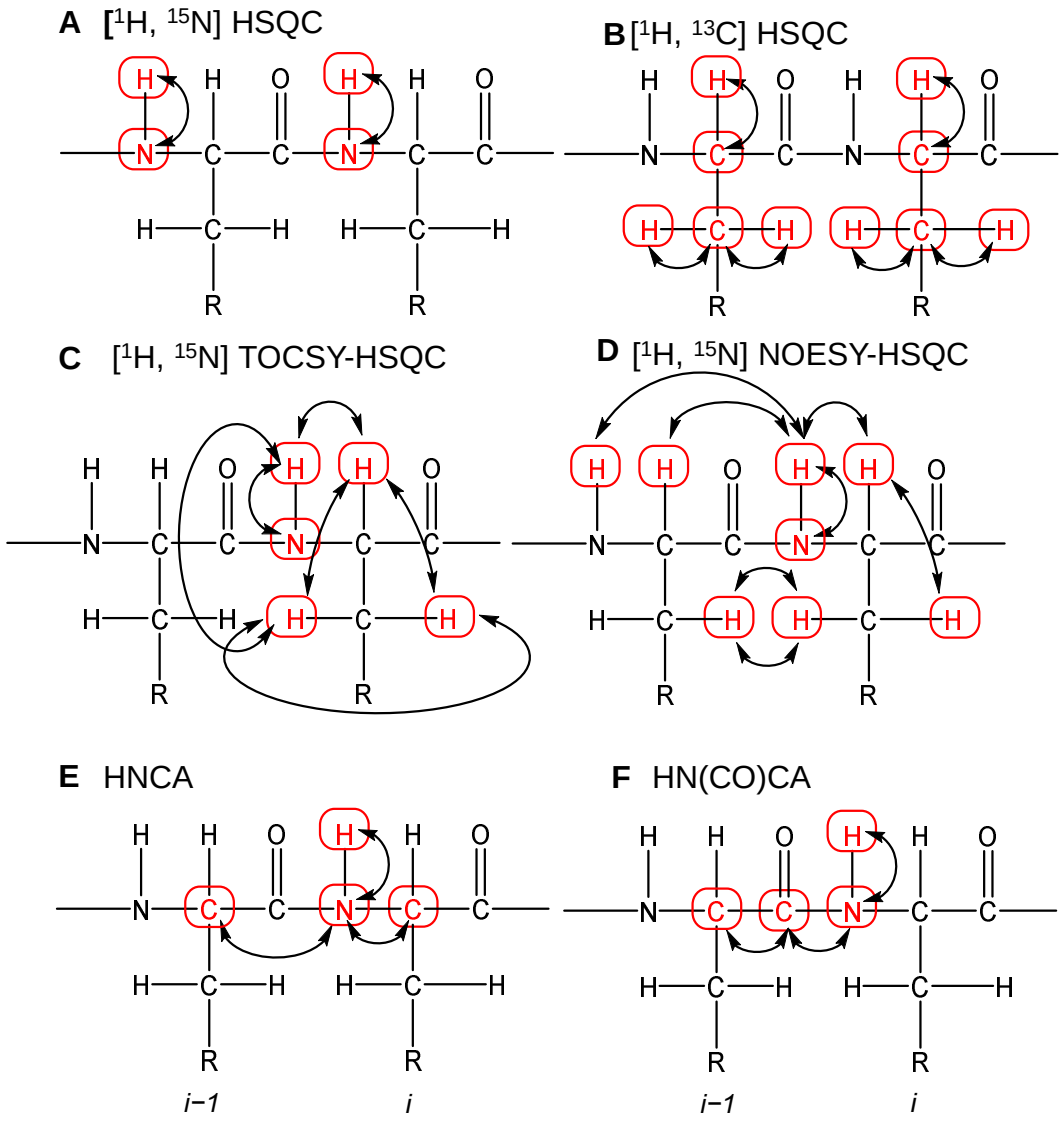

Figure 4.4 Schematic diagrams of different NMR spectroscopic techniques. Magnetization transfer mechanism (A) [^{1}H, ^{15}N] HSQC, (B) [^{1}H, ^{13}C] HSQC, (C) [^{1}H, ^{15}N] TOCSY-HSQC, (D) [^{1}H, ^{15}N] NOESY-HSQC, (E) HNCA and (F) HN(CO)CA. Figures are adapted from Protein NMR: A practical guide (www.protein-nmr.org.uk)

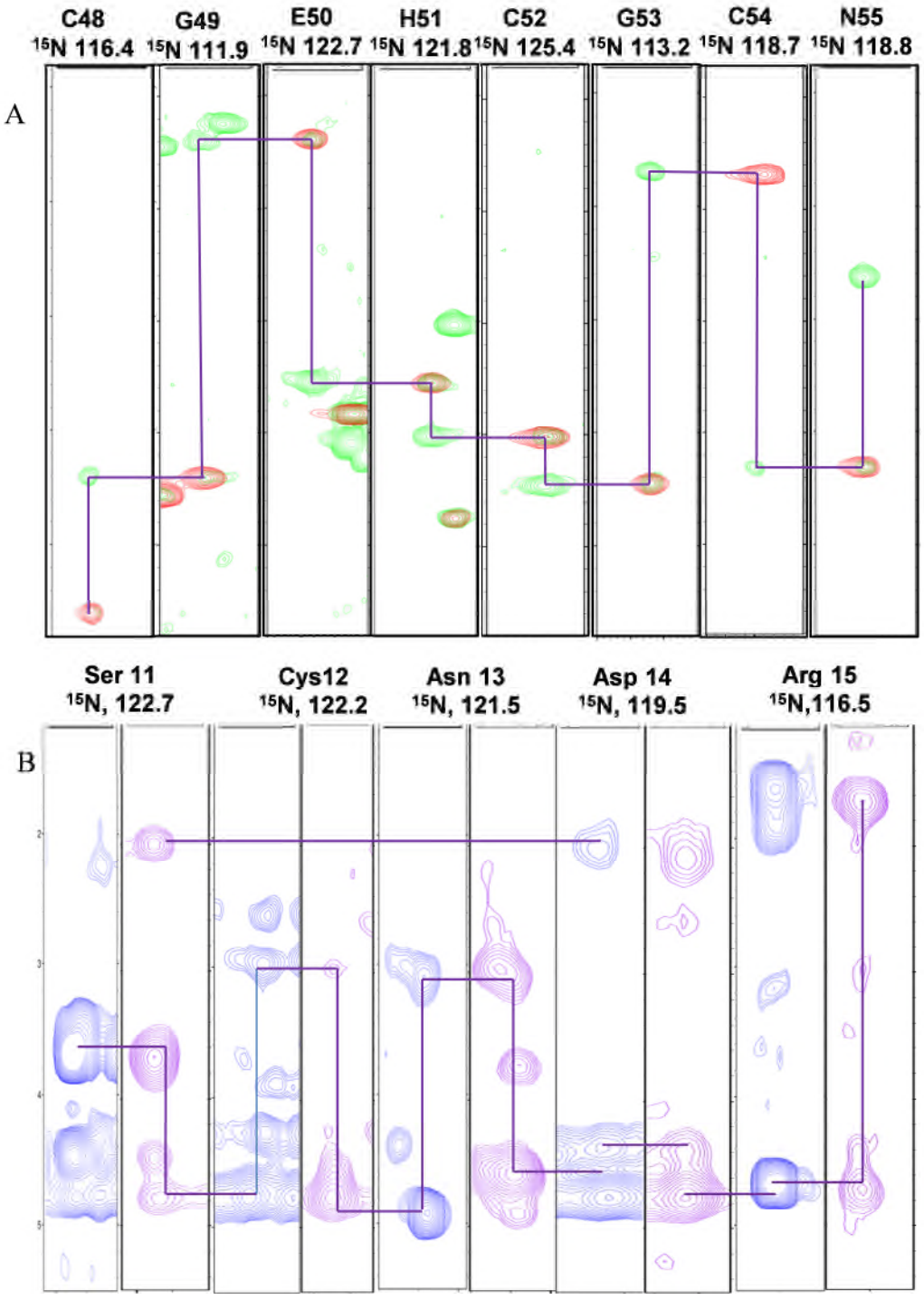

Figure 4.5 Sequential assignments of 3D spectra of MT4b. A. Overlay spectra of HNCA (green) and HNCOCA (red). HNCA spectrum generates two peaks – the intra residual Cα and preceding residue of Cα-1 whilst HNCOCA produces Cα-1, thus starting from Cys48 helps assignment of eight residues up to Asn55. B. Assignment of five residues from Ser11 to Arg15 with the help of 3D HSQC-TOCSY (Blue) and 3D HSQC-NOESY (Purple). A homogenously labelled (^{13}C and ^{15}N) protein sample (~500 µM, 50 mM Tris-D_{11}, 10 % D_2O, 50 mM NaCl, pH 7.4) at an operating frequency of 700.24 MHz for ^{1}H using a TCI cryoprobe at 25 °C was used for these experiments.

As 2D NMR spectra already allowed assigning some residues unambiguously, taking that advantage, HNCA and HNCOCA spectra helped assigning residues starting with Cys48 to Asn55. These two experiments along with the aid of a [^{1}H, ^{13}C] HSQC spectrum helped assigning proline residues which due to the absence of a backbone amide H were otherwise difficult to detect in unlabelled 2D ^{1}H experiments. These experiments were indispensable for unambiguous assignment. ^{15}N-edited 3D TOCSY-HSQC and NOESY-HSQC experiments were performed for side-chain assignment and for assisting with backbone sequential assignment. These two experiments are similar to 2D experiments, only a third dimension (^{15}N) is added to the former two. In 3D TOCSY-HSQC magnetisation is transferred between ^{1}H and $^{1}H_N$ then to ^{15}N and then again to ^{1}H. For NOESY-HSQC magnetization is transfer to all ^{1}H through NOE then transfer to neighbour ^{15}N and again to ^{1}H. As the ^{15}N dimension is added and ^{15}N has higher chemical shift dispersion (ca. 35 ppm), overlapped peaks can be assigned with less ambiguity. A sequential assignment of a 5-amino-acid stretch starting with Ser11 to Arg15 is shown in Figure 4.5 (B). These two experiments were used to resolve overlapping spin systems and also to assign side-chain proton resonances.

4.3 Zinc coordination to histidines: Identification of mononuclear zinc binding site

The coordination of histidines to zinc in MTs was first observed in bacterial SmtA where two Cys_3His sites form part of a $Zn_4Cys_9His_2$cluster (Blindauer et al., 2001). In type 4 plant MTs, two histidine residues were found to be conserved

(Leszczyszyn et al., 2007). Previously, in wheat E_C it has been demonstrated that both histidine residues, along with two cysteines, coordinate a single zinc to form a mononuclear $ZnHis_2Cys_2$ site (Leszczyszyn et al., 2010). MT4b has two histidines in its amino acid sequence. To investigate whether MT4b also coordinates zinc via histidines, like their homolog E_C from wheat, extended [^{1}H ^{15}N] HSQC NMR spectroscopy has been employed. This experiment is designed to observe two-bond couplings between imidazole nitrogens and the protons bound to the adjacent carbons, unlike the one-bond coupling observed in conventional [^{1}H, ^{15}N] HSQC spectra.

The side-chain imidazole nitrogens Nδ1 and Nε2 of histidine exhibit characteristic crosspeaks with the Hε1 and Hδ2 protons for their neutral, protonated, and metal-coordinated forms, thus providing a means to detect metal coordination of histidines. Which nitrogen exhibits which chemical shift range depends on which tautomer prevails. In general, the nitrogen with the lone pair exhibits a chemical shift range between 200 and 250 ppm (Table 4.1). When zinc-bound, values between 199.5-220.0 ppm have been observed. When solvent exposed, and in unprotonated imidazole, much higher chemical shifts (close to 250 ppm) are observed, and when this nitrogen accepts a hydrogen bond, a chemical shift of around 239.5 ppm is observed. The chemical shifts of the N-H nitrogen also depend on whether or not imidazole is protonated, hydrogen-bonded, or metallated (Table 4.1), but the N: nitrogen shift is more discriminating. Recorded spectra as presented in Figure 4.6 support the idea that the histidines were coordinated to zinc in MT4b. From the pattern of crosspeaks, it can also be

deduced that zinc coordination occurs to His43 through Nδ1 and His51 through Nε2 with chemical shifts of 213.5 ppm and 213.9, respectively.

Table 4.1 Chemical shift values of histidine ring nitrogens in different states.

Histidines	Unprotonated ring N: ppm	Protonated ring N-H ppm	Unprotonated ring N-H ppm
Zinc coordinated	199.5-220.0	n/a	169.5-177.0
Solvent exposed	249.5	176.5	167.5
Hydrogen bonded	239.5	186.5	177.5

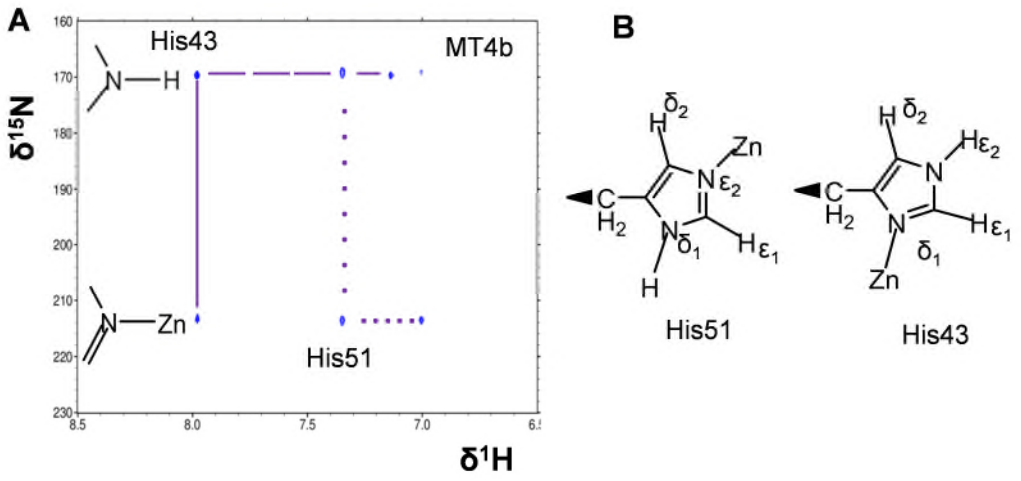

Figure 4.6 Histidine coordination to zinc in MT4b, as revealed by extended [^{1}H, ^{15}N] HSQC spectra. (A) The 2-bond-coupling crosspeaks between imidazole Nε2 and Nδ1 nitrogens and Hε1 and Hδ2 protons for zinc-coordinated His43 (purple solid line) and His51 (purple dotted line) are shown. (B) Schematic representation of zinc-coordinated histidine residues illustrating that His43 binds zinc through Nδ1 and His51 through Nε2, as derived from the observed coupling pattern.

Importantly, histidines in MT4b were not in solvent exposed or hydrogen bonded states, as suggested by comparing their chemical shifts with the reference values presented in Table 4.1.

As the coordination of the two histidines to zinc was established, it was of interest to find out which cysteines bind to zinc to form the mononuclear zinc binding site. With the aid of 2D TOCSY and NOESY spectra, it was possible to find out that Cys59 and Cys57 were the other two ligands to bind zinc in this site as shown in Figure 4.7.

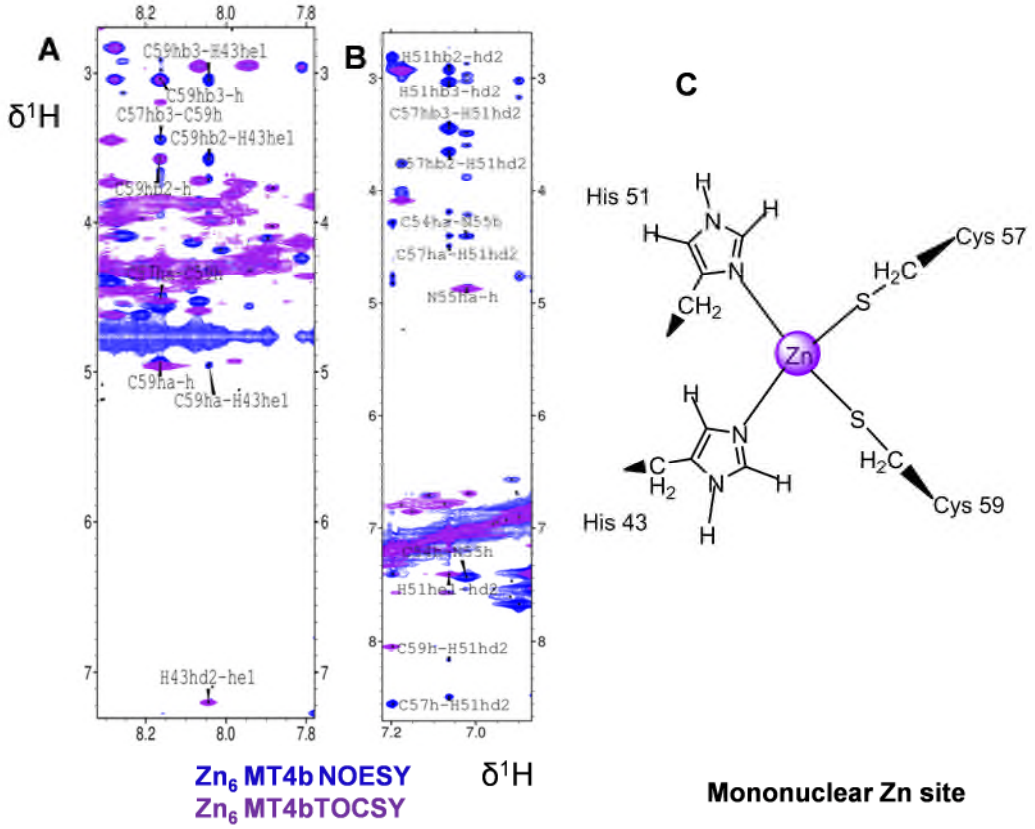

Figure 4.7 Overlaid 2D NOESY and TOCSY spectra of MT4b. (A) Cys57 and Cys59 Hα and Hβ crosspeaks with His43 Hε1. The Hβ protons of Cys57 are also near Cys59 NH. (B) Cys57 NOESY crosspeaks with His51 Hδ2. (C) Representation of the mononuclear zinc binding site formed by His43, His51, Cys57 and Cys59 for MT4b, respectively.

From Figure 4.7 (A and B), it is clear that Cys59 and Cys57 NH, Hα and -CH_2 (β) protons are close in space to His43 and His51 of MT4b, as corresponding NOESY crosspeaks are observed. Moreover, Cys57 Hα-to-Cys59 NH crosspeaks as

observed suggested that these two residues were also in close proximity, consistent with the known structure for the mononuclear site in wheat E_C.

4.4 Fully cadmium-exchanged MT4b: Protein folding and metal clusters

To understand the protein folding and cluster nature in fully exchanged cadmium form of MT4b, 2D [^{1}H, ^{1}H] TOCSY, 1D ^{111}Cd and 2D [^{1}H, ^{111}Cd] HSQC NMR spectra were recorded on a sample prepared from Zn_6MT4b by incubation with 6-7 equivalents of Cd^{2+}, as mass spectrometry suggested a stable Cd_6 metallo-species formed with 6-7 equivalents of Cd^{2+} as shown in inset in Figure 4.8. These experiments have also merit in order to make a comparison of protein folding nature with wheat E_C. As for wheat E_C, complete replacement of zinc with cadmium resulted in misfolding of domain II as shown in Figure 4.8. For the Zn_6 form, MT4b was well-folded as indicated by the number and dispersion of peaks (also see section 4.2.2). However, in the Cd_6 form, the number of peaks observed was much lower than for the Zn_6 form, suggesting non-isostructural replacement of zinc by cadmium. Like wheat E_C, most resonances for the Cd_6 form originated from the first cysteine-rich region that comprises domain I. 1D ^{111}Cd NMR spectroscopy of a sample containing six molar equivalents of $^{111}Cd^{2+}$ showed two intense peaks at 654.2 and 656.3 ppm, suggesting two cadmium environments. 2D [^{1}H, ^{111}Cd] HSQC experiments also produced two sets of -CH_2(β)-^{111}Cd crosspeaks.

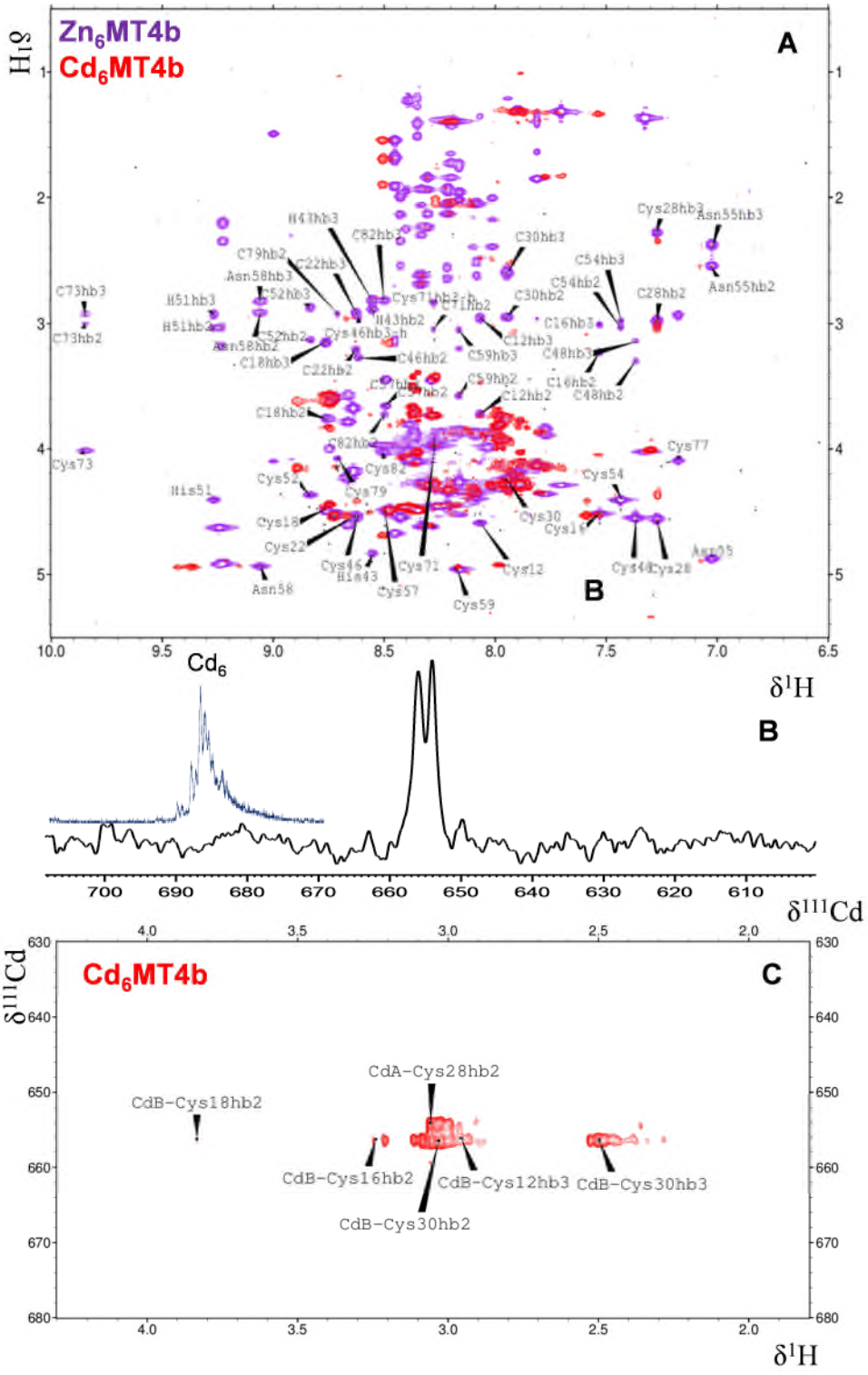

Figure 4.8 Effect of cadmium on protein folding. (A) Superimposed [^{1}H, ^{1}H] TOCSY spectra of **Zn_6MT4b** and **Cd_6MT4b.** (B) 1D ^{111}Cd NMR spectrum shows two peaks at 654.2 and 656.3 ppm**,** Inset figure - mass spectrometry suggests fully exchanged Cd_6 form in a different sample preparation (C) The [^{1}H, ^{111}Cd] HSQC spectrum consists of two sets of -CH_2 (β)-^{111}Cd crosspeaks. Spectra were recorded at 25 °C (1-1.5 mM protein, 50 mM Tris-D_{11}, 10 % D_2O, 50 mM NaCl, pH 7.42).

These observations indicated that in the fully exchanged Cd_6 form, domain I remained folded, whereas domain II underwent some conformational and/or configurational exchange – essentially, there is no stable protein fold for domain II in the exclusive presence of Cd^{2+}. The mis-folding of domain II also seems to influence domain I, as the peak intensities of Cys12 and Cys16 in the 2D ^{1}H spectra were hugely affected suggesting that these residues of domain I might be in close vicinity to domain II.

The above observations are closely similar to those made for wheat E_C. It is thus inferred that mis-folding of domain II in the fully exchanged cadmium form is perhaps a general phenomenon for type 4 plant MTs.

The mis-folding of domain II was the reason why the organisation of zinc or cadmium ions within this domain could not be determined by means of Cd NMR spectroscopy, which is otherwise a standard approach required for MT structure determination. In the case of His_2Cys_{11} in domain II of wheat E_C and MT4b, 11 cysteines could, in principle, bind 4 Cd^{2+}. Thus, given the presence of sufficient available binding sites other than histidines, it was suggested for E_C that Cd^{2+} can form one or more alternative clusters of Cd_4Cys_{11} in domain II, where all the available 11 cysteines will coordinate to Cd^{2+} (Leszczyszyn et al., 2010); however, in the Zn_6 form of the protein, formation of the $ZnHis_2Cys_2$ site plus the Zn_3Cys_9 cluster is energetically more favourable. Recently, chemical modification of histidines residues by diethyl pyrocarbonate (DEPC), it has also been shown that cadmium does not bind to histidines in fully cadmium exchanged sunflower MT4s (HaMT4) (Tomas et al., 2014). While mass spectrometry suggests predominant Cd_6 species in fully exchanged Cd-MT4b, in 1D ^{111}Cd and also in 2 [^{1}H, ^{111}Cd]

HSQC, only two Cd peaks were observed, suggesting if a cluster of Cd_4Cys_{11} is formed, it is not a single species, but rather many species with similar energy and these would undergo conformational and configuration exchange and were hence not observed by NMR spectroscopy, under the accessible experimental conditions.

As it was previously shown for wheat E_C that the $ZnHis_2Cys_2$ site plays a significant role for domain II folding (Leszczyszyn et al., 2010), further proving the same phenomenon for MT4s from *Arabidopsis thaliana* by site-directed mutagenesis was not a priority. Instead, it was hoped that it would be possible to generate mixed Zn/Cd MT4 species which would contain Zn^{2+} in the isolated His_2Cys_2 site to achieve ordered protein folding, with most of the other sites occupied by NMR-active Cd^{2+}. However, finding an appropriate Zn/Cd stoichiometry was the main concern - as it was unknown at what protein to cadmium stoichiometry zinc would remain within the His_2Cys_2 site and also cadmium will be in other sites within domain II. To prepare mixed-metal species, the mass balance technique was chosen where sub-stoichiometric to stoichiometric amounts of cadmium were titrated into the zinc-saturated proteins.

4.5 Zinc replacement by cadmium: UV-visible spectroscopy and mass spectrometry

Zinc replacement by cadmium from MTs can be easily monitored by UV-Visible spectroscopy because of different metal-thiolate absorption bands exhibited by these two metal ions. Whilst the Zn-thiolate ligand-to-metal charge transfer

(LMCT) band is observed at 220-230 nm, the Cd-thiolate LMCT band appears at 254 nm. Incremental additions of Cd^{2+} (0-9 equivalents) to the zinc form of protein results in displacement of Zn^{2+} by Cd^{2+} as observed by an increasing absorption at 254 nm as displayed in Figure 4.9. Interestingly, plots of equivalents of Cd^{2+} added vs absorption at 254 nm suggested that MT4b can bind more Cd^{2+} than expected. Ideally, six Zn^{2+} should be replaced by six Cd^{2+} ions.

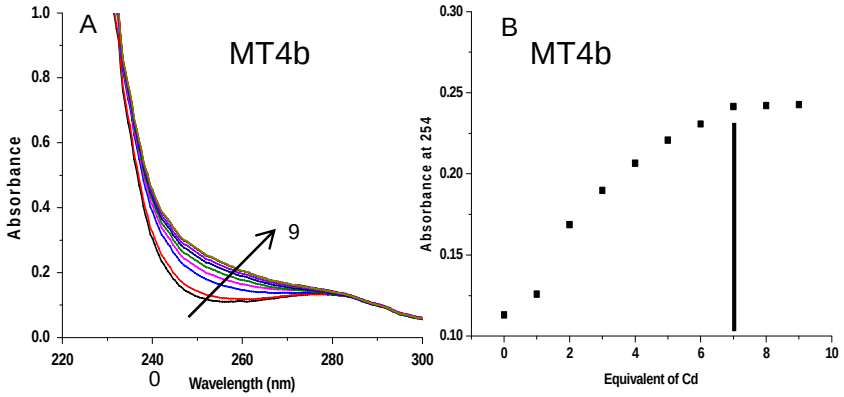

Figure 4.9 Cadmium exchanged with Zn from MT4b monitored by UV-Visible spectroscopy. Raw spectra (A) Up to 9 equivalents of Cd^{2+} addition. (B) Absorbance changes vs equivalents of cadmium addition as measured at 254 nm for Cd-thiolate bonds. Proteins samples (2 µM, 0.2 M Tris buffer, pH 7.58).

However, experimental results suggested that up to seven equivalents of Cd^{2+} could be bound to the protein, but it should be noted that the higher than expected Cd^{2+} stoichiometry to the protein may be largely due to inaccuracies either in protein or Cd^{2+} concentration, as very small amounts (2 µM) of protein were used.

Mass spectrometry was employed to understand the metallo-species formed during cadmium exchange reactions.

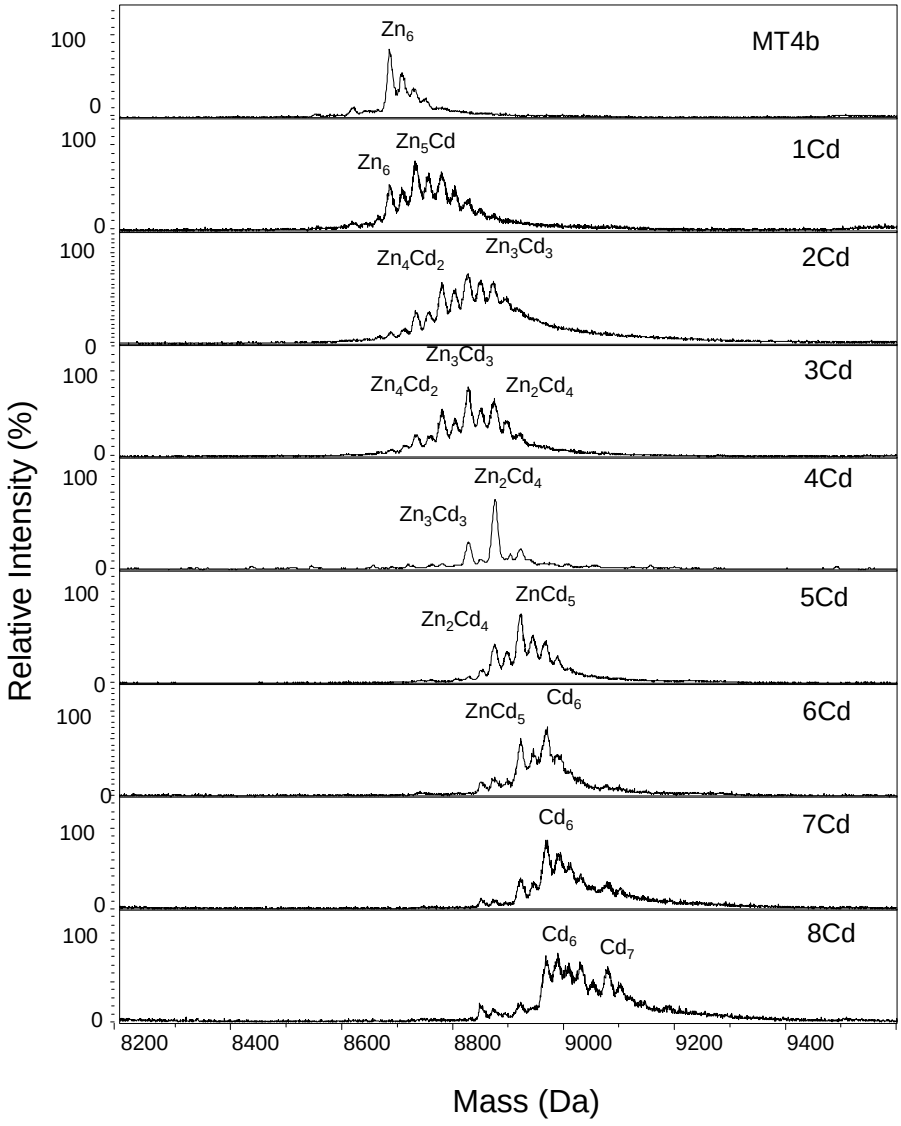

Figure 4.10 Deconvoluted mass spectra of MT4b at different Cd stoichiometry (25 µM protein, 10% v/v CH_3OH, 10 mM NH_4HCO_3 buffer).

For doing so, a set of protein samples were incubated with 1-8 equivalents of Cd^{2+} and desalted prior to recording their mass spectra at neutral pH. Initially, the predominant peak observed was Zn_6 for MT4b. Addition of 1 molar equivalent of Cd^{2+} resulted in $Zn_5CdMT4b$ as predominant species. With continuing addition of cadmium up to 6 equivalents, different mixed metal species of Zn_4Cd_2, Zn_3Cd_3, Zn_2Cd_4 and $ZnCd_5$ were observed. Interestingly, fully cadmium exchanged Cd_6

species was observed at 7 equivalents of cadmium; again, this may be because of small concentration inaccuracies. Addition of 8 equivalents of cadmium resulted in the appearance of Cd_7 species. An intriguing and promising feature was the formation of Zn_2Cd_4 as a major species at 4 equivalents of cadmium. Formation of prominent Zn_2Cd_4 species as observed, possibly retaining a folded nature of protein, thus support the viability of the idea of mixed Zn/Cd species for protein folding study.

4.6 Protein folding of mixed metal species: NMR spectroscopy

A series of 2D [^{1}H, ^{1}H] TOCSY and NOESY NMR spectra were recorded at 2 to 5 equivalents of cadmium for screening the best stoichiometry, the idea being to maximise both protein folding and Cd^{2+} content. In agreement with mass spectrometry data (Figure 4.10), where at 3-4 equivalents of Cd^{2+}, a Zn_2Cd_4 species was observed, NMR spectroscopy also indicated mostly well-folded protein at 3-4 equivalents of Cd^{2+}, as shown in Figure 4.11.

Unlike with 6 equivalents of Cd^{2+}, many of the domain II resonances were still observed at 4 equivalents of Cd^{2+}, particularly, Cys52, Cys81, Cys71, Cys59, Cys46 and Cys79 resonances were observed. However, the resonance from Cys73 was not observed. All resonances from domain I except for Cys12 were also observed at 4 equivalents of cadmium.

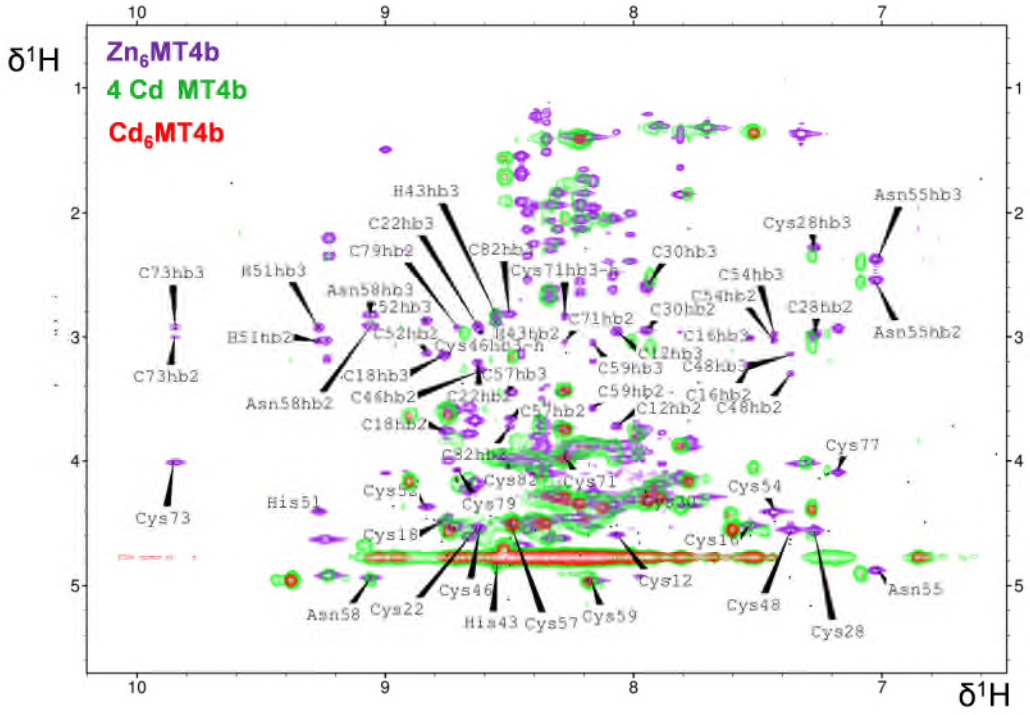

Figure 4.11 Comparison of protein folding. [^{1}H, ^{1}H] Superimposed TOCSY spectra of **Zn_6MT4b**, **4 Cd** and **Cd_6MT4b.** Spectra were recorded at 25 °C (1-1.5 mM protein, 50 mM Tris-D_{11}, 10 % D_2O, 50 mM NaCl, pH 7.42).

Not unexpectedly, zinc/cadmium replacement results in chemical shift perturbation for both metal-binding cysteines and non-metal binding residues due to larger size of Cd^{2+} (0.92 Å) compared to Zn^{2+} (0.70 Å) in a tetrahedral geometry.

To better understand the effect of zinc/cadmium replacement on protein folding, a ^{15}N labelled MT4b sample was prepared and NMR spectra were recorded with incremental additions of Cd^{2+}, to monitor the cadmium-induced chemical shift perturbation. At 2 equivalents of cadmium, protein folding remained very similar to the zinc- bound form, as almost all of the metal binding cysteine residues were still observable.

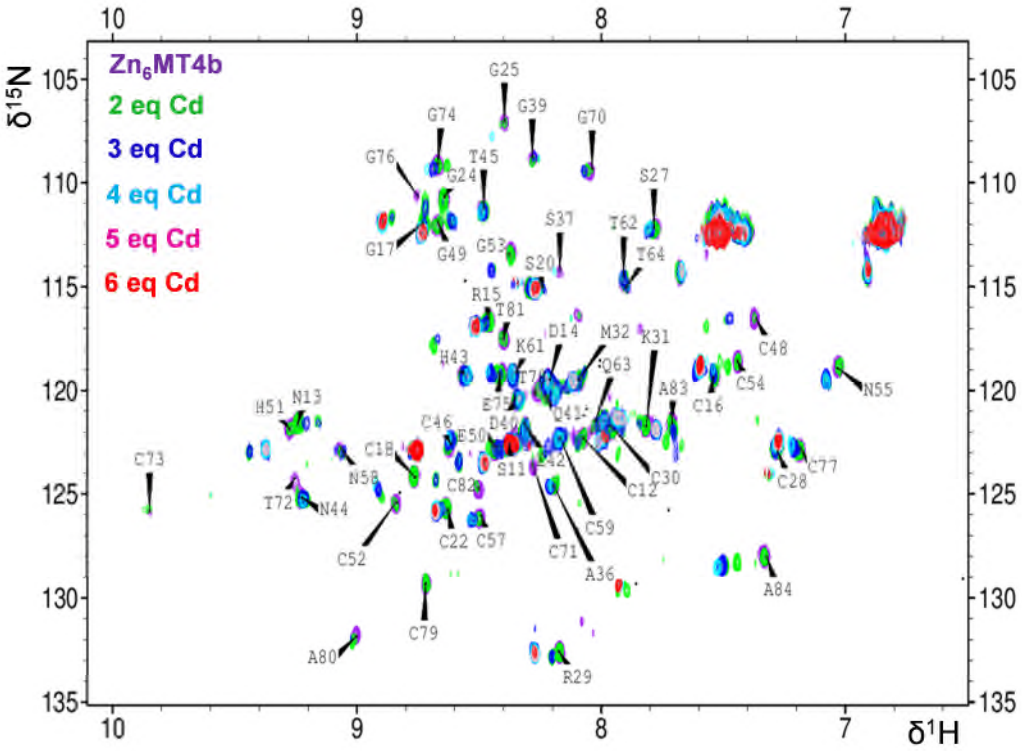

Figure 4.12 Overlay of [^{1}H, ^{15}N] HSQC spectra of cadmium titration to zinc form of MT4b. Incremental cadmium addition to zinc form of MT4b results in gradual and domain-specific protein misfolding. (**Zn_6MT4b**, **2 Cd**, **3 Cd**, **4 Cd**, **5 Cd** and **6 Cd**. Spectra recorded at 25 °C (250 µM protein, 50 mM Tris-D_{11}, 10 % D_2O, 50 mM NaCl, pH 7.42).

However, only very weak resonances were observed for Cys82, Cys73, Cys71, Cys54 and Cys48, suggesting zinc binding to these residues was affected. Following addition of another equivalent of Cd^{2+}, Cys79 and Cys73 were completely diminished. Moreover, Cys77, Cys52, Cys57, Cys46 and His51 were also affected as lower peak intensities were observed. At 4 equivalents of Cd, metal coordinating cysteine residues remained the same as observed for 3 equivalents, however, weaker resonances were observed for non-binding residues originating from domain II. Interestingly, the crosspeak for His43 had completely disappeared at 5 equivalents of cadmium. At this and 6 equivalents, only domain I remained, with most domain I crosspeaks having shifted by small amounts.

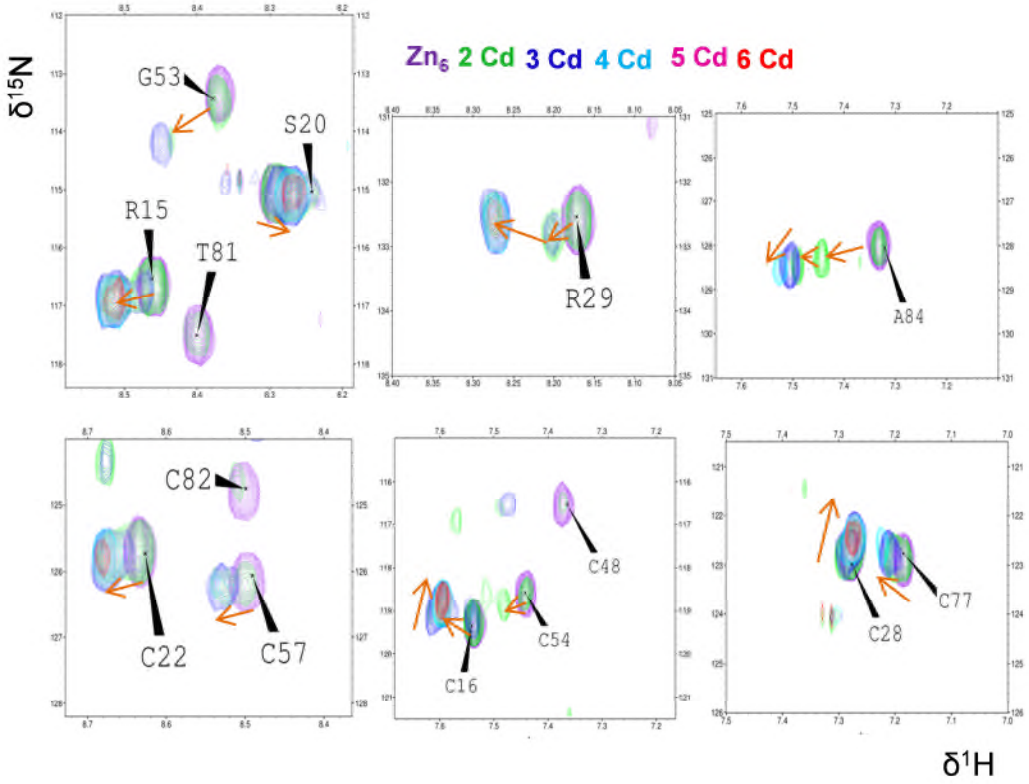

Figure 4.13 Chemical shift perturbation of metal coordinating and non-coordinating residues of MT4b as a result of cadmium addition. Superimposed slices of [^{1}H, ^{15}N] HSQC spectra of incremental cadmium addition to zinc form of MT4b (**Zn_6MT4b**, **2 Cd, 3 Cd, 4 Cd, 5 Cd** and **6 Cd**). Spectra were recorded at 25 °C (250 µM protein, 50 mM Tris-D_{11}, 10 % D_2O, 50 mM NaCl, pH 7.42).

Both metal coordinating and non-coordinating residues were affected by cadmium addition. Among the non-coordination residues, remarkable perturbations were observed for Ala84, Arg29 and Gly53. Chemical shift perturbation (CSP) as determined by the following equation suggested that among the non-coordinating residues, Gly53 was most affected, with a value of 0.47 ppm. Ala84 was also affected considerably.

Table 4.2 Chemical shift perturbation data for some metal coordinating and non-coordinating residues of MT4b as determined by using the following equation:

$$\Delta\delta = \sqrt{(\Delta\delta_{^1H}^2 + (1/9\Delta\delta_{^{15}N}^2)}$$

Where $\Delta\delta$ = chemical shift perturbation, $\Delta\delta_H$= difference in chemical shift in H axes, $\Delta\delta_{N=}$ difference in chemical shift in N axes.

Amino acids	CSP($\Delta\delta$) ppm	Amino acids	CSP($\Delta\delta$) ppm
Ala84	0.27	Cys77	0.14
Gly53	0.47	Cys57	0.05
Arg29	0.1	Cys54	0.06
Ser20	0.03	Cys28	0.22
Arg15	0.12	Cys16	0.17

Among the coordinating ligands, Cys28 was found to be considerably influenced by cadmium addition as CSP value observed was 0.22 ppm. Cys77 and Cys16 were also perturbed with values of 0.14 and 0.17 ppm.

4.7 Effect of cadmium on zinc-binding histidines

The hypothesis on mixed metal species was to keep zinc within the His_2Cys_2 site. It was therefore important to understand how cadmium influenced this site in MT4b. Here, 2D [^{1}H, ^{1}H] TOCSY and NOESY and extended [^{1}H, ^{15}N] HSQC NMR spectroscopy was employed to understand the effect of cadmium on histidines and their tautomeric state in MT4b.

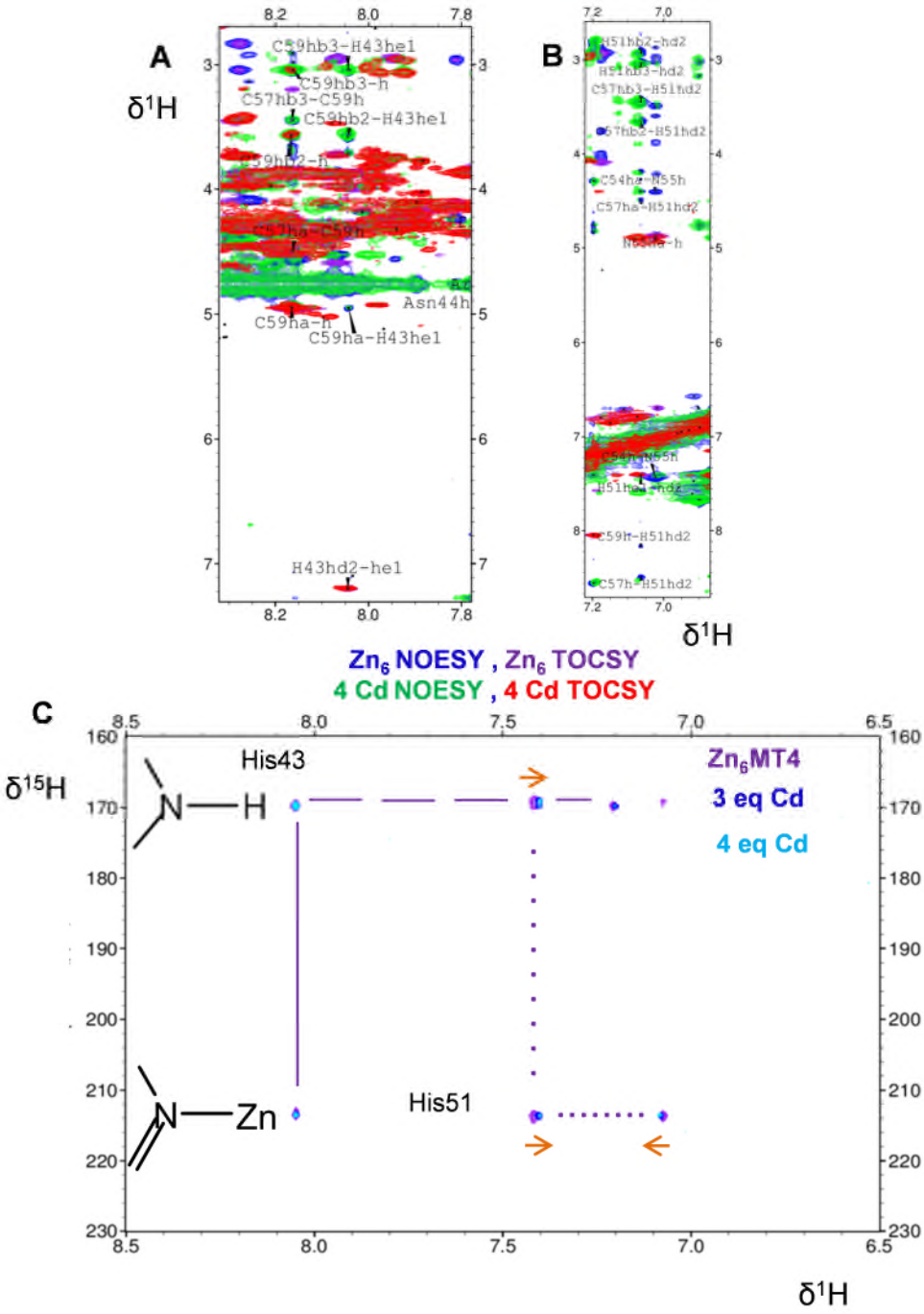

Figure 4.14 Effect of cadmium on histidines resonances. (A-B) Overlay of 2D TOCSY and NOESY of Zn_6MT4b and addition of 4 Cd to Zn_6MT4b suggests that zinc is still bound to the His_2Cys_2 site. (C) Superimposed of expended [^{1}H, ^{15}N] HSQC spectra of incremental cadmium addition to zinc form of MT4b (**Zn_6MT4b**, **3 Cd,** and **4 Cd.** Spectra were recorded at 25 °C (250 µM protein, 50 mM Tris-D_{11}, 10 % D_2O, 50 mM NaCl, pH 7.42).

From Figure 4.14 (A-B), it was evident that at 4 equivalents of cadmium, resonances from His43, His51, Cys57 and Cys59 were still observed, although Hδ2 of His51 had slightly shifted, suggesting that the His_2Cys_2 site remained largely folded at 4 equivalent of cadmium. Moreover, the extended region of the [^{1}H, ^{15}N] HSQC spectra as displayed in Figure 4.14 (C) confirmed that cadmium addition influenced the histidine resonances of His51. Whilst His43 resonances remained steady up to 4 equivalents of cadmium, shifts of His51 resonances were observed. Moreover, His51 Hε1 shifted upfield, whilst Hδ2 shifted downfield at 3 and 4 equivalents of cadmium. The shift of His51 side-chain resonances suggests that perhaps His51 senses the changes that happen in the adjacent cluster within domain II due to cadmium addition, as His51 is near to several of the other metal-binding residues within this domain. Intriguing features observed were that after addition of 4 equivalents of cadmium, resonances for His51 and His43 were still observed. This suggests that up to 4 equivalents of cadmium, the His_2Cys_2 site remains largely stable and loaded with zinc.

4.8 Paving the way to metal-ligand connectivities: ^{111}Cd NMR spectroscopy

The studies so far suggest that addition of cadmium to the zinc-saturated protein resulted in different mixed metallo-species as observed by mass spectrometry Figure 4.10. Formation of these mixed metal species also contributed to the nature of the protein folding as shown in Figure 4.12. Importantly, for up to 4 equivalents of cadmium, the mononuclear site, well-folded domain I and mostly folded domain II resonances were observed. However, at 5 and 6 equivalents of

cadmium, the mononuclear site was disintegrated and domain II resonances had disappeared as shown in Figure 4.12.

The various 2D NMR experiments, in agreement with MS data, had indicated that at various stoichiometries, several mixed metallo-species co-existed (also see Figure 4.15 B). Therefore, in order to better understand the species that may be present in the NMR spectra, it is helpful to consider all possible mixed metallo-species at various Cd:Zn ratios.

At 2 equivalents of cadmium, as the mononuclear site will be occupied by zinc, the 2 cadmium could occupy 5 of the 6 binding sites in 10 possible ways (Figure 4.15 A).

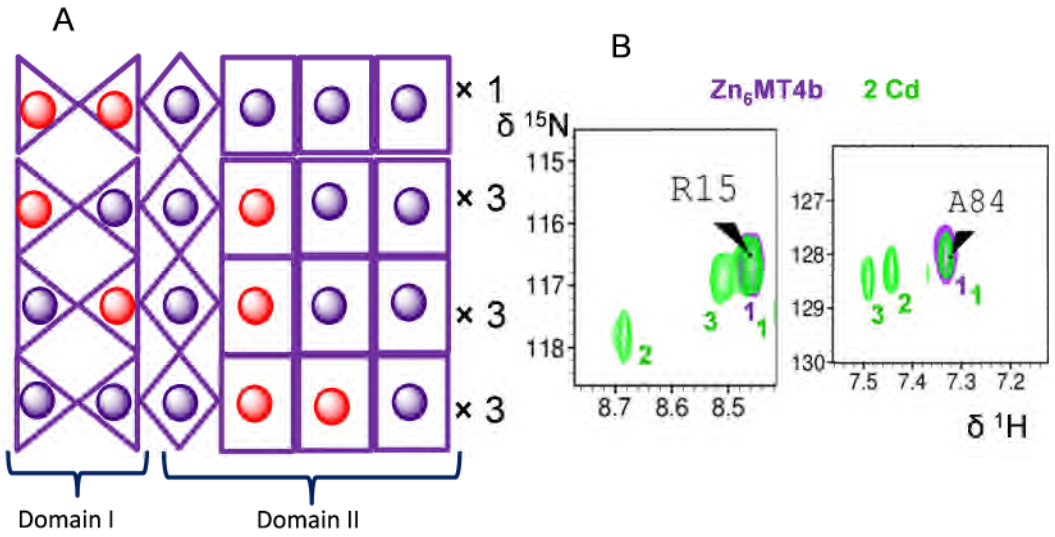

Figure 4.15 Possible localization of Zn and Cd in the metal binding sites of MT4b at 2 equiv. mol Cd^{2+}. (A) Schematic diagram of possible organisation of 2 Cd in 5 binding sites provided that the mononuclear site will be occupied by Zn. (B) [^{1}H, ^{15}N] HSQC peaks perturbation of R15 and A84 at 2 mol equiv of Cd.

If 2 cadmium ions occupy domain I, leaving domain II loaded with 4 zinc ions, then only one arrangement is possible. If only one of the cadmium ions is placed

in domain I, then two sets of arrangements will be possible, depending on the position of cadmium in the two binding sites in domain I. This means that one of the cadmium ions will be in domain II. In domain II, one cadmium could in principle occupy one of 3 binding sites, i.e. in 3 possible ways, together with the two possible positions for cadmium in domain I, 6 arrangements are possible. Another possibility, if both cadmium ions go to domain II, this leaves domain I for zinc, then 2 cadmium ions in domain II would be arranged in 3 possible ways.

Mass spectrometry result suggested that at 2 equivalents of cadmium Zn_6, Zn_5Cd , Zn_4Cd_2 and Zn_3Cd_3 metallo-species were formed; however, Zn_4Cd_2 and Zn_3Cd_3 were observed as predominant peaks. In the ^{15}N HSQC spectra, 3 species were detected for R15 as shown in Figure 4.15 (B). Peak (1) is Zn_6 form, Peak (2) and (3) for R15 could perhaps refer to Zn-Cd mixed or fully-exchanged Cd-Cd domain I, respectively, for example in a Zn_4Cd_2 species with a fully Cd-occupied domain I. For A84, peak (1) is Zn_6 species, peak (2) and peak (3) could be for mixed Zn-Cd sites and perhaps fully Cd occupied sites in domain II, respectively, as low abundance Zn_3Cd_3 species was observed in mass spectrometry. The three distinct peaks observed for R15 from domain I and A84 from domain II suggest that cadmium went into both domains at 2 equivalents of cadmium.

At 3 equivalents of cadmium, it can be expected that at least one cadmium will occupy domain II. In total, 10 arrangements are possible for 3 cadmium ions to bind within 5 binding sites, depending on whether domain I is fully occupied, partially occupied or fully unoccupied. Again, since only folded species are considered, all assumptions are based on the mononuclear site being occupied by zinc. Predominant species observed in mass spectrometry at 3 equivalents of

cadmium were Zn_4Cd_2, Zn_3Cd_3 and Zn_2Cd_4. As R15 has still three peaks, this suggests either peak 2 or peak 3, one of them corresponding to mixed Zn/Cd domain I, could originate from any of the 3 mixed metal species observed in mass spectrometry.

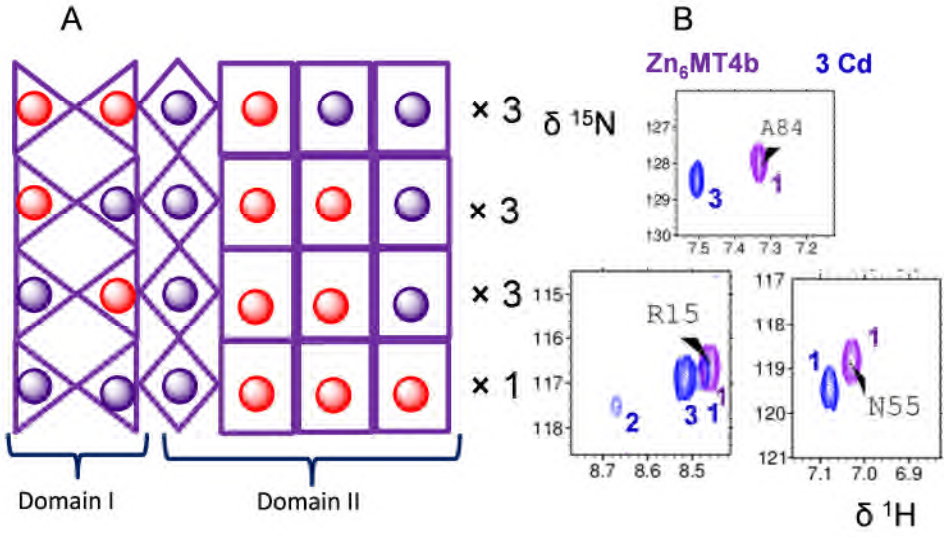

Figure 4.16 Localization of Zn and Cd in the metal binding sites of MT4b at 3 equiv. mol. Cd^{2+}. (A) Schematic diagram of possible orientation of 3 Cd in 5 binding sites provided mononuclear site will be occupied by Zn. (B) [^{1}H, ^{15}N] HSQC peaks perturbation of R15, N55 and A84 at 3 mol. equiv. of Cd.

However, as the peak 2 intensity decreases and peak 3 intensity increases, this suggested strongly that peak 2 corresponds to the mixed Zn-Cd domain I, and peak 3 to fully Cd-exchanged domain I, as with increased Cd concentration, the likelihood of Cd-occupied sites will be increased. The binding sites for domain II are expected to be observed predominantly from Zn_3Cd_3 and Zn_2Cd_4 species. Surprisingly, the [^{1}H, ^{15}N] HSQC spectrum suggested only one dominant species for domain II, as indicated from N55 and A84 (Figure 4.16 B); for each of these, single peaks, different from the original ones, were observed. Formation of single

species for domain II could be attributed to any of Zn_4Cd_2, Zn_3Cd_3 or Zn_2Cd_4 species. The previous peak 2 for A84 had completely disappeared.

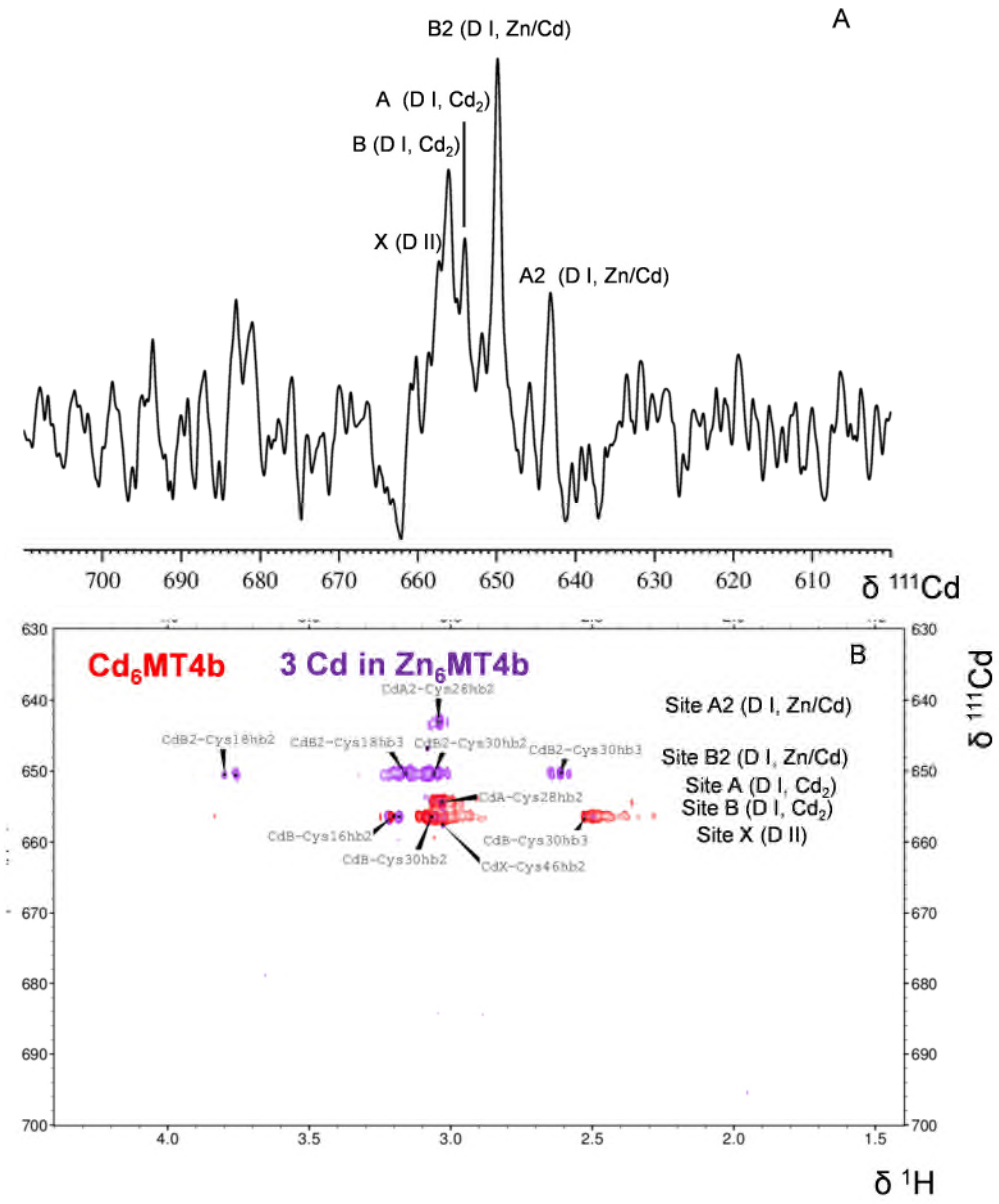

Figure 4.17 1D and 2D ^{111}Cd NMR spectra of mixed metal species at 3 equiv. mol $^{111}Cd^{2+}$. (A) 1D^{111}Cd NMR spectra of MT4b at 3 equivalents of cadmium - peaks from domain I and domain II are shown. (B) Overlaid 2D [^1H, ^{111}Cd] HSQC NMR spectra of **Cd_6MT4b** and **3Cd in Zn_6MT4b** illustrates -CH_2 (β)-^{111}Cd connectivities. Spectra recorded at 25 °C (1-1.5 mM protein, 50 mM Tris-D_{11}, 10 % D_2O, 50 mM NaCl, pH 7.42).

This suggests that peak 2 refers to species with one Cd in domain II, and peak 3 to species with two Cd in domain II. Significantly, even though there are three possible arrangements for this, only one species is observed by ^{1}H and ^{15}N NMR spectroscopy. Three species for domain I, Cd_2 and mixed Zn/Cd, were also identified in 1D ^{111}Cd and 2D [^{1}H, ^{111}Cd] HSQC spectroscopy. At 3 equivalents of cadmium, five peaks were identified in 1D ^{111}Cd and 2D [^{1}H, ^{111}Cd] HSQC spectra: (A2) 643.1 (B2) 650.1 (A) 654.2 (B) 656.3 and (X) 657.6 ppm. Peaks also appeared in the 1D ^{111}Cd NMR spectrum; however, with different intensities, confirming that various sites were differentially populated by ^{111}Cd nuclei. Also, because the same two ^{111}Cd resonances for domain I were observed (Figure 4.17 B) at 3 and 6 equivalents of cadmium (sites A and B), this illustrates that at least in some species present at 3 mol equiv, domain I was fully occupied by Cd. Furthermore, there was at least one set of crosspeaks with a pattern similar to B, namely B2, which was particularly prominent at this Cd:ZnMT4b ratio. This suggests that these two peaks correspond to the same site, but whilst B corresponds to Cd in a fully Cd-loaded domain I, B2 corresponds to the same Cd, but with a Zn neighbour. Similarly, peaks A and A2 both refer to the same domain I site, but in slightly different Cd environments; while A2 has Cd with a Zn neighbour, site A refers to this Cd ion in a fully occupied domain I. Peak (X) is a completely new peak, likely to correspond to a domain II metal site. Thus, at 3 mol. equiv. of Cd, one site of domain II can be identified.

At 4 equivalents of cadmium, and with the Zn_2Cd_4 species dominating speciation as judged from MS results, only 5 arrangements are possible to accommodate 4 cadmium ions in 5 binding sites. If domain I is fully occupied by Cd, then the

remaining 2 cadmium ions again could bind to 3 binding sites in 3 possible ways. If however domain I is only partially occupied, then 3 cadmium ions would populate all 3 binding sites. In the [^{1}H, ^{15}N] HSQC spectrum, a single species is observed for domain II, this species could be from the dominating Zn_2Cd_4 species, and have (at least) two Cd ions in domain II. However, some heterogeneity with respect to Zn-Cd was observed as illustrated in Figure 4.18 (C) shows the ^{15}N HSQC resonance of R29 for which three species of either fully Cd-Cd or mixed Cd-Zn were observed - peak 3 could be fully Cd-Cd site while peak 1 and 2 could be mixed Zn-Cd site. Unlike R15 and A84, R29 which is border line can sense both domains.

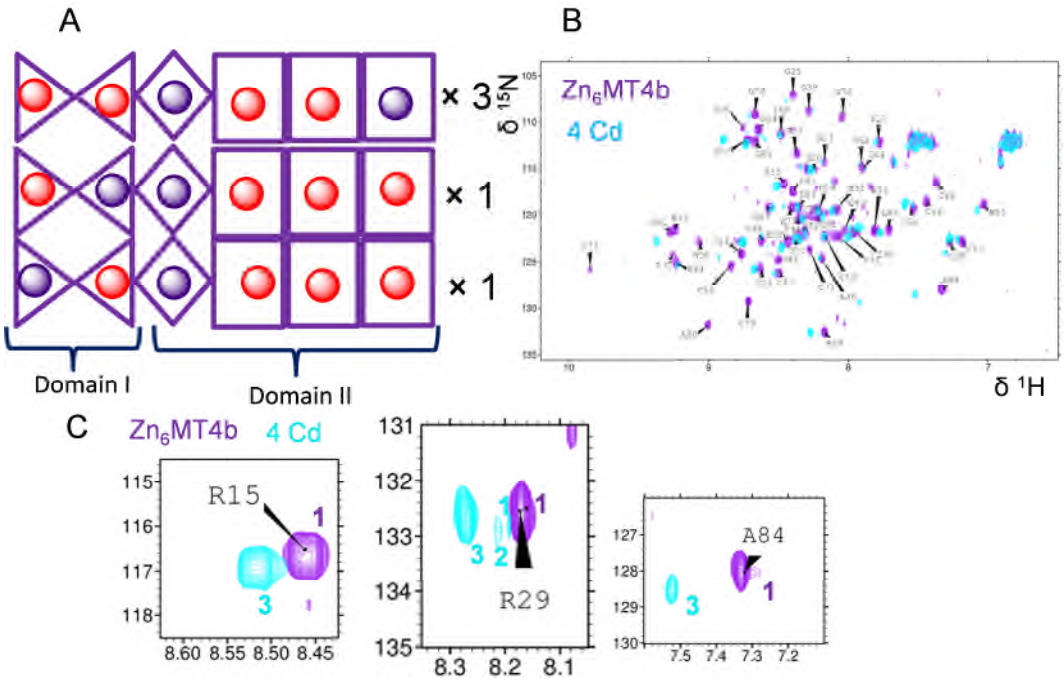

Figure 4.18 Possible localization of Zn and Cd in the metal binding sites of MT4b at 4 equiv.mol Cd^{2+}. (A) Schematic diagram of possible orientation of 4 Cd in 5 binding sites provided that the mononuclear site will be occupied by Zn. (B) Overlaid [^{1}H, ^{15}N] HSQC spectra of Zn_6MT4b and 4 mol equiv of Cd:MT4b. (C) Overlaid Crosspeaks of R15, R29 and A84. At 4 equivalents of cadmium with Zn_6MT4b

Peak 1 in R29 could be fully Zn site but as one Zn remained in the mononuclear site that will make maximally one Zn available for binding to domain I. However, high intensity of peak 3 in both R15 and R29 suggested that the predominant species in domain I is mostly fully occupied Cd. In that circumstance, it is obvious that 2 Cd will be in domain II. 1D ^{111}Cd NMR and 2D [^{1}H, ^{111}Cd] HSQC spectra as displayed in Figure 4.19.

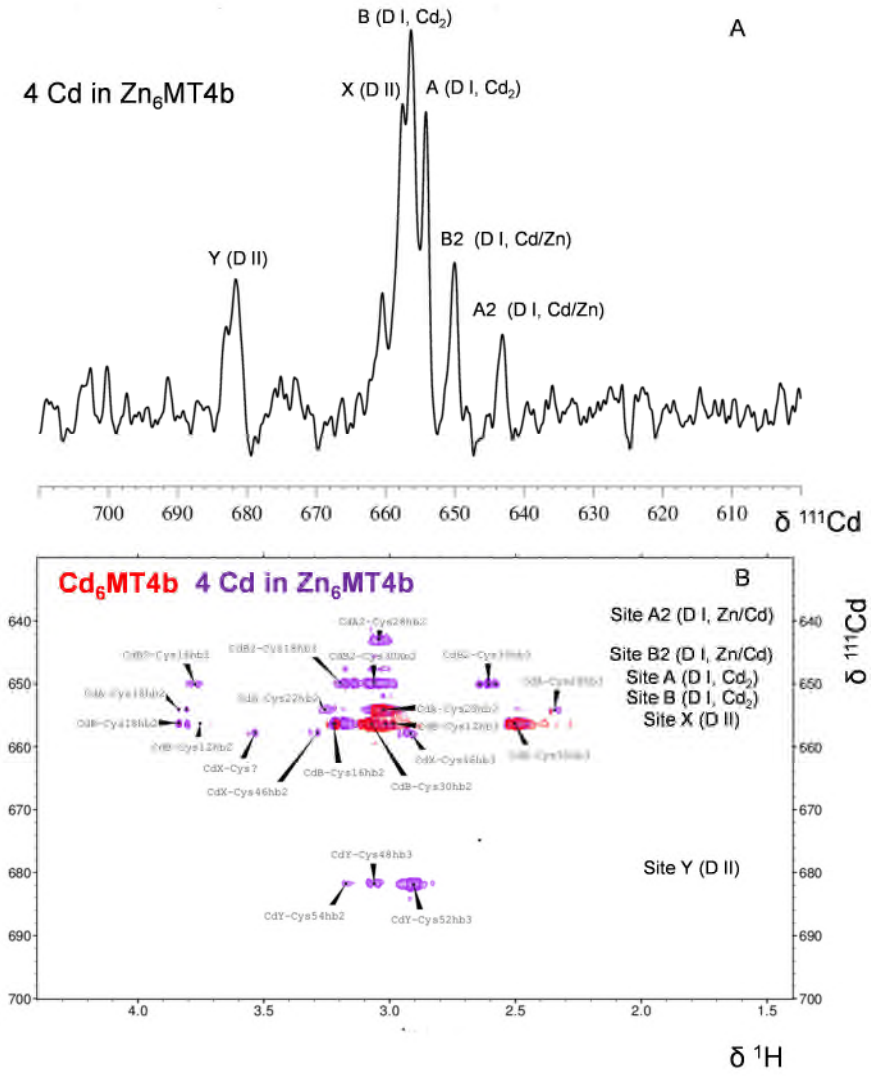

Figure 4.19 1D and 2D ^{111}Cd NMR spectra of mixed metal species at 4 equiv. mol $^{111}Cd^{2+}$. (A) 1D^{111}Cd NMR spectra of MT4b at 4 equivalents of cadmium - peaks from domain I and domain II are shown. (B) Overlaid 2D [^{1}H,^{111}Cd] HSQC NMR spectra of **Cd_6MT4b** and **4Cd in Zn_6MT4b** illustrates -CH_2(β)-^{111}Cd connectivities. Spectra recorded at 25 °C (1-1.5 mM protein, 50 mM Tris-D_{11}, 10 % D_2O, 50 mM NaCl, pH 7.42).

Figure 4.19 illustrate that addition of 4 equivalents of cadmium resulted in appearance of a new resonance at 681.6 ppm, designated as Y, along with the peaks previously observed at 3 equivalents of cadmium. These were also observed for 3 mol equiv. of Cd. It was inferred that the new peak (Y) belonged to domain II. It was also observed that the number of crosspeaks for site X has increased at 4 equivalents of Cd. At 4 equivalents of Cd, two prominent sites for domain II have been identified, one of these sites (X) was also observed (weakly) at 3 equivalents of Cd.

At 5 mol. equiv. of cadmium, mass spectrometry indicated $ZnCd_5$ and Zn_2Cd_4 species. However, 2D [^{1}H, ^{15}N] HSQC NMR spectrum at 5 mol. equiv. of cadmium suggests that domain II was largely unfolded; however, resonances were observed

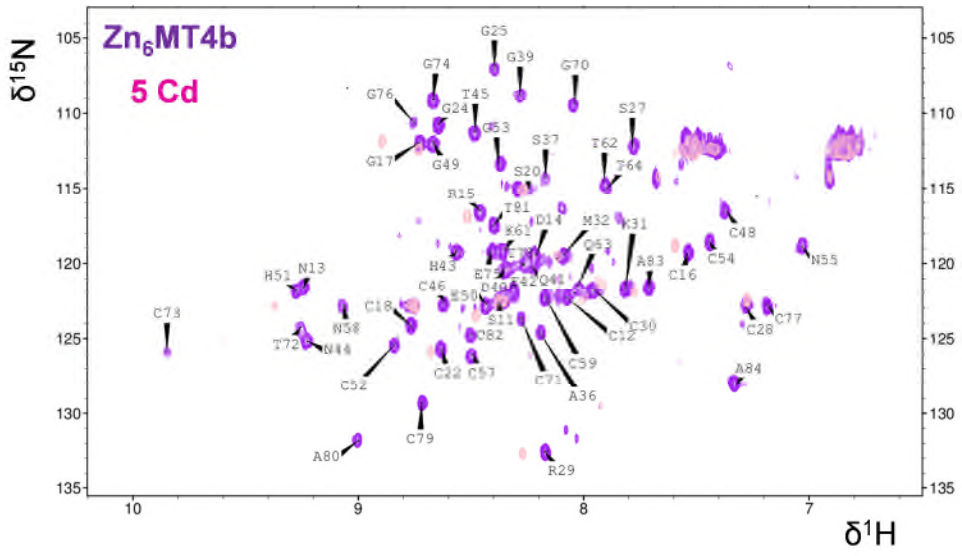

Figure 4.20 Overlaid [^{1}H, ^{15}N] HSQC spectra of Zn_6MT4b and 5 mol equv of Cd MT4b. Spectra recorded at 25 °C (250 µM protein, 50 mM Tris-D_{11}, 10 % D_2O, 50 mM NaCl, pH 7.42).

for domain I. It was also observed that backbone and side-chain resonances from both histidines had vanished; this could indicate that in the $ZnCd_5$ species, the mononuclear site is no longer present, and that the remaining zinc ion is part of alternative mixed-metal clusters.

Results so far observed by mass spectrometry, 1D ^{111}Cd, 2D [^{1}H, ^{15}N] HSQC and 2D [^{1}H, ^{111}Cd] HSQC NMR spectroscopy suggests that at 4 mol. equiv. Cd, the predominant species observed is Zn_2Cd_4. As a maximal number of CH_2 (β)-^{111}Cd crosspeaks were observed at 4 equivalents of cadmium in [^{1}H, ^{111}Cd] HSQC spectra, this preparation was considered the best possible for connectivity studies.

Table 4.3 1D ^{111}Cd NMR resonances observed in fully exchanged and mixed metal species of MT4b.

Species	Number of peaks	^{111}Cd chemical shifts Ppm					
		643.1 A2 (D I, Zn-Cd)	650.1 B2 (D I, Zn-Cd)	654.2 A D I, Cd-Cd)	656.3 B D I, Cd-Cd)	657.6 X DII, Cd-Cd)	681.6 Y DII, Cd-Cd)
Cd_6MT 4b	2	×	×	√	√	×	×
3 equiv Cd^{2+}	5	√	√	√	√	√	×
4 equiv Cd^{2+}	6	√	√	√	√	√	√

All the above experimental results allow some conclusive remarks on domain I, the mononuclear His_2Cys_2 site and domain II.

Domain I: Domain I can accommodate two metal ions to form a cluster. In the fully exchanged Cd_6 form, two sets of connectivities were identified in the 2D [^{1}H, ^{111}Cd] HSQC NMR spectrum - although for site A, only connectivity with Cys28 was determined. However, Cys12, Cys16, Cys 18 and Cys30 were found

to form site B. Moreover, at 4 mol. equiv. of cadmium, 4 sets of resonances for domain I were observed in a 2D [^{1}H, ^{111}Cd] HSQC NMR spectrum. Apart from site A and site B, which were also observed for the fully exchanged form, two new sets of resonances observed were A2 and B2, referring to the same sites as A and B, but having Zn as neighbour. At 4 equivalents of cadmium, the maximal number of connectivities were observed for sites A and B, referring to the fully Cd-exchanged form of domain I. Cys18, Cys22 and Cys28 bound to site A and site B connected to Cys12, Cys16,Cys18 and Cys30. It is clear that Cys18 is common to both sites, suggesting that this acts as a bridging ligand. Site A has two more ligands, Cys22 and Cys28; as site B is fully occupied by four other cysteines so Cys22 and Cys28 should be terminal ligands. Other cadmium site could be terminally coordinated by Cys16, Cys30 or Cys12, but only two of them, with the third residue acting as a bridging ligand. Because Cys16 and Cys18 are very close to each other in the amino acid sequence, perhaps Cys16 and Cys18 as bridging ligand would not be energetically favourable; thus it is plausible that Cys16 would be one of the terminal cysteines for site B. Thus, of the remaining Cys12 and Cys30, one would be bridging and one would be terminal. In wheat E_C (Loebus et al., 2011), one of the bridging ligands was Cys8 equivalent to Cys18 in MT4b, for the other bridging ligand Cys20 and Cys2, equivalent to Cys30 and Cys12 in MT4b, were considered and in both cases Cys8-Cys20 and Cys8-Cys2 as bridging ligand structure was energetically favourable. For MT4b, Cys12 was considered as the missing bridging ligand, and Cys30 as terminal ligand, however, alternatively Cys30 as bridging and Cys12 as terminal could also be a possible option.

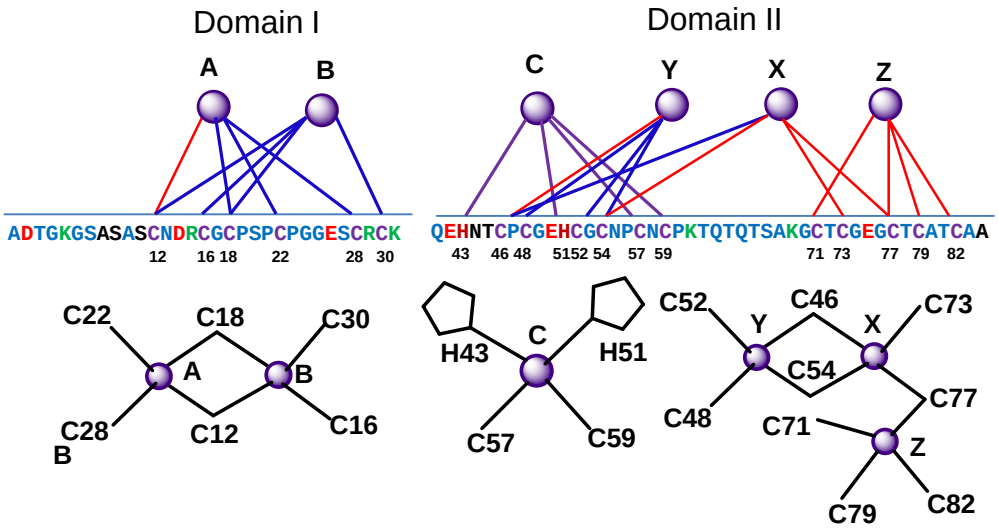

Figure 4.21 Schematic connectivity diagram. The blue lines are experimentally determined Cd connectivities; purple lines refer to experimentally determined Zn connectivities, and red lines are most likely connectivity based on nearest Zn-thiolate distances.

Domain II: Domain II has four metals to be bound by 11 cysteines and 2 histidines.

Mononuclear His_2Cys_2 site: A single zinc ion coordinated to His43, His51, Cys57 and Cys59 forms a $ZnHis_2Cys_2$ site. Both in the Zn_6 form and at 4 equivalents of cadmium, the mononuclear site was observed. This mononuclear site was derived from analysis of 2D TOCSY, NOESY and ^{15}N HSQC data.

Organization of three metals in Domain II: As one metal binds to the mononuclear His_2Cys_2 site, this leaves three metals to bind to the remaining nine cysteines. All these nines cysteines were observed in the Zn_6 form and these cysteines, apart from Cys73, Cys79 and Cys82, were observed at 4 equivalents of cadmium. However, resonances from Ala80, Thr81, Ala83 and Ala84 were observed, suggesting that perhaps the missing cysteine NH resonances experienced severe

chemical shift perturbation due to cadmium addition. For Zn_2Cd_4 species, only two cadmium sites (X and Y) were observed in 2D [^{1}H, ^{111}Cd] HSQC NMR spectroscopy. Only one cysteine – Cys46 connectivity was identified for Site X. Three cysteine connectivities were observed for site Y, corresponding to Cys54, Cys52 and Cys48. Initially, a model was prepared using all the experimental data - Cys54, Cys52, Cys48 and Cys46, then further likely ligands were connected to site X and Y. Finally, site Z was connected to the remaining 3 cysteines and then the most likely bridging residue was chosen. The connectivity for the final model was site Y (Cys46, Cys48, Cys52 and Cys54), Site X (Cys46, Cys54, Cys73 and Cys77) and Site Z (Cys71, Cys77, Cys79 and Cys81) where Cys46 and Cys54 were bridging sites X and Y to form a binuclear cluster, and with Cys77 bringing sites X and Z.

4.9 Studies with MT4a

4.9.1 Peaks assignment: [^{1}H, ^{15}N] HSQC

With the aid of 2D TOCSY and NOESY and aided by the MT4b assignments, 46 amino acid residues accounting for 55% of MT4a sequence coverage have been assigned as shown in Figure 4.22. Like MT4b, the first 10 amino acid residues have not been assigned. Importantly, all the metal binding residues - cysteines and histidines – have been assigned, thus in principle, this partial assignment will provide adequate information to study the metal-ligand connectivities and cluster dynamics (chapter 5 and 6).

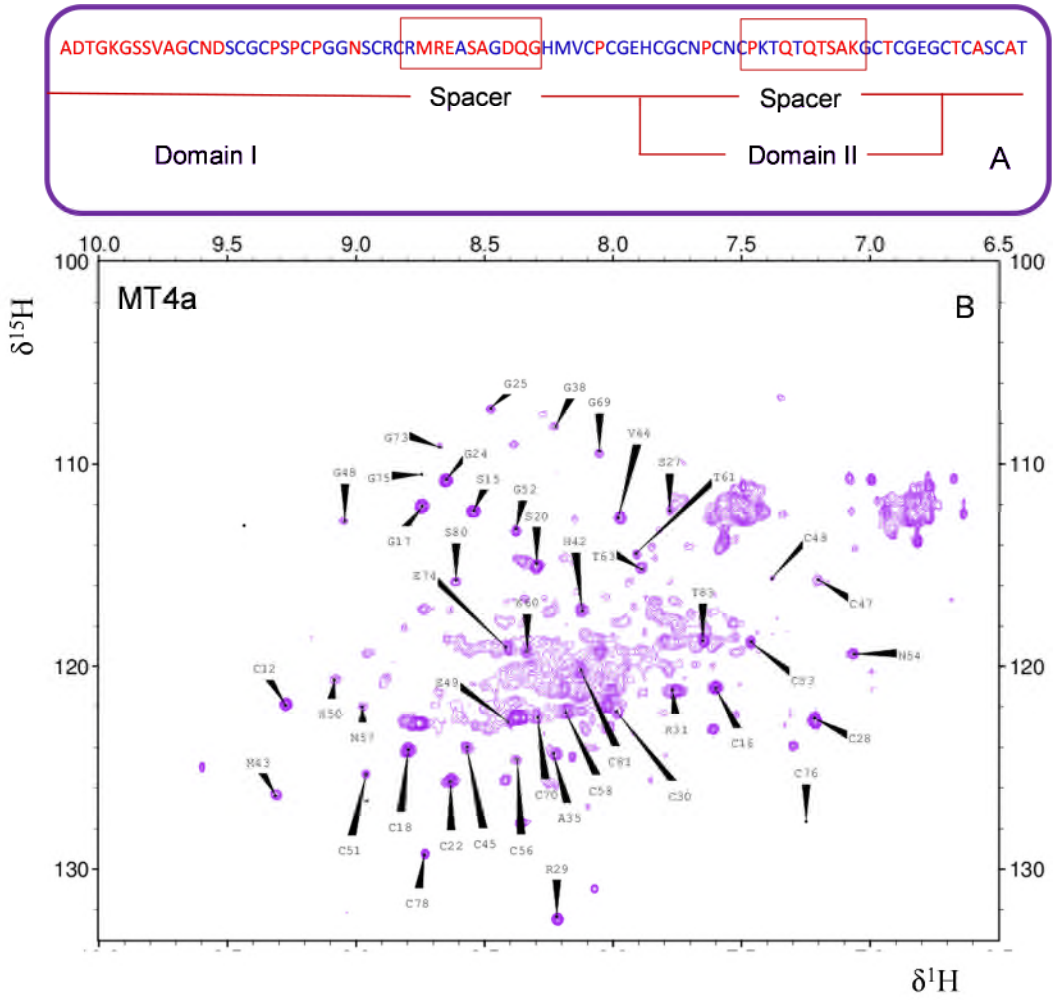

Figure 4.22 Assignment of MT4a. (A) Schematic sequence coverage diagram (B) partially assigned [^{1}H, ^{15}N] HSQC spectrum. Among the 83 amino acids, 46 residues were assigned including all cysteines and the two histidines, giving 54% of sequence coverage.

4.9.2 Involvement of histidines to zinc coordination

The extended region [^{1}H, ^{15}N] HSQC spectrum suggests that the two histidines, His42 and His50, bind zinc through Nδ1 and Nε2, respectively, very similar to MT4b. Because of the very similar Zn-to-histidines coordination patterns observed for MT4b and MT4a, it is thus plausible that MT4a will also form a mononuclear $ZnHis_2Cys_2$ site involving two cysteines - Cys56 and Cys58.

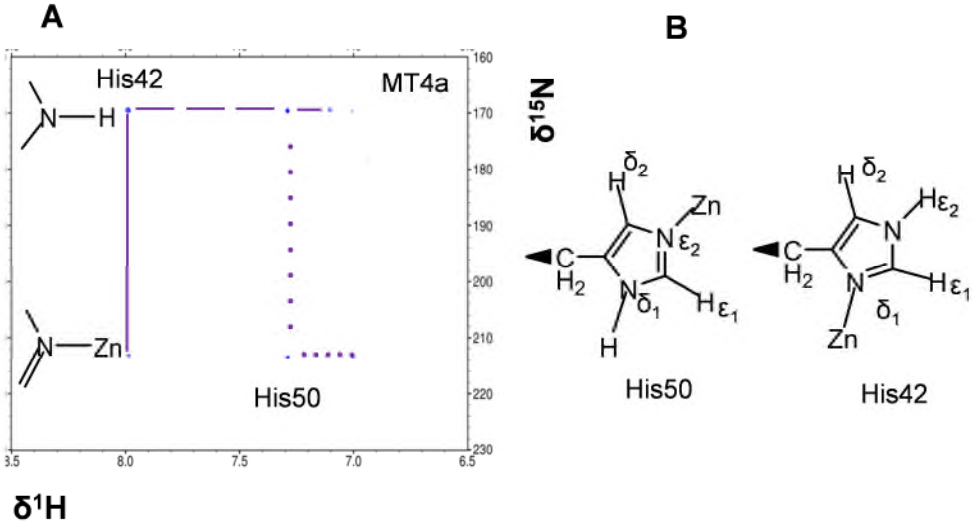

Figure 4.23 Histidine coordination to zinc in MT4a, as revealed by extended [^{1}H, ^{15}N] HSQC spectra. (A) The 2-bond-coupling crosspeaks between imidazole Ne2 and Nd1 nitrogens and He1 and Hd2 protons for zinc-coordinated His42 (purple solid line) and His50 (purple dotted line) are shown. (B) Schematic representation of zinc-coordinated histidine residues illustrating that His42 binds zinc through Nδ1 and His50 through Nε2, as derived from the observed coupling pattern.

4.9.3 Fully exchanged cadmium form: Protein folding

Like MT4b, fully exchanged Cd of MT4a resulted in domain II misfolding. At fully Cd exchanged form, resonances only belonging to domain I were observed. However, among the metal binding residues, Cys12 resonances were not observed.

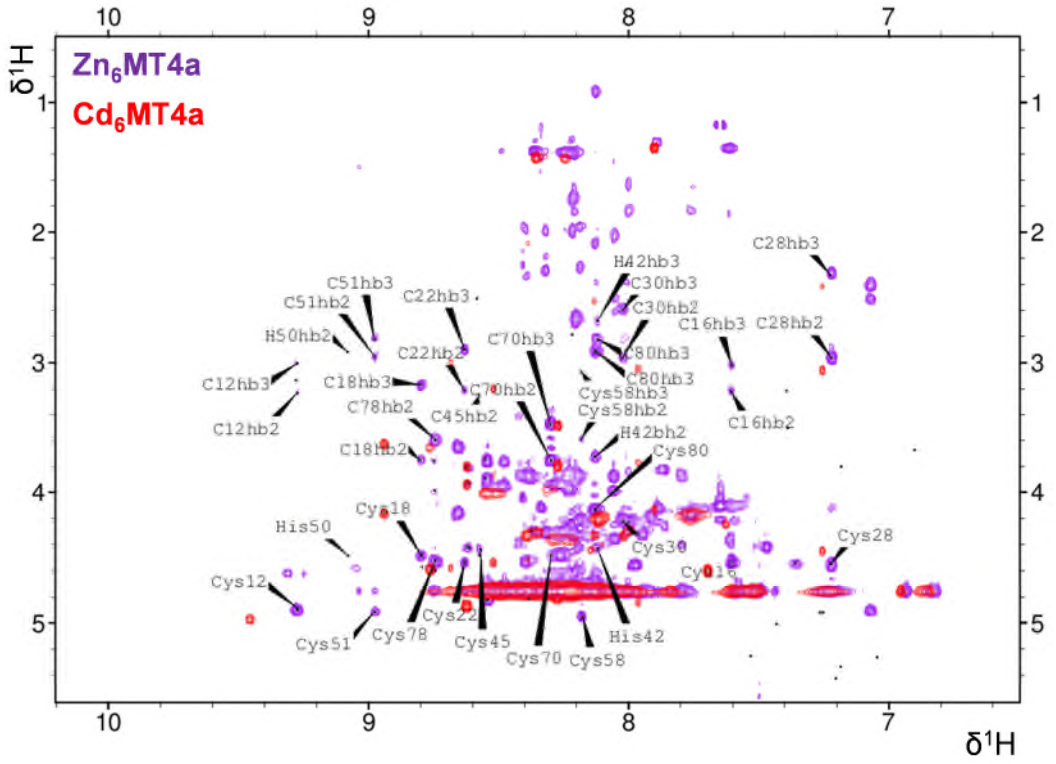

Figure 4.24 Effect of cadmium on protein folding of MT4a. Superimposed [^{1}H, ^{1}H] TOCSY spectra of **Zn_6MT4a** and **Cd_6MT4a.**. Spectra were recorded at 25 °C (0.8 mM protein, 50 mM Tris-D_{11}, 10 % D_2O, 50 mM NaCl, pH 7.42).

4.9.4 Exchange with cadmium: Mixed metal species

To investigate whether MT4a exhibited similar Cd exchange properties like MT4b, Cd exchange with Zn saturated MT4a was monitored by UV-Visible spectroscopy and mass spectrometry, the ultimate goal was to screen for mixed metal species.

Addition of Cd^{2+} (1-9 equivalents) to Zn_6MT4a produced characteristic Cd-thiolate bands at 254 nm suggesting replacement of Zn^{2+} by Cd^{2+}. The plot of equivalents of Cd^{2+} added against absorbance change at 254 nm, showed saturation at 8 equivalents of Cd^{2+} suggesting MT4a binds up to 8 Cd^{2+} ions. The

reason yet again could perhaps be small error in concentration either for MT4a or for Cd^{2+} solution.

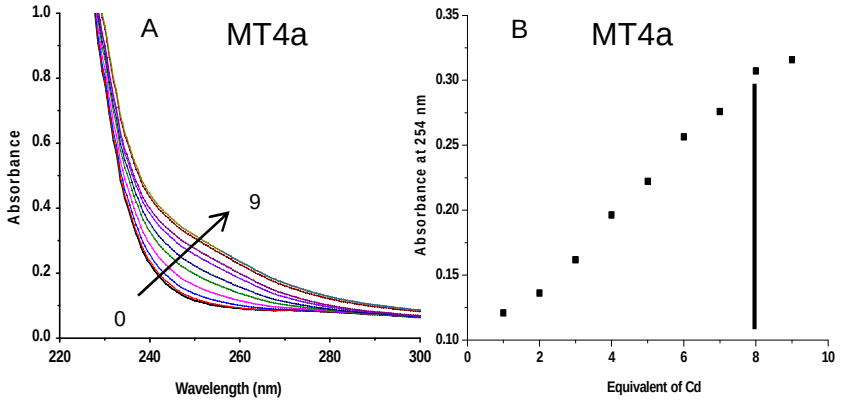

Figure 4.25 Cadmium replacements to Zn from of MT4a monitored by UV-Visible spectroscopy. Raw spectra (A) MT4a recorded up to 9 equivalents of cadmium addition. (B) Absorbance changes vs equivalents of cadmium addition as measured at 254 nm for Cd-thiolate bonds. Proteins samples (2µM, 0.2M Tris buffer, pH 7.58).

Metal speciation by mass spectrometry suggests addition of Cd^{2+} resulted in formation of different metallo species. Yet again, at 4 equivalents of Cd^{2+}, Zn_2Cd_4 metallo species was found predominant. Although a Cd_6 species was formed at 7 equivalents of cadmium (perhaps tiny concentration error), NMR spectroscopy revealed that protein was mostly unfolded in the fully Cd exchanged form as shown in Figure 4.24.

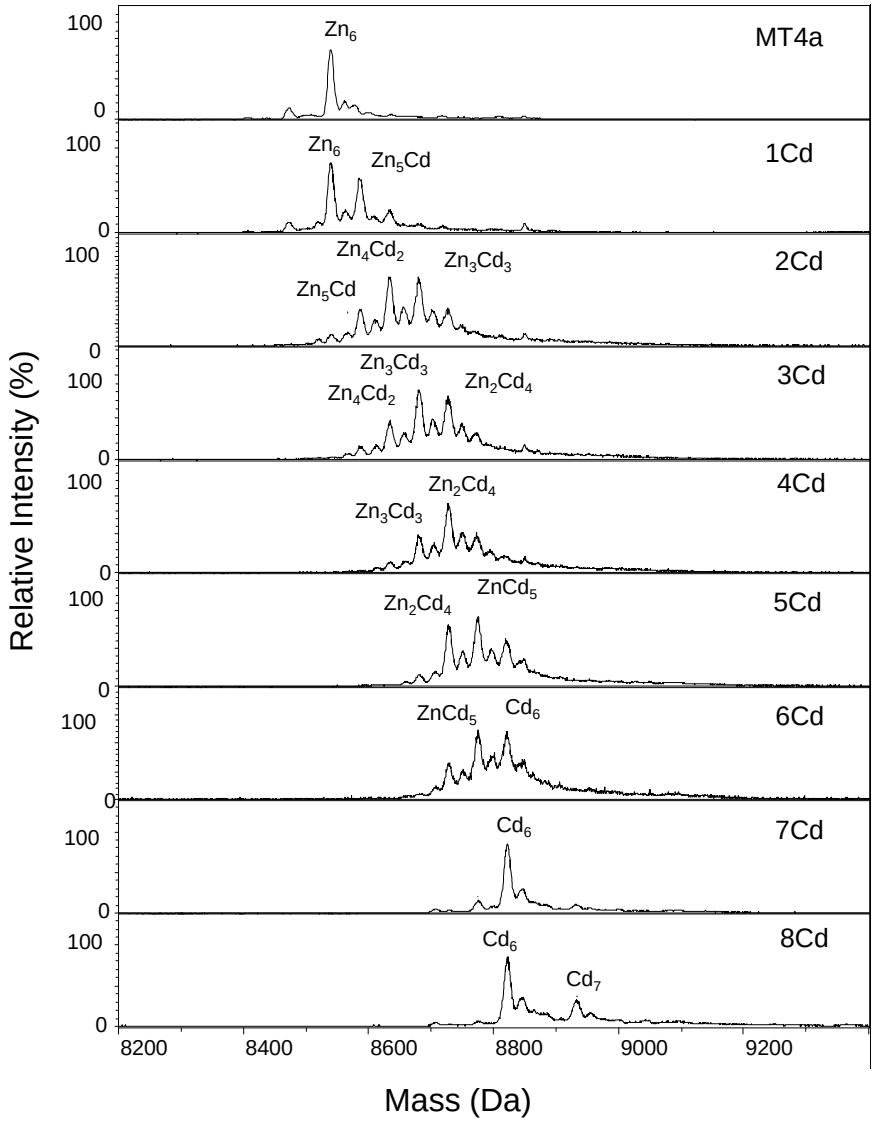

Figure 4.26 Deconvoluted mass spectra of MT4a at different Cd stoichiometry. Protein samples for mass spectra were prepared as (25µM, 10% v/v CH_3OH, 10 mM NH_4HCO_3 buffer, pH 7.8).

4.9.5 Mixed metal species: Protein folding and metal-ligand connectivity

At 4 equivalents of Cd^{2+} resonances from His42, His50, Cys56 and Cys58 constituting the mononuclear site were observed. Many other metal binding residues from domain II were observed for MT4a at 4 equivalents of cadmium, particularly, Cys51, Cys80, Cys70, Cys45 and Cys78 resonances. All but cysteine

12 resonances from domain I were also observed. The result was consistent with that was observed for MT4b.

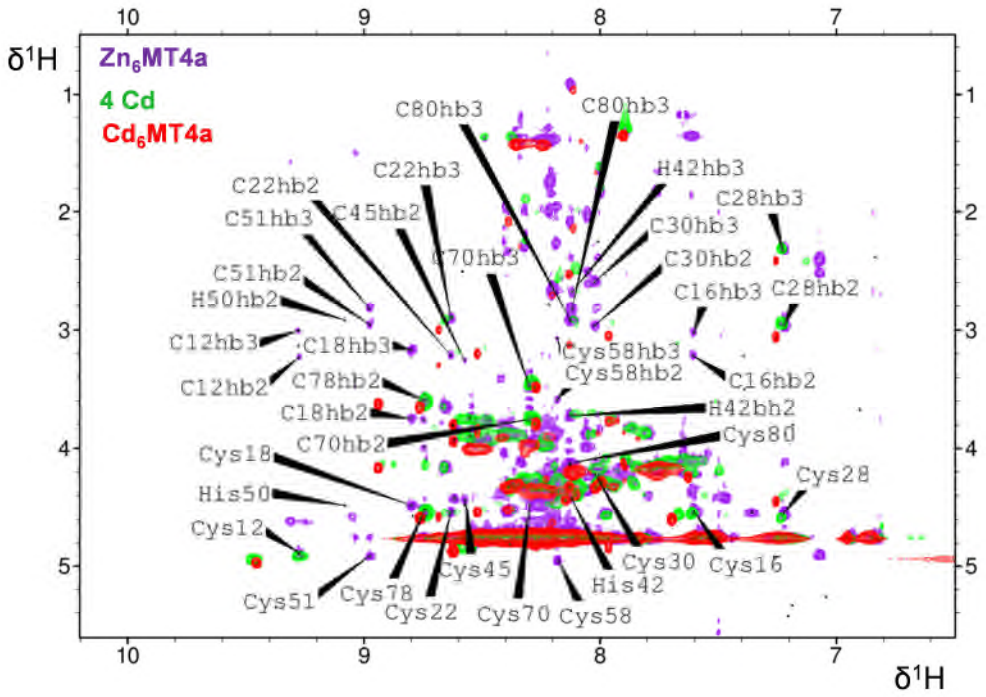

Figure 4.27 Comparison of protein folding. [^{1}H, ^{1}H] Superimposed TOCSY spectra of **Zn_6MT4a**, **4 Cd** and **Cd_6MT4a.** Spectra were recorded at 25 °C (0.8 mM protein, 50 mM Tris-D_{11}, 10 % D_2O, 50 mM NaCl, pH 7.42).

1D ^{111}Cd and 2D [^{1}H, ^{111}Cd] HSQC NMR spectra of 4 equivalents of Cd produced 5 well resolved peaks at 640.5 ppm assigned as site A2 for Cd site in domain I having Zn neighbour (D I, Zn-Cd), peak at 649.1 ppm for B2 (D I, Zn-Cd), peak at 652.0 ppm for site A (D I, Cd-Cd), peak at 656.6 for site B (D I, Cd-Cd) and peak 682.0 ppm for site Y (D II, Cd-Cd). For MT4a no site X was observed as it was observed for MT4b. However, differences in the peaks chemical shifts were observed, for site A resonance was observed at 652.0 ppm for MT4a but for MT4b that resonance was observed at 654.2 ppm, 2 ppm higher than MT4a. However, Site B resonances remained very close at 656.6 and 656.3

ppm for MT4a and MT4b respectively. Similar result observed for Zn neighbouring Cd site of A as assigned A2, for which resonances observed at 640.5 ppm, some 2.6 ppm lower than A2 resonances of MT4b. Resonances for Site B2 for both isoforms were very similar with values of 649.1 and 650.1 ppm for MT4a and MT4b respectively. Moreover, site

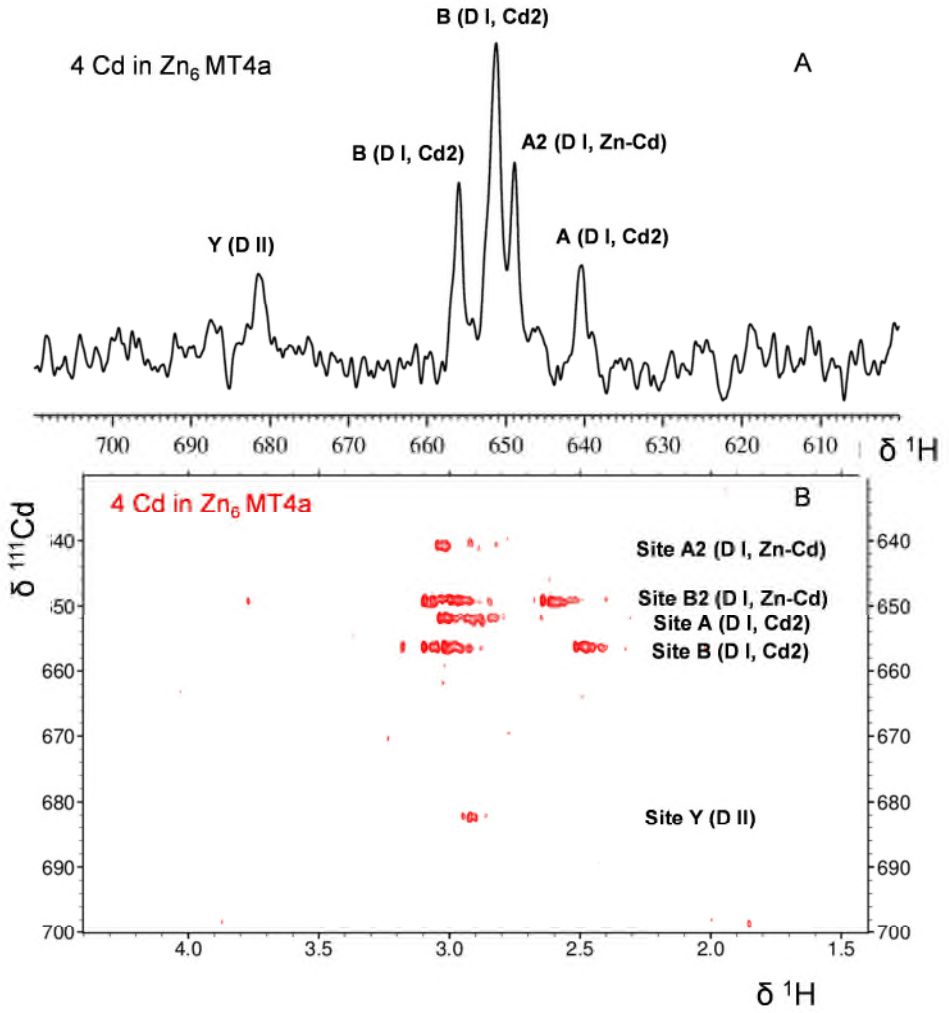

Figure 4.28 1D and 2D ^{111}Cd NMR spectra of mixed metal species at 4 equiv. mol $^{111}Cd^{2+}$. (A) 1D^{111}Cd NMR spectra of MT4a at 4 equivalents of cadmium- peaks from domain I and domain II have shown. (B) 2D [^{1}H, ^{111}Cd] HSQC NMR spectrum **4Cd in Zn_6MT4a** illustrates -CH_2 (β)-^{111}Cd connectivity. Spectra recorded at 25 °C (1-1.5mM protein, 50 mM Tris-D_{11}, 10 % D_2O, 50 mM NaCl, pH 7.42).

Table 4.4 1D ^{111}Cd NMR resonances observed in fully exchanged and mixed metal species of MT4a.

Species	Number of peaks	111Cd chemical shifts Ppm				
		640.5 A2 (D I, Zn-Cd)	649.1 B2 (D I, Zn-Cd)	652.0 A D I, Cd-Cd)	656.6 B D I, Cd-Cd)	682.0 Y DII, Cd-Cd)
3 equiv Cd^{2+}	4	√	√	√	√	×
4 equiv Cd^{2+}	5	√	√	√	√	√

Y resonances were also very close at 682.0 ppm for MT4a and 681.6 ppm for MT4b. Apart from little differences in resonances for site A, observed ^{111}Cd resonances sites were very similar for MT4a and MT4b, thus it was plausible that perhaps MT4a will also adopt similar connectivity pattern as it was applied for MT4b.

4.10 Homology models

Homology models of domain I and domain II of MT4a and MT4b were constructed using the published structures of the two domains of wheat E_C (Loebus et al., 2011; Peroza et al., 2009) as templates. Wheat E_C was selected as template because E_C is a homolog of MT4a and MT4b and importantly, they have fully conserved metal binding residues (Cys and His), and for E_C, solution NMR structures are available. Nevertheless, a search for template was carried out using MT4a and MT4b sequences by the Phyre2 (Kelley et al., 2015) homology search engine. Unsurprisingly, the Phyre2 result suggested that the wheat E_C structures

are the best templates. However, for domain I, three structures are available in the protein data bank (PDB) - 2L61, 2L62 and 2MFP. 2MFP is modified circular domain 1, and was therefore not considered as template. The other two structures comprise 26 residues, and while 2L61 contains $Cd^{2+,}$ 2L62 contains Zn^{2+} as bound metals. For both structures, Phyre2 gave 59% identity over 24 residues. Thus to generate homology models for zinc-containing domain 1, 2L62 was selected as a template. To generate models for domain II, 2KAK (containing Zn^{2+}) was used as template.

4.10.1 Model of Domain I

Domain I consists of 33 residues starting from the N-terminal alanine. However, the first 10 residues, ADTGKGSSVAG for MT4a and ADTGKGSSVAG for MT4b, which were not present in the template, were found disordered in the model. However, in the model a small helix was observed for both isoforms formed by residues 14-16 corresponding to DSC and DRC for MT4a and MT4b, respectively. Within the models, metals were incorporated based on the Cd-Cys connectivities observed in 2D [^{1}H, ^{111}Cd] HSQC spectra. Ligands were connected to Zn to produce a tetrahedral geometry. Cys18 had been identified as a bridging ligand; this is also consistent with the connectivities observed in the template. The other most likely bridging ligand is Cys12 which is also in agreement with the template, but Cys30 was also a possible bridging ligand. The terminal residues for one Zn centre (site A) were Cys22 and Cys28, and the remaining two cysteines,

Cys16 and Cys30, connected to the other Zn centre (site B) to form a binuclear metal cluster. Similar clusters were observed for E_C domain I.

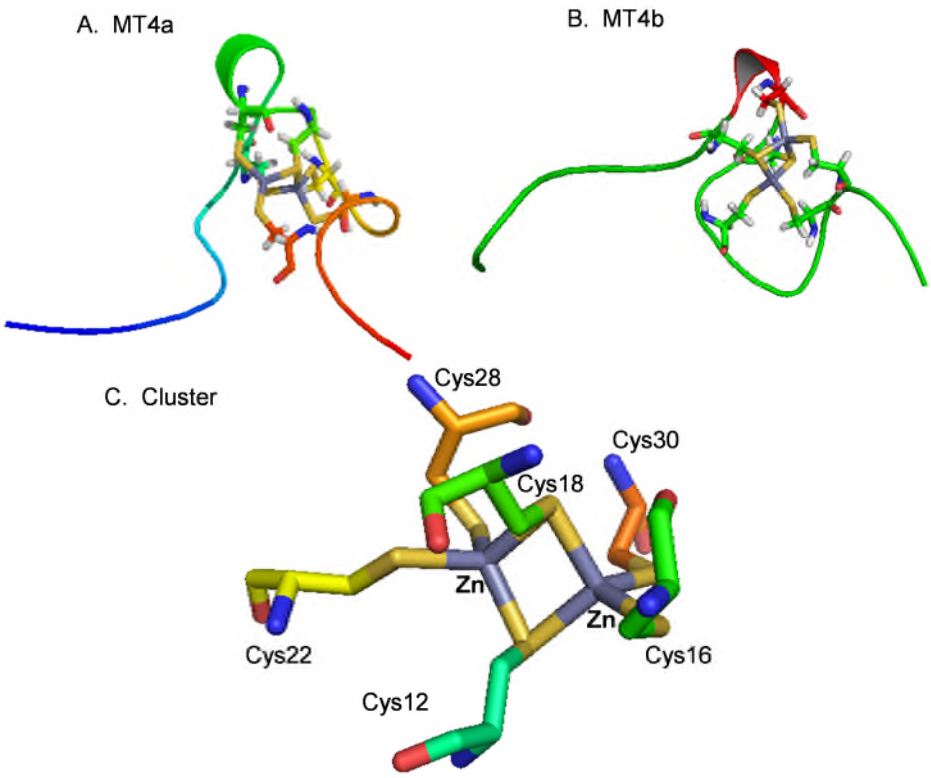

Figure 4.29 Homology models and cluster structures of Domain I of MT4a (A) and MT4b (B). (C) The binuclear metal cluster with name and number of metal binding ligands is shown. Models were constructed using wheat E_C domain I (PDB 2L62) as a template. Figures were prepared using PyMOL.

The final protein structures were validated by the program WHATIF and were found to be acceptable. It was also suggested that chirality, dihedral angles, tau angles and side-chain planarities were within normal regions after incorporation of Zn. Comparison of the models of MT4a and of MT4b domain I with the template structure highlights some differences. The amino acid residues belonging to the region 1-10 are not present in the template (E_C). Therefore, these sections are modelled de-novo, which is highly unreliable. The dissimilarities observed for MT4a and MT4b, together with the fact that no sequential assignments could be

obtained for them, is consistent with the suggestion that this stretch of the proteins is disordered and flexible. Furthermore, both MT4a and MT4b formed a small helical structure comprising residues DSC and DRC, however, such a structure had not been observed for E_C. In the region of 17-21, there was homogeneity in structural motifs observed for the three proteins.

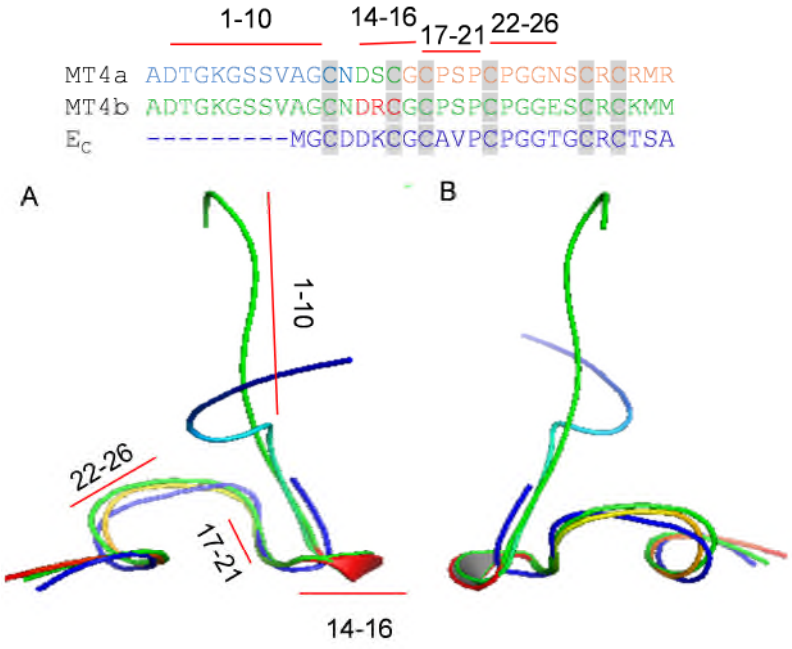

Figure 4.30 Comparison of homology models with template E_C domain I (PDB 2L62). MT4a is shown with the backbone in green, MT4b in red, and the template in blue. Figures were prepared using PyMOL.

However, all three proteins show distinctive differences in the region of 22-26. Calculated RMS value of deviation between MT4a and MT4b was 1.98 Å and with template was 1.07 Å as produced by the program PyMOL.

4.10.2 Model of domain II

Domain II comprises 44 residues. Zn was incorporated into the model generated by homology modelling, initially with known connectivities as determined from

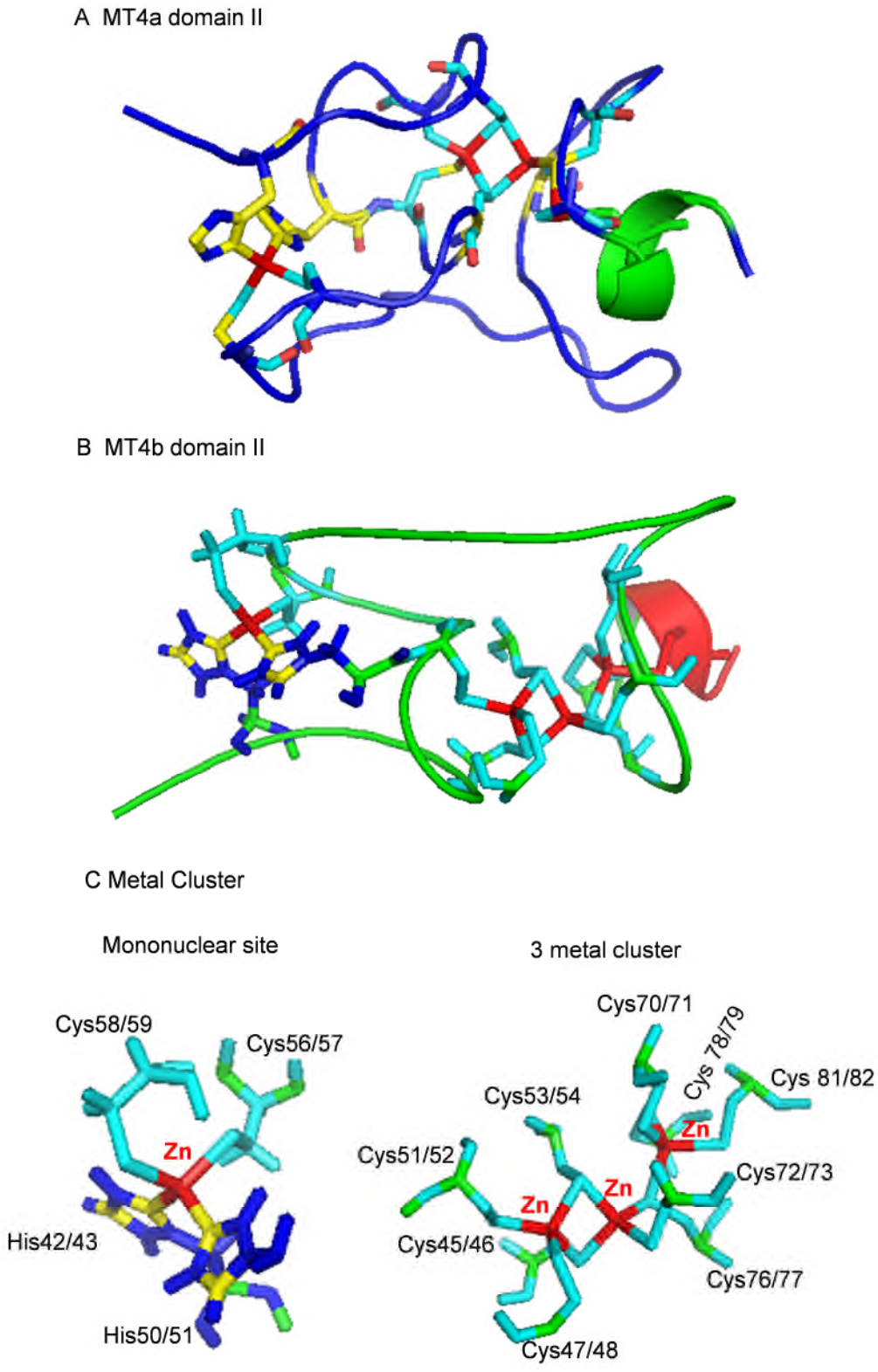

Figure 4.31 Homology model and cluster structure of Domain II of MT4a (A) and MT4b (B). (C) Metal cluster- mononuclear site and 3 metal cluster: name and number of metal binding ligands are shown. Models were constructed using wheat E_C domain II (PDB 2KAK) as a template. Figures were prepared using PyMOL.

2D [^{1}H, ^{111}Cd], 2D TOCSY, NOESY and ^{15}N HSQC. All other sites were then connected based on shortest Zn-thiolate distances, and an acceptable Zn-thiolate cluster was suggested. The metal-connected model was then checked with WHATIF.

In comparison with the template, the shapes of the models were found similar, but deviations were noticed. Observed RMS value was 2.60 Å, as evaluated by PyMOL. Deviations observed are perhaps due to the presence of gap in the cysteine-free region. Both for template and for MT4a and MT4b, a helical structure was detected near the C-terminal region. However, in the region of 55-64 there was structural homogeneity observed.

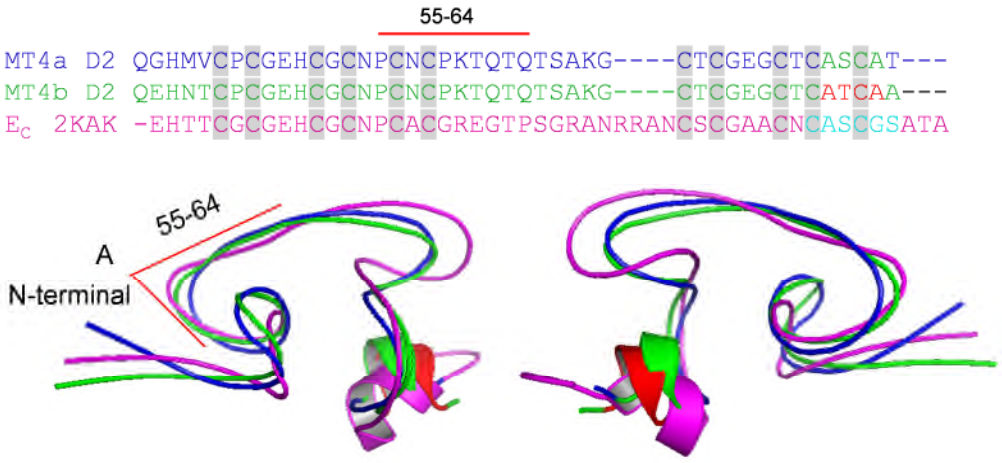

Figure 4.32 Comparison of homology models with template E_C domain II (PDB 2KAK). MT4a is blue with green helix, MT4b is green with red helix and template is in magenta. Figures were prepared using modelling program PyMOL

In summary, both MT4a and MT4b were well folded in the presence of Zn^{2+}, and for the Zn^{2+} form of the proteins 54 and 84 % of sequential assignment has been completed for MT4a and MT4b, respectively. Like their homolog from wheat E_C,

a mononuclear Zn^{2+} binding site of $ZnHis_2Cys_2$ has also been identified in MT4a and MT4b. In the Cd^{2+} saturated proteins, non-isostructural Zn^{2+} replacement for domain II has been observed, resulting in misfolding of domain II. However, well-folded domain I was observed. For domain I, a binuclear cluster of $Zn_2Cys_{6,}$ similar to wheat E_C, has been proposed. The idea on exploiting mixed metal species that has been developed to study domain II, particularly the 3-metal cluster, was found to be partially successful. From the mixed-metal species at 4 equivalents of Cd^{2+}, domain I, mononuclear $ZnHis_2Cys_2$ site and 2 binding sites from the 3-metal cluster have been observed. In addition, for domain I mixed Zn-Cd sites have also been identified. Considering all the experimental connectivities and nearest cysteines distances, a cluster topology for the 3-metal cluster has been proposed – a binuclear cluster bridging to a single metal connected to three terminally bonded cysteines.

Chapter 5

Metal binding dynamics of MT4a and MT4b

5.1 Introduction

A majority of proteins require metal ions for structural or for functional purposes. MTs are among the proteins that bind metal ions, and play significant roles in metal detoxification, homeostasis and sequestration. Type 4 MTs from the plant phylum are zinc binding proteins. It has been hypothesised that the function of these proteins is to transfer or donate zinc to nascent zinc-requiring proteins or peptides during seed germination which could perhaps help germination and seedling growth. To support this hypothesis, this chapter aims to investigate zinc release from MT4a and MT4b and zinc transfer to the metal chelators Ethylediaminetetraacetic acid (EDTA) and 4-(2-pyridylazo)resorcinol (PAR) as mimics of biomolecules. It will also discuss the influences of pH variations and effects of phytate on zinc binding dynamics of MT4a and MT4b. Of particular interest was to find out whether these two very similar protein isoforms differ in their metal binding dynamics.

5.2 Zinc binding dynamics: Effects of pH variation

Metal clusters, specifically the metal-sulfur bonds in MTs, have characteristic charge-transfer bands which can be easily detected by UV-Visible spectroscopy. Zn-thiolate clusters give rise to a shoulder at 220-230 nm for the sulfur ligand-to-metal-charge-transfer (LMCT) transition (Freisinger, 2007). Protons compete with metal ions for thiolates, leading to the release of metal ions. Addition of acid causes the release of the metal ions thus lowering the absorbance due to Zn-thiolate bonds which is reflected in Figure 5.1 (A and B).

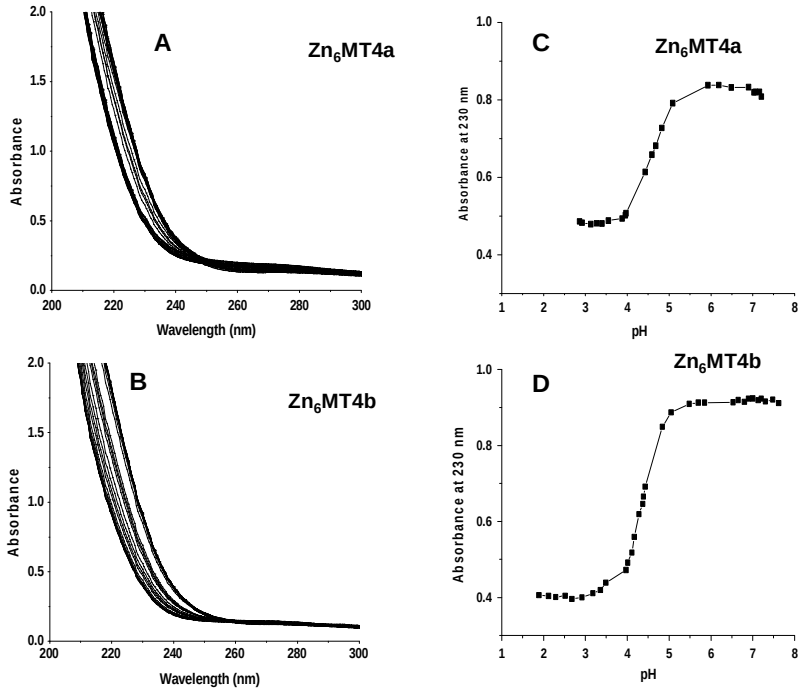

Figure 5.1 Influence of pH change on Zn forms of MT4a and MT4b studied by UV-Visible spectroscopy. Raw spectra (absorbance against wavelength) (A) Zn_6MT4a and (B) Zn_6MT4b recorded at different pH values with protein concentration of 10 µM in 1 mM Tris-Cl buffer. Absorbance changes with pH measured at 230 nm for Zn-thiolate bonds (C) Zn_6MT4a (D) Zn_6MT4b.

The pH stability of the cluster is expressed by means of apparent pK_a values, which is defined as the pH value at half maximum UV absorbance ½(A_{max} + A_{min}) of the respective ligand-to-metal-charge transfer band. The study of apparent pK_a values has long been used as a means of characterising different MTs. The pH of half-dissociation values are similar for all MTs, around 3 for Cd forms, and 4 for Zn forms. In contrast, the pH at which metals begin to be released is characteristic for a particular MT. For the determination of the half-dissociation constant, the absorbances at 230 nm were plotted against pH as shown in Figure 5.1 (C and D). From the plots, the pK_a values were found to be 4.55 and 4.56 for Zn-loaded MT4a and MT4b, respectively. These values were similar to the values of 4.70 and 4.68, observed for their homolog E_C from wheat, measured by two independent experiments (Leszczyszyn et al., 2007b; Peroza and Freisinger, 2007). It should be noted that the value 4.7 was measured by AAS in 10 mM ammonium acetate buffer while 4.68 was determined by UV-Visible spectroscopy in 1 mM Tris-Cl buffer with 10 mM NaCl. In the present study, 1 mM Tris-Cl and UV-Visible spectroscopy was used. However, pK_a values of MT4a and MT4b were yet higher than the values observed for mammalian MTs which lie around 4.3-4.4 (Jiang et al., 2000) and 4.1 for bacterial SmtA (Blindauer et al., 2002). This observation suggests that the two *A. thaliana* MT4 isoforms have lower zinc affinities compared to MTs from other phyla, but have comparable values to other plant MTs including 4.94 for *C. arietinum* MT1 (Schicht and Freisinger, 2009), 4.51 for *C. arietinum* MT2 (Wan and Freisinger, 2009), and lower than 5.41 for *P. sativum* MT1 (Tommey et al., 1991). Another intriguing feature observed in Figure 5.1 (C and D) was the shape of the curves. It was apparent from the

Figures 5.1 (C and D) that down to pH 6, both proteins isoforms were very much in stable form. However, within one pH unit, from 5 to 4, there was a very sudden drop of absorbance observed. Absorbance for MT4a dropped from ~0.81 to ~0.45, and for MT4b, absorbance dropped from ~0.87 to ~0.48. The sharp change in absorbance within a rather narrow pH range may suggest that clusters collapse co-operatively. Furthermore, more subtle differences in the curve shapes indicated that there could perhaps be a difference in metal release from the two isoforms.

In order to find out which different metallo-species formed upon pH changes, mass spectrometry was used (Figure 5.2). Metal speciation by mass spectrometry demonstrated that there were indeed differences in proton-induced metal release from MT4a and MT4b, as formation of different metallo-species at comparable pH values was observed. At pH ~6.4, both isoforms contained predominantly Zn_6 species, suggesting intact folded proteins. The changes in speciation occurring between pH 4.90 and 4.40 for MT4a, or between pH 4.80 and 4.20 for MT4b, were quite dramatic. A predominant Zn_5 metalloform was observed for MT4b at pH 4.76, while Zn_2 became the major species for MT4a already at pH 4.90. Interestingly, at this pH value, the Zn_6 species had almost completely disappeared and the apo-form was the second-most abundant species for MT4a. In contrast, for MT4b at pH 4.76, the Zn_6 species was still present, but no apo-form was observed. However, both isoforms produced under-metallated species of Zn_4, Zn_3, and Zn_2 at pH 4.76 or 4.90. Surprisingly, a new over-metalled Zn_7 species was observed for MT4b at pH 4.76. The reason for the formation of over-metallated species is not clear but was also evident in human MT3 (Palumaa, 2005). Further lowering the pH to 4.41 for MT4a resulted in formation of apo-MT4a as

dominating species, along with under-metallated species of Zn_1, Zn_2 Zn_3 and a very low abundance Zn_4 species. For MT4b at pH 4.20, the apo form also became the major species, followed by Zn_2 as the second-most abundant species, with the Zn_6 species almost completely disappeared. At pH 2.37 for MT4a and 2.76 for MT4b, the apo forms were the major species, but interestingly, the Zn_1 species was still observed for both isoforms, albeit at very low abundance.

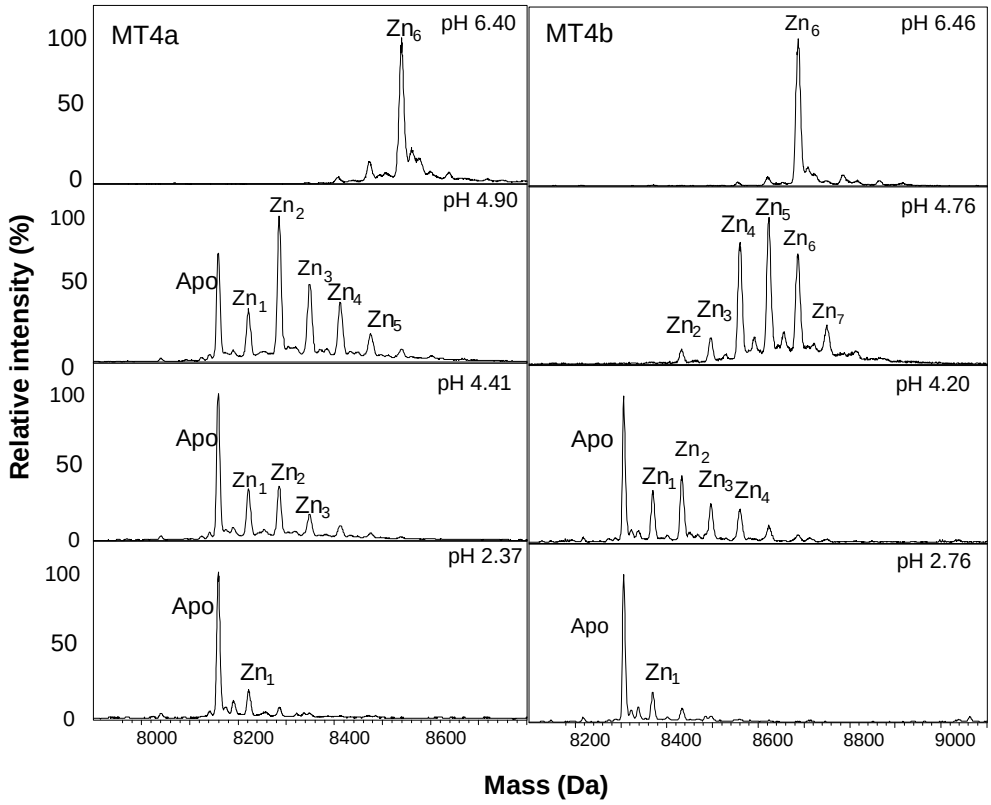

Figure 5.2 Deconvoluted mass spectra of MT4a and MT4b at different pH values. Protein samples for mass spectrometry were 25 µM, in 10 mM NH_4HCO_3 buffer with 10% v/v CH_3OH. The pH was lowered by incremental addition of HCOOH.

Furthermore, 1D ^{1}H NMR spectroscopy was used to investigate the nature of proton attack on MT4s and the consequences of zinc-thiolate cluster reactivity on protein folding. Interestingly, ^{1}H NMR spectroscopy data suggested that proton

competition with zinc resulted in domain-specific zinc release from these two isoforms. ^{1}H NMR data suggested that initially zinc was preferentially released from domain II for both the isoforms, as displayed in Figure 5.3.

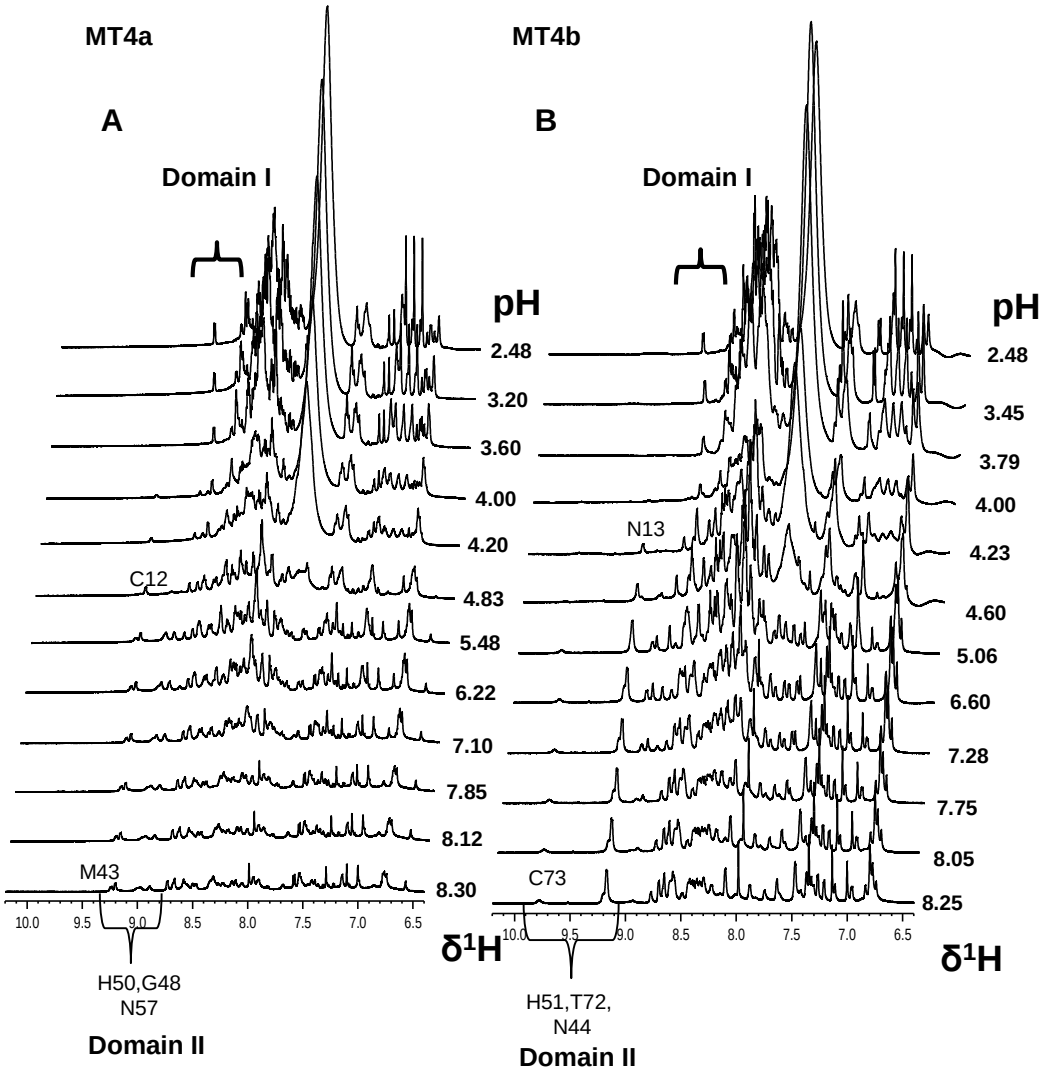

Figure 5.3 Stacked plot of 1D ^{1}H-NMR spectra of MT4a and MT4b at various pH values recorded at 700.24 MHz and 298 K. Disappear or decrease in peaks intensity belongs to Domain II and Domain I suggested domain specific reactivity of MT4a and MT4b upon pH variation.

In Figure 5.3 (A), peaks resonating in the downfield region around of 9.27 and 8.80 ppm belong to backbone NH resonances of MT4a domain II residues, and

were found to disappear first with lowering the pH. However, one peak at 9.26 ppm originating from domain I was Cys12 and persisted down to pH 4.0. A very similar trend was also observed for MT4b as shown in Figure 5.3 (B). A peak at 9.78 ppm for Cys73 disappeared with lowering the pH to 4.6. The intense peaks between 9.24 and 9.11 ppm were the resonances for NH of His51, Thr72, Asn44 and Asn13, whereas the peak that was still observed at pH 4.23 was likely Asn13 of domain I. It was also evident from Figure 5.3 that abrupt changes happen between pH 5 and 4, as intense broad peaks observed in the random coil region suggested a transition from folded to unfolded proteins. These observations thus also supported the results from observed mass spectrometry and UV-Visible data (Figures 5.1 and 5.2)

Development of the Zn_5 species for MT4b (Figure 5.2) as observed by mass spectrometry and the conclusion from ^{1}H NMR spectroscopy suggesting that zinc was initially released from domain II, indicated that (at least) one of the four zinc sites within domain II was most labile to initial proton attack. However, it was not clear whether this single labile site was the mononuclear site or from the three-metal cluster. During the pH changes from 6.46 to 4.20, the MS spectra did not reveal dominating peaks corresponding to either fully loaded domain II, which would show up as a Zn_4 species, or fully loaded domain I, which is expected to be seen as a Zn_2 species. This would suggest a non-cooperative metal release from both domains of MT4b. For MT4a, the major Zn_2 species observed at pH 4.90 by mass spectrometry might correspond to the fully loaded domain I, suggesting cooperative metal release from both domains of this isoform, with domain II being significantly more pH-labile than domain I. Upon pH variation, domain

specific and non-cooperative metal release was previously observed for E_C from wheat (Leszczyszyn and Blindauer, 2010). However, the observed result was quite different from those in the present work, where E_C domain II released two zinc ions at pH 5.5 to produce an abundant Zn_4 species, yet with complete disappearance of domain II backbone NH resonances.

Finally, an increase in pH value from ~2.5 to neutral regenerated spectra that looked very similar to the native ones as shown in Figure 5.4. This indicates that pH-induced metal loss and unfolding is likely fully reversible. However, it would be interesting to find out whether regenerated MTs behave in completely similar ways as native proteins.

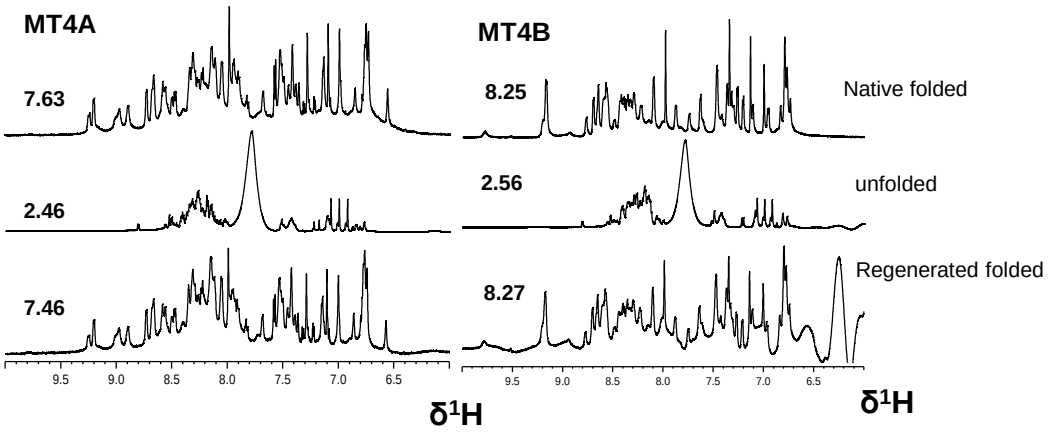

Figure 5.4 1D ^{1}H NMR spectra of regenerated MT4a and MT4b. Increase in pH from ~2.5 to 7.46-8.27 results in regeneration of native-like proteins.

In the case of mammalian MTs, doubts about this question have led to recent controversies (Ejnik et al., 2010; Jiang et al., 2000).

5.3 Zinc transfer to Ethylediaminetetraacetic acid (EDTA)

The metal chelator EDTA has long been used as a mimic of metal-binding proteins as it contains both amine and carboxyl groups as found in amino acids (Li et al., 1980). EDTA has been used in this study to get insights into the metal transfer dynamics of MT4a and MT4b, as the affinity constant of log K = 16.5 for the Zn(EDTA) complex is higher than that of Zn-MTs (Leszczyszyn and Blindauer, 2010), particularly for wheat Zn_6-E_C, an affinity constant of log K = 8.6 (Leszczyszyn et al., 2007b) was observed. Zinc transfer to EDTA was monitored as a decrease in absorbance of Zn-S bonds at 220 nm using UV-Visible spectroscopy. However, reactions were performed at three different EDTA concentrations of 0.05 mM, 0.25 mM and 0.5 mM respectively, with a fixed protein concentration (5 µM) to understand the EDTA dependence on metal transfer as displayed in Figure 5.5. It was apparent from Figure 5.5 (A) that MT4a transferred zinc faster than MT4b, as there were clear differences observed between the curves for MT4a and MT4b. In the case where a large excess of EDTA (0.5 mM; 100-fold excess compared to protein concentration) was used for the reaction, data were fitted to pseudo-first order kinetics to quantify the reaction rate. Fitted data suggested that MT4a followed essentially monophasic kinetics with a reaction rate of 5.2×10^{-4} s^{-1}. Interestingly, zinc transfer from MT4b appeared biphasic with an initial faster step followed by a slower step. The reaction rate calculated for step 1 was 2.1×10^{-4} s^{-1} and for step 2, was1.1×10^{-4} s^{-1}. Observed reaction rates clearly suggested that initial zinc release from MT4a was almost 2-fold faster than from MT4b.

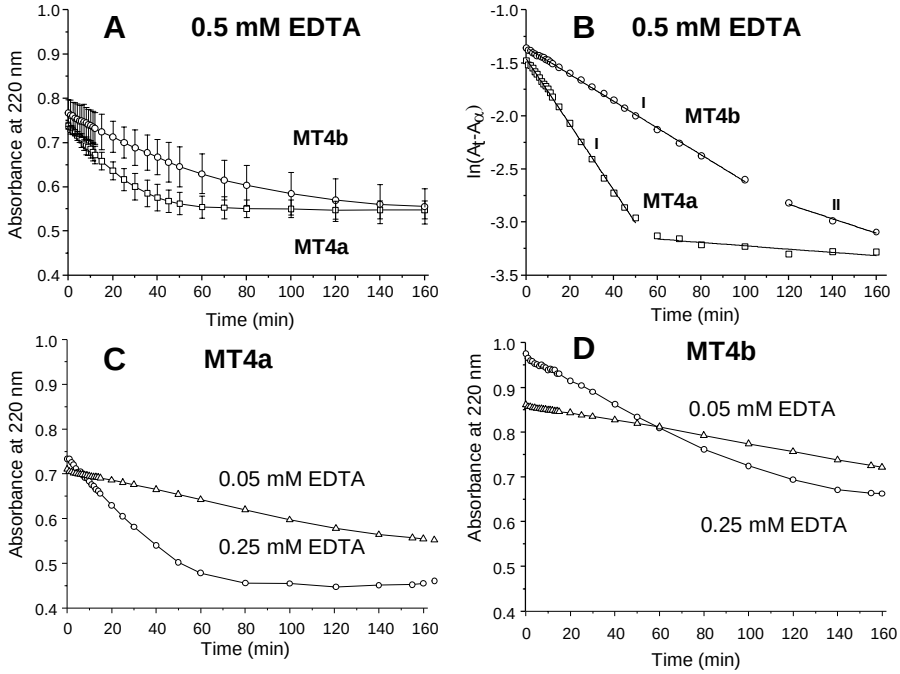

Figure 5.5 Reactions of MT4a and MT4b with EDTA. (A) Comparison of time course reactions of MT4a and MT4b with 0.5 mM EDTA. (B) Pseudo-first order reaction kinetics of MT4a and MT4b with 0.5 mM EDTA. Concentrations depending reactions: (C) MT4a and (D) MT4b with 0.05 mM and 0.25 mM EDTA respectively. In all reactions, the protein concentration was 5 µM in 25 mM Tris-Cl buffer, pH 7.33.

The results observed in this study are somewhat different from the results previously observed for E_C from wheat (Leszczyszyn and Blindauer, 2010). Under the same experimental conditions, triphasic reaction kinetics were observed for E_C where step 1 was too fast to be measured, followed by two slower reaction steps. Biphasic kinetics with a fast and a slow reaction rate were also observed for rabbit liver $^{111}Cd_7MT$ (Gan et al., 1995). Under pseudo-first order reaction conditions, multiphasic reaction kinetics were also observed for mammalian MTs (Li et al., 1980) and bacterial SmtA (Leszczyszyn et al., 2007a).

Furthermore, the reactions of MT4a and MT4b with EDTA were also found to be depending on EDTA concentration, as illustrated in Figure 5.5 (C and D). With

lowering the EDTA concentration, the decrease in absorbance at 220 nm became markedly slower. This suggests a bimolecular reaction involving direct protein-EDTA interactions.

To further extend insights on metallo-species formed during the reaction with EDTA, mass spectrometry was employed. These reactions were carried out with equimolar amounts of EDTA (with respect to zinc concentration), but at much higher protein concentrations than the UV-Vis experiments. Results obtained are presented both in qualitative and semi-quantitative way as shown in Figure 5.6. Initial metal transfer to EDTA was found to be a relatively slow process as shown in Figure 5.6 (B and C). In the first 5 minutes, metallo-species observed were predominantly Zn_6 for both isoforms (Figure 5.6 B and C - black lines). A distinct difference in zinc transfer was observed after 16 minutes (Figure 5.6 A) where the Zn_6 metallo-form of MT4a had almost completely disappeared, leading to the build-up of Zn_3 as a major species. At the same time-point, the Zn_6 species was still the major metallo-form for MT4b, along with Zn_5, Zn_4, Zn_3, Zn_2 and Zn_1 species, all with low intensities. Interestingly, and similar to the results from pH titrations (Figure 5.2), no Zn_5 metallo-form was observed for MT4a. Also, the apo-form was observed for MT4a at the 16 min time-point (Figure 5.6 A), but no apo-species was visible for MT4b. After 25 minutes, Zn_6 was still the predominant species for MT4b, closely followed by a Zn_3 species, while for MT4a, the Zn_6 metallo-form had completely disappeared. The Zn_3 species remained predominant for MT4a, along with Zn_4, Zn_2, Zn_1 and the apo-form. A semi-quantitative relative intensity measurement suggested that Zn_3 and Zn_2 contributed 55% and 40 % of

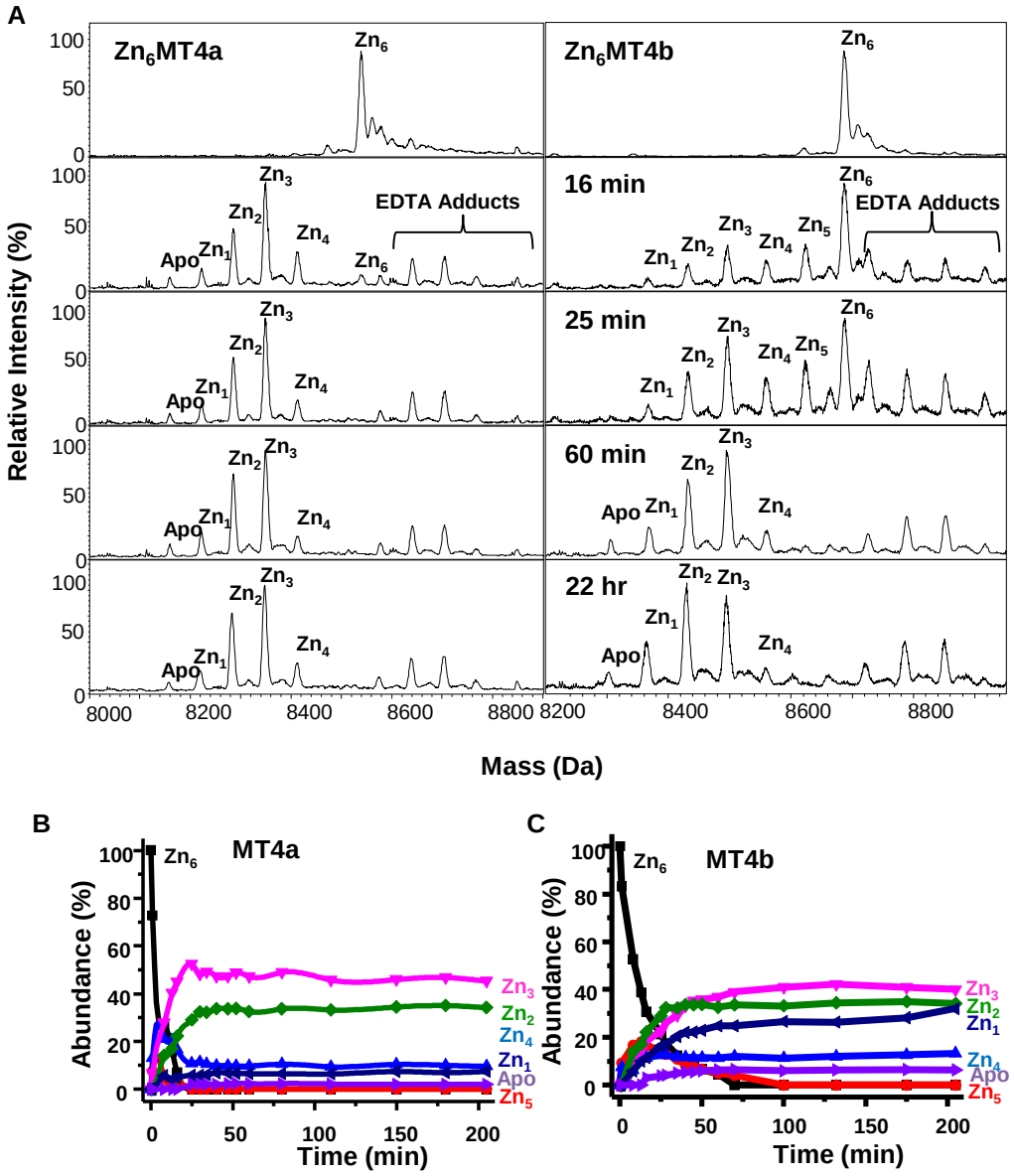

Figure 5.6 Reactions of MT4a and MT4b with EDTA studied by mass spectrometry. (A) Deconvoluted mass spectra of time dependent reactions of MT4a and MT4b with EDTA. Semi-quantitative presentation of abundances in percentages of different metallo-species formed during the time-course reactions of (B) MT4a and (C) MT4b with EDTA. Abundance (%) was calculated as relative intensity of each metallo-species formed as a function of percentage of total relative intensity of all metallo-species. Reaction conditions: desalted proteins (277 µM, i.e. 1620 µM Zn), 10 mM NH_4HCO_3 buffer, pH 7.8) were reacted with EDTA (1620 µM; 1:1 with respect to Zn).

total relative intensity for both the isoforms respectively, as shown in Figure 5.6 (B and C). One of the intriguing features was that Zn_3 and Zn_2 metallo-forms

remained as major species even after 22 hours (Figure 5.6 A), suggesting less reactive sites for metal transfer to EDTA. Formation of a less reactive site could perhaps maintain partial protein folding and may have biological significance for re-uptake of metal ions. Moreover, EDTA adducts formation was also observed, as high molecular mass peaks corresponding to MT-EDTA were observed. Adduct formation also supported the idea of direct attack of EDTA on MT4s, and hence a bimolecular reaction as observed by UV-Visible spectroscopy. EDTA adducts formation has been previously observed for SmtA (Leszczyszyn et al., 2007a) and wheat E_C (Leszczyszyn and Blindauer, 2010). However, the formation of stable Zn_3 metalloforms for MT4a and MT4b was a significant difference from the result observed for E_C from wheat for which Zn_1 species remained the major species after 150 minutes.

Subsequently, 1D ^{1}H NMR spectroscopy was used to understand the domain reactivity of MT4a and MT4b. Unsurprisingly, the observed results suggest that MT4a transferred zinc faster than MT4b, as shown in Figure 5.7. During the first 8 minutes, many of the resonances in the region of 8.80 to 9.50 ppm disappeared or were affected for MT4a as displayed in Figure 5.7 (A). Decreasing intensities of imidazole side-chain proton resonances of His42 and His50 also supported the idea that metals and ordered structure were lost from domain II. At 13 minutes, most resolved resonances from both domains had disappeared. As the reaction continued, the spectra remained almost the same, even after 65 minutes.

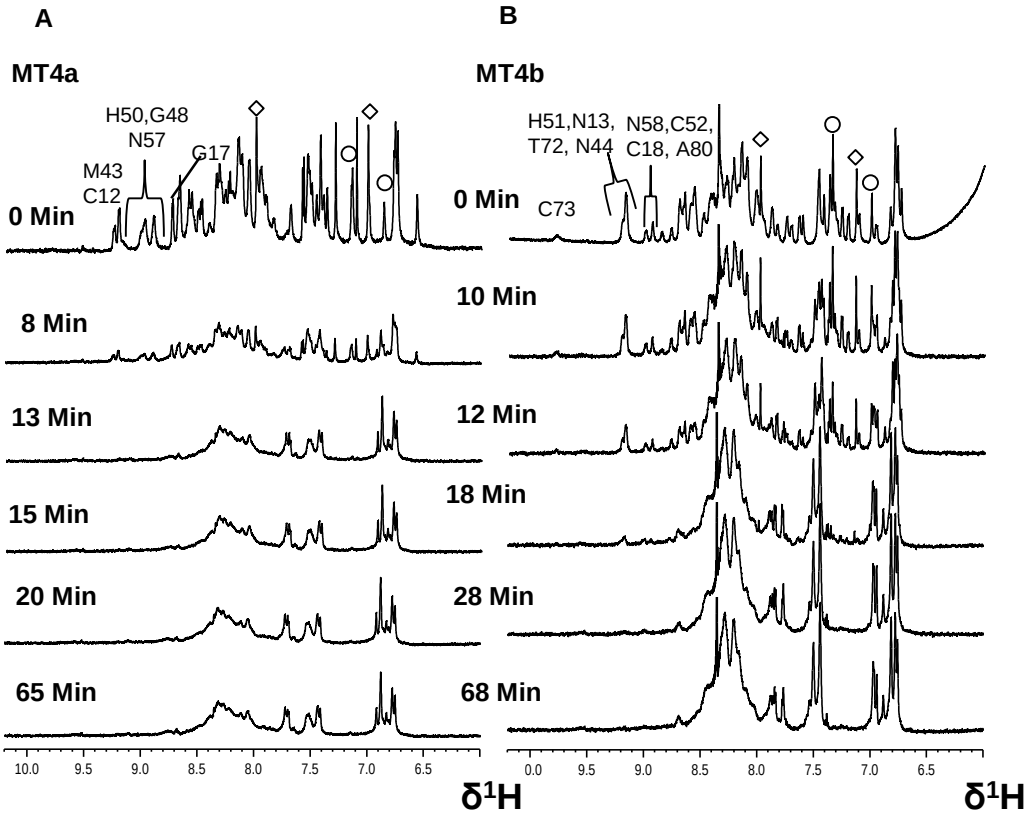

Figure 5.7 1D ^{1}H NMR time course reactions of MT4a and MT4b with EDTA. Spectra were recorded at 700.24 MHz with protein concentrations of 267 µM (50 mM Tris-D_{11}, 10 % D_2O, 50 mM NaCl, pH 7.4). Samples were mixed with EDTA (1:6 with respect to protein concentration). Resonances from domain I and domain II have shown. Imidazole ring protons are denoted ◊ and ○ for His42/His43 and His50/His51, respectively.

For MT4b, even though reacting more slowly, it was difficult to see any domain-specific metal transfer. The weak downfield peak at 9.70 ppm which corresponds to Cys73 had almost disappeared within the first 10 minutes, however, the side-chain proton resonances for both His43 and His51 were still prominent at that time. Subsequently, gradual changes in peak intensities were observed for both domains. As the reaction progressed to 18 minutes, most of the domain II resonances in the downfield region were completely diminished. However, a peak in the downfield region corresponding to Asn13 was still visible at that time point.

Thus, unlike for MT4a, domain I resonances were visible at that time point. However, those peaks had also disappeared after 28 minutes. Later, up to 68 minutes, not much further change in resonances was observed. However, the build-up of broad peaks at 8-8.5 ppm for both isoforms suggested unfolding of the proteins with metal loss.

The fast reaction of MT4a as observed by ^{1}H NMR spectroscopy did not give any scope to make conclusive suggestions on its domain-specific reactivity. Moreover, peak broadening and peak overlap make it difficult to distinguish the reactivity between domain I and domain II for both isoforms. In order to gain insight into domain specificity and the nature of reactive sites, 2D [^{1}H, ^{15}N] HSQC spectra were recorded, in the hope that this would help discerning the involvement of zinc binding ligands (cysteines and histidines) in the reactivity towards EDTA, and would also help explaining at least partially the origin of different reactivity of MT4a and MT4b, as this technique is more sensitive and gives direct information on changes in the environment of specific backbone protons.

Addition of EDTA to MT4a resulted in losses of many of the domain II signals including resonances from Cys81, Cys78, Cys76, Cys53, Cys51, His50, Cys48, His42, Met43, Asp54 Gly74, Gly69 and Gly73 within the first 10 minutes as displayed in Figure 5.8 (A). Moreover, resonances originating from Cys70 and Cys47 were also affected as decreases in peaks intensities were observed. At that time point, weak resonances from Cys56 (mononuclear site) and all cysteine resonances from domain I were still visible. Following the next 5 minutes, resonances for Cys45 from domain II and Cys12 from domain I had disappeared.

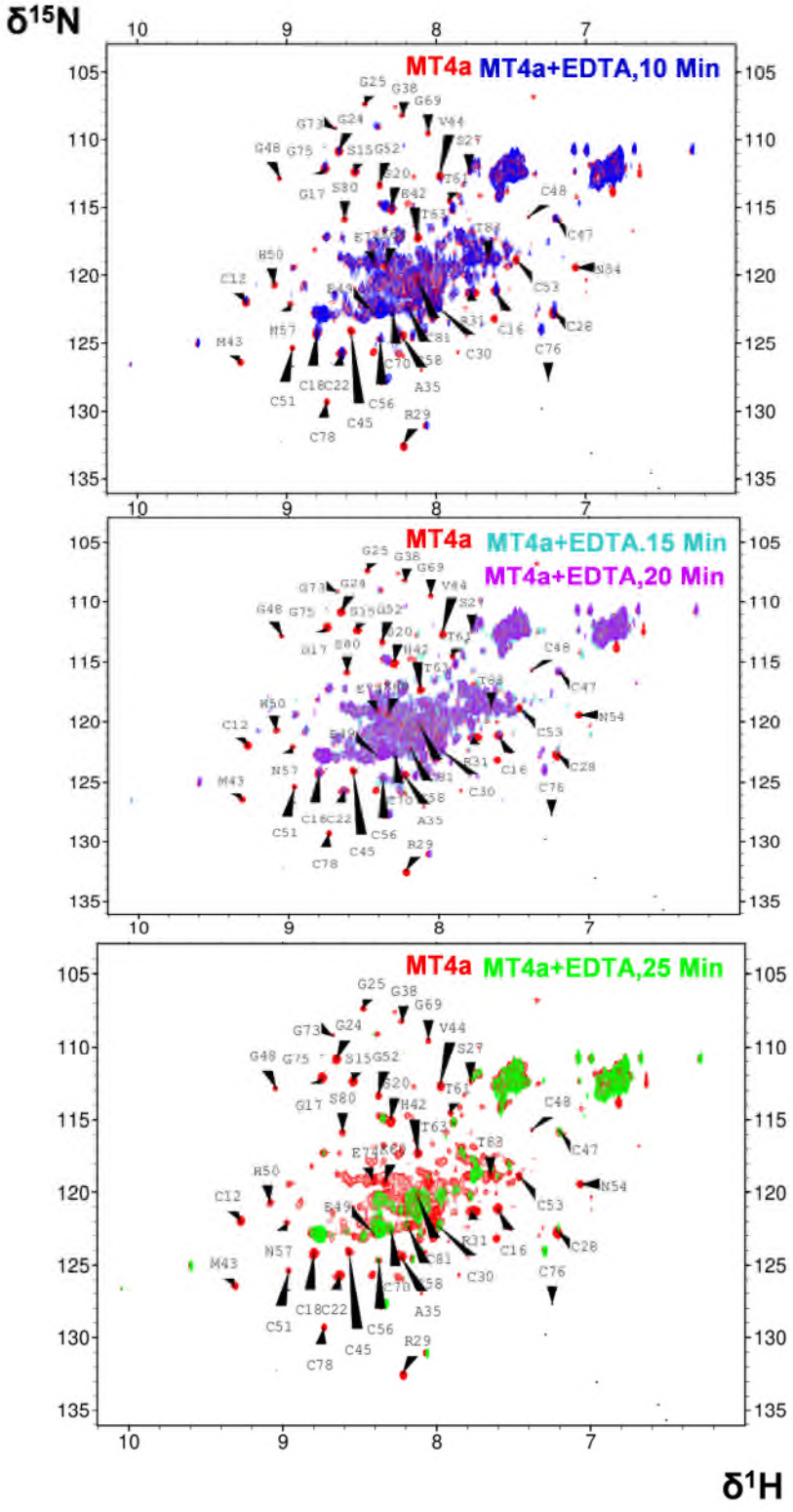

Figure 5.8 Superimposed [^{1}H, ^{15}N] spectra of MT4a in absence (Red) and presences of EDTA at various time intervals (shown in different colours). (A) At 10 minutes, MT4a+EDTA (Blue). (B) At 15 and 20 minutes, MT4a+EDTA (Turquoise) and MT4a+EDTA (Magenta). At 25 minutes, MT4a+EDTA (Green). Spectra were recorded in 700.24 MHz. Protein (251µM, 50 mM Tris-D_{11}, 10 % D_2O, 50 mM NaCl, pH 7.4) was mixed with EDTA (1:6 with respect to protein concentration).

However, peaks for Cys16, Cys18, Cys22 and Cys30 from domain I, and the remaining Cys residues from domain II were still observed (Figure 5.8 B). Interestingly, at 20 minutes, resonances form Cys16 and Cys28 of domain I had completely vanished, and Cys22 was greatly affected. Other domain II resonances as observed earlier remained steady as shown in Figure 5.8 (B). A further drastic change was observed at 25 minutes as displayed in Figure 5.8 (C). Apart from Cys70, Cys58, Cys56, Cys47 and Cys30, all other Cys resonances from both domains had disappeared. These results suggested that within the first 10 min, both domains were affected by metal loss and protein unfolding, perhaps with a slight preference for domain II. These observations were in good agreement with the results observed by 1D ^{1}H NMR spectroscopy.

Interestingly, after 9 hours, peaks for the entire domain I, Cys12, Cys16, Cys18, Cys22, Cys28, Cys30, had reappeared. Resonances from Ser15, Gly17, Gly24 and Asn29 also reappeared. The reason for refolding of domain I is not clear but a plausible explanation could be that the five cysteines residues (Cys70, Cys58, Cys56, Cys47 and Cys30) that were initially least affected, perhaps retained some bound zinc that was subsequently re-distributed to form a fully loaded domain I. This would indicate that when zinc is present at sub-stoichiometric levels, the thermodynamically preferred product is a full domain I. Distinct changes in ligand environment were also observed upon zinc transfer to EDTA from MT4b as shown in Figure 5.9. During the first 10 minutes as displayed in Figure 5.9 (A), Cys73 and Cys71 resonances disappeared completely, suggesting that zinc was lost from the C-terminal part of domain II and also indicating that zinc bound to

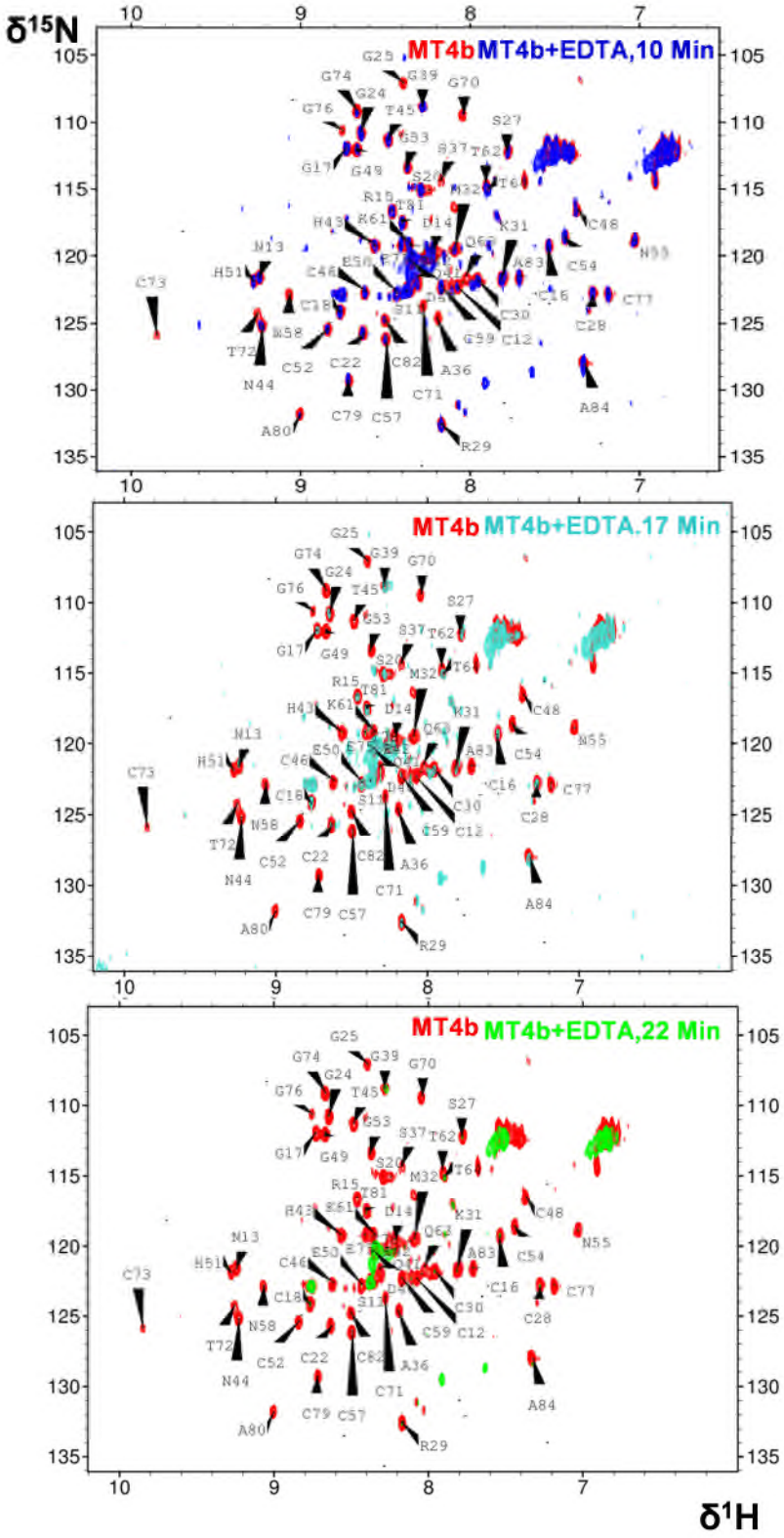

Figure 5.9 Superimposed [^{1}H, ^{15}N] spectra of MT4b in absence (Red) and presences of EDTA at various time intervals (shown in different colours). (A) At 10 minutes, MT4b+EDTA (Blue). (B) At 17 MT4b+EDTA (Turquoise). At 22 minutes, MT4b+EDTA (Green). Spectra were recorded at 700.24 MHz. Protein (267 µM, 50 mM Tris-D_{11}, 10 % D_2O, 50 mM NaCl, pH 7.4) was mixed with EDTA (1:6 with respect to protein concentration)

these two cysteines was the most labile for EDTA attack. However, Cys82 was also greatly affected as only a very low intensity peak remained. In contrast, the two histidine residues were less affected, suggesting that initial zinc transfer did not happen from the unique mononuclear site. After the next 7 minutes, a dramatic change was observed as shown in Figure 5.9 (B): resonances from the entire domain II were completely diminished. However, Cys12 resonance from domain I had also disappeared. Interestingly, the remainder of the domain I resonances still remained. After a further 5 minutes, resonances corresponding to domain I also had largely disappeared as shown in Figure 5.9 (C), however, very low intensity resonances of Cys16, Cys18 and Cys30 were still observed. Interestingly, Cys28 reappeared after 50 minutes and Cys22 reappeared after 11 hours. These observations suggested that metals were released from domain II somewhat faster than from domain I. The fact that resonances for the mononuclear site of domain II remained visible in the initial stages strongly suggests that initial zinc release occurs preferentially from the three-metal cluster. Development of a Zn_5 species as observed by mass spectrometry implies that one of the sites in the three-metal cluster of MT4b is significantly more reactive towards EDTA. Its removal seems to disturb protein structure only locally. Tentatively, it is suggested that the most labile zinc ion might be one that is bound through a single thiolate bridge, as suggested in the model presented for MT4b in Chapter 4. In this model, one zinc is bound by Cys71, Cys77, Cys79, and Cys82, with Cys77 acting as bridge. Initially, both the isoforms released zinc faster from domain II than domain I, however, domain II of MT4a was found to be more reactive than that of MT4b.

5.4 Zinc transfer to 4-(2-Pyridylazo)resorcinol (PAR)

The metallochromic dye PAR forms a 2:1 coloured $Zn(PAR)_2$ complex. Formation of the complex can easily be monitored by UV-Visible spectroscopy at a wavelength of 500 nm. The $Zn(PAR)_2$ complex has also a high binding constant of log β = 14.3 (Shaw III, 1990). The relatively high zinc affinity and the formation of a coloured zinc complex makes PAR a suitable probe for studying zinc transfer and competition reactions with metalloproteins including MTs by means of UV-Visible spectroscopy. In this study, a 100-fold excess of PAR was allowed to react with MT4a and MT4b and the zinc transfer was monitored at 500 nm as displayed in Figure 5.10 (A). The plots suggest that initially zinc was lost more rapidly from MT4a than from MT4b, as a higher absorbance for the $Zn(PAR)_2$ complex was observed for MT4a from the start of monitoring. Time-dependent absorbance data were fitted to pseudo-first order kinetics as shown in Figure 5.10 (B).

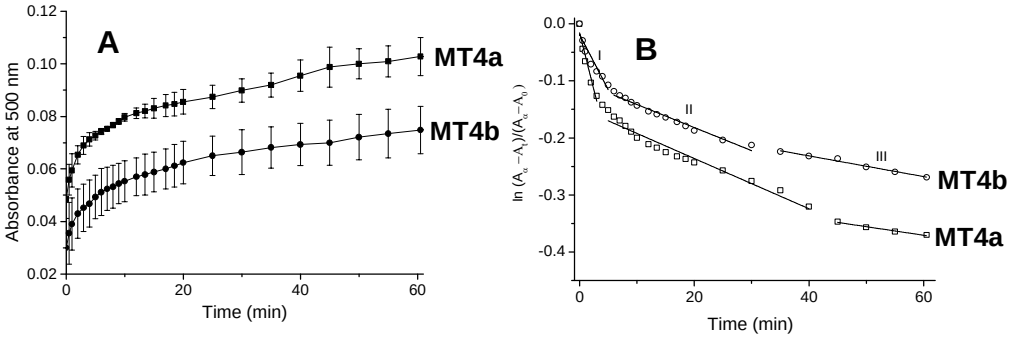

Figure 5.10 Zinc transfer reaction from MT4a and MT4b to PAR. (A) Reaction with PAR monitored at 500 nm. (B) Pseudo-first order kinetic plots suggest a triphasic reaction. 2 µM proteins were reacted with 200 µM of PAR.

This suggested that the reactions progressed in a triphasic manner, with both fast and slow reaction rates observed. It was also evident from the kinetics results (Figure 5.10) that again there were differences in zinc transfer rates between MT4a and MT4b. Initially, MT4a transferred zinc about 2 times faster than MT4b as evaluated from their reaction rates of 6.6×10^{-4} and 3.3×10^{-4} s^{-1} respectively, for the fast step. The second phase was slow for both isoforms with reaction rates of 7.3×10^{-5} and 6.6×10^{-5} s^{-1} for MT4a and MT4b, respectively.

A theoretical estimation (www.acadsoft.co.uk), considering two stability constant for Zn-MT4s of 8.6 and 11 suggested that at least 89.9 % and 24.4 % of zinc respectively, should be distributed to PAR from ZnMT4s to form $Zn(PAR)_2$ complex at pH 7.5. Initial absorbance values suggested that at the beginning of the monitoring, some zinc had already reacted within the time to start absorbance measurement. Considering an extinction co-efficient of 6.6×10^{4} $M^{-1}cm^{-1}$ for the $Zn(PAR)_2$ complex (Hunt et al., 1985) it was revealed that initially 0.5-0.7 µM and at the end of the monitored reactions 1.2-1.5 µM of zinc had been transferred to PAR from proteins containing 12 µM of total zinc, which accounted for about 1 zinc released from both MT4s within the timeframe of the experiment.

Biphasic zinc transfer to PAR from wheat E_C was observed under similar reaction conditions (Leszczyszyn, 2010). Biphasic reaction kinetics were also exhibited by both individual domains of human MT2 (Jiang, 2000). Observed results also suggested that MT4a and MT4b tend to transfer zinc to PAR more slowly compared to wheat E_C (Leszczyszyn and Blindauer, 2010) for which fast and slow steps observed proceeded with rates of 3.4×10^{-3} and 4.3×10^{-4} s^{-1}, respectively. However, the values were comparable to individual α and β domains of human

MT2 (Jiang et al., 2000) where observed fast and slow steps proceeded with rates of 8.4×10^{-4} and 9.9×10^{-4} s^{-1} for the α domain and 3.5×10^{-4} and 4.3×10^{-5} s^{-1} for the β domain.

Mass spectrometry was employed to further investigate zinc transfer from MT4a and from MT4b to PAR.

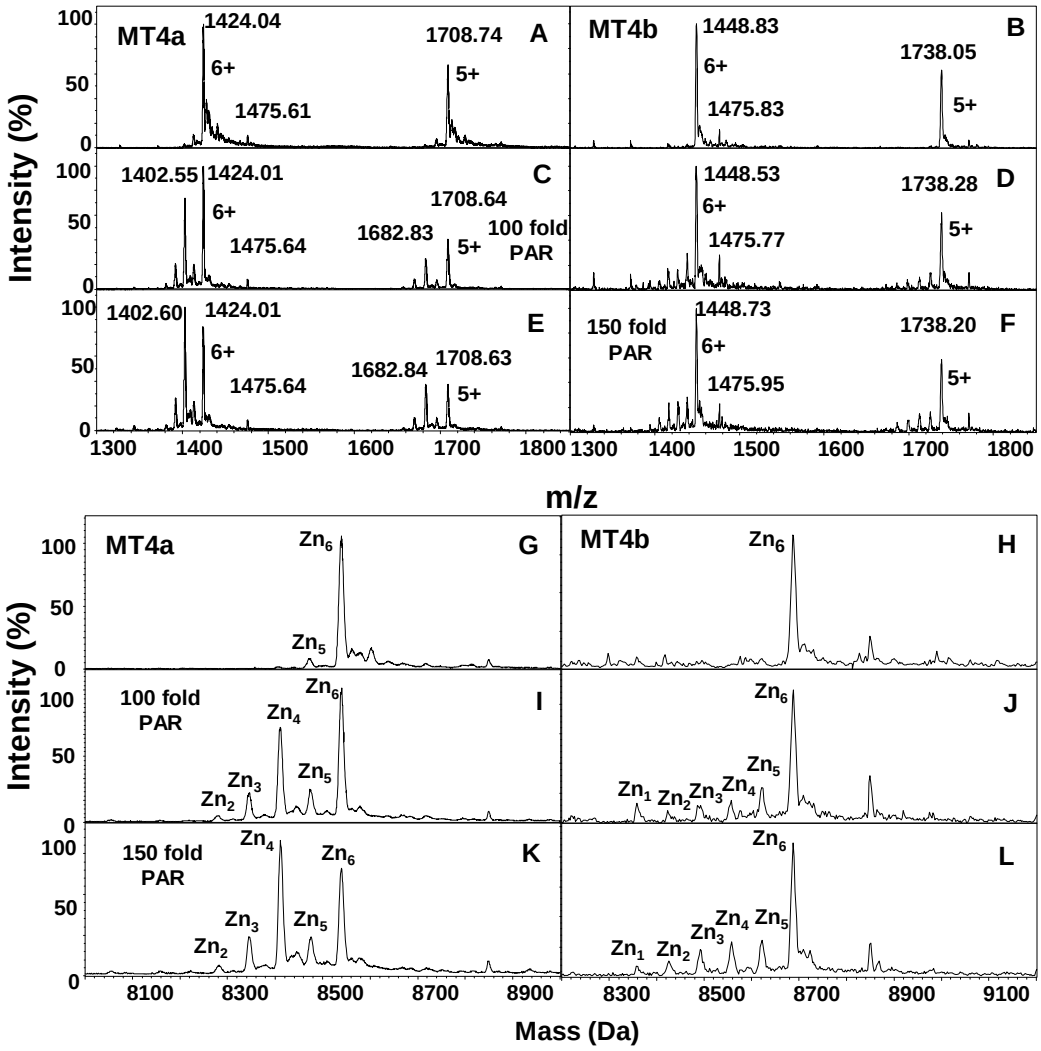

Figure 5.11 Reactions of MT4a and MT4b with PAR observed by mass spectrometry. Raw spectra showing the charge states of 6+ and 5+ (A) MT4a, (B) MT4b. 100-fold excess of PAR (C) MT4a (D) MT4b, 150-fold excess of PAR (E) MT4a, (F) MT4b. Deconvoluted mass spectra (G) MT4a, (H) MT4b, 100-fold excess of PAR, (I) MT4a, (J) MT4b, 150-fold excess of PAR (K) MT4a, (L) MT4b. A high molecular weight peak observed at 1475.66 m/z for both proteins in presence and absence of PAR is likely a contamination.

A kinetics study with PAR by mass spectrometry was hindered as it was observed that zinc transfer to PAR was a slow process and also that a large excess of PAR was required for releasing zinc from MT4s. Therefore, an equilibrium approach was attempted where 100- and 150-fold excesses of PAR were allowed to react with MT4s for 18-20 hours. To remove excess PAR and to avoid any salt contamination, the protein samples were passed through gel filtration columns, and mass spectra were recorded as displayed in Figure 5.11. Initially Zn_6 was the most abundant peak for both isoforms. Incubation with a 100-fold excess of PAR still resulted in Zn_6 as a major species for both isoforms. However, remarkable differences were observed for new under-metallated, but less-abundant peaks. MT4a formed Zn_4 species with almost 70% intensity (with respect to Zn_6 set to 100%), while Zn_5 appeared as the second-most abundant peak, with low intensity (35%) for MT4b. Interestingly, with an increase in PAR concentration to 150 equivalents, the Zn_4 species became the predominant peak for MT4a. Surprisingly, at the same concentration, Zn_6 was still the major peak for MT4b, with undermetallated species at much lower abundances. A noteworthy feature was that neither of the protein isoforms formed apo-species, as evident from Figure 5.11. Zn_2 was the least metallated species observed for MT4a, while MT4b produced Zn_1 as least metallated species. This suggests that these species bound zinc with at least 150-fold higher affinity than PAR. An interesting finding was also that PAR did not form adducts with either of these protein isoforms as no peaks corresponding to PAR-Zn-MT or PAR-MT were observed.

In order to gain more insight into effects on protein dynamics due to metal transfer to PAR, ^1H NMR spectra were recorded. Protein samples were prepared

as mentioned earlier for mass spectrometry but with 100 fold excess of PAR, and after the reaction, protein samples were transferred into NMR buffer, with removal of PAR by using PD10 column. Distinct differences in proton resonances between the two isoforms were observed as displayed in Figure 5.12. Because the experiments were performed under equilibrium rather than kinetics conditions, it is not possible to draw conclusions about the domain specific reactivity for either isoform.

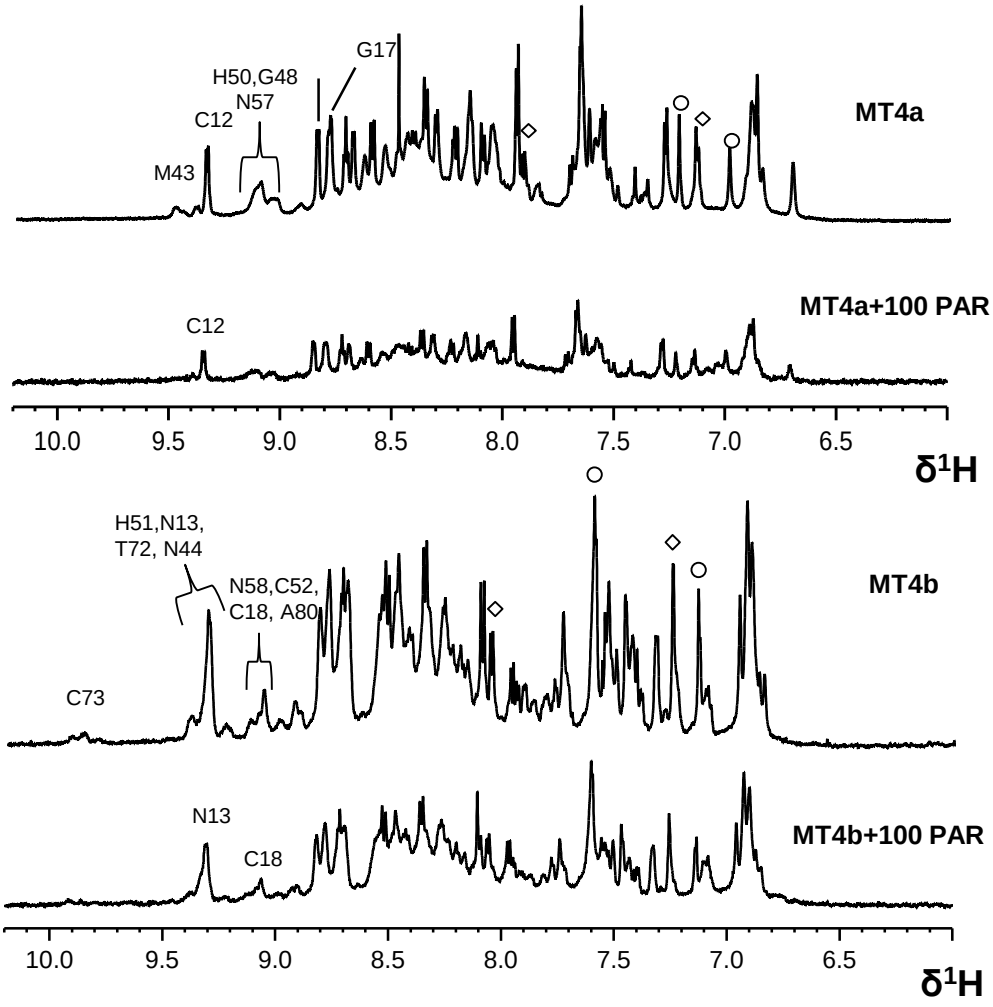

Figure 5.12 ^{1}H-NMR spectra of amide regions of MT4a and MT4b before and after reaction with PAR. Proteins samples (250 µM, 50 mM Tris-D_{11}, 10 % D_2O, 50 mM NaCl, pH 7.42). Changes in amino acid residues belonging to domain II and domain I are shown. Little changes were observed for both isoforms. Imidazole ring protons are denoted ◊ and ○ for His42/His43 and His50/His51, respectively.

However, since the intensities of peaks from both domains were observed, it appears likely that both domains were stable within the reaction timeframe. Moreover, histidine side-chain proton resonances were also observed.

Some peaks intensities decreased in the downfield regions of 8.8 ppm to 10.0 ppm; perhaps due to decrease in signal-to-noise ratio of the reacted samples. As resonances from both domains are still observed, the origin in differences of the metal released as observed by mass spectrometry still remains elusive. An explanation could perhaps be the metal release mechanism. Formation of Zn_4 species for MT4a suggests a cooperative metal release. Interestingly, MT4b exhibited very similar metal-release trends as observed by pH variation. Formation of Zn_5 species as observed by mass spectrometry again suggested that one zinc site was less stable.

In agreement with the mass spectrometry results, ^{1}H NMR spectroscopy also suggested that PAR did not form any adduct with either of the MTs as no proton resonances corresponding to PAR were observed in the amide region or in the upfield aliphatic regions. The bulky size of PAR could possibly hinder PAR to directly attack on solvent exposed protein surface area of MT4s. In this case zinc transfer from MT4a and MT4b to PAR could be a result of a dissociative process. Dissociative zinc transfer was previously observed from individual domains of human MT2 to apo-sorbitol dehydrogenase (Jiang et al., 2000).

5.5 Zinc release from MT4a and MT4b: Influence of phytate

Myo-inositol-1,2,3,4,5,6-hexakisphosphate (IP_6), better known as phytate, is one of the prime constituents of seeds and pollen, contributing 1-5% of total dry weight and accounting for 50-80% of total plant phosphorous contents (Barrientos et al., 1994). Phytate binds to a range of divalent metal ions like zinc, iron and manganese to form phytate complexes *in vivo* and makes the ions unavailable for absorption from plant-based diets. Its high abundance in the aleurone layer and its low occurrence in embryos in cereal seeds (Ockenden et al., 2004) makes phytate an interesting biomolecule to study its interactions with metalloproteins, in particular with MTs.

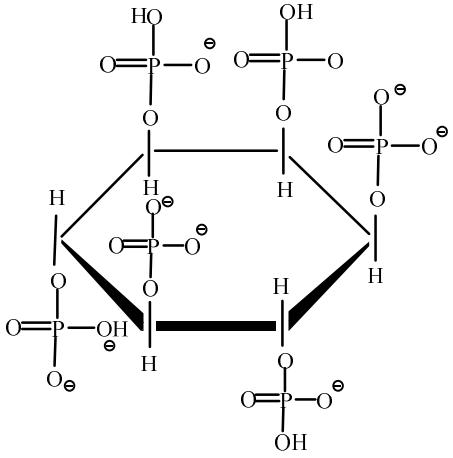

Figure 5.13 Chemical structure of phytate.

Previously, inorganic phosphate binding to Cd-loaded rabbit liver MT2 has been studied, and it was suggested that there are possibilities of physiologically relevant organic phosphate binding to other MTs (Palumaa and Vasák, 1992).

Later, the binding of the phosphorous-containing biomolecule ATP to mammalian MT2 and its effect of zinc binding has been studied (Jiang et al., 1998).

Controversially, Armitage and co-workers reviewed that work and suggested that there was no ATP binding site in MTs (Zangger et al., 2000). This study aims to explore the influences of phytate on zinc binding properties of MT4a and MT4b. Purified MT4a and MT4b were allowed to react with 1 and 10 equivalents of phytate with respect to protein concentration. Excess phytate was removed using gel filtration columns, and mass spectra were recorded. Raw mass spectra of the samples after reaction with 1 and 10 equivalents are shown in Figure 5.14 (A).

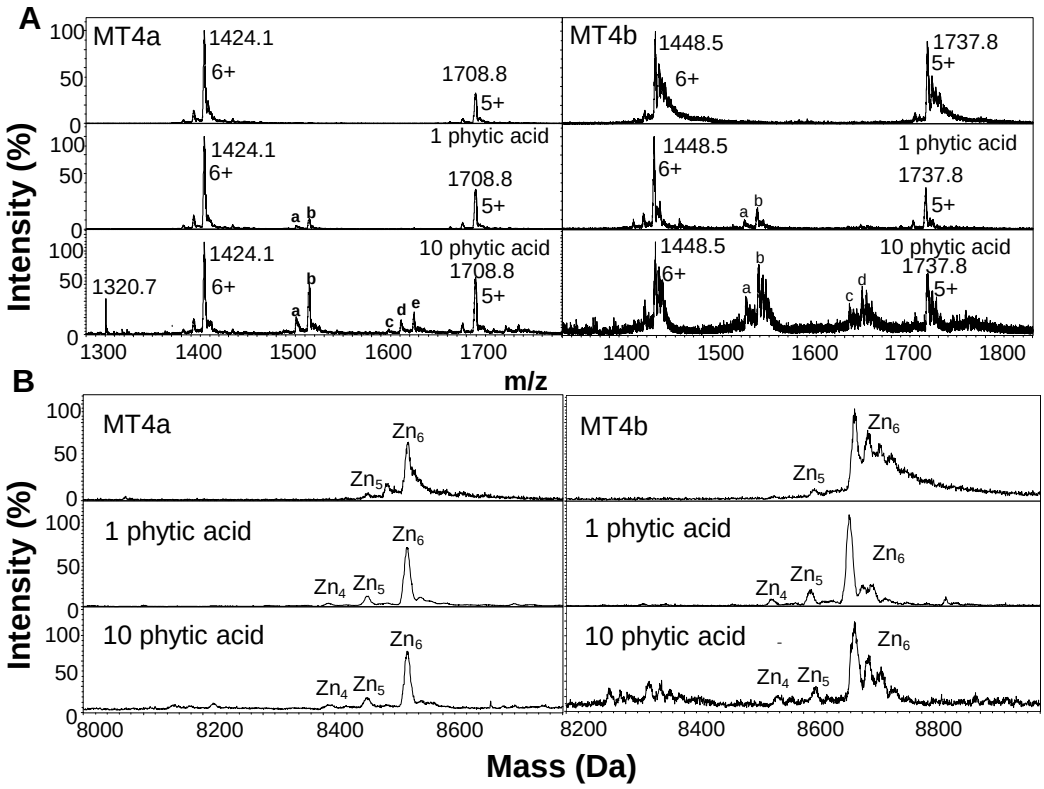

Figure 5.14 Reactions of MT4a and MT4b with phytate studied by mass spectrometry. (A) Raw mass spectra showing 6+ and 5+ charge states of the proteins. (B) Deconvoluted mass spectra. Proteins (30 µM in 20 mM NH_4HCO_3 buffer, pH 7.8) were incubated with 1 and 10 equivalents of phytate. Desalted protein samples (25 µM in 10 mM NH_4HCO_3 buffer, 10% MeOH, pH 7.8) were analysed by ESI-MS.

The two intense peaks in each spectrum correspond to the 6+ and 5+ charge states of the proteins. Deconvoluted mass spectra as shown in Figure 5.14 (B) suggested

that the initial predominant species was Zn_6, however, a very low intensity Zn_5 species was also observed for both isoforms in this preparation. Phytate-treated samples produced Zn_6 as an abundant species and a very slight increase in intensity of Zn_5 species was observed. In addition, a Zn_4 species with very low intensity appeared for both the isoforms. The very low intensity of Zn_5 and Zn_4 species compared to Zn_6 species suggested relatively small effects of phytate to induce zinc release or transfer from MT4a and MT4b. Elemental analysis by ICP-OES also suggested that less that 2% of zinc was released from the proteins at 50 equivalents of phytate.

Interestingly, phytate was found to form adducts as shown in Figure 5.14 (A). At 1 equivalent of phytate, two adducts were formed, labelled a and b for the 6+ charge states. Peaks labelled a-e with mass/charge ratios of (a) 1520.8, (b) 1533.9, (c) 1617.7, (d) 1630.7 and (e) 1644.1 for MT4a, and (a) 1545.28, (b) 1558.54, (c) 1655.43 and (d) 1668.72 for MT4b, correspond to (a) [Zn_6MT4a-IP_5] or [Zn_6MT4b-IP_5] which has a mass of 580 Da higher than Zn_6MT4a or Zn_6MT4b. This indicates binding of IP_5 acid, with a loss of one HPO_3 group from phytate (IP_6) with a mass of 660 Da. Peak (b) represents [Zn_6MT4a-IP_6] or [Zn_6MT4b-IP_6], suggesting that one molecule of phytate is bound to both isoforms. When increasing the phytate concentration to 10-fold excess, very similar results were observed. However, in that case, interestingly, two new sets of peaks appeared where two equivalents of IP_5 and IP_6 were found to bind to MT4a and MT4b as assigned as c, d, and e. Further increasing the phytate concentration to higher ratios resulted in an increased number of adducts formation and very complex spectra (Figure 5.16 E and F). Formation of a single adduct at a ratio as low as 1:1

suggests that there might be a preferential binding site for phytate on MT4a and MT4b. One of the interesting features observed was that IP_5, a cleaved product of phytate (IP_6), also formed adducts. Raw mass spectra incorporating the low m/z range confirmed the presence of IP_5(-H) at m/z = 580; the large intense peak at m/z = 660 represent free phytate (IP_6) (Figure 5.15).

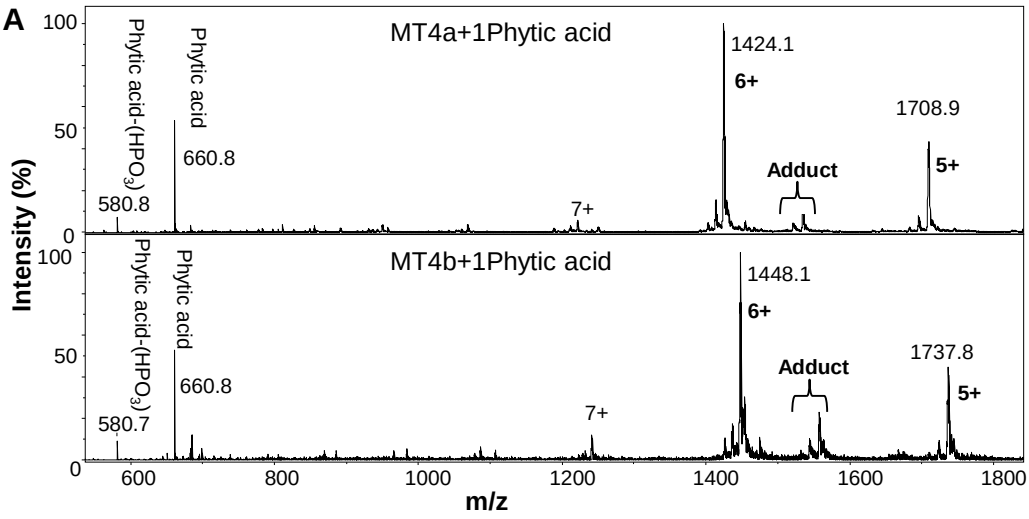

Figure 5.15 Reactions of MT4a and MT4b with 1 equivalent of phytate. A) Binding of phytate as an adducts and loss of one -PO_3H from phytate has shown.

Subsequently, phytate-treated protein samples were subjected to low pH to understand zinc participation in adduct formation and also the adducts' stability against low pH. Lowering the pH to 2 resulted in disappearance of MT4a adducts, but interestingly, the 1:1 adducts formed with MT4b were still persistent suggesting that these MT4b adducts have a higher pH stability than the corresponding MT4a adducts. Moreover, the adducts had masses of 660 and 580 Da higher than apo-MT4b (with mass of 8305.2 Da) suggesting that zinc did not

take part in adduct formation. However, at higher phytate concentrations, even at pH 2, adducts were observed for both isoforms (Figure 5.16 (G and H).

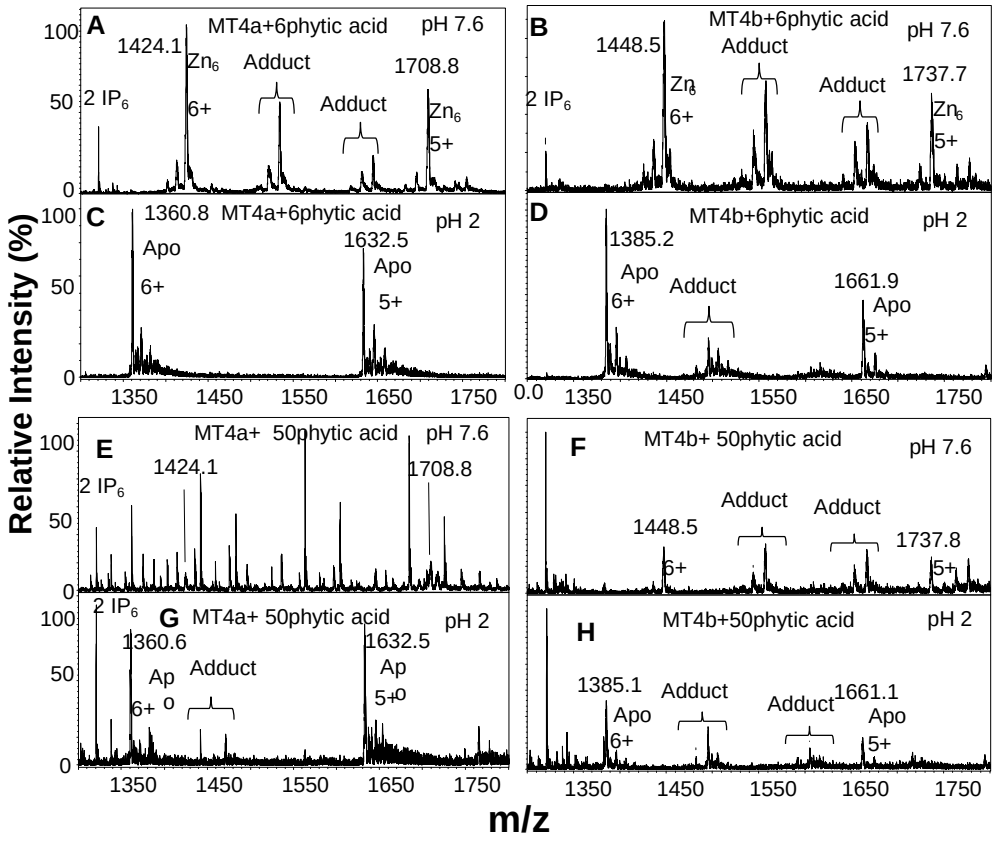

Figure 5.16 pH stability of MT-phytate adducts. Adducts formed with MT4a have a lower pH stability than adducts formed with MT4b. Proteins (30 µM in 20 mM NH_4HCO_3 buffer, pH 7.8) were incubated with 6 equivalents of phytate. Desalted protein samples (25 µM in 10 mM NH_4HCO_3 buffer, 10% MeOH, pH 7.8) were analysed with and without addition of HCOOH by ESI-MS.

Phytate-treated MT4a and MT4b did not release or transfer zinc to a significant extent. However, like EDTA, phytate has negatively charged groups forming adducts, potentially with positively charged amino acids, which might perhaps result in protein modification or change in protein environments.

To investigate whether phytate helps or influences metal release or transfer to other molecules, metal transfer properties of MT4a and MT4b to PAR were

studied in presence and in absence of phytate by means of UV-Visible spectroscopy. The metal chelator PAR was used as it exhibits absorbance at 500 nm for $Zn(PAR)_2$ complex whereas phytate itself has no absorbance at 500 nm.

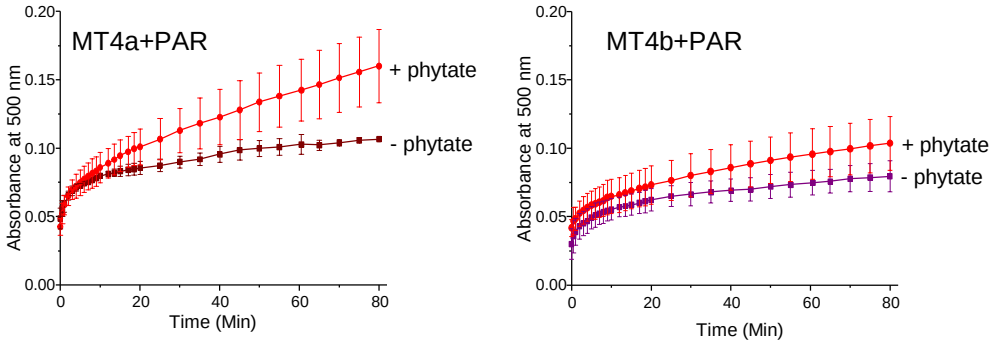

Figure 5.17 Zinc transfer from MT4a and MT4b to PAR in presence and absence of phytate. Proteins (2 µM, 0.2 M Tris buffer, pH 7.54) were allowed to react with a 100-fold excess of PAR (200 µM) in absence and presence of 1 mM phytate. The blank contained equivalent quantities of PAR with/without phytate.

The experimental results indicate that phytate facilitated zinc transfer to PAR, as higher absorbance at 500 nm was observed in presence of 1 mM phytate compared to PAR only as shown in Figure 5.17. However, the results also suggest that the effect of phytate on zinc release was more profound on MT4a than on MT4b. Previously, another biomolecule, oxidised glutathione (GSSG) was found to promote zinc transfer to PAR from mammalian MT2 (Jiang et al., 1998b). A redox drug, Ebselen, was also found to facilitate complete zinc transfer to PAR from human MT2 (Jacob et al., 1998), but in either case, this was a redox-mediated process, which is not a likely mechanism for phytate-induced zinc release.

Subsequently, ^{1}H-NMR spectroscopy was employed to understand whether the interaction with phytate influenced specific protein residues. A large excess of

phytate, i.e. 50 equivalents, was used for this study as earlier it was observed that low phytate concentration had very little effect on zinc transfer dynamics of both isoforms. Even at this high concentration of phytate there was not much change observed in the proteins' amide region. However, subtle decreases in peak intensities were observed. Interestingly, in the upfield region of 1.5-1.6 ppm, subtle changes in chemical shifts were observed as shown in Figure 5.18. The affected protons may originate from Arg or Lys as they are positively charged they might interact with negatively charged phytate.

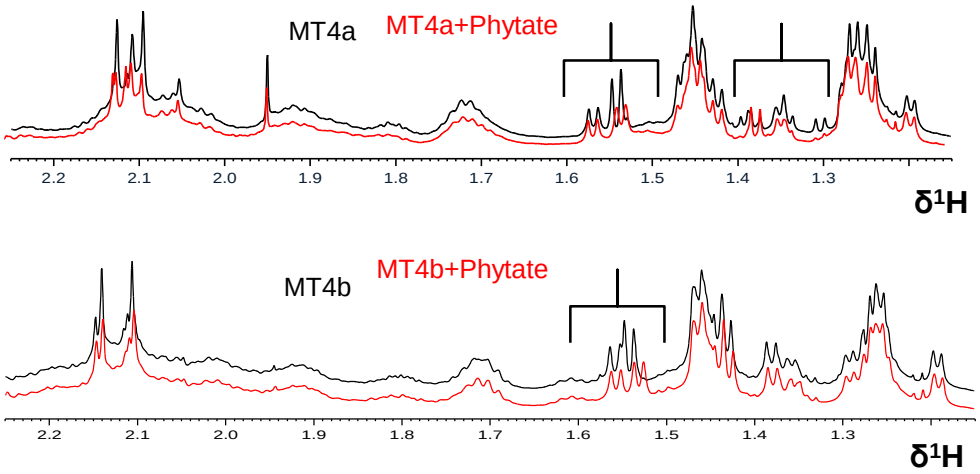

Figure 5.18 1D ^{1}H NMR spectra of upfield regions of MT4a and MT4b before (Black) and after (Red) addition of phytate. Proteins (250 µM, 50 mM Tris-d_{11},50 mM NaCl,10% D_2O pH 7.42) were allowed to react with phytic acid (12.5 mM, 50 mM Tris-d_{11},50 mM NaCl, 10% D_2O, pH 7.42).

There are possibilities of how phytate may trigger zinc transfer to PAR; one of the possibilities may perhaps be through interactions with positively-charged amino acid residues which could allow PAR to interact better with the proteins than in absence of phytate. Another possibility is that phytate may directly extract a labile

zinc ion from the proteins, and that the subsequent dissociation of the Zn-phytate complex helps PAR to acquire zinc. Low stability constant of Zn-Phytate (Lasztity and Lasztity, 1988) complex (Zn-IP_6 log K ~ 3.26 and Zn-IP_5 ~ 5.06) compared to Zn $(PAR)_2$ complex (Shaw III et al., 1990) of log β = 14.3 support the later mechanism.

In summary, results so far observed in this chapter suggest remarkable differences in zinc transfer dynamics between the two isoforms. While both isoforms have similar pH half dissociation values, cooperative metal release was observed for MT4a and non-cooperative release was observed for MT4b. Cooperative and non-cooperative zinc transfer to PAR was also observed for MT4a and MT4b, respectively. However, in zinc transfer reactions to EDTA, both isoforms exhibited non-cooperative behaviour, suggesting cooperative and non-cooperative metal release or transfer behaviour is not entirely based on the properties of the proteins, it also depends on the nature of the external reactant. Faster zinc transfer properties of MT4a illustrate that MT4a might be a better zinc donor than MT4b. Domain specificity suggests that perhaps these domains are designed to perform different specific functions *in vivo*. Protein-phytate interactions accelerated zinc transfer rates of both isoforms, suggesting that interactions of such kind *in vivo* could potentially increase functional efficiency of these proteins as zinc donors.

Chapter 6

Metal binding properties of MT4a and MT4b: Effect of redox active reactants

6.1 Introduction

Metallothioneins are believed to play roles in cellular zinc distribution (Bell and Vallee, 2009; Maret, 2011). Despite their high thermodynamic stability, the kinetic lability of the bound metal ions allows to release and transfer them to other biological molecules or apo-proteins *in vitro* and *in vivo* (Maret, 1994). Apart from the acidic environment in lysosomes, there is not much pH variation in the cells to release metal ions from MTs. The cellular redox couple glutathione/glutathione disulfide (GSH/GSSG) and reactive oxygen species are thought to play an important role in modulating the metal binding properties of MTs (Maret, 1995). This chapter aims to understand the influences of the redox couple GSH/GSSG on metal binding properties of MT4b. It will also discuss the effect of the synthetic disulfide reagent 5,5'-dithiobis (2-nitrobenzoic acid (DTNB) and the reactive oxygen species H_2O_2 on zinc mobilization from MT4a and MT4b and the consequences for protein folding.

6.2 Interaction of MT4b with GSSG, GSH and GSH/GSSG: Mass spectrometry

It has been postulated that the cellular glutathione redox couple GSH/GSSG plays a pivotal role in regulating metal binding properties of MTs. Glutathione (GSH) is the most abundant cellular non-protein thiol, distributed mostly in its reduced form in plants, bacteria and mammalian cells at concentrations ranging from 0.5 to 10 mM. Previously, it has been shown that glutathione disulfide (GSSG) released metals from MTs (Savas et al., 1993). It was also found that the glutathione redox couple (GSH/GSSG) facilitates the zinc release from MTs (Maret, 1994b). Moreover, zinc mobilization from human MTs to zinc-depleted sorbitol dehydrogenase was found to be regulated by the GSH/GSSG couple (Jiang et al., 1998). Furthermore, an equilibrium binding and molecular modelling study of Cd,Zn-MT from rabbit liver with GSSG and GSH has proposed a binding site for these compounds on mammalian MTs (Brouwer et al., 1993).

To investigate the effect of GSSG on zinc release from MT4b, here experiments were performed in absence and presence of two different GSSG concentrations of 2.5 mM and 5.5 mM. The concentrations were selected because they were in the middle of physiological concentrations of GSH/GSSG. Mass spectrometry results as displayed in Figure 6.1 suggested that initially the most abundant peaks observed were the 6+ and 5+ charge states corresponding to Zn_6MT4b. Addition of GSSG resulted in three sets of protein species: fully metallated Zn_6 (1448.7 m/z for 6+ charge state), apo species (1385.5 m/z), and oxidised under-metallated species of Zn_5, Zn_3, Zn_2 and Zn_1. However, glutathione oligomer of $[(GS)_{14}]^{3+}$

with a corresponding peak of 1430.6 m/z and $[(GS)_9]^{2+}$ at peak of 1379.9 m/z were also observed. However, the considerable decrease in the relative intensity of 6+ and 5+ charge states peaks (as also seen by a decreased signal-to-noise ratio), and the emergence of apo and under-metallated species suggested that zinc was released from the protein. The effect was more pronounced at the higher concentration of GSSG. The reacted and desalted protein samples were also subjected to elemental analysis. The ICP-OES results revealed that 22% and 45% of zinc were released from Zn_6MT4b to produce $Zn_{4.6}$MT4b and $Zn_{3.4}$MT4b upon treatment with 2.5 mM and 5.5 mM of GSSG, respectively. For wheat E_C, a 40-42% decrease in bound zinc was found when treated with 4.5 mM GSSG (Peroza et al., 2013).

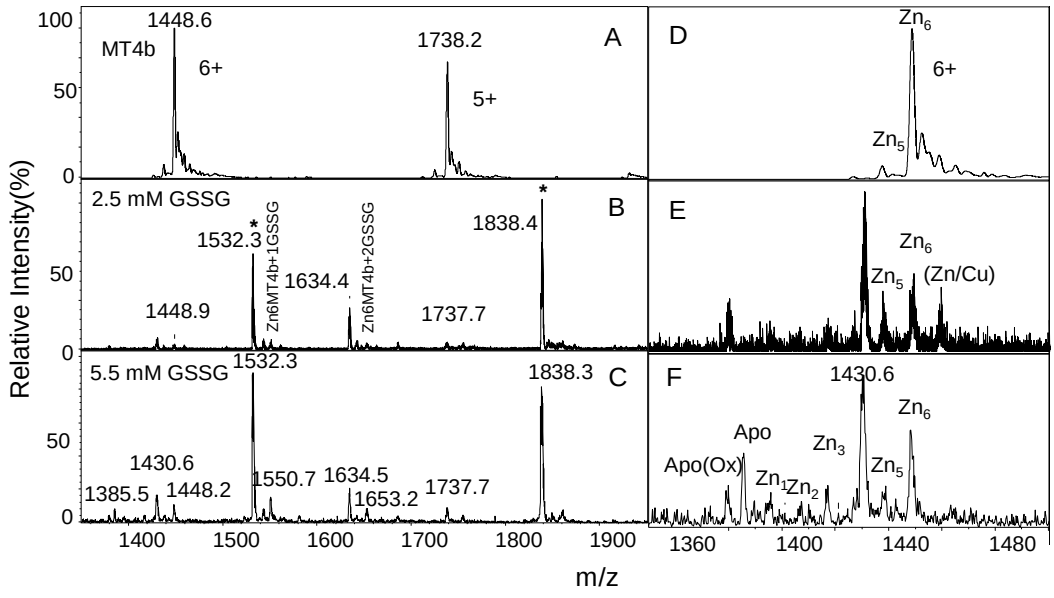

Figure 6.1 Reactions of MT4b with GSSG observed by mass spectrometry. Raw spectra showing the charge states of 6+ and 5+ (A) Zn_6MT4b, (B) Zn_6MT4b + 2.5 mM GSSG (C) Zn_6MT4b + 5.5 mM GSSG. Expanded raw spectra of the 6+ charge state (D) Zn_6MT4b (E) Zn_6MT4b +2.5 mM GSSG (F) Zn_6MT4b + 5.5 mM GSSG. Protein (35 µM, 20 mM NH_4HCO_3 buffer) was incubated with GSSG (2.5 mM and 5.5 mM) for 18-20 hours. Desalted protein samples were subjected to ESI-MS analysis. The peaks at 1532.3 m/z and 1838.4 m/z are glutathione oligomers (+1 charge state; 5- and 6-mers); peaks at 1550.7 m/z and 1653.2 m/z are protein-GSSG adducts; the peak at 1634.5 m/z is an unidentified +1 species. A trace amount of Cu was detected by ICP-OES.

Subsequently, the effect of GSH on metal release from MT4b by GSSG was studied, as previously it was observed that GSH helps GSSG facilitating zinc transfer from MTs (Maret, 2000). The experiments were performed in a series of physiological stoichiometries of GSH/GSSG as suggested by previous work (Jiang et al., 1998). Surprisingly, recorded mass spectra as shown in Figure 6.2 indicated three sets of species: fully zinc-loaded at 1448.7 m/z, and oxidised Zn_5 and Zn_4 and oligomer $[(GS)_9]^{2+}$ at 1379.3 m/z, Interestingly, Zn_2 and Zn_3 were observed in their reduced form. However, the peak at ~1430 m/z for oligomer $[(GS)_{14}]^{3+}$, previously observed for GSSG, was present again, and a further peak at 1442.2 m/z appeared, the deconvoluted mass of which was 25 and 28.9 Da higher than the oxidised or reduced Zn_5 species, respectively.

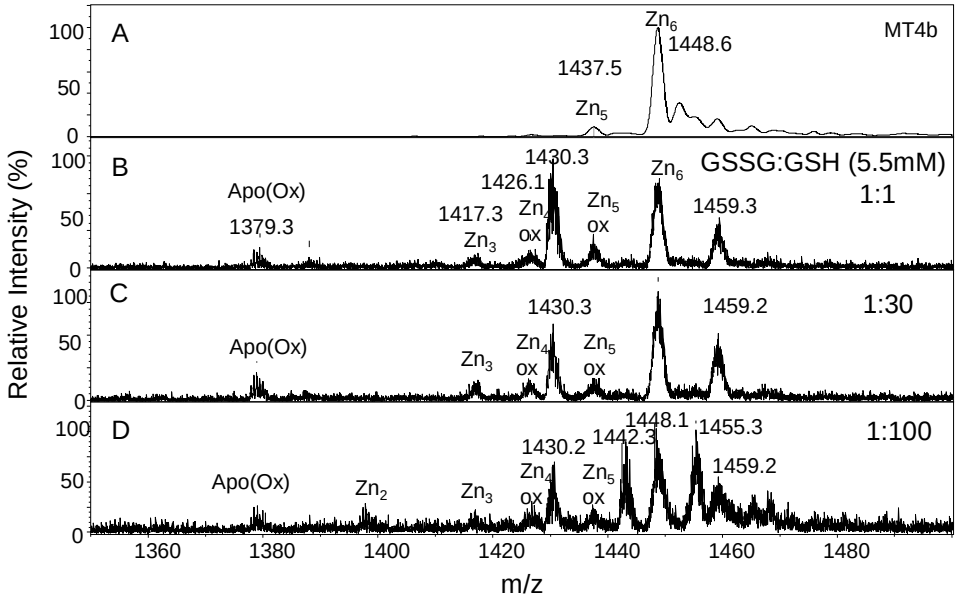

Figure 6.2 Reactions of MT4b with the GSSG/GSH redox couple observed by mass spectrometry. Raw spectra of 6+ charge state showing (A) Zn_6MT4b, (B) Zn_6MT4b + 1:1 GSSG/GSH (C) Zn_6MT4b + 1:30 GSSG/GSH (D) Zn_6MT4b + 1:100 GSSG/GSH. Protein (30 µM, 20 mM NH_4HCO_3 buffer) was incubated with different GSSG/GSH ratios (total glutathione at 5.5 mM) for 18-20 hours. Peaks at 1459.2 m/z correspond to Zn_7MT4b**.** Weak peak intensity as observed for B, C and D is likely due to protein loss during desalting and concentrating prior to ESI-MS analysis.

However, oxidised protein was observed at high GSH concentration. Further, the influence of GSH alone on MT4b was studied. Results as displayed in Figure 6.3 suggested that after reaction with 2.5 mM of GSH, the protein existed predominantly in oxidised apo form at 1382.9 m/z. The oxidised Zn_1 species was also observed. Increasing the GSH concentration to 5.5 mM resulted in the emergence oligomer $[(GS)_9]^{2+}$ at 1379.8 m/z, with the fully-loaded Zn_6 species still present. The relative abundance of this form was very low at 2.5 mM GSH, but the reason for its persistence at the higher concentration was not clear but one plausible explanation could be that the reaction time (15-16 hours) was not sufficient for completion of the reaction. The results observed in this study can be explained by oxidant behaviour of GSH in the presence of oxygen (Petzold and Sadler, 2008). It was proposed that oxidation of glutathione may produce highly reactive peroxo sulfenic acid (GSOOH) which subsequently may react to produce GSSG and H_2O_2. At the prolonged reaction times used in the present study, GSH oxidation to GSOOH and GSSG is a plausible mechanism for protein oxidation. Interestingly, subtle differences were observed between the reaction of MT4b with GSH and GSSG. One of the intriguing features was the development of the full range of under-metallated species (Zn_5-Zn_2) that were observed in the presence of GSSG. In contrast, the Zn_1 species was prominent after the reaction with 2.5 mM GSH alone. However, under-metallated species were also observed for GSH/GSSG mixture. Like rabbit liver MT2a (Afonso et al., 2002), MT4b was found to form adducts with GSSG and GSH. Interestingly, both GSSG and GSH produced the same adducts, as two sets of peaks were observed at 1532.0, 1550.0 and 1634.2 and 1653.0 m/z. The peaks at 1550.0 m/z and 1653.0 m/z correspond

to the +6 charge states of Zn_6MT4b+GSSG(-2H) and Zn_6MT4b+2GSSG(-4H). However, at higher concentration of GSH and GSSG, the relative intensity of both these peaks decreased and the emergence of 1532.0 m/z and 1634.2 m/z peaks was observed. Collision induced dissociation (CID) mass spectrometry of the peak at 1532.0 suggests that this peak was a singly charged oligomer of 5 GS units as shown in Figure 6.4.

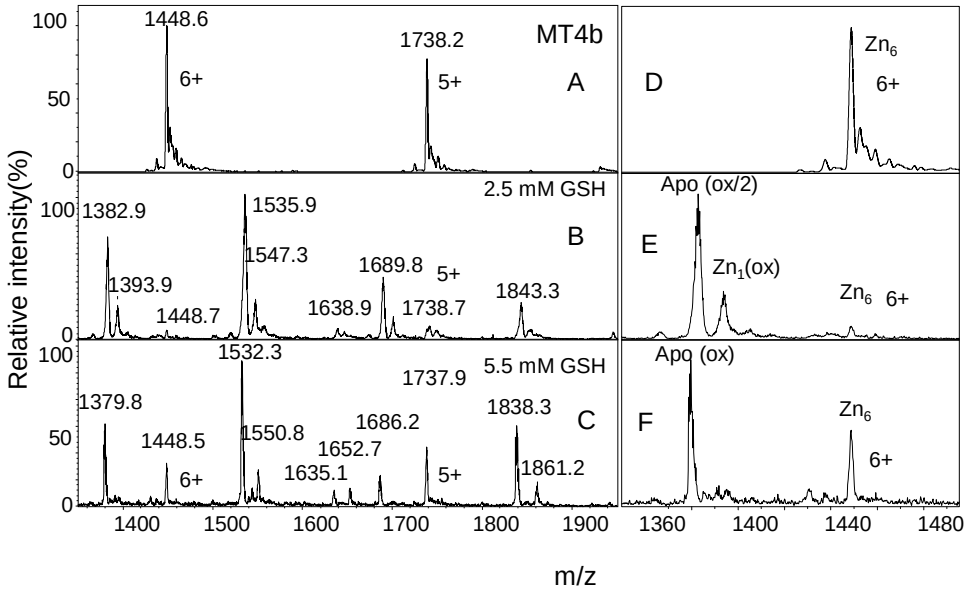

Figure 6.3 Reactions of MT4b with GSH observed by mass spectrometry. Raw spectra showing the charge state of 6+ and 5+ (A) Zn_6MT4b, (B) Zn_6MT4b +2.5 mM GSH (C) Zn_6MT4b +5.5 mM GSH. Expanded raw spectra of 6+ charge state (D) Zn_6MT4b (E) Zn_6MT4b +2.5 mM GSH (F) Zn6MT4b +5.5 mM GSH. Protein (30 µM, 20 mM NH_4HCO_3 buffer) was incubated with GSH (2.5 mM and 5.5mM) for 18-20 hours. Desalted protein samples were subjected to Mass spectrometry analysis.

From Figure 6.4, it was also evident that the oligomer underwent cleavage to produce 4GS, 3GS and 2GS units. In addition, GS units fragmented on carboxyl and glutamate sites (y2) to produce truncated GS units. However, the peak corresponding to 531.1 m/z has a mass difference of 64 from 2(GS-H_2O) and neither of the fragment patterns (y_2, a_2 or b_2 or z_2) produced a mass difference of

64. The peak at 466.1 m/z which was assigned as 2 (GS-y_2)-H_2O has also a mass difference of 65 from the 531.1 peak. Furthermore, high molecular mass peaks of 1837.3 and 2449.0 observed were possibly monocharged oligomer of $[(GS)_6]^+$ and $[(GS)_8]^+$ respectively . The peak of 1837.3 was also observed in the raw spectra as displayed in Figure 6.3. This peak has a mass difference of 306 Da from the peak at 1532.1; this suggests that the peak at 1838.0 could be an oligomer of 6 GS units.

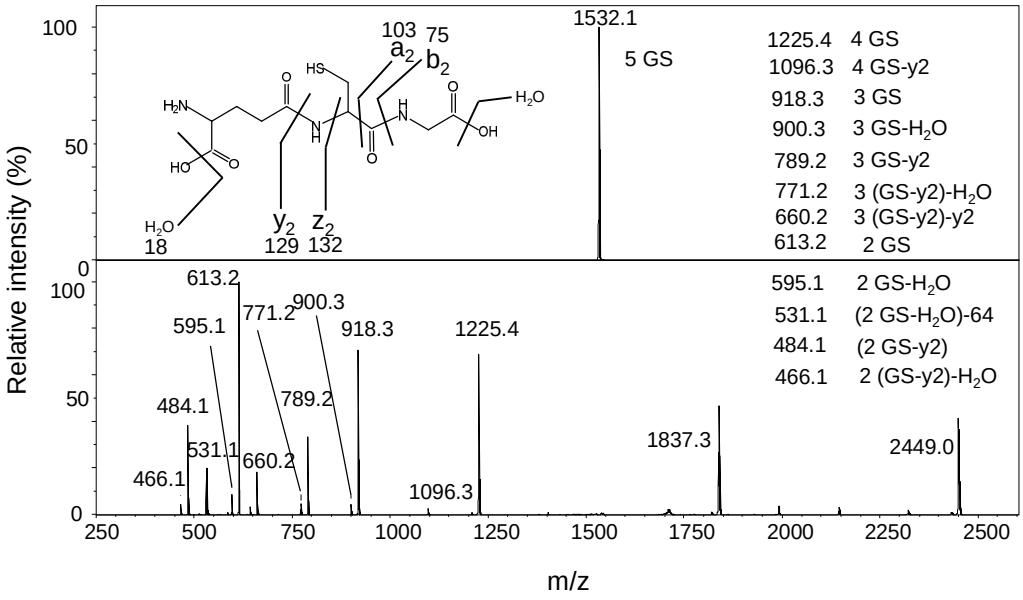

Figure 6.4 Collision induced dissociation tandem mass spectra of peak 1532.1 m/z. Different fragmentation patterns are shown. Tandem mass spectra suggested peak 1532.1 was an oligomer of glutathione.

However, peak of 1635 has a mass of 102 higher than the peak at 1532.0 and 204 lower than the 1838.0 peak. One of the plausible explanations for the peak at 1635 could possibly be a truncated residue from peak 1838 for which y_2 and a_2 cleavage happened to produce a mass differences of 204 Da.

Interestingly, GSSG adducts were formed with the Zn_6 form of the protein as there were no such adducts observed with under-metallated species. Thus it was of interest to see whether metal mediates this adduct formation; two approaches were investigated - lowering pH and zinc replacement by cadmium shown in Figure 6.5.

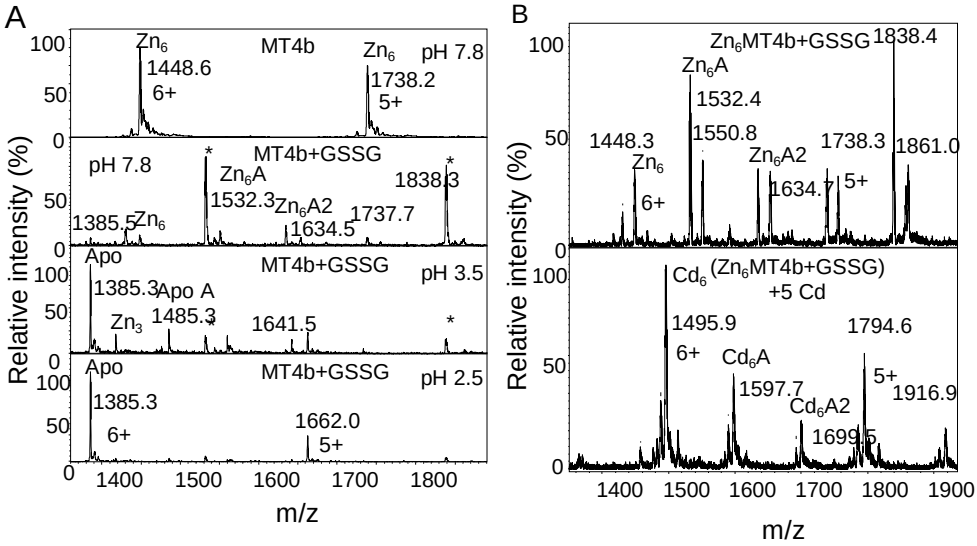

Figure 6.5 Effect of pH and Cd^{2+} on [Zn_6MT4b+nGSSG] complexes. (A) Effect of pH variation. Desalted [Zn_6MT4b+nGSSG] (25µM in 10 mM NH_4HCO_3 buffer, 10% MeOH, pH 7.8) samples were analysed with addition of HCOOH by ESI-MS. (B) Effect of Cd addition. [Zn_6MT4b+nGSSG] (25 µM in 10 mM NH_4HCO_3 buffer, pH7.8) was incubated with 5 equivalents of $Cd(CH_3COO)_2$. Desalted protein samples (25 µM in 10 mM NH_4HCO_3 buffer, 10% MeOH, pH 7.8) were analysed by ESI-MS.

Lowering the pH to 3.5 resulted in a decrease in peak intensity for both metallated adducts. The apo protein peak appeared, alongside a new peak at 1485.3 m/z, corresponding to a neutral mass of 8905.8 Da. This is consistent with the mass for partially oxidised apo protein with two "GS" units (8305.2 + 2*306.2 – 12) suggestingg zinc was not involved with adduct formation as adduct was formed with apo protein. Moreover, at pH 2.5, these adduct peaks had completely disappeared suggesting adduct formation was non-covalent. Zinc replacement by

cadmium resulted in a shift of the adduct to m/z values corresponding to the +6 charge states of Cd_6MT4b+GSSG (-2H) and Cd_6MT4b+2GSSG (-4H). Upon cadmium addition, a mass shift of the Zn_6 adduct to the corresponding Cd_6-adduct suggests that adduct formation was independent of metal ions. (Krężel and Bal, 2004; Piątek et al., 2009).

To obtain insights into protein folding under the influence of GSH and GSSG, 1D ^{1}H NMR spectra were recorded with GSSG and GSH at stoichiometries of 1:30 and 30:1, with a fixed concentration of 5 mM as displayed in Figure 6.6. At 1:30 GSSG to GSH ratio, an intense peak appeared at 8.3 ppm, likely due to the amide proton resonances from GSH and GSSG.

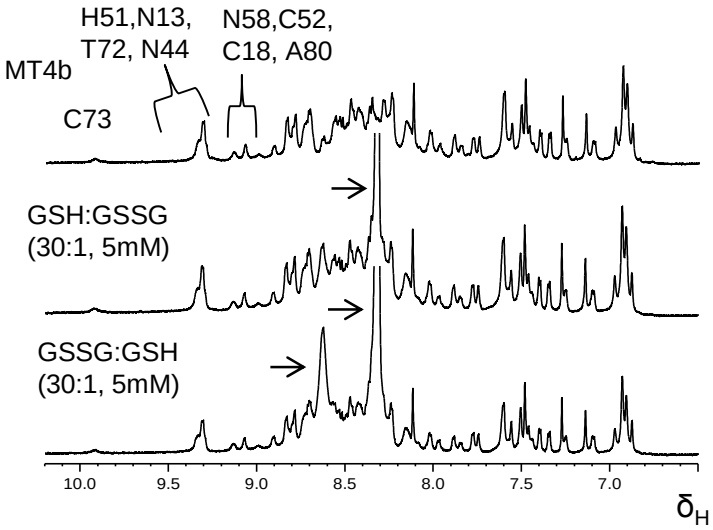

Figure 6.6 1D ^{1}H NMR spectra of MT4b treated with 1:30 and 30:1 (GSSG/GSH) at a fixed concentration of 5 mM. Resonance peaks corresponding to domain I and domain II are shown. Also, the appearance of intense NH peaks from glutathione are shown by arrows. Spectra were recorded at 700.24 MHz (220 µM protein, 50 mM Tris-D_{11}, 10 % D_2O, 50 mM NaCl, pH 7.33). The protein was mixed with GSH/GSSG (5 mM, 30:1 and 1:30, Tris-D_{11}, 10 % D_2O, 50 mM NaCl, pH 7.33).

Switching to a GSSG/GSH stoichiometry to 30:1 means a more oxidising environment. Again, the resonance of Cys73 disappeared. However, a new peak

appeared in the downfield region of 8.6 ppm, perhaps due to the differences in resonances of amide protons of GSSG. Disappearance of Cys73 peak as observed in 1D ^{1}H NMR suggests that domain II released zinc preferentially. For better understanding of domain-specific zinc release and its consequences on protein folding, 2D [^{1}H, ^{1}H] TOCSY spectra were recorded with the same samples, displayed in Figure 6.7. 2D [^{1}H, ^{1}H] TOCSY NMR spectroscopy was useful in distinguishing changes occurring for individual amino acids. Addition of 1:30 GSSG/GSH resulted in disappearance of Cys73 as shown in Figure 6.7 (Blue).

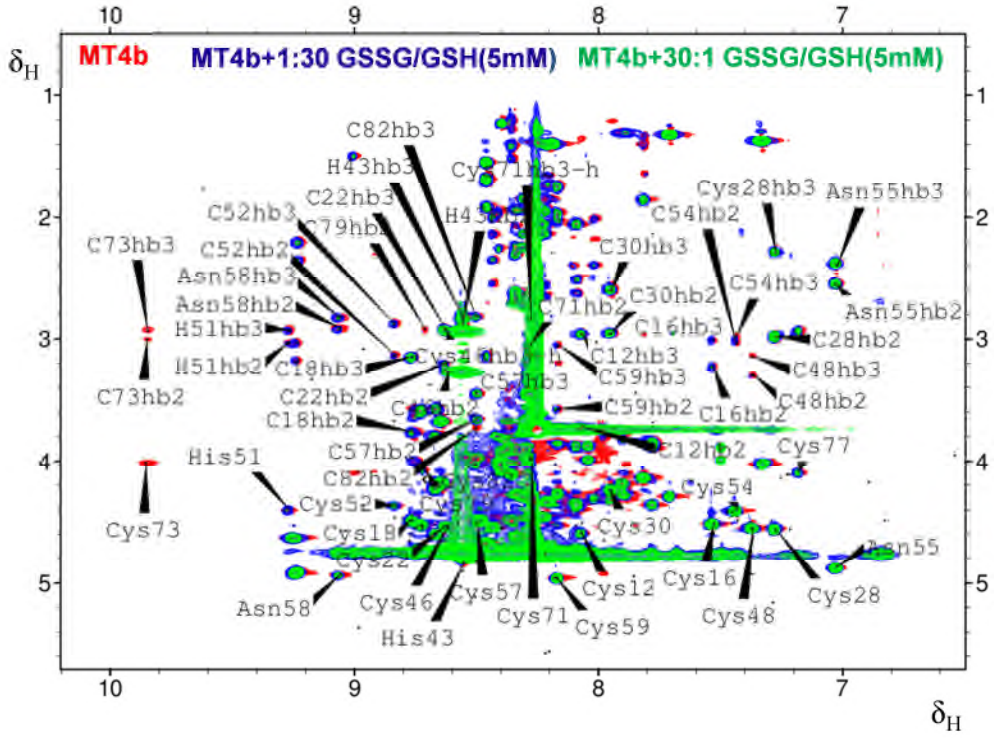

Figure 6.7 Superimposed [^{1}H, ^{1}H] TOCSY spectra of MT4b in absence (Red, 1 mM protein) and presence of 1:30 (Blue) and 30:1 (Green) GSSG/GSH at a fixed concentration of 5 mM. Spectra were recorded at 700.24 MHz, protein (220 µM, 50 mM Tris-D_{11}, 10 % D_2O, 50 mM NaCl, pH 7.33). The protein was mixed with GSH/GSSG (5 mM, 30:1 and 1:30, Tris-D_{11}, 10 % D_2O, 50 mM NaCl, pH 7.33).

A decrease in crosspeak intensities was also observed for Cys79, Cys82, Cys54 and Cys48. Moreover, a small downfield shift of 0.012 ppm of NH-CH(α) and –

CH (β) crosspeaks of Cys59 was observed. In contrast, peak intensities for Cys12, Cys16, Cys18, Cys22, Cys28 and Cys30, i.e., all domain I ligands, remained largely unaffected. However, a small downfield shift of 0.01 ppm was observed for the NH-CH(α) and –CH(β) crosspeaks of Cys16. The resonances from the two histidines and all other cysteine resonances also remained unaffected. Upon increasing the GSSG concentration to a stoichiometry of 30:1 GSSG/GSH, there were pronounced effects observed for domain II residues as displayed in Figure 6.7 (Green). The NH-CH(α) and –CH(β) crosspeaks from Cys73 had completely disappeared, as previously observed. In addition, the NH-CH(β) crosspeaks from Cys48, Cys54, Cys59, Cys52 and Cys79 were almost completely diminished, even though the NH-CH(α) crosspeaks were still detected. Moreover, the NH-CH(β) crosspeaks from Cys59 and His51 were also affected as observed by their decreased intensity. The rest of the domain II resonances from Cys77, Cys46 and Cys57 were largely unaffected. Interestingly, apart from Cys16 all other cysteines resonances from domain I remained unchanged suggesting mostly resilient nature of domain I against redox environment. The experimental observation suggested that domain II was more susceptible to zinc release upon the influence of glutathione redox couple. However, under the more reducing condition at 1:30 GSSG/GSH stoichiometry, the fact that only very few changes in proton resonances were observed was in good agreement with mass spectrometry results and also previously observed results for other MTs (Maret, 1994). Complete or partial disappearance of NH-CH(β) crosspeaks could be the result of a reduction in the amount of the fully zinc-loaded species (with the resulting undermetallated species not observed), consistent with zinc release from the protein. The effect

was more prominent under oxidising conditions than under reducing conditions. However, under more oxidising conditions, domain II appeared to be more vulnerable towards the GSH/GSSG couple while domain I remained less affected within the experimental timeframe.

6.3 Zinc release and thiol reactivity: Effect of 5, 5'-dithiobis (2-nitrobenzoic acid (DTNB)

The exogenous disulfide reagent 5,5'-dithiobis (2-nitrobenzoic acid) (DTNB) has long been used to study the thiol reactivity of MTs. Reactions between MTs and DTNB are usually a two-step process; the reaction products depend on the DTNB concentration, and on whether the thiol attacked first is in the vicinity of a second thiol. If there is an excess of DTNB and/or no second thiol in the vicinity, then the reaction may stop with step 1 and the formation of mixed disulfides. On the other hand, formation of inter- and/or intra-protein disulfide bonds via step 2 can occur when there is an excess of protein, or in cases where protein thiols are close in space (Savas et al., 1993).

$$MTCys + DTNB = MTCys\text{-}TNB + TNB^{-} + H^{+} \qquad \text{step 1}$$

$$MTCys\text{-}TNB + MTCys = MTCys\text{-}CysMT + TNB^{-} + H^{+} \qquad \text{step 2}$$

Previously, thiol reactivity of MTs was studied mostly for MTs from mammalian sources where 20 cysteines bind 7 metal ions in two different cluster arrangements of the 4-metals α-cluster and the 3-metals β-cluster. It was thus interesting to understand the thiol reactivity of plant MTs, in particular the type 4 MT4a and

MT4b for which 17 cysteines and 2 histidines bind 6 metal ions forming two metal clusters of Zn_2Cys_6 and Zn_3Cys_9 and a mono-nuclear metal binding site of $ZnHis_2Cys_2$.

Reactions of MT4s with DTNB were monitored at 412 nm as an indication of formation of TNB^- by means of UV-Visible spectrometry. The experiments were performed in two different reaction conditions where [MT] >> [DTNB] and [MT] << [DTNB] as shown in Figure 6.8. Under both conditions, the thiolates of MT4a reacted faster than those of MT4b. However, at low DTNB concentration, the differences in thiol reactivity were more prominent as seen in Figure 6.7A. Different reactivity observed for very similar MTs was thought to originate from different cluster reactivity, participation of bridging and terminal thiolate ligands and also the position of metal-coordinating cysteines (Munoz et al., 2002).

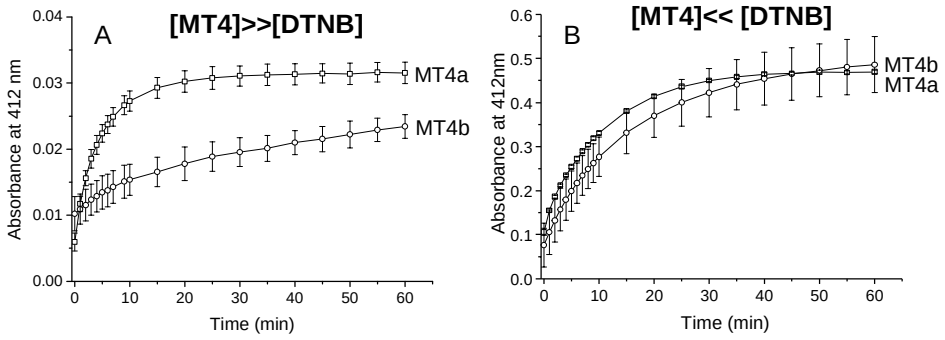

Figure 6.8 Time courses for the reactions of MT4a and MT4b with DTNB under two different reaction conditions: (A) [MT4]>>[DTNB] and (B) [MT4]<<[DTNB]. Reaction conditions: (A) [MT4]>>[DTNB]; proteins (5 µM (85 µM thiol), 0.2 M Tris buffer, pH 7.33) were reacted with DTNB (2 µM, 0.2 M Tris buffer, pH 7.33) (B) [MT4]<<[DTNB], proteins (2.5 µM (42.5µM thiol), 0.2 M Tris buffer, pH 7.33) were reacted with DTNB (1 mM, 0.2 M Tris buffer, pH 7.33). In both cases, the formation of TNB^- was monitored at 412 nm.

However, it was observed that the reversal of the amino-acid sequence of the α-domain of human MT2 had very little effect on reactivity towards DTNB (Pan et al., 1999).

Subsequently, mass spectrometry was used to monitor the metallo-species formed as a result of oxidation by DTNB at 1:1 and 1:17 stoichiometry with respect to protein concentration as shown in Figures 6.9 and 6.10.

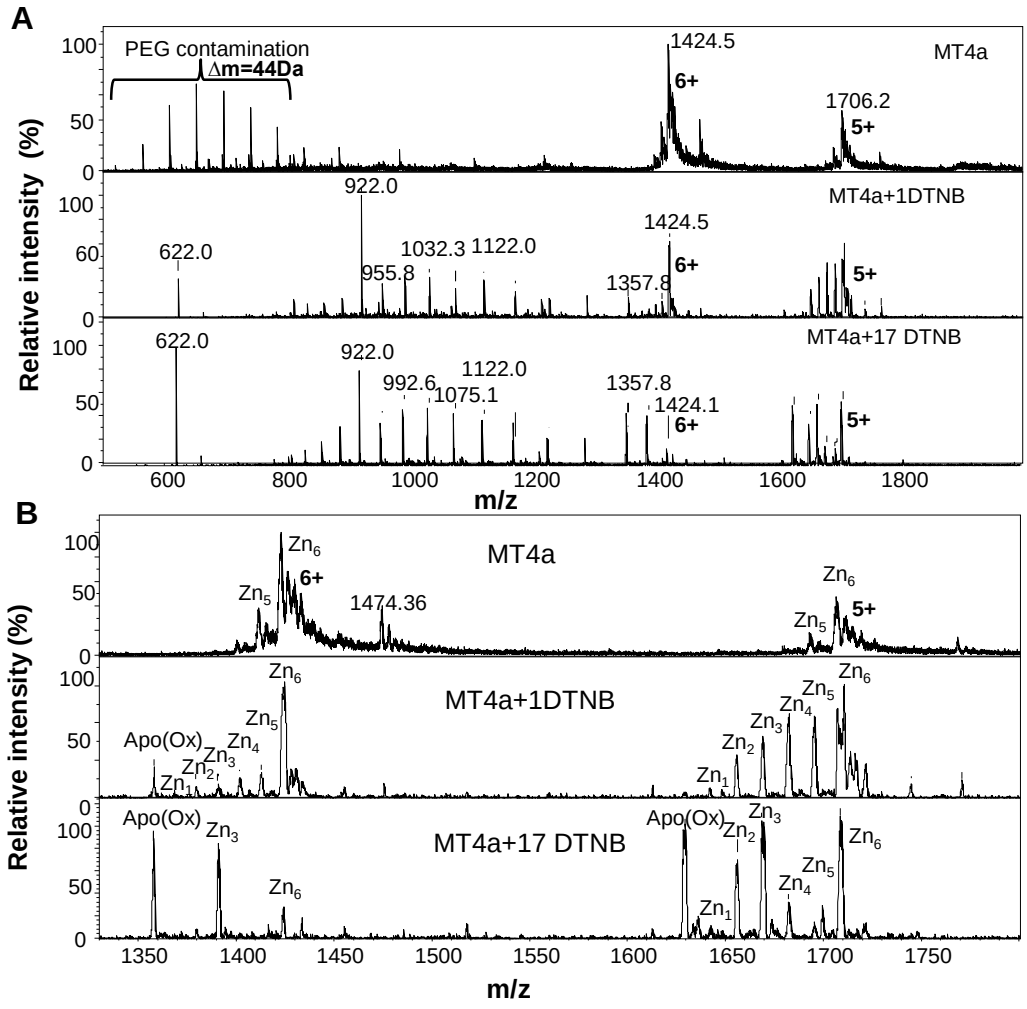

Figure 6.9 Reactions of MT4a with DTNB observed by mass spectrometry. (A) Raw spectra of MT4a in absence and presence of DTNB. (B) Raw spectra showing the charge states of 6+ and 5+ with different metallo-species as formed upon the reaction with DTNB. Reaction condition: Protein (25 μM, 20 mM NH_4HCO_3 buffer) was incubated with DTNB (1 or 17 equivalents) for 2-3 hours. Desalted protein samples (25 μM, 10% v/v CH_3OH, 10 mM NH_4HCO_3 buffer, pH 7.8) were subjected to mass spectrometry analysis.

Protein samples were desalted prior to mass spectrometry. Addition of 1 equivalent of DTNB to MT4a resulted in the formation of oxidised under-metallated species of Zn_5, Zn_4, Zn_3 Zn_2 and Zn_1 as shown in Figure 6.9. Interestingly, fully oxidised apo along with fully metallated Zn_6 species were also observed. Increasing the DTNB concentration to 17-fold (equimolar with respect to thiols) produced oxidised Zn_3 and fully oxidised apo as most abundant species with comparable intensities for their 6+ charge states. Surprisingly, the Zn_6 species was still observable. One of the intriguing features was that unusually, different metallo-species were observed for the 6+ and 5+ charge states. For the 5+ charge state, Zn_6, Zn_3 Zn_2 and oxidised apo-species became the major species. However, low intensity Zn_5, Zn_4 and Zn_1 species were also observed.

Different metallo-species formed as observed for 5+ charge states suggested that in the gas phase, metallo-species with a 5+ charge state were perhaps in more stable conformations compared to the same metallo-species in their 6+ charge state. Ion mobility mass spectrometry could perhaps help elucidating conformational changes in the gas phase.

For MT4b, the results observed were also interesting as displayed in Figure 6.10. At 1 equivalent of DTNB, there was not much change observed for neither 6+ nor 5+ charge states, but interestingly, the 7+ and 8+ charge states produced different metallo-species. However, there was a very intense peak at 1646.8 m/z. If this corresponded to a 6+ charge state, the deconvoluted mass would be 9874.8 Da, consistent with a mass of [Zn_6MT4b+6TNB]. However, no such peak corresponding to a 5+ charge state was observed; furthermore, an adduct with 6 TNB moieties is highly unlikely at such low DTNB concentrations, and would be

expected to produce under-metallated species due to the conversion of coordinating cysteines to oxidised cysteines with much lower metal affinity. This peak was also not the result of backbone cleavage as no such mass was observed in findpept. Presumably, the peak (1646.8 m/z) corresponds to a contaminant introduced during sample preparation. At 17 equivalents of DTNB, Zn_4 and Zn_3 species emerged; however Zn_3 was the major species. Yet again, the Zn_6 species was also observed, but at lower intensity. Interestingly, and in contrast to MT4a, no apo-species was observed for MT4b. A close look at the raw spectra suggests that oxidation resulted in cleavage of the protein, as the overall peak intensity had decreased, and many peaks with low mass/charge ratio (m/z) were observed but with low intensity at 1:17 equivalents. Cleaved peptide analysis by findpept also suggested that those low m/z peaks were cleaved peptides from MT4b. However, cleavage of MT4a was also observed. Interestingly, neither of the isoforms formed any mixed disulfides of Cys-TNB as no masses corresponding to mixed disulfides were observed. However, intra-disulfide bond formation of Cys-Cys was confirmed as deficits in m/z were observed for each undermetallated metallo-species, including fully oxidised apo-species in the case of MT4a. Formation of mixed disulfides had been observed for rabbit liver MT2 at low DTNB concentration (Munoz et al., 1999); at high concentration of DTNB intra-molecular disulfides were observed. Mass spectrometry data also support the results observed by UV-Visible spectroscopy for MT4a and MT4b. As no mixed disulfides were observed, both reaction steps occurred for both MTs, indicating preferential reaction of the protein-TNB adducts that must have formed in step 1.

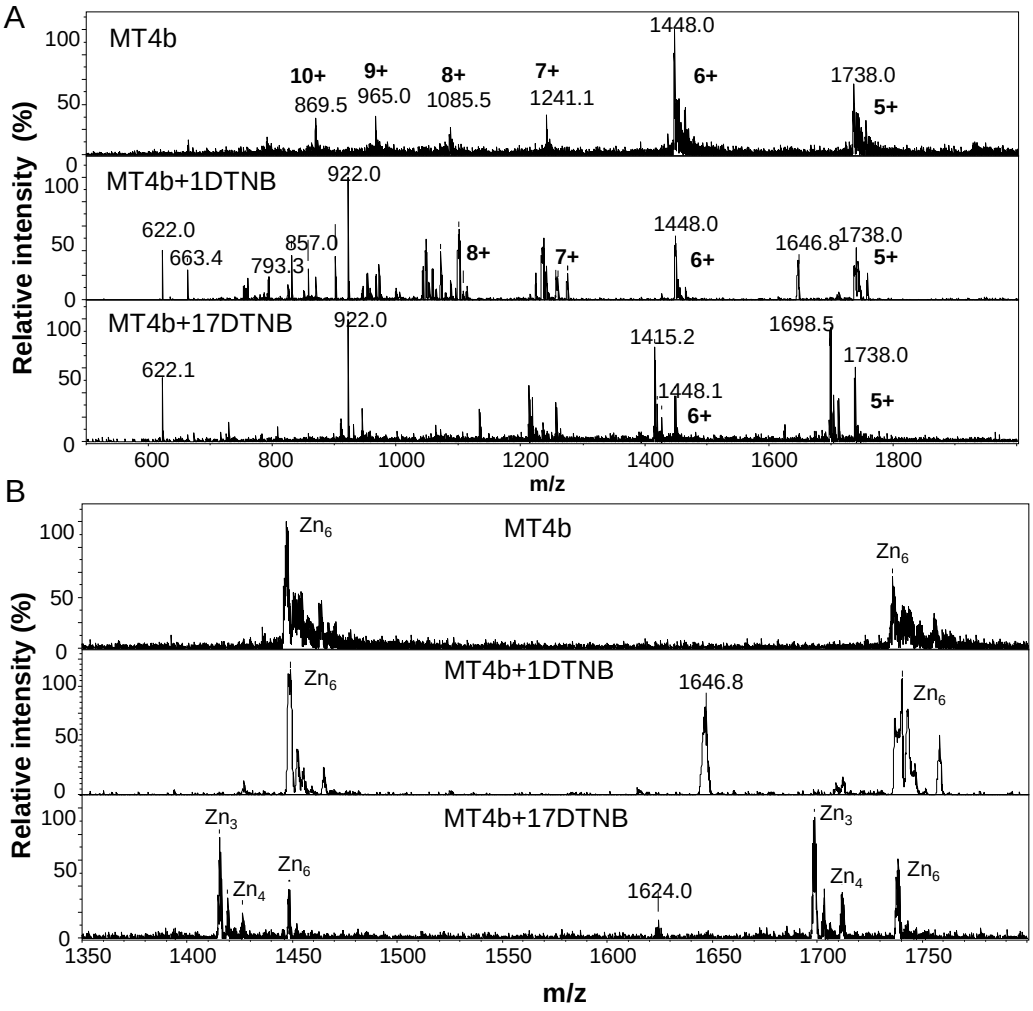

Figure 6.10 Reactions of MT4b with DTNB observed by mass spectrometry. (A) Raw spectra of MT4b in absence and presence of DTNB. (B) Raw spectra showing the charge states of 6+ and 5+ with different metallo-species as formed upon the reaction with DTNB. Reaction conditions: Protein (25 µM, 20 mM NH_4HCO_3 buffer) was incubated with DTNB (1 or 17 equivalents) for 2-3 hours. Desalted protein samples (25 µM, 10% v/v CH_3OH, 10 mM NH_4HCO_3 buffer, pH 7.8) were subjected to mass spectrometry analysis.

To further explore the reactivity of the MT4 domains with DTNB, ^{1}H NMR spectroscopy was used. The proteins were allowed to react with DTNB at 1:1 stoichiometry with respect to cysteine concentrations or 1:17 with respect to

protein concentration and spectra were recorded at 4-5 minutes intervals. Spectra as shown in Figure 6.11 suggested that MT4a reacted faster than MT4b.

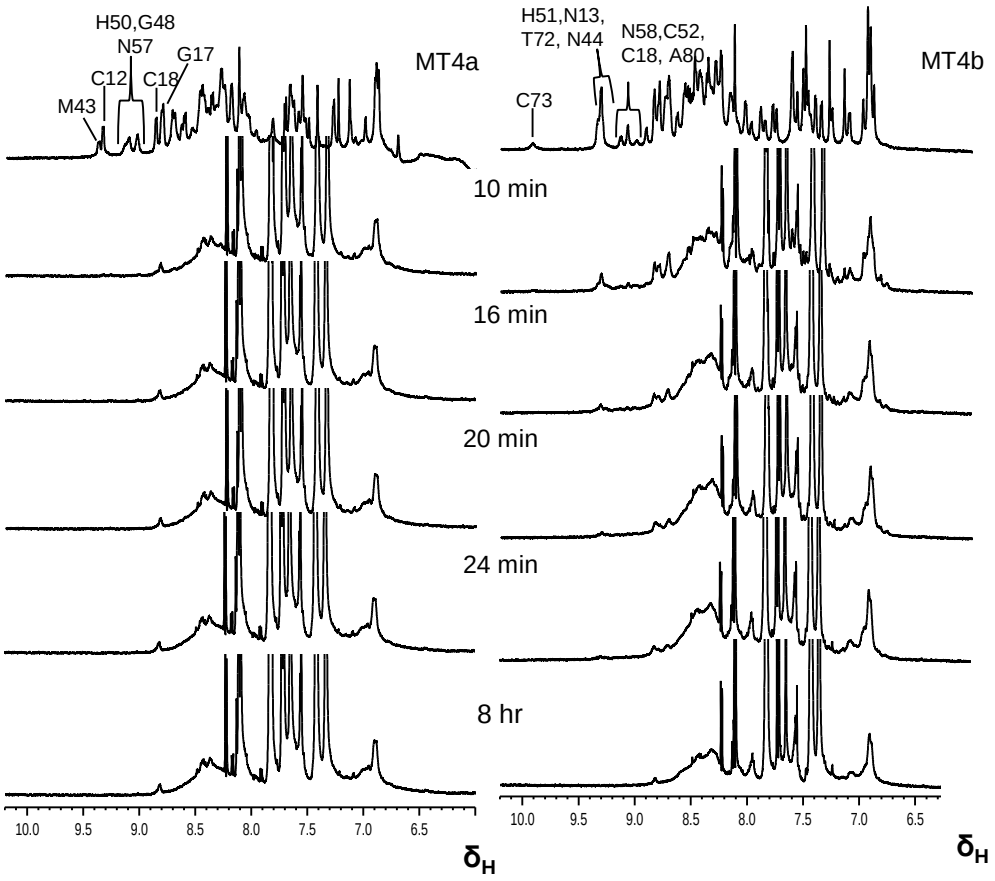

Figure 6.11 1D ^{1}H NMR spectroscopic time course reactions of MT4a and MT4b with DTNB. Spectra were recorded at 700.24 MHz, proteins (298 µM, 50 mM Tris-D_{11}, 10 % D_2O, 50 mM NaCl, pH 7.33). Proteins were mixed with DTNB (5.066 mM, 1:1 with respect to [thiol] or 1:17 with respect to [protein]).

At 10 minutes, most of the resonances from domain I and domain II for MT4a had completely disappeared. After 14 minutes, not much further change was observed. However, some low-field resonances at 8.6-8.9 ppm and some upfield resonances at 6.7-7.2 ppm were still visible but with very low intensity. These resonances could perhaps originate from domain I as at the low-field region G17 peak was

still observed. On the other hand, initially DTNB attack on MT4b was found to be slower compared to MT4a. Many of the peaks corresponding to domain II were diminished after 10 minutes. Although domain I resonances were also affected, they were still visible, e.g. the resonance from N13. At 20 minutes, the latter resonance had completely disappeared. After 8 hours both spectra looked very similar and were consistent with completely unfolded proteins. Addition of DTNB resulted in very intense peaks in the 7.3 to 8.3 ppm region, corresponding to the four nitrobenzoate protons. Their intensities were so high that they obscured any peaks from the proteins within this region. At higher concentration of DTNB, both domains reacted too fast; hence NMR spectroscopy could not give any further results on domain reactivity. Moreover, both UV-Vis and NMR spectroscopy suggested that MT4a reacted faster than MT4b. Furthermore, as under-metallated species of Zn_3 along with low intensity Zn_6 were still observed by mass spectrometry suggested that perhaps domain II was more susceptible to DTNB attack than domain I.

6.4 Zinc release and thiol reactivity: Influence of hydrogen peroxide (H_2O_2)

There is a shortfall of studies to evidence the role of MTs as an antioxidant with various reactive oxygen species (ROS) in general and hydrogen peroxide in particular. Previously it has been shown that hypocholorous acid (HOCl) and the superoxide radical anion ($^{\cdot}O_2^-$) were more effective than hydrogen peroxide (H_2O_2) to elicit oxidation and subsequent metal release from MTs (Fliss and Ménard, 1992). However, later it has been demonstrated that H_2O_2 can influence metal release from MTs (Jimenez et al., 1997). Furthermore, a study in HL-60

cells suggested a direct reaction of MTs with H_2O_2 to protect from DNA damage (Quesada et al., 1996). It has also been shown that the *in vitro* reaction with H_2O_2 resulted in the oxidation of MT thiols, with substantial loss of metal ions (Zeitoun-Ghandour et al., 2011). All these studies were conducted with mammalian MTs. Very little is known about the interactions of H_2O_2 with plant MTs. Although some work on plant MTs has already been done on the gene level (Mir et al., 2004; Zhu et al., 2009), not much work has been done on the protein level, especially not with seed-specific type 4 MTs. This is despite the fact that H_2O_2 plays an important role in the seed life cycle, especially during germination (El-Maarouf-Bouteau and Bailly, 2008). As it has been hypothesised that MT4s help seed germination by providing zinc, the reaction of MT4s with H_2O_2 is of immediate relevance. This section explores whether zinc mobilization from MT4s upon the influence of H_2O_2 may occur.

Mass spectrometry was employed to understand which metallo-species formed during the reaction. Metallo-species formed are presented as observed for 6+ charge state of MT4a and MT4b (Figure 6.12). At the start of the reaction, the spectra are dominated by the fully zinc-loaded Zn_6MT4a and Zn_6MT4b. Addition of an equimolar amount of H_2O_2 (with respect to thiols) resulted in Zn_6 and Zn_5 species at 4 minutes for both isoforms; however, for the latter with lower intensity. With progressing time to 10 minutes, very low intensity Zn_4 and Zn_3 appeared and a very small increase in intensity was observed for the Zn_5 metallo-forms. At that time point Zn_6 was still the major species for both isoforms. Interesting differences between MT4a and MT4b were observed at 15 minutes and subsequent time points up to 17-18 hours. While metallo-species formed for

MT4a remained the same up to 18 hours, MT4b exhibited a gradual metal release with progression of time. At 15 minutes, the Zn_2MT4b metallo-form was observed, and it took 25 minutes for Zn_1 to appear. During the next 60 minutes and then up to 18 hours there were gradual increases in the intensities of Zn_1, Zn_2, Zn_3, Zn_4 and Zn_5 species and a corresponding decrease for the Zn_6 species.

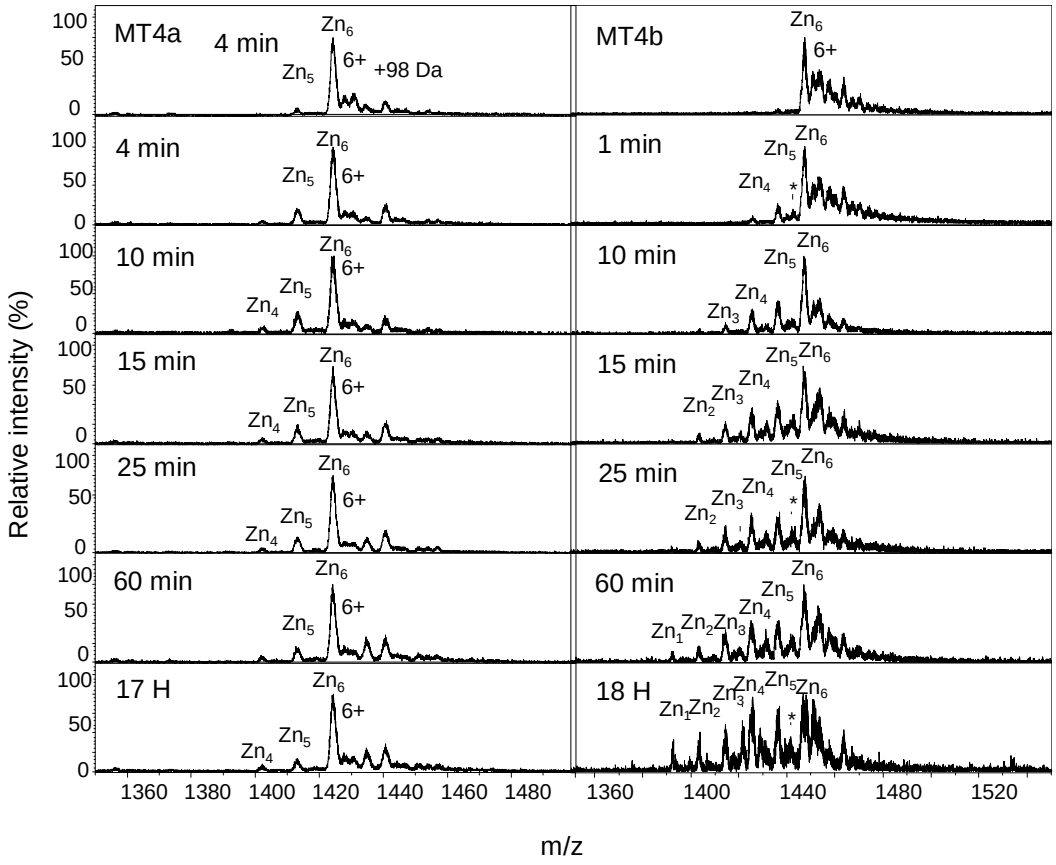

Figure 6.12 Raw mass spectra showing the 6+ charge states for the time dependent reactions of MT4a and MT4b with H_2O_2. Desalted protein samples (250 µM, 10 mM NH_4HCO_3 buffer) were mixed with H_2O_2 (4.25 mM, 1:1 with respect to [thiol] or 1:17 with respect to [protein]). Immediately after mixing, aliquots (10 µL) were taken out from the reaction solution at different time intervals, and diluted samples (25 µM, 10% v/v CH_3OH, 10 mM NH_4HCO_3 buffer, pH 7.7) were analysed by mass spectrometry.

However, the intensity of the Zn_6MT4b species remained abundant even after 18 hours. Interestingly, no apo species was observed, in contrast to observations for the two isoforms of CeMT1 and CeMT2 for *C. elegans* (Zeitoun-Ghandour et al.,

2011). However, formation of no apo species was previously predicted for mammalian MT2 by using chromatographic methods and a metal displacement reaction (Quesada et al., 1996). Although cysteine oxidation was observed for both isoforms, interestingly, no masses corresponding to sulfinic or other related acids as a results of cysteine oxidation were observed. Sulfinic acid adducts were observed for CeMT1 which, like plant MT4s, possesses an odd number of cysteines. A close analysis on the observed peaks between the metallo-species for MT4b indicated that these were adducts of Na/K salts. Formation of Na/K salt adducts were evident from reaction between XPA zinc fingers with H_2O_2 (Smirnova et al., 2007).

To explore whether H_2O_2-induced zinc release displayed any domain specificity, 2D [^{1}H, ^{1}H] TOCSY NMR spectroscopy was employed (Figure 6.13). Data for MT4a as shown in Figure 6.13 suggested that there was no significant change observed with the protein before and after addition of H_2O_2. Only resonances from His42, His50, Cys45 and Cys58 were somewhat affected as decreases in cross-peak intensities were observed. Interestingly, neither of these peaks was completely diminished. These data were in good agreement with observations from mass spectrometry, as very little change was observed. Interestingly, for MT4b, domain II was found to be susceptible to oxidation as indicated by a loss of crosspeak intensity. The 2D [^{1}H, ^{1}H] TOCSY NMR spectrum after reaction with H_2O_2 suggested that resonances from Cys73 and Cys79 had completely disappeared while Cys77 was almost absent, too. In addition, NH-to-CH (β)-proton crosspeaks from Cys46, Cys71, Cys82, Cys48, Cys54 and Cys59 had

disappeared. Moreover, the respective crosspeaks from Cys57 and Cys59 were hugely affected as lower peak intensities were observed.

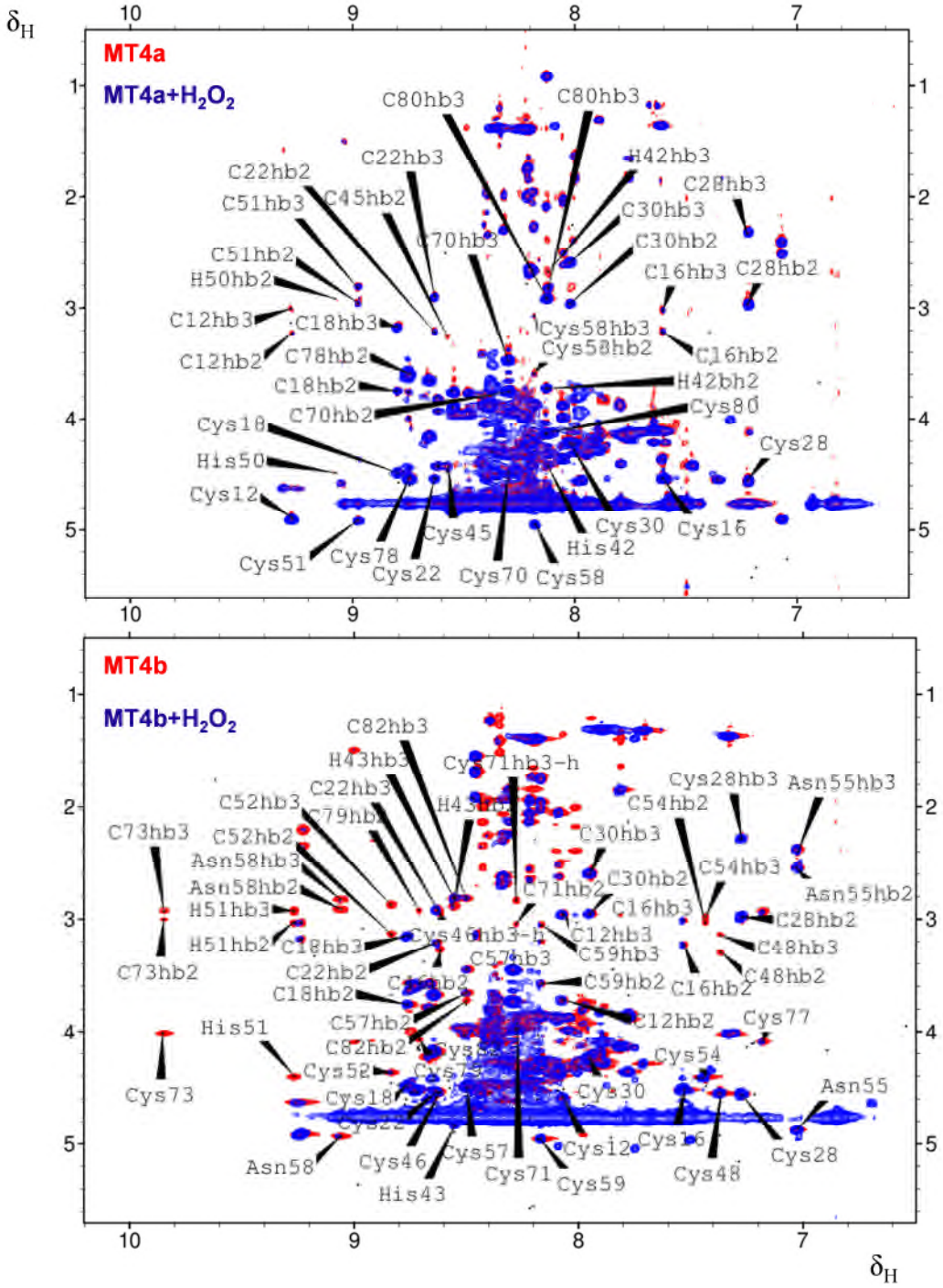

Figure 6.13 Superimposed [^{1}H,^{1}H] TOCSY NMR spectra of MT4a and MT4b in absence (Red) and after reaction (Blue) with H_2O_2. Proteins (250 µM, 50 mM Tris-D_{11}, 10 % D_2O, 50 mM NaCl, pH 7.33) were mixed with H_2O_2 (4.25 mM, 1:1 with respect to [thiol]).

Interestingly, both histidine residues were also affected as resonances from His51 had completely disappeared while the NH-to-β proton crosspeaks of His43 were decreased. Importantly, cysteine resonances from Domain I remained largely unaffected, suggesting that this domain resisted oxidation. However, lower peak intensity for Cys22 and a downfield shift of 0.01 ppm observed for Cys16 could originate from the unfolding of the neighbouring domain II.

Both mass spectrometry and NMR spectroscopy suggested that MT4a was less reactive toward oxidation by H_2O_2. However, MT4b underwent H_2O_2 oxidation. Interestingly, oxidation was found to be domain-specific where domain II was more reactive while domain I remained largely inert towards oxidation within the experimental conditions.

In summary, GSH and GSSG/GSH (GSH in large excess) had very little effect on zinc mobilistion from MT4b, while GSSG and GSSG/GSH (GSSG in large excess) helped release zinc from MT4b, resulting in partially and fully oxidised protein. However, GSSG formed non-covalent adducts with MT4b, suggesting that the presence of such binding sites could perhaps allow manipulating functional properties of this protein. Moreover, GSSG formed a stable adduct of Cd_6MT4b-GSSG by replacing Zn^{2+} from Zn_6MT4b-GSSG; this suggests that protein misfolding due to Cd^{2+} had no effects on adduct formation. Faster reaction of MT4a with DTNB than MT4b suggests that thiols in MT4a are more reactive in disulfide interchange reactions than thiols in MT4b. However, the resistant nature of MT4a against oxidation by H_2O_2 suggests that perhaps *in vivo*, a surge of H_2O_2

during seed germination has little effects on MT4a. This could indicate that the two isoforms retain/release zinc to perform distinct functions, perhaps at different timepoints during seed germination to meet different Zn^{2+} demands.

Chapter 7

Conclusions: Structure and Properties relationships

7.1 Introduction

Variation in amino acid sequences, occurrence in almost every phyla and diversity in functional properties make metallothioneins important proteins to study their structure and functional relationships. Plant MTs are a family of proteins for which very limited structural and functional properties information is available in general. It has been hypothesised that type 4 plant MTs donate zinc to zinc-requiring proteins or peptides during seed germination and help seedling growth. A better understanding of structural and functional properties of type 4 MTs may have benefits for future food safety and nutritional demands. Here, two type 4 MT isoforms -MT4a and MT4b from the dicotyledonous plant *Arabidopsis thaliana* - have been studied. Protein isoforms were recombinantly expressed in *E. coli*, purified by chromatographic methods, identified by SDS-PAGE and characterised by mass spectrometry and NMR spectroscopy. Both isoforms were found to bind 6 zinc ions. To understand how metal (Zn and/or Cd) ions are organised to form clusters within the proteins, multinuclear and multi-dimensional NMR spectroscopy was employed. Moreover, to study the metal-cluster dynamics of these protein isoforms, a range of biomimetic and biological reagents were used. The aim of this chapter is to summarise and explain all the results achieved.

7.2 MT4a and MT4b bind zinc

Proteins recombinantly expressed in *E. coli* were purified by chemical precipitation and chromatographic methods. During identification of purified proteins, erratic migration was observed in SDS and Native PAGE, however, erratic migration on SDS gels is a common phenomenon for MTs (Meloni et al., 2005). Incomplete destruction of metal clusters or oxidative dimerisation/oligomerisation was considered to be the origin of this behaviour. Consequently, metal chelator EDTA and reducing agent DTT treated MT4a samples have shown that not oxidative oligomerisation but the high metal cluster stability against denaturation was responsible for slow migration of MT4s on SDS gels. Mass speciation by mass spectrometry and elemental analysis by ICP-OES revealed that like their homolog from wheat, E_C (Leszczyszyn et al., 2007; Peroza and Freisinger, 2007), both the isoforms bind six zinc ions.

7.3 Mixed metal species: Towards cluster topology

Both the isoforms were well-folded in presence of zinc. However, the six zinc ions were distributed in two domains, namely domain I - binding 2 zinc ions with 6 cysteines - and domain II – binding 4 zinc ions with 11 cysteines and 2 histidines. However, within domain II, one zinc ion binds to two cysteines and two histidines to form a mononuclear site. This mononuclear site has been identified in both MT4a and MT4b. For determining the metal connectivity to cysteines, ^{111}Cd NMR spectroscopy has been employed as standard technique for metal-to-ligand connectivity studies for MTs.

Like for their homolog E_C from wheat, domain II of MT4a and MT4b was misfolded in Cd-saturated proteins. However, domain I remained folded in the cadmium forms, and connectivities to cysteines for these two Cd ions have been identified. A previous study on wheat E_C (Leszczyszyn et al., 2010) illustrates that the mononuclear $ZnHis_2Cys_2$ site is critical for proper folding of domain II, however, this occurs in presence of zinc only. An idea of mixed metal (Zn/Cd) species has been developed for cluster study. The goal was to prepare mixed Zn/Cd samples where Zn would be exclusively in the mononuclear site. To achieve the right stoichiometry of Cd to Zn, for which Zn would remain in the mononuclear site, whereas other binding sites would be occupied mostly by Cd, the metal-exchange reaction of Zn by Cd has been studied. Sub-stoichiometric to stoichiometric cadmium addition to the fully zinc-loaded proteins formed different $Zn_{6-n}Cd_n$ (n= 1, 2, 3, 4, 5 and 6) species. Mixed species co-exist in solution. At higher cadmium stoichiometries of 5 and 6 molar equivalents, the mononuclear site was not observed, and the entire domain II was misfolded. However, a homogeneous domain I with respect to Cd was observed. Moreover, at 4 equivalents of Cd the foldedness of mixed metal species, as assessed by multinuclear NMR spectroscopy, suggested that the mononuclear site was present and occupied by Zn. The zinc-bound mononuclear site was also observed at lower Cd ratios; however, the maximal number of cadmium resonances, and hence metal-to-ligand connectivities, was observed at 4 molar equivalents of Cd.

7.3.1 Cluster topology of mixed metal species at 4 equivalents of Cd^{2+}

In the presence of 4 molar equivalents of Cd, two cadmium ions were found to bind to two binding sites in domain I, but mixed Cd-Zn sites were also identified within domain I. One Zn bound to the mononuclear site, and two further Cd resonances were detected in 2D [^{1}H, ^{111}Cd] HSQC spectra. Connectivities to domain II cysteines were detected, hence this suggested that the remaining three sites in domain II were predominantly occupied by two Cd and one Zn.

Domain I: The cluster structure of domain I has been determined experimentally by ^{111}Cd NMR spectroscopy. 4 terminal and 2 bridging cysteines were identified in the binuclear cluster of Zn_2Cys_6 similar to E_C (Loebus et al., 2011). Among 8 Cys-Cd connectivities within this domain, 7 connectivities have been determined.

Domain II: A mononuclear and a three metal binding site

Mononuclear site: Two cysteines and two histidines bind to one zinc to form a $ZnCys_2His_2$ mononuclear site; this has been identified using 2D [^{1}H, ^{1}H] TOCSY, NOESY and [^{1}H, ^{15}N] HSQC spectra. Although no direct metal-to-ligand connectivity information is obtainable for this site, the presence of characteristic through-space NOESY peaks between the four ligands strongly suggests that this site is also present in MT4a and MT4b.

The three remaining metal sites: A binuclear cluster bridging to a single metal binding site?

Six cysteines bind 2 metals to form a binuclear site, similar to that seen in domain I, but one of the “terminal” cysteines binds a further single metal, with the single

metal also terminally connected to three further cysteines, thus providing a binuclear cluster bridging to a single metal binding site. Two binding sites in the binuclear cluster have been partially identified experimentally by ^{111}Cd NMR spectroscopy. Three connectivities for site Y (chapter 4) and one connectivity for site X (chapter 4) were confirmed by 2D [^{1}H, ^{111}Cd] HSQC NMR spectroscopy. The site X was connected to 3 nearest cysteines based on Zn-thiolate distances. Connectivity of the third site Z was based on the results of dynamics studies (Chapter 5). Among 12 connectivities, 4 connectivities were determined experimentally by ^{111}Cd NMR spectroscopy. Of the remaining 8 connectivities, 3 connectivities were based on dynamics results and the remaining 5 connectivities were based on assumptions considering nearest Zn-thiolate bond distance.

For domain I and domain II together, out of 24 connectivities, 15 connectivities are supported by experimental data.

7.4 MT4a and MT4b can transfer or release zinc

The role of type 4 MTs is hypothesised to release or transfer zinc to zinc-requiring proteins, peptides or small molecules during seed germination to help seedling growth. It was therefore important to understand whether both isoforms can release or transfer zinc to meet functional criteria as a zinc donor. The zinc transfer ability of MT4a and MT4b to two metal chelators - EDTA and PAR – was compatible with a role for MT4a and MT4b as zinc donors. However, the differences in readiness to transfer zinc to the small and strong metal chelator

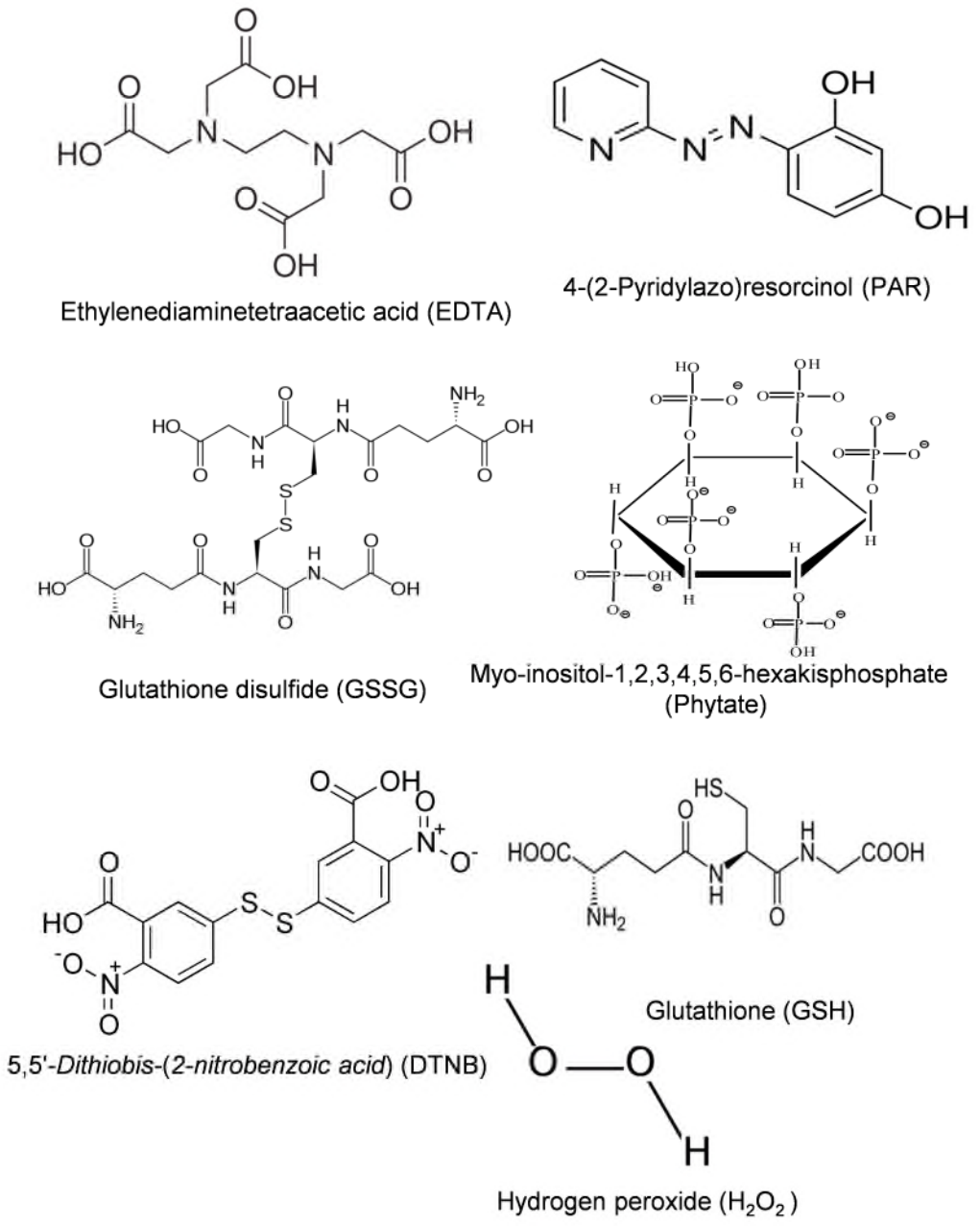

Figure 7.1 Chemical structures of metal chelators and oxidants used in zinc binding dynamics studies.

EDTA in comparison to the bulky and moderately strong PAR indicates that the zinc donor ability of these isoforms depends on the properties of the acceptors as well. Importantly, this, as well as kinetic parameters for the reaction with EDTA

that pointed towards a bimolecular mechanism, suggested that efficient zinc transfer required the direct interaction between MT and acceptor.

MT4a and MT4b bind zinc and they can act as zinc donors, however, it was also important to understand any factors that could help MT4s to release or mobilize zinc. The reaction of MT4a and MT4b with redox-active glutathione, disulfides, reactive oxygen species, variation of pH, and phytate suggests they can play significant roles in cellular context. MT4a and MT4b exhibited very similar pH of half dissociation; however, somewhat lower than their homolog E_C from wheat. The GSH/GSSG redox couple and DTNB alone led to zinc release. The reactive oxygen species H_2O_2 also released zinc from MT4b, but resistant behaviour was observed for MT4a. On its own, the anti-nutrient phytate had very little effect on zinc mobilization from MT4a and MT4b, however, phytate accelerated and increased zinc transfer to PAR from both isoforms suggesting phytate can modify metal transfer dynamics *in vivo*.

7.5 MT4a transfers/releases zinc faster than MT4b

Based on biological function studies, it has been suggested that *A. thaliana* MT4a and MT4b work cooperatively where the role of MT4a is to distribute zinc and MT4b functions as a store for zinc (Ren et al., 2011) . Thus a role assigned for MT4a as a zinc distributor, it is assumed that zinc transfer will be a fast process, while for MT4b as a storage protein, the process should be slow. Faster zinc transfer from MT4a to EDTA and PAR compared to zinc transfer from MT4b would be consistent with a zinc distribution role of MT4a. Comparatively slower

zinc transfer reactions for MT4b suggest that MT4b may store zinc a little longer than MT4a. Phytate accelerated zinc transfer to PAR from both MT4a and MT4b, however the effect was more pronounced in MT4a than MT4b. MT4a thiols were more reactive than thiols in MT4b towards oxidation by DTNB, however, at low DTNB concentration, the effect was more pronounced. While zinc released from MT4b due to H_2O_2 mediated oxidation was observed, on contrary, MT4a resisted zinc release through oxidation by H_2O_2. This is mirrored by observation that *in vivo* MT4a gene expression was not affected by H_2O_2 while an increase in MT4b gene expression was observed (Ren et al., 2011).

7.6 MT4a and MT4b transfer or release zinc in domain specific manner

MT4a and MT4b transferred or released zinc in domain specific ways, where domain II was more vulnerable to pH variation and EDTA attack than domain I, and consequently transferred or released zinc first. MT4b domain II was also affected by H_2O_2, DTNB, GSSG/GSH in oxidising condition. MT4a resisted H_2O_2 oxidation, whilst oxidation by DTNB was too fast to draw any conclusions regarding domain specificity. Reaction with PAR was an equilibrium process; hence, no comments can be made regarding the domain specificity of the reaction. However, the fact that MT4a formed a stable Zn_4 species as monitored by mass spectrometry suggested cooperative metal transfer. Cooperative metal release was also observed during pH titrations, for which a stable Zn_2 species was observed for MT4a. Zinc release or transfer from MT4b to metal chelator and due to pH

variation was non-cooperative as no predominant metallo-species corresponding to any domain was observed.

Some intriguing features were

I. Development of a Zn_5 species for MT4b in reactions with H^+, EDTA and PAR suggested a labile zinc site within domain II, site Z as proposed in the cluster model.

II. After zinc transfer from the most labile site of MT4b to EDTA, the rest of the protein remained mostly folded as evident from [^{1}H, ^{15}N] HSQC spectra, suggesting that the labile site had very little effect on global protein folding.

III. Both domains of MT4a reacted almost simultaneously with EDTA and DTNB; however, initially a slight preference for domain II was observed.

IV. Domain I of both MTs was refolded a few hours after the reaction with EDTA, suggesting that domain I of MT4a and MT4b can act as strong zinc chelator if sub-stoichiometric amount of zinc is present.

Domain specific zinc transfer or release as observed for MT4a and MT4b suggests that these two isoforms can act as multi-targeting zinc donors, where two domains will be able to donate zinc to different zinc-requiring sites at the same time (in terms of germination and seedling development) or at different times.

7.7 Origins of cluster reactivity

In spite of 84% sequence identity, MT4a and MT4b have shown remarkable differences in cluster reactivity against pH, metal chelators and different oxidants as discussed in chapters 5 and 6. Small variations in amino acid sequences and charge distribution might be the reason for differential reactivity. A change in single non-cysteine residues in lobster MT was found to have a profound effect on the cluster reactivity (Muñoz et al., 2000). Moreover, a sequence of C(6)P(7)C(8)P(9) is important for the biological function of human MT3 (Sewell et al., 1995) The sequences of MT4a and MT4b have some dissimilarities as highlighted in Figure 7.1.

```
     1        10        20        30        40        50        60        70
MT4a ADTGKGSSVAGCNDSCGCPSPCPGGNSCRCRMR-EASAGDQGHMVCPCGEHCGCNPCNCPKTQTQTSAKGCTCGEGCTCASCAT
MT4b ADTGKGSASASCNDRCGCPSPCPGGESCRCKMMSEASGGDQEHNTCPCGEHCGCNPCNCPKTQTQTSAKGCTCGEGCTCATCAA
```

Figure 7.2 Protein sequence alignment of MT4a and MT4b. Yellow color highlights dissimilarities in amino acids between the sequences. Number considers alanine (A) as position 1, since the terminal methionine is cleaved during purification.

In domain I, dissimilarities are observed at positions 8 (S-A), 9 (V-S), 11 (G-S), 15 (S-R) and 26 (N-E) for MT4a and MT4b, respectively. At the beginning of the 1st Cys-free stretch, dissimilarities are observed at position 31 (R-K), 33 (R-M), 34 (missing-S), 37/38 (A-G). Remarkable dissimilarities are observed near the 1st histidine residues (H42 or H43). Whilst for MT4a a sequence of GHMV (41-44) is observed, for MT4b the sequence is EHNT (42-45). The presence of the negatively charged residue E42 in the vicinity of H43 and another extra negatively charged residue (E26) in MT4b could perhaps hamper the interaction of anionic

molecules like EDTA, PAR and phytate to attack, resulting in slower metal release than from MT4a.

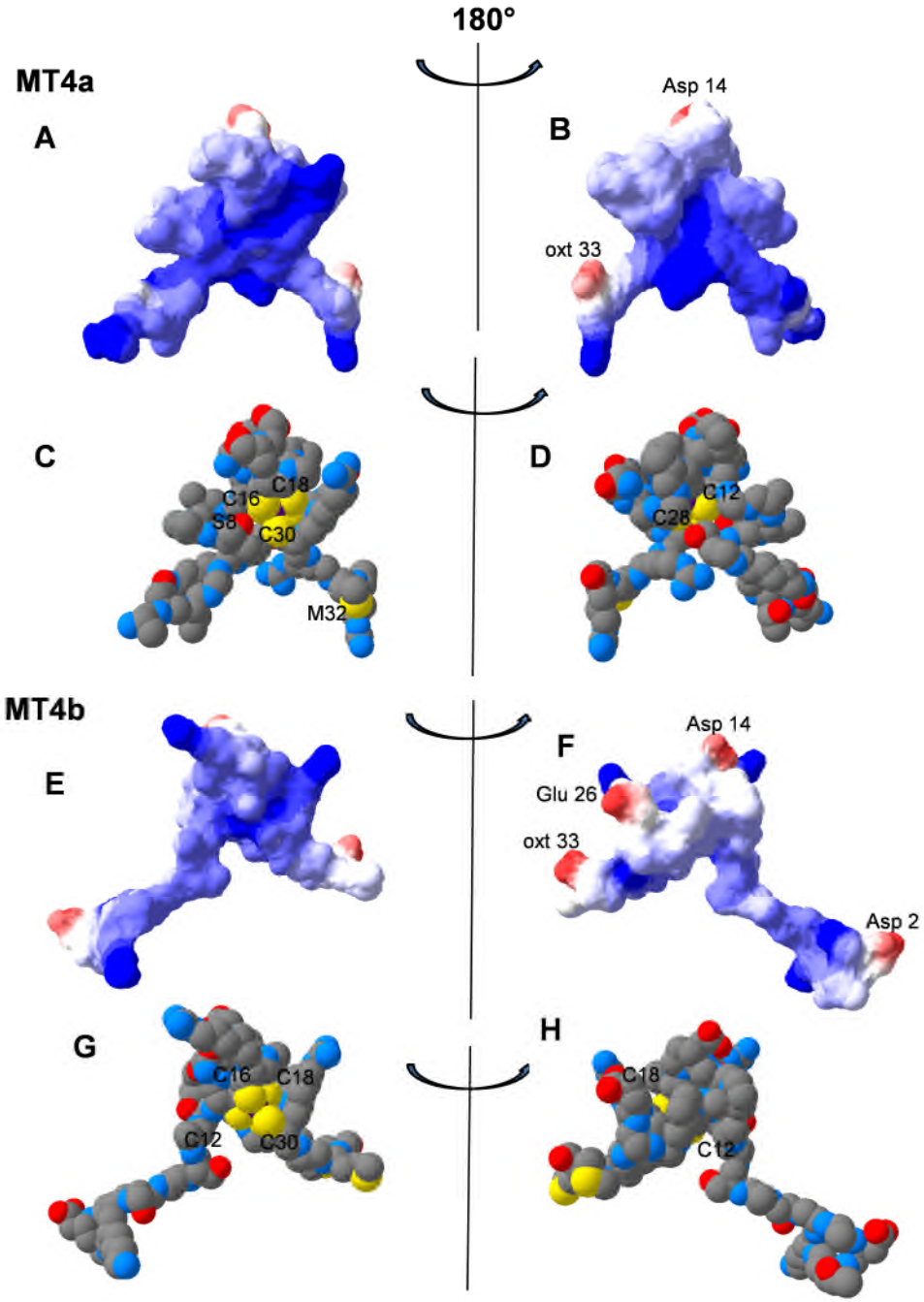

Figure 7.3 Surface plots of domain I. Electrostatic charge distribution (A) and (B) for MT4a domain I, (E) and (F) for MT4b with different views. Space filling models (C) and (D) for MT4a and (G) and (H) for MT4b. Surface accessible cysteines are labelled on the figures. In surface figures red and blue corresponds to negatively and positively charged regions. In space-filling figures red, blue and yellow corresponds to Oxygen, Nitrogen and Sulfur, respectively. Figures are prepared using swiss pdb viewer.

Surface exposure of metal ions and their coordinating atoms is thought to be an important factor determining reactivity in metal-exchange and metal-transfer reactions. Exposed Zn ions may be amenable to direct attack by metal chelators or zinc-requiring biomolecules, whilst exposed sulfurs may be points of attack for both disulfide-based and oxygen-based oxidants.

The electrostatic potential surface for domain I as shown in Figure 7.3 (A, B) for MT4a suggested the presence of a highly positively charged region on the surface. However, at the top within a very small region a negative charge was observed due to the presence of Asp14. Analysis of space-filling models suggests that for domain I (Figure 7.3 (C-D)) of MT4a, the sulfurs of Cys16, Cys30, Cys18 and one Zn ion from site B are surface-exposed. On the opposite side of the domain I, accessible residues are Cys28 and Cys12, however, Cys28 is less exposed. Solvent accessibility studies using MOLMOL (Figure 7.5 A), suggested that Cys18 is the least accessible metal binding residue, whereas Cys16 and Cys30 are highly accessible residues, thus it is possible that attack by DTNB occurs preferentially through Cys16 and Cys30.

For MT4b domain I (Figure 7.3 (E-H)), the sulfurs of Cys16 and Cys30 are also highly surface-exposed, possibly offering suitable sites for DTNB, GSSG and H_2O_2 attack; however, Cys12 and Cys18 are also visible but more buried. All four residues lie in a crevice. This could be a position suitable for attack, but only by small molecules like EDTA. Furthermore, solvent accessibility results (Figure 7.4 C) also suggested that Cys30 is the most highly accessible residue and Cys16 is also readily accessible. The reverse face (Figure 7.3 (F and H)), suggesting that this side of the protein is less suitable for attack.

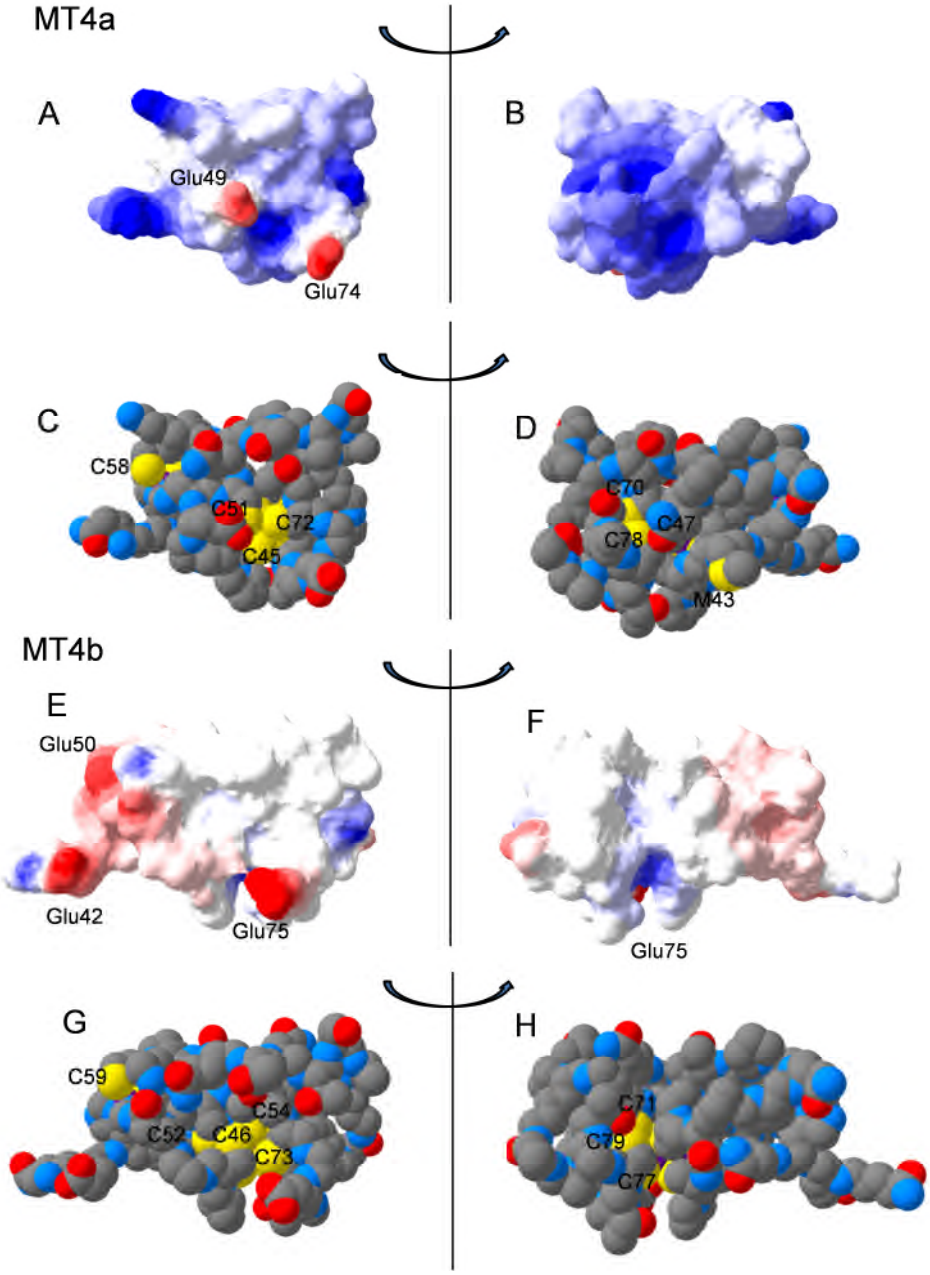

Figure 7.4 Surface plot analysis of domain II. Electrostatic charge distribution (A) and (B) for MT4a, and (E) and (F) for MT4b of domain II, with different views. Space filling representations (C) and (D) for MT4a, and (G) and (H) for MT4b. In surface figures red and blue corresponds to negatively and positively charged regions. In space-filling figures red, blue and yellow corresponds to Oxygen, Nitrogen and Sulfur, respectively. Figures are prepared using swiss pdb viewer.

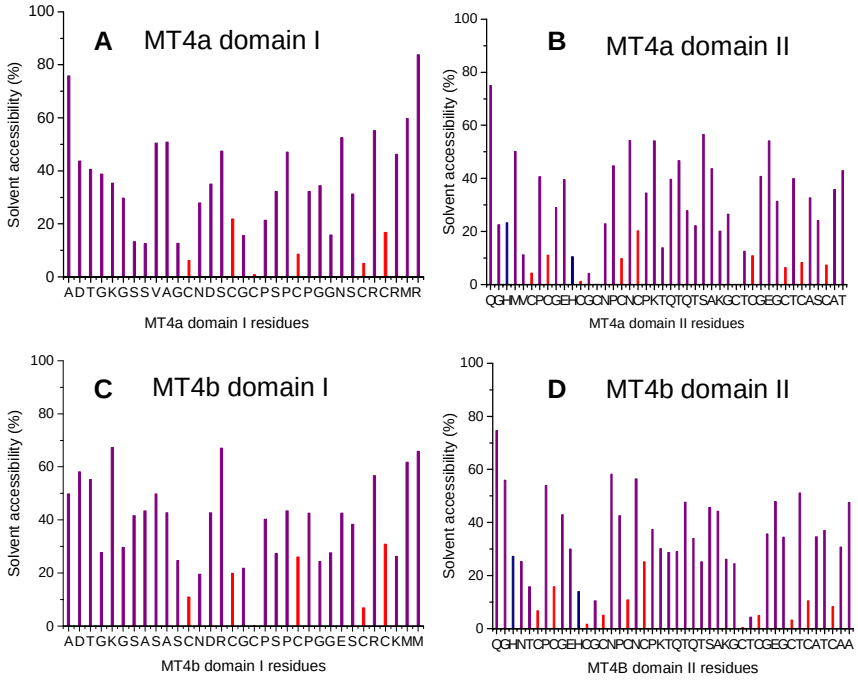

Figure 7.5 Solvent accessible residues in both domains. Solvent accessibility for domain I for MT4a (A) and MT4b (C), and for domain II for MT4a (B) and MT4b (D). Data were calculated using MOLMOL.

For domain II of MT4a (Figure 7.4 (A-D)), surface charge distribution suggested that the mononuclear site is flanked by two positively charged regions; this could be suitable for nucleophiles to readily attack on this site. However, two negatively charged region due to Glu49 and Glu74 were also observed. It was observed from space filling models (Figure 7.4 (C and D)) that Cys45, Cys51 and Cys72 were surface exposed, these are the residues that bind Zn in site X and site Y. However, Cys45 was buried and Cys51 was least solvent-accessible and Cys72 was the most accessible residue, as shown in Figure 7.5 (B). Cys58 from the mononuclear site was also surface exposed. On the reverse side, the surface is also largely positively charged and Cys70, Cys78 and Cys47 are found surface-exposed. Cys70 and Cys78 are part of the binding site that is proposed to have three

terminal Cys ligands. Exposure of this site was also observed in MT4b (Figure 7.4 (E and F)). Given its surface accessibility, and the presence of three negatively charged terminal cysteines, it is plausible that this site is a primary target for attack by electrophilic agents such as H_2O_2 and disulfides.

The comparison between the individual domains of MT4a and MT4b indicates in both cases that MT4a is much more positively (or less negatively) charged than MT4b, consistent with the fact that the latter has two extra negative charges, one in each domain. The effect of this on overall surface charges seen in Figures 7.3 and 7.4 is quite striking. Furthermore, it is apparent from the surface charge figures that the reacting ligands (EDTA, PAR, phytate, all negatively charged) are likely to attack from the reverse side (binding site Z of domain II) as for MT4b development of Zn_5 species observed in mass spectrometry in reaction with EDTA, PAR and pH variation, ^{1}H NMR spectroscopy suggested that zinc released from domain II and ^{15}N HSQC NMR clearly suggested that the single metal site (Z) in domain II released zinc first in reaction with EDTA. However, for MT4a, no such development of Zn_5 species was observed, rather Zn_4 species with PAR and Zn_3 species with EDTA were observed in mass spectrometry; in all these reactions domain II released zinc first as observed by ^{1}H NMR spectroscopy, particularly for EDTA. One explanation could be that these ligands attack MT4a from the side where Cys46, Cys51, Cys58 and Cys72 were surface exposed. Reaction of MT4a with EDTA monitored by ^{15}N HSQC suggested that the mononuclear site in MT4a reacted simultaneously with the other metal binding sites within domain II. Perhaps positive charge surrounding the mononuclear site in MT4a makes the process suitable. For MT4b, the more negative surface charge

near the mononuclear site may repulse negatively charged ligands (EDTA, PAR, phytate) thus slowing the reaction. Both isoforms have surface and solvent exposed sulfurs, thus allowing oxidant reagent to react with them. Surface exposed cysteines in mononuclear site and other cysteines in domain II and domain I perhaps allow oxidation by DTNB to proceed faster for MT4a than for MT4b. However, the resilient nature of MT4a against oxidation by H_2O_2 is not clear.

7.8 Future work

Future work of this project could be elaborated into three avenues - structural, metal binding, and reactivity for better understanding of structure-function relationship.

I. Structural
    a. Complete assignment of MT4a and MT4b to obtain NOE restraints and generate proper structures using CYANA.
    b. Mutation studies: Mutation or deletion of the single Zn binding site in domain II to understand its impact on the global protein folding.
    c. Structural study of individual domain II
    d. Structural study by solid state NMR or Crystallography particularly the domain II.

II. Metal binding studies

a. Metal binding studies with other metal ions particularly with Cu^{+} to understand the effect of monovalent ions on protein folding and reactivity.
b. Metal (Zn^{2+}/Cd^{2+}/ Cu^{+}) binding to both isoforms individually and as mixtures of isoforms to understand whether these two isoforms show any discrimination in metal binding.
c. Reactions between two isoforms - apoMT4a with metallated MT4b and vice versa.
d. Reactions with apo-enzymes and apo-zinc fingers. The expected outcomes would be two-fold: to understand structural properties of MT4s after Zn donation to apo-biomolecules and to understand whether apo-enzymes and apo-zinc fingers may recover their activity after Zn uptake from MT4s.

III. Reactivity: Reaction with biomolecules

a. Metal uptake or release between MT4s and cytoplasmic extracts from *A. thaliana*, a mimic of the *in vivo* system amenable to *in vitro* studies.
b. MT4 reaction with natural chelators, in particular, nicotianamine- a plant metabolite, which plays an important role in intracellular metal transport, particularly Zn^{2+}.

References

Abdullah, S.N.A., Cheah, S., and Murphy, D.J. (2002). Isolation and characterisation of two divergent type 3 metallothioneins from oil palm, Elaeis guineensis. *Plant Physiol. Biochem.,**40***, 255-263.

Afonso, C., Hathout, Y., and Fenselau, C. (2002). Qualitative characterization of biomolecular zinc complexes by collisionally induced dissociation. *J. Mass Spectrom. **37***, 755-759.

Akashi, K., Nishimura, N., Ishida, Y., and Yokota, A. (2004). Potent hydroxyl radical-scavenging activity of drought-induced type-2 metallothionein in wild watermelon. *Biochem. Biophys. Res. Commun., **323*****,*** 72-78.

Armitage, I.M., and Otvos, J.D. (1982). Principles and applications of 113Cd NMR to biological systems. *Biological Magnetic. Resonances, 4th ed. ED. Lawrence J B and Jacques R,* Springer, US, pp. 79-144.

Arseniev, A., Schultze, P., Wörgötter, E., Braun, W., Wagner, G., Vasák, M., Kägi, J.H.R., and Wüthrich, K. (1988). Three-dimensional structure of rabbit liver [Cd7] metallothionein-2a in aqueous solution determined by nuclear magnetic resonance. *J. Mol.Biol., **201*****,*** 637-657.

Barrientos, L., Scott, J.J., and Murthy, P.P. (1994). Specificity of hydrolysis of phytic acid by alkaline phytase from lily pollen. *Plant physiol., **106***, 1489-1495.

Bertini, I., Hartmann, H.J., Klein, T., Liu, G., Luchinat, C., and Weser, U. (2000). High resolution solution structure of the protein part of Cu7 metallothionein. *Eur. J. Biochem*., ***267***, 1008-1018.

Bilecen, K., Ozturk, U.H., Duru, A.D., Sutlu, T., Petoukhov, M.V., Svergun, D.I., Koch, M.H., Sezerman, U.O., Cakmak, I., and Sayers, Z. (2005). Triticum durum Metallothionein Isolation of the gene and structural characterization of the protein using solution scattering and molecular modeling. *J. Biol. Chem., **280*****,*** 13701-13711.

B**inz, P.A., and Kägi, J.H.R.** (1999). Metallothionein: molecular evolution and classification. Metallothionein IV, Advences in life sciences, *ED*. Curtis D K, Birkhauser, Basel., pp. 7-13.

Blindauer, C.A. (2008). Metallothioneins with unusual residues: histidines as modulators of zinc affinity and reactivity. *J. Inorg. Biochem., **102*,** 507-521.

Blindauer, C.A., Harrison, M.D., Parkinson, J.A., Robinson, A.K., Cavet, J.S., Robinson, N.J., and Sadler, P.J. (2001). A metallothionein containing a zinc finger within a four-metal cluster protects a bacterium from zinc toxicity. *Proc. Natl. Acad. Sci.,U.S.A.*, ***98***, 9593-9598.

Blindauer, C.A., Harrison, M.D., Robinson, A.K., Parkinson, J.A., Bowness, P.W., Sadler, P.J., and Robinson, N.J. (2002). Multiple bacteria encode metallothioneins and SmtA-like zinc fingers. *Mol. Microbiol.*, ***45***, 1421-1432.

Blindauer, C.A., and Leszczyszyn, O.I. (2010). Metallothioneins: unparalleled diversity in structures and functions for metal ion homeostasis and more. *Nat. Prod. Rep., **27***, 720-741.

Blindauer, C.A., Razi, M.T., Campopiano, D.J., and Sadler, P.J. (2007). Histidine ligands in bacterial metallothionein enhance cluster stability. *J. Biol. Inorg.Chem.*, ***12*,** 393-405.

Blindauer, C.A., and Schmid, R. (2010). Cytosolic metal handling in plants: determinants for zinc specificity in metal transporters and metallothioneins. *Metallomics, **2*,** 510-529.

Bofill, R., Capdevila, M., and Atrian, S. (2009). Independent metal-binding features of recombinant metallothioneins convergently draw a step gradation between Zn-and Cu-thioneins. *Metallomics, **1***, 229-234.

Boulanger, Y., and Armitage, I.M. (1982). 113 Cd nmr study of the metal cluster structure of human liver metallothionein. *J. Inorg. Biochem., **17***, 147-153.

Bower, MJ, Cohen FE, Dunbrack RL Jr. (1997). Prediction of protein side-chain rotamers from a backbone-dependent rotamer library: a new homology modeling tool. *J. Mol.Biol.*, **267**, 1268-1282.

Bradshaw, R.A., Brickey, W.W., and Walker, K.W. (1998). N-terminal processing: the methionine aminopeptidase and N α -acetyl transferase families. *Trends Biochem. Sci.*, ***23***, 263-267.

Braun, W., Vasak, M., Robbins, A., Stout, C., Wagner, G., Kägi, J., and Wüthrich, K. (1992). Comparison of the NMR solution structure and the x-ray crystal structure of rat metallothionein-2. *Proc. Natl. Acad. Sci.,U.S.A.,**89***, 10124-10128.

Braun, W., Wagner, G., Wörgötter, E., Vasák, M., Kägi, J.H.R., and Wüthrich, K. (1986). Polypeptide fold in the two metal clusters of metallothionein-2 by nuclear magnetic resonance in solution. *J. Mol.Biol.,* ***187*****,** 125-129.

Broadley, M.R., White, P.J., Hammond, J.P., Zelko, I., and Lux, A. (2007). Zinc in plants. *New Phytol.,****173***, 677-702.

Brouwer, M., Hoexum-Brouwer, T., and Cashon, R.E. (1993). A putative glutathione-binding site in CdZn-metallothionein identified by equilibrium binding and molecular-modelling studies. *Biochem. J.,* ***294*****,** 219-225.

Calderone, V., Dolderer, B., Hartmann, H.J., Echner, H., Luchinat, C., Del Bianco, C., Mangani, S., and Weser, U. (2005). The crystal structure of yeast copper thionein: the solution of a long-lasting enigma. *Proc. Natl. Acad. Sci.,U.S.A.,* ***102***, 51-56.

Capasso, C., Carginale, V., Crescenzi, O., Di Maro, D., Parisi, E., Spadaccini, R., and Temussi, P.A. (2003). Solution structure of MT_nc, a novel metallothionein from the Antarctic fish Notothenia coriiceps. *Structure,* ***11***, 435-443.

Capdevila, M., Bofill, R., and Atrian, S. (2011). State-of-the-art of metallothioneins at the beginning of the 21st century. *Coord. Chem.Rev.,****256****,46-62*

Castiglione, S., Franchin, C., Fossati, T., Lingua, G., Torrigiani, P., and Biondi, S. (2007). High zinc concentrations reduce rooting capacity and alter metallothionein gene expression in white poplar (Populus alba L. cv. Villafranca). *Chemosphere,* ***67*****,** 1117-1126.

Chang, T., Liu, X., Xu, H., Meng, K., Chen, S., and Zhu, Z. (2004). A metallothionein-like gene htMT2 strongly expressed in internodes and nodes of Helianthus tuberosus and effects of metal ion treatment on its expression. *Planta ,****218*****,** 449-455.

Chatthai, M., Kaukinen, K.H., Tranbarger, T.J., Gupta, P.K., and Misra, S. (1997). The isolation of a novel metallothionein-related cDNA expressed in somatic and zygotic embryos of Douglas-fir: regulation by ABA, osmoticum, and metal ions. *Plant Mol. Biol.,* ***34***, 243-254.

Chyan, C.L., Lee, T.T.T., Liu, C.P., Yang, Y.C., Tzen, J.T.C., and Chou, W.M. (2005). Cloning and expression of a seed-specific metallothionein-like protein from sesame. *Biosci., Biotechnol., Biochem.,* ***69***, 2319-2325.

Cismowski, M.J., and Huang, P. (1991). Effect of cysteine replacements at positions 13 and 50 on metallothionein structure. *Biochemistry.,* ***30***, 6626-6632.

Cobbett, C., and Goldsbrough, P. (2002). Phytochelatins and metallothioneins: roles in heavy metal detoxification and homeostasis. *Annu. Rev. Plant Biol.,* ***53***, 159-182.

Cobine, P.A., McKay, R.T., Zangger, K., Dameron, C.T., and Armitage, I.M. (2004). Solution structure of Cu6 metallothionein from the fungus Neurospora crassa. *Eur. J. Biochem.,****271*****,** 4213-4221.

Collett, H., Shen, A., Gardner, M., Farrant, J.M., Denby, K.J., and Illing, N. (2004). Towards transcript profiling of desiccation tolerance in Xerophyta humilis: construction of a normalized 11 k X. humilis cDNA set and microarray expression analysis of 424 cDNAs in response to dehydration. *Physiol. Plant.,* ***122*****,** 39-53.

Dallinger, R., Wang, Y., Berger, B., Mackay, E.A., and Kägi, J.H. (2001). Spectroscopic characterization of metallothionein from the terrestrial snail, Helix pomatia. *Eur. J. Biochem.*, **268**, 4126-4133.

Dell, A., Williams, D.H., Morris, H.R., Smith, G.A., Feeney, J., and Roberts, G.C. (1975). Structure revision of the antibiotic echinomycin. *J. Am. Chem. Soc*., ***97*****,** 2497-2502.

Domènech, J., Mir, G., Huguet, G., Capdevila, M., Molinas, M., and Atrian, S. (2006). Plant metallothionein domains: functional insight into physiological metal binding and protein folding. *Biochimie,* ***88*****,** 583-593.

Domenech, J., Orihuela, R., Mir, G., Molinas, M., Atrian, S., and Capdevila, M. (2007). The Cd II-binding abilities of recombinant Quercus suber metallothionein: bridging the gap between phytochelatins and metallothioneins. *J. Inorg. Biochem.,****12*****,** 867-882.

Domènech, J., Tinti, A., Capdevila, M., Atrian, S., and Torreggiani, A. (2007). Structural study of the zinc and cadmium complexes of a type 2 plant (Quercus suber) metallothionein: Insights by vibrational spectroscopy. *Biopolymers,* ***86*****,** 240-248.

Dong, J.-Z., and Dunstan, D.I. (1996). Expression of abundant mRNAs during somatic embryogenesis of white spruce [Picea glauca (Moench) Voss]. *Planta,* ***199***, 459-466.

Ejnik, J., Shaw III, C.F., and Petering, D.H. (2010). Mechanism of Cadmium Ion Substitution in Mammalian Zinc Metallothionein and Metallothionein α Domain: Kinetic and Structural Studies. *Inorg. Chem.*, ***49***, 6525-6534.

El Ghazi, I., Martin, B.L., and Armitage, I.M. (2010). New proteins found interacting with brain metallothionein-3 are linked to secretion. *Int. J. Alzheimers Dis.*, ***2011***.

El-Maarouf-Bouteau, H., and Bailly, C. (2008). Oxidative signaling in seed germination and dormancy. *Plant Signal. Behav., **3***, 175-182.

Fernandez, L.R., Vandenbussche, G., Roosens, N., Govaerts, C., Goormaghtigh, E., and Verbruggen, N. (2012). Metal binding properties and structure of a type III metallothionein from the metal hyperaccumulator plant Noccaea caerulescens.*B Biochim. Biophys. Acta.*, **1824**,1016-1023

Fliss, H., and Ménard, M. (1992). Oxidant-induced mobilization of zinc from metallothionein. *Arch. Biochem. Biophys. **293***, 195-199.

Foley, R.C., Liang, Z.M., and Singh, K.B. (1997). Analysis of type 1 metallothionein cDNAs in Vicia faba. *Plant Mol. Biol., **33***, 583-591.

Freisinger, E. (2007). Spectroscopic characterization of a fruit-specific metallothionein: M. acuminata MT3. *Inorganica. Chimica. Acta., **360*****,*** 369-380.

Freisinger, E. (2008). Plant MTs—long neglected members of the metallothionein superfamily. *Dalton Trans.,* 6663-6675.

Freisinger, E. (2011). Structural features specific to plant metallothioneins. *J. Biol. Inorg. Chem., **16,*** 1035-1045.

Gan, T., Munoz, A., Shaw, C.F., and Petering, D.H. (1995). Reaction of 111Cd7-Metallothionein with EDTA A REAPPRAISAL. *J. Biol. Chem.*,***270*****,*** 5339-5345.

Guo, W.J., Bundithya, W., and Goldsbrough, P.B. (2003). Characterization of the Arabidopsis metallothionein gene family: tissue-specific expression and induction during senescence and in response to copper. *New Phytol.*, ***159*****,*** 369-381.

Guo, W.J., Meetam, M., and Goldsbrough, P.B. (2008). Examining the specific contributions of individual Arabidopsis metallothioneins to copper distribution and metal tolerance. *Plant physiol., **146*****,*** 1697-1706.

Hacisalihoglu, G., and Kochian, L.V. (2003). How do some plants tolerate low levels of soil zinc? Mechanisms of zinc efficiency in crop plants. *New Phytol., **159*****,*** 341-350.

Hanley-Bowdoin, L., and Lane, B.G. (1983). A novel protein programmed by the mRNA conserved in dry wheat embryos. *Eur. J. Biochem.*,***135***, 9-15.

Hao, Q., and Maret, W. (2006). Aldehydes release zinc from proteins. A pathway from oxidative stress/lipid peroxidation to cellular functions of zinc. *FEBS J*., ***273***, 4300-4310.

Hathout, Y., Fabris, D., and Fenselau, C. (2001). Stoichiometry in zinc ion transfer from metallothionein to zinc finger peptides. *Int. J. Mass Spectrom.* ***204*****,** 1-6.

Hegelund, J.N., Schiller, M., Kichey, T., Hansen, T.H., Pedas, P., Husted, S., and Schjoerring, J.K. (2012). Barley Metallothioneins: MT3 and MT4 Are Localized in the Grain Aleurone Layer and Show Differential Zinc Binding. *Plant Physiol.,* ***159***, 1125-1137.

Higham, D.P., Sadler, P.J., and Scawen, M.D. (1983). Bacterial cadmium-binding proteins. *Inorganica Chimica Acta.,* ***79***, 140-142.

Hirel, P.-H., Schmitter, M., Dessen, P., Fayat, G., and Blanquet, S. (1989). Extent of N-terminal methionine excision from Escherichia coli proteins is governed by the side-chain length of the penultimate amino acid. *Proc. Natl. Acad. Sci.,U.S.A.,* ***86***, 8247-8251.

Huang, G.-Y., Wang, Y.-S., Ying, G.-G., and Dang, A.-C. (2012). Analysis of type 2 metallothionein gene from mangrove species (Kandelia candel). *Trees.,* ***26*****,** 1537-1544.

Huang, G.Y., Wang, Y.S., and Ying, G.G. (2011). Cadmium-inducible BgMT2, a type 2 metallothionein gene from mangrove species (Bruguiera gymnorrhiza), its encoding protein shows metal-binding ability. *J. Exp. Mar. Biol. Ecol.,* ***405***, 128-132.

Huang, M., Shaw Iii, C.F., and Petering, D.H. (2004). Interprotein metal exchange between transcription factor IIIa and apo-metallothionein. *J. Inorg. Biochem*., ***98***, 639-648.

Hunt, J.B., Neece, S.H., and Ginsburg, A. (1985). The use of 4-(2-pyridylazo) resorcinol in studies of zinc release from Escherichia coli aspartate transcarbamoylase. *Anal. Biochem*., ***146***, 150-157.

Iavarone, A.T., Udekwu, O.A., and Williams, E.R. (2004). Buffer loading for counteracting metal salt-induced signal suppression in electrospray ionization. *Anal. Chem.*, ***76***, 3944-3950.

Jacob, C., Maret, W., and Vallee, B.L. (1998). Control of zinc transfer between thionein, metallothionein, and zinc proteins. *Proc. Natl. Acad. Sci.,U.S.A.,* ***95*****,** 3489-3894.

Jacob, C., Maret, W., and Vallee, B.L. (1999). Selenium redox biochemistry of zinc–sulfur coordination sites in proteins and enzymes. *Proc. Natl. Acad. Sci*.,U.S.A., ***96***, 1910-1914.

Jacob, C., Maret, W., and Vallee, B.L. (1998). Ebselen, a selenium-containing redox drug, releases zinc from metallothionein. *Biochem. Biophys., Res. commun.*, ***248***, 569-573.

Jiang, L.-J., Maret, W., and Vallee, B.L. (1998a). The ATP–metallothionein complex. *Proc. Natl. Acad. Sci.,U.S.A.*,***95***, 9146-9149.

Jiang, L.J., Maret, W., and Vallee, B.L. (1998b). The glutathione redox couple modulates zinc transfer from metallothionein to zinc-depleted sorbitol dehydrogenase. *Proc. Natl. Acad. Sci.,U.S.A.*, ***95***, 3483-3488.

Jiang, L.-J., Vašák, M., Vallee, B.L., and Maret, W. (2000). Zinc transfer potentials of the α-and β-clusters of metallothionein are affected by domain interactions in the whole molecule. *Proc. Natl. Acad. Sci*.,U.S.A., ***97***, 2503-2508.

Jimenez, I., Gotteland, M., Zarzuelo, A., Uauy, R., and Speisky, H. (1997). Loss of the metal binding properties of metallothionein induced by hydrogen peroxide and free radicals. *Toxicol., **120***, 37-46.

Kaegi, J.H., and Schaeffer, A. (1988a). Biochemistry of metallothionein. *Biochemistry, **27***, 8509-8515.

Kägi, J., and Kojima, Y. (1987). Chemistry and biochemistry of metallothionein. *Experientia Supplementum., **52*****,** 25-61.

Kägi, J.H.R., and Vallee, B.L. (1960). Metallothionein: a cadmium-and zinc-containing protein from equine renal cortex. *J. Biol. Chem., **235*****,** 3460-3465.

Kane, J.F. (1995). Effects of rare codon clusters on high-level expression of heterologous proteins in Escherichia coli. *Curr. Opin., Biotechnol.*, ***6***, 494-500.

Kawashima, I., Kennedy, T.D., Chino, M., and Lane, B.G. (1992). Wheat Ec metallothionein genes. *E. J. Biochem.*,***209***, 971-976.

Kelley, L.A., Mezulis, S., Yates, C.M., Wass, M.N., and Sternberg, M.J. (2015). The Phyre2 web portal for protein modeling, prediction and analysis. *Nat. Protoc*., ***10***, 845-858.

Khatai, L., Goessler, W., Lorencova, H., and Zangger, K. (2004). Modulation of nitric oxide-mediated metal release from metallothionein by the redox state of glutathione in vitro. *Eur. J. Biochem.,* ***271***, 2408-2416.

Kille, P., Winge, D.R., Harwood, J.L., and Kay, J. (1991). A plant metallothionein produced in E. coli. *FEBS Lett.*, ***295***, 171-175.

Kim, S.H., Lee, H.S., Song, W.Y., Choi, K.S., and Hur, Y. (2007). Chloroplast-targeted BrMT1 (Brassica rapa type-1 metallothionein) enhances resistance to cadmium and ros in transgenicatabidopsis plants. *J. Plant Biol.*, ***50*****,** 1-7.

Kim, Y.O., Lee, Y.G., Patel, D.H., Kim, H.M., Ahn, S.J., and Bae, H.J. (2012). Zn tolerance of novel Colocasia esculenta metallothionein and its domains in Escherichia coli and tobacco. *J. Plant Res.,* **125,** 793-804.

Kim, Y.O., Patel, D.H., Lee, D.S., Song, Y., and Bae, H.J. (2011). High Cadmium-Binding Ability of a Novel Colocasia esculenta Metallothionein Increases Cadmium Tolerance in Escherichia coli and Tobacco. *Biosci., Biotechnol., Biochem.,****75***, 1912-1920.

Kowald, G.R. (2012). Structure and properties of earthworm metallothionein-2 (University of Warwick).

Krepkiy, D., Antholine, W.E., and Petering, D.H. (2003). Properties of the reaction of chromate with metallothionein. *Chem. Res. Toxicol.*, ***16*****,** 750-756.

Krężel, A., and Bal, W. (2004). Studies of zinc (II) and nickel (II) complexes of GSH, GSSG and their analogs shed more light on their biological relevance. *Bioinorg. Chem. Appl.****2***, 293.

Krezel, A., Hao, Q., and Maret, W. (2007). The zinc/thiolate redox biochemistry of metallothionein and the control of zinc ion fluctuations in cell signaling. Arch. Biochem. Biophys., ***463***, 188-200.

Krężel, A., and Maret, W. (2008). Thionein/metallothionein control Zn (II) availability and the activity of enzymes. *J. Biol., Inorg., Chem.*, ***13***, 401-409.

Kurland, C., and Gallant, J. (1996). Errors of heterologous protein expression. *Curr. Opin., Biotechnol., **7***, 489-493.

Lane, B., Kajioka, R., and Kennedy, T. (1987). The wheat-germ Ec protein is a zinc-containing metallothionein. *Biochem. Cell Biol.,* ***65*****,** 1001-1005.

Lasztity, L., and Lasztity, R. (1988). Investigation of the formation of phytate-metal complexes. *Chem. Eng*., ***32***, 299-304.

Lecina, J., Palacios, Ò., Atrian, S., Capdevila, M., and Suades, J. (2014). Rhenium and technetium tricarbonyl,$M(CO)_3$+(M= Tc, Re), binding to mammalian metallothioneins: new insights into chemical and radiopharmaceutical implications. *J. Biol. Inorg.Chem.,**20**, 465-474.*

Lee, J., Donghwan, S., Won-yong, S., Inhwan, H., and Youngsook, L. (2004). Arabidopsis metallothioneins 2a and 3 enhance resistance to cadmium when expressed in Vicia faba guard cells. *Plant Mol.Biol., **54***, 805-815.

Lemkuil, D.C., Nettesheim, D., Shaw, C.F., and Petering, D.H. (1994). Reaction of Cd7-metallothionein with cis-dichlorodiammine platinum (II). *J. Biol. Chem., **269***, 24792-24797.

Leszczyszyn, O.I., and Blindauer, C.A. (2010). Zinc transfer from the embryo-specific metallothionein EC from wheat: a case study. *Phys Chem Chem Phys*., ***12***, 13408-13418.

Leszczyszyn, O.I., Evans, C.D., Keiper, S.E., Warren, G.Z., and Blindauer, C.A. (2007a). Differential reactivity of individual zinc ions in clusters from bacterial metallothioneins. *Inorg., Chimica. Acta **360***, 3-13.

Leszczyszyn, O.I., Imam, H.T., and Blindauer, C.A. (2013). Diversity and distribution of plant metallothioneins: a review of structure, properties and functions. *Metallomics* ,**5**,1146-69.

Leszczyszyn, O.I., Schmid, R., and Blindauer, C.A. (2007). Toward a property/function relationship for metallothioneins: Histidine coordination and unusual cluster composition in a zinc-metallothionein from plants. *Proteins: Struct., Funct., Bioinf., **68***, 922-935.

Leszczyszyn, O.I., White, C.R.J., and Blindauer, C.A. (2010). The isolated Cys2His2 site in EC metallothionein mediates metal-specific protein folding. *Mol BioSyst., **6***, 1592-1603.

Li, T.-Y., Kraker, A.J., Shaw, C.F., and Petering, D.H. (1980). Ligand substitution reactions of metallothioneins with EDTA and apo-carbonic anhydrase. *Proc. Natl. Acad. Sci.,U.S.A.,**77***, 6334-6338.

Loebus, J., Peroza, E.A., Blüthgen, N., Fox, T., Meyer-Klaucke, W., Zerbe, O., and Freisinger, E. (2011a). Protein and metal cluster structure of the wheat metallothionein domain γ-E c-1: the second part of the puzzle. *J. Biol. Inorg. Chem., 2011*., **16**, 683-694.

Loebus, J., Peroza, E.A., Blüthgen, N., Fox, T., Meyer-Klaucke, W., Zerbe, O., and Freisinger, E. (2011b). Protein and metal cluster structure of the wheat metallothionein domain γ-E c-1: the second part of the puzzle. *Biol. Inorg. Chem., 2011*., **16**, 683-694

Loo, J.A. (2000). Electrospray ionization mass spectrometry: a technology for studying noncovalent macromolecular complexes. *Int. J. Mass Spectrom.*, ***200*****, 175-186.**

Lv, Y., Deng, X., Quan, L., Xia, Y., and Shen, Z. (2013). Metallothioneins BcMT1 and BcMT2 from Brassica campestris enhance tolerance to cadmium and copper and decrease production of reactive oxygen species in Arabidopsis thaliana. *Plant Soil*., **367**:507–519

Maret, W. (1994). Oxidative metal release from metallothionein via zinc-thiol/disulfide interchange. *Proc. Natl. Acad. Sci.,U.S.A.,****91***, 237-241.

Maret, W. (2009). Molecular aspects of human cellular zinc homeostasis: redox control of zinc potentials and zinc signals. *Biometals, **22***, 149-157.

Maret, W. (1995). Metallothionein/disulfide interactions, oxidative stress, and the mobilization of cellular zinc. *Neurochem. Int. **27***, 111-117.

Maret, W. (2000). The function of zinc metallothionein: a link between cellular zinc and redox state. *J. Nutr., **130***, 1455-1458.

Maret, W., Heffron, G., Hill, H.A.O., Djuricic, D., Jiang, L.J., and Vallee, B.L. (2002). The ATP/metallothionein interaction: NMR and STM. *Biochemistry, **41***, 1689-1694.

Margoshes, M., and Vallee, B.L. (1957). A cadmium protein from equine kidney cortex. *J. Am. Chem.Soc., **79***, 4813-4814.

Marquès, L., and Oomen, R.J.F.J. (2011). On the way to unravel zinc hyperaccumulation in plants: a mini review. *Metallomics., **3***, 1265-1270.

Meloni, G., Knipp, M., and Vašák, M. (2005). Detection of neuronal growth inhibitory factor (metallothionein-3) in polyacrylamide gels and by Western blot analysis. *J.Biochem., Biophys., Methods.*, ***64*****,** 76-81.

Messerle, B.A., Schäffer, A., Vasák, M., Kägi, J.H.R., and Wüthrich, K. (1992). Comparison of the solution conformations of human [Zn7]-metallothionein-2 and [Cd7]-metallothionein-2 using nuclear magnetic resonance spectroscopy. *J. Mol. Biol., **225***, 433-443.

Mir, G., Domenech, J., Huguet, G., Guo, W.J., Goldsbrough, P., Atrian, S., and Molinas, M. (2004). A plant type 2 metallothionein (MT) from cork tissue responds to oxidative stress. *J. Exp. Bot*. ***55***, 2483-2493.

Mounaji, K., Erraiss, N., and Wegnez, M. (2002). Identification of Metallothionein in Pleurodeles waltl., *J. Biosci.*, ***57***, 727-731.

Munoz, A., Försterling, H.F., Shaw, F.C., and Petering, D.H. (2002). Structure of the 113Cd3ß domains from Homarus americanus metallothionein-1: hydrogen bonding and solvent accessibility of sulfur atoms. *J. Biol. Inorg.Chem., **7*,** 713-724.

Muñoz, A., Petering, D.H., and Shaw, C.F. (2000). Structure-reactivity relationships among metallothionein three-metal domains: Role of non-cysteine amino acid residues in lobster metallothionein and human metallothionein-3. *Inorg. Chem*., **39**, 6114-6123.

Murphy, A., Zhou, J., Goldsbrough, P.B., and Taiz, L. (1997). Purification and immunological identification of metallothioneins 1 and 2 from Arabidopsis thaliana. *Plant Physiol., **113***, 1293-1301.

Namdarghanbari, M.A., Meeusen, J., Bachowski, G., Giebel, N., Johnson, J., and Petering, D.H. (2010). Reaction of the zinc sensor FluoZin-3 with Zn 7-metallothionein: inquiry into the existence of a proposed weak binding site. *J. Inorg. Biochem., **104***, 224-231.

Narula, S.S., Brouwer, M., Hua, Y., and Armitage, I.M. (1995). Three-dimensional solution structure of Callinectes sapidus metallothionein-1 determined by homonuclear and heteronuclear magnetic resonance spectroscopy. *Biochemistry., **34***, 620-631.

Nordberg, M., and Kojima, Y. (1979). Metallothionein and other low molecular weight metal-binding proteins. *Experientia Suppl.*, **34**, 41-135.

Ockenden, I., Dorsch, J.A., Reid, M.M., Lin, L., Grant, L.K., Raboy, V., and Lott, J.N. (2004). Characterization of the storage of phosphorus, inositol phosphate and cations in grain tissues of four barley (Hordeum vulgare L.) low phytic acid genotypes. *Plant Sci*., ***167***, 1131-1142.

Otvos, J.D., and Armitage, I.M. (1980). Structure of the metal clusters in rabbit liver metallothionein. *Proc. Natl. Acad. Sci.,U.S.A*., ***77***, 7094-7098.

Otvos, J.D., Engeseth, H.R., and Wehrli, S. (1985). Preparation and cadmium-113 NMR studies of homogeneous reconstituted metallothionein: reaffirmation of the two-cluster arrangement of metals. *Biochemistry, **24***, 6735-6740.

OtvosS, J.D., Olafsony, R.W., and Armitage, I.M. (1982). Structure of an Invertebrate Metallothionein from ScyZZu Serruta. *J. Biol. Chem.*, **257**, 2427-2431.

Öz, G., Zangger, K., and Armitage, I.M. (2001). Three-dimensional structure and dynamics of a brain specific growth inhibitory factor: metallothionein-3. *Biochemistry, **40**,* 11433-11441.

Pagani, M.A., Tomas, M., Carrillo, J., Bofill, R., Capdevila, M., Atrian, S., and Andreo, C.S. (2012b). The response of the different soybean metallothionein isoforms to cadmium intoxication. *J. Inorg. Biochem.*, **117**, 306-315

Page, R., Peti, W., Wilson, I.A., Stevens, R.C., and Wüthrich, K. (2005). NMR screening and crystal quality of bacterially expressed prokaryotic and eukaryotic proteins in a structural genomics pipeline. *Proc. Natl. Acad. Sci.,U.S.A., **102***, 1901-1905.

Palmer, C.M., and Guerinot, M.L. (2009). Facing the challenges of Cu, Fe and Zn homeostasis in plants. *Nat. Chem. Biol., **5***, 333-340.

Palumaa, P., and Vasák, M. (1992). Binding of inorganic phosphate to the cadmium-induced dimeric form of metallothionein from rabbit liver. *Eur. J. Biochem*. ***205***, 1131-1135

Pan, P.K., Zheng, Z., Lyu, P., and Huang, P. (1999). Why reversing the sequence of the α domain of human metallothionein-2 does not change its metal-binding and folding characteristics. *Eur. J. Biochem*. ***266***, 33-39.

Pan, T., and Coleman, J.E. (1989). Structure and function of the Zn (II) binding site within the DNA-binding domain of the GAL4 transcription factor. *Proc. Natl. Acad. Sci.,U.S.A., **86***, 3145-3149.

Peroza, E.A., dos Santos Cabral, A., Wan, X., and Freisinger, E. (2013). Metal ion release from metallothioneins: proteolysis as an alternative to oxidation. *Metallomics, **5***, 1204-1214.

Peroza, E.A., and Freisinger, E. (2007). Metal ion binding properties of Tricium aestivum E c-1 metallothionein: evidence supporting two separate metal thiolate clusters. *J. Biol. Inorg. Chem., **12***, 377-391.

Peroza, E.A., Schmucki, R., Güntert, P., Freisinger, E., and Zerbe, O. (2009). The [β] E-Domain of Wheat Ec-1 Metallothionein: A Metal-Binding Domain with a Distinctive Structure. *J. Mol.Biol., **387***, 207-218.

Peterson, C.W., Narula, S.S., and Armitage, I.M. (1996). 3D solution structure of copper and silver-substituted yeast metallothioneins. *FEBS Lett., **379***, 85-93.

Petering, D.H., Zhu, J., Krezoski, S., Meeusen, J., Kiekenbush, C., Krull, S., Specher, T., and Dughish, M. (2006). Apo-metallothionein emerging as a major player in the cellular activities of metallothionein. *Exp. Biol. Med.*, ***231***, 1528-1534.

Petzold, H., and Sadler, P.J. (2008). Oxidation induced by the antioxidant glutathione (GSH). *Chem. Commun,* 4413-4415.

Piątek, K., Hartwig, A., and Bal, W. (2009). Physiological levels of glutathione enhance Zn (II) binding by a Cys4 zinc finger. *Biochem. Biophys. Res. Commun., **389***, 265-268.

Pinter, T.B., and Stillman, M.J. (2014). The Zinc Balance: Competitive Zinc Metalation of Carbonic Anhydrase and Metallothionein 1A. *Biochemistry, **53***, 6276-6285.

Pitt-Rivers, R., and Impiombato, F. (1968). The binding of sodium dodecyl sulphate to various proteins. *Biochem. J*., ***109***, 825-830.

Prinz, R., and Weser, U. (1975). Cuprodoxin. *FEBS Lett*., ***54***, 224-229.

Quesada, A.R., Byrnes, R.W., Krezoski, S.O., and Petering, D.H. (1996). Direct reaction of H2O2 with sulfhydryl groups in HL-60 cells: zinc-metallothionein and other sites. *Arch. Biochem. Biophys., **334***, 241-250.

Rana, U., Kothinti, R., Meeusen, J., Tabatabai, N.M., Krezoski, S., and Petering, D.H. (2008). Zinc binding ligands and cellular zinc trafficking: apo-metallothionein, glutathione, TPEN, proteomic zinc, and Zn-Sp1. *J. Inorg. Biochem., **102***, 489-499.

Rauser, W.E. (1999). Structure and function of metal chelators produced by plants. *Cell Biochem. Biophys*., ***31***, 19-48.

Rauser, W.E., and Curvetto, N.R. (1980). Metallothionein occurs in roots of Agrostis tolerant to excess copper. *Nature*, **287**, 563-564.

Ren, Y., Liu, Y., Chen, H., Li, G., Zhang, X., and Zhao, J. (2011). Type 4 metallothionein genes are involved in regulating Zn ion accumulation in late embryo and in controlling early seedling growth in Arabidopsis. *Plant, Cell. Environ.*,**35**,770-789.

Riek, R., Pręcheur, B., Wang, Y., Mackay, E.A., Wider, G., GuÈntert, P., Liu, A., KaÈgi, J.H.R., and WuÈthrich, K. (1999). NMR structure of the sea urchin (Strongylocentrotus purpuratus) metallothionein MTA. *J. Mol. Biol. **291***, 417-428.

Rodríguez-Llorente, I.D., Pérez-Palacios, P., Doukkali, B., Caviedes, M.A., and Pajuelo, E. (2010). Expression of the seed-specific metallothionein mt4a in plant vegetative tissues increases Cu and Zn tolerance. *Plant Sci., **178***, 327-332.

Roosens, N.H., Leplae, R., Bernard, C., and Verbruggen, N. (2005). Variations in plant metallothioneins: the heavy metal hyperaccumulator Thlaspi caerulescens as a study case. *Planta **222***, 716-729.

Rosenberg, A.H., Goldman, E., Dunn, J., Studier, F., and Zubay, G. (1993). Effects of consecutive AGG codons on translation in Escherichia coli, demonstrated with a versatile codon test system. *J. Bacteriol*., ***175*****,** 716-722.

Sadler, P.J., Bakka, A., and Beynon, P.J. (1978). 113 Cd nuclear magnetic resonance of metallothionein: Non-equivalent CdS4 sites. *FEBS Lett., **94***, 315-318.

Sali A, Potterton L, Yuan F, van Vlijmen H, Karplus M. (1995). Evaluation of comparative protein modeling by MODELLER. *Proteins: Struct., Funct., Bioinf.,* **23**, 318-326.

Samardžić, J.T., Nikolić, D.B., Timotijević, G.S., Jovanović, Ž.S., Milisavljević, M.Đ., and Maksimović, V.R. (2010). Tissue expression analysis of FeMT3, a drought and oxidative stress related metallothionein gene from buckwheat (Fagopyrum esculentum). *J. Plant physiol.*, ***167*****,** 1407-1411.

Savas, M.M., Shaw III, C.F., and Petering, D.H. (1993). The oxidation of rabbit liver metallothionein-II by 5, 5′-dithiobis (2-nitrobenzoic acid) and glutathione disulfide. *J. Inorg. Biochem*., ***52***, 235-249.

Savas, M.M., Petering, D.H., and Shaw III, C.F. (1991). On the rapid, monophasic reaction of the rabbit liver metallothionein. α .-domain with 5, 5'-dithiobis (2-nitrobenzoic acid)(DTNB). *Inorg. Chem*., ***30***, 581-583.

Schicht, O., and Freisinger, E. (2009). Spectroscopic characterization of Cicer arietinum metallothionein 1. *Inorg., Chimica Acta., **362***, 714-724.

Sekhar, K., Priyanka, B., Reddy, V., and Rao, K. (2011). Metallothionein 1 (CcMT1) of pigeonpea (Cajanus cajan, L.) confers enhanced tolerance to copper and cadmium in Escherichia coli and Arabidopsis thaliana. Environmental and *Exp. Bot. **72***, 131-139.

Sewell, A.K., Jensen, L.T., Erickson, J.C., Palmiter, R.D., and Winge, D.R. (1995). Bioactivity of Metallothionein-3 Correlates with Its Novel. β. Domain Sequence Rather Than Metal Binding Properties. *Biochemistry* , **34**, 4740-4747.

Shaw III, C.F., Laib, J.E., Savas, M.M., and Petering, D.H. (1990). Biphasic kinetics of aurothionein formation from gold sodium thiomalate: a novel metallochromic technique to probe zinc (2+) and cadmium (2+) displacement from metallothionein. *Inorg. Chem.*, ***29***, 403-408.

Smirnova, J., Zhukova, L., Witkiewicz-Kucharczyk, A., Kopera, E., Olędzki, J., Wysłouch-Cieszyńska, A., Palumaa, P., Hartwig, A., and Bal, W. (2007). Quantitative electrospray ionization mass spectrometry of zinc finger oxidation: the reaction of XPA zinc finger with H_2O_2. *Anal.biochem*., ***369***, 226-231.

Sørensen, H.P., and Mortensen, K.K. (2005). Advanced genetic strategies for recombinant protein expression in Escherichia coli. *J. Biotechnol.*, ***115*****,** 113-128.

Tarasava, K., Johannsen, S., and Freisinger, E. (2013). Solution Structure of the Circular γ-Domain Analog from the Wheat Metallothionein Ec-1. *Molecules., **18***, 14414-14429.

Tomas, M., Pagani, M.A., Andreo, C.S., Capdevila, M., Bofill, R., and Atrian, S. (2014). His-containing plant metallothioneins: comparative study of divalent metal-ion binding by plant MT3 and MT4 isoforms. *J. Biol. Inorg. Chem., **19***, 1149-1164.

Tommey, A.M., Shi, J., Lindsay, W.P., Urwin, P., and Robinson, N.J. (1991). Expression of the pea genePsMTA inE. coli Metal-binding properties of the expressed protein. *FEBS Lett., **292***, 48-52.

Valls, M., Bofill, R., González-Duarte, R., González-Duarte, P., Capdevila, M., and Atrian, S.l. (2001). A new insight into metallothionein (MT) classification and evolution The in vivo and in vitro metal binding features of Homarus americanus recombinant MT. *J. Biol., Chem.*, ***276*****,** 32835-32843.

Van Oss, C. (1989). On the mechanism of the cold ethanol precipitation method of plasma protein fractionation. *J. Protein Chem.*, ***8***, 661-668.

Vašák, M. (1998). Application of 113Cd NMR to metallothioneins. *Biodegradation., **9***, 501-512.

Vasak, M., Galdes, A., Hill, H.A.O., Kaegi, J.H., Bremner, I., and Young, B.W. (1980). Investigation of the structure of metallothioneins by proton nuclear magnetic resonance spectroscopy. *Biochemistry., **19***, 416-425.

Vriend, G. (1990). WHAT IF: a molecular modeling and drug design program. *J.Mol., Graphics*, **8**, 52-56.

W**an, X., and Freisinger, E.** (2009). The plant metallothionein 2 from Cicer arietinum forms a single metal–thiolate cluster. *Metallomics., **1***, 489-500.

Wang, H., Zhang, Q., Cai, B., Li, H., Sze, K.H., Huang, Z.X., Wu, H.M., and Sun, H. (2006). Solution structure and dynamics of human metallothionein-3 (MT-3). *FEBS Lett. **580***, 795-800.

Wang, Y., Mackay, E.A., Kurasaki, M., and Kägi, J.H. (1994). Purification and characterisation of recombinant sea urchin metallothionein expressed in Escherichia coli. *Eur. J. Biochem., **225***, 449-457.

White, C.N., and Rivin, C.J. (1995). Characterization and expression of a cDNA encoding a seed-specific metallothionein in maize. *Plant Physiol. **108***, 831-832.

Winter, D., Vinegar, B., Nahal, H., Ammar, R., Wilson, G.V., and Provart, N.J. (2007). An “Electronic Fluorescent Pictograph” browser for exploring and analyzing large-scale biological data sets. *PloS one., **2***, e718.

Wishart DS, Bigam CG, Yao J, Abildgaard F, Dyson HJ, Oldfield E, Markley JL, Sykes BD (1995). 1H, 13C and 15N chemical shift referencing in biomolecular NMR. *J. Biomol.NMR.,* **6**, 135-140.

Xue, T., Li, X., Zhu, W., Wu, C., Yang, G., and Zheng, C. (2009). Cotton metallothionein GhMT3a, a reactive oxygen species scavenger, increased tolerance against abiotic stress in transgenic tobacco and yeast. *J. Exp. Bot.*, ***60***, 339-349.

Yang, Z., Wu, Y., Li, Y., Ling, H.Q., and Chu, C. (2009). OsMT1a, a type 1 metallothionein, plays the pivotal role in zinc homeostasis and drought tolerance in rice. *Plant Mol. Biol., **70***, 219-229.

Yu, X., Wojciechowski, M., and Fenselau, C. (1993). Assessment of metals in reconstituted metallothioneins by electrospray mass spectrometry. *Anal. Chem*., ***65*****,** 1355-1359.

Zaia, J., Fabris, D., Wei, D., Karpel, R.L., and Fenselau, C. (1998). Monitoring metal ion flux in reactions of metallothionein and drug-modified metallothionein by electrospray mass spectrometry. *Protein Science., **7***, 2398-2404.

Zaia, J., Jiang, L., Han, M.S., Tabb, J.R., Wu, Z., Fabris, D., and Fenselau, C. (1996). A binding site for chlorambucil on metallothionein. *Biochemistry. **35***, 2830-2835.

Z**angger, K., ÖZ, G., Armitage, I.M., and Otvos, J.D.** (1999). Three-dimensional solution structure of mouse [Cd7]-metallothionein-l by homonuclear and heteronuclear NMR spectroscopy. *Protein Sci., **8**,* 2630-2638.

Zangger, K., Öz, G., Haslinger, E., Kunert, O., and Armitage, I.M. (2001). Nitric oxide selectively releases metals from the amino-terminal domain of metallothioneins: potential role at inflammatory sites. The *FASEB J.*, ***15*,** 1303-1305.

Zangger, K., Öz, G., and Armitage, I.M. (2000). Re-evaluation of the binding of ATP to metallothionein. *J. Biol. Chem.*, ***275***, 7534-7538.

Zeitoun-Ghandour, S., Leszczyszyn, O.I., Blindauer, C.A., Geier, F.M., Bundy, J.G., and Stürzenbaum, S.R. (2011). C. elegans metallothioneins: response to and defence against ROS toxicity. *Mol. BioSyst*., *7*, 2397-2406.

Zhigang, A., Cuijie, L., Yuangang, Z., Yejie, D., Wachter, A., Gromes, R., and Rausch, T. (2006). Expression of BjMT2, a metallothionein 2 from Brassica juncea, increases copper and cadmium tolerance in Escherichia coli and Arabidopsis thaliana, but inhibits root elongation in Arabidopsis thaliana seedlings. *J. Exp.Bot.*, ***57***, 3575-3582.

Zhou, G.-K., Xu, Y.-F., and Liu, J.-Y. (2005). Characterization of a rice class II metallothionein gene: tissue expression patterns and induction in response to abiotic factors. *J. Plant Physiol., **162***, 686-696.

Zhu, J., Meeusen, J., Krezoski, S., and Petering, D.H. (2010a). Reactivity of Zn-, Cd-, and apo-metallothionein with nitric oxide compounds: in vitro and cellular comparison. *Chem. Res. Toxicol.*, ***23***, 422-431.

Zhu, J., Zhang, Q., Wu, R., and Zhang, Z. (2010b). HbMT2, an ethephon-induced metallothionein gene from Hevea brasiliensis responds to H(2)O(2) stress. *Plant Physiol. Biochem., **48***, 710-715.

Zhu, W., Zhao, D.-X., Miao, Q., Xue, T.-T., Li, X.-Z., and Zheng, C.-C. (2009). Arabidopsis thaliana metallothionein, AtMT2a, mediates ROS balance during oxidative stress. *J. Plant Biol., **52***, 585-592.

Zhu, Z., Goodrich, M., Isab, A.A., and Shaw III, C.F. (1992). Biphasic reactions of DTNB with lobster Cd6-and Cd5Cu-metallothionein-2 which have two type-B (M3S9) clusters. *Inorg. Chem., 31*, 1662-1667.

Appendix

A1

Thesis reference: Chapter 2, Section 2.4.3

Recipe for Labelled protein expression

Recipe for labelled protein expression (500 ml)- 5xM9 salt= 100 ml, $MgSO_4$= 500µL, (1M), $FeCl_3$= 250 µL, (15mg/ml), Metal Mix= 250 µL Yeast extract= 250 µL (5g/50ml), Biotin= 500 µL (10mg/ml), Thiamine=125 µL (2mg/ml), $^{15}NH_4Cl$= 5 ml (1g/10 ml), ^{13}glucose/glucose= 12.5 ml (5g/25ml, 20%), $CaCl_2$= 50 µL (1M), Kanamycin=500 µL (50 µg/ml), chloramphenicol= 500 µL (34µg/ml). 5xM9 salt(100 ml)-(Na_2HPO_4= 6.4g,KH_2PO_4=1.5g, NaCl=0.25g) and metal mix(100 ml) ($ZnSO_4.7H_2O$= 0.115, $MnSO_4.5H_2O$ = 0.0169, H_3BO_3= 0.029g, $CuSO_4.5H_2O$= 0.0175)

A2

Thesis reference: Chapter 4, Section 4.2.1

Temperature dependent ^{1}H NMR spectra of Zn_6MT4a and Zn_6MT4b

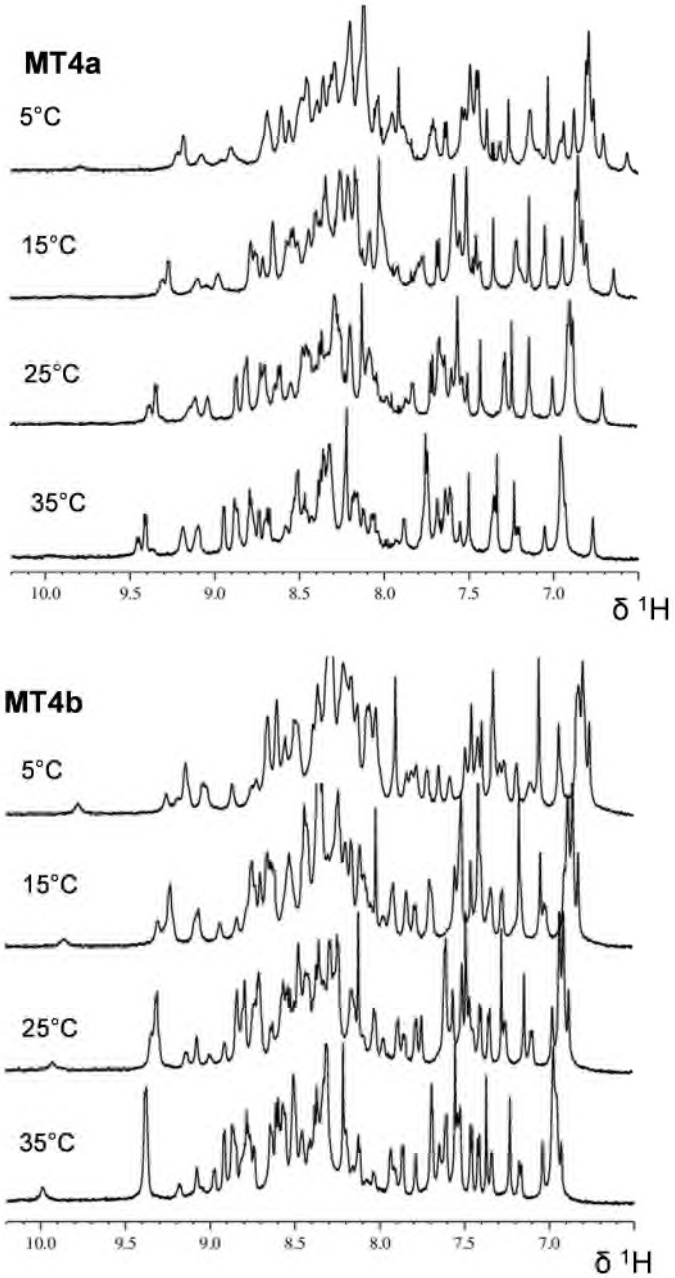

Figure A2 1D ^{1}H NMR spectra of MT4a and MT4b at different temperature. Spectra were recorded at 700.24 MHz, proteins (250 µM, 50 mM Tris-D_{11}, 10 % D_2O, 50 mM NaCl, pH 7.33).

A3

Thesis reference: Chapter 4, Section 4.2 (4.2.1-4.2.3

Resonance assignment table for Zn_6MT4b

Table A3

Residues	Ca	N	NH	Hα	Hβ	Others
Ser11	55.45	122.7	8.372	4.463	3.720, 3.666	
Cys12	58.74	122.2	8.056	4.589	3.720, 2.980	
Asn13	50.09	121.5	9.244	4.928	3.176, 3.027	Hδ 6.901 7.672
Asp14	52.80	119.5	8.215	4.453	2.646	
Arg15	52.62	116.5	8.457	4.679	1.910, 1.684	CH2δ 2.927, CH2γ 1.543
Cys16	57.79	119.1	7.540	4.525	3.220, 3.034	
Gly17	42.26	111.9	8.722	4.531	3.601	
Cys18	58.17	124.1	8.721	4.489	3.773, 3.149	
Pro19	60.65					
Ser20	50.98	115.0	8.287		3.745, 3.450	
Pro21	60.17			4.734	2.294, 1.895	CH2 δ 3.535, 3.448, CH2γ 1.795
Cys22	54.86	125.7	8.635	4.531	3.218 2.933	
Pro23	60.60					
Gly24	41.22	110.6	8.641	4.176	3.675	
Gly25	43.22	106.9	8.395	3.890		
Glu26	55.74		4.082	2.073, 1.992		CH2γ 2.299
Ser27	56.36	112.1	7.776	4.360	3.888	
Cys28	56.37	122.7	7.271	4.534	2.993 2.315	
Arg29	54.92	132.6	8.146	4.240	2.019, 1.961	CH2γ 1.981 CH2δ3.194
Cys30	59.30	121.8	7.942	4.245	3.007, 2.567	
Lys31	54.62	121.7	7.812	4.144	1.851	CH2γ 2.959, 1.635
Met32	53.72	119.5	8.088	4.364	2.618	2.072, 2.053
Glu35	54.03					
Ala36	49.88	124.8	8.189	4.354	1.398	
Ser37	55.77	115.0	8.247		3.871	
Gly38	42.73	110.6	8.396			
Gly39	42.48	108.7	8.279	4.620	3.930	
Asp40	51.63	120.2	8.337	4.618	2.680	
Gln41	52.67	119.6	8.211	4.339	2.085,2.133	Hδ 6.857
Glu42	53.68	121.6	8.304	4.293	1.837	CH2γ2.236, 1.859
His43	52.57	119.3	8.556	4.830	2.885 2.815	Hδ2 7.198, Hε1 8.043
Asn44	49.24	125.3	9.226	4.896	2.345 2.201	Hδ 6.857 7.409
Thr45	57.01	111.3	8.480	4.488	3.980	CH2γ 0.5394
Cys46	55.42	122.8	8.619	4.543	3.273, 2.954	
Pro47	62.99			4.404	2.357 2.011	CH2δ 3.896, CH2δ 1.804
Cys48	56.97	116.4	7.369	4.547	3.298 3.136	
Gly49	41.96	111.9	8.665	4.606	3.569	
Glu50	52.77	122.7	8.429	4.547	2.137	CH2γ 2.537, 2.030
His51	55.15	121.8	9.268	4.407	3.033, 2.926	Hδ2 7.064, Hε1 7.408
Cys52		57.26	125.4	8.835	4.378 3.127 2.872	
Gly53	43.47	113.2	8.366	3.895		
Cys54	56.58	118.7	7.435	4.413	3.024, 2.977	
Asn55	48.16	118.8	7.024	4.873	2.539, 2.373	Hδ 6.858
Pro56	61.26		4.210	2.289, 2.055		CH2δ 3.598, 3.494
Cys57	55.52	126.3	8.497	4.493	3.653, 3.446	
Asn58	50.17	122.6	9.060	4.935	2.910, 2.826	Hδ 6.834, 7.432
Cys59	54.85	122.2	8.165	4.955	3.574, 3.047	
Pro60	62.61			4.378	2.115, 1.975	CH2δ 3.945
Lys61	55.50	119.1	8.352	4.111	1.421	CH2γ 1.508
Thr62	61.24	114.7	7.898	4.273	4.184	CH2γ 1.293
Gln63	53.91	121.7	8.014	4.295	2.174, 2.003	Hδ 6.801 7.486
Thr64		49.55	115.1	7.888	4.281	CH2γ 1.011
Gln65	55.26	125.5	7.852	4.083		
Ala68	53.67					
Lys69	53.27	119.6	8.210	4.322		CH2γ 1.844
Gly70	42.10	109.3	8.040	3.874	3.985	
Cys71	56.81	123.4	8.277	3.976	3.044, 2.833	
Thr72	58.21	124.3	9.243	4.626		CH2γ 1.186
Cys73	58.19	125.7	9.846	4.013	3.003, 2.920	
Gly74	41.19	108.9	8.662	4.417	3.787	
Glu75	55.22	119.2	8.409	4.026	1.957	
Gly76	42.11	110.5	8.750	3.997		
Cys77	58.20	122.8	7.178	4.082	2.926, 2.941	
Thr78	58.17	119.9	8.256	4.539	4.449	CH2γ 1.126
Cys79	57.05	129.3	8.713	4.075	2.921	
Ala80	52.17	131.9	9.001	4.422	1.504	
Thr81	63.18	117.4	8.393	4.079		CH2γ 1.226
Cys82	60.66	124.9	8.499	4.024	3.721, 2.813	
Ala83	49.77	121.6	7.705	4.285	1.323	
Ala84	51.48	128.1	7.326	4.022	1.357	

A4

Thesis reference: Chapter 4, Section 4.10

Homology model of MT4a and MT4b

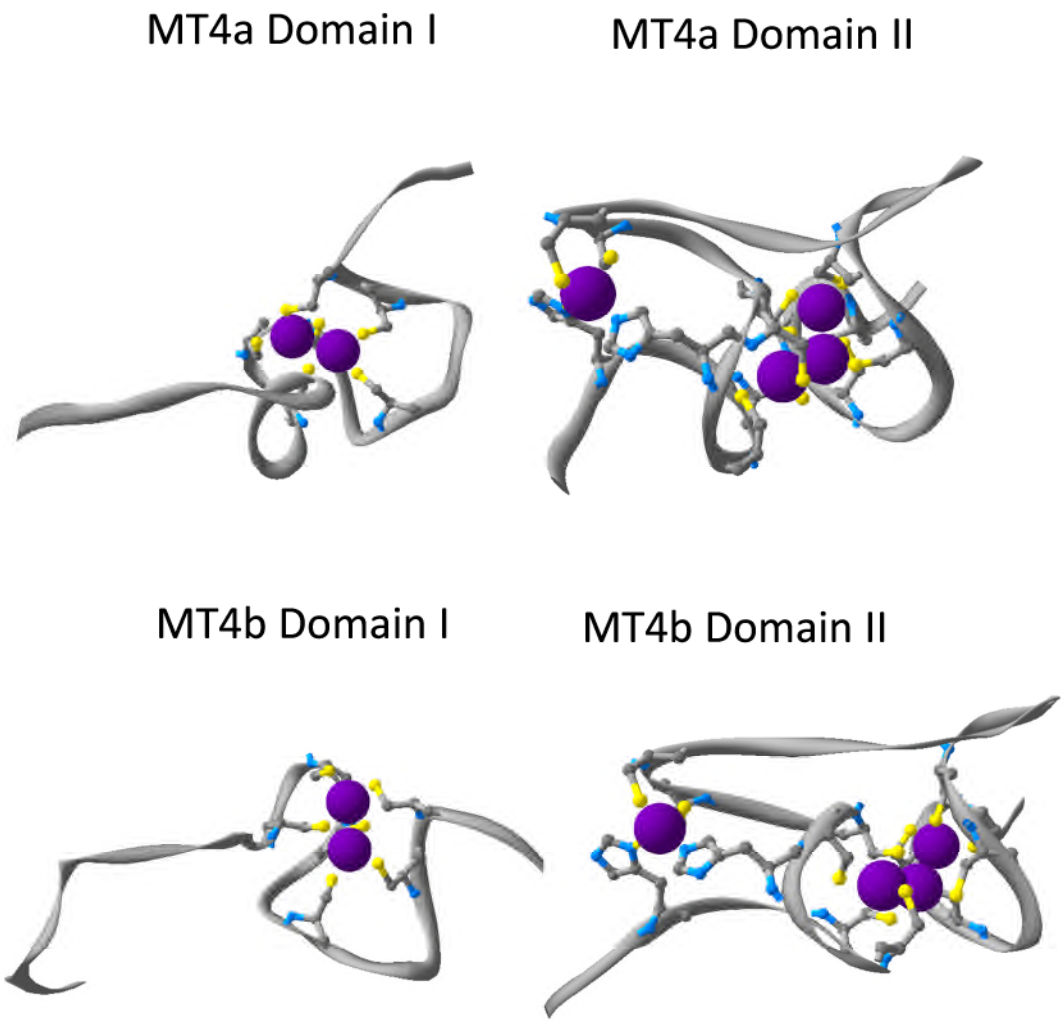

Figure A4 Homology model of MT4a and MT4b. Models are prepared using swiss pdb viewer.

A5

Thesis reference: Chapter 5, Section 5.3

Zinc transfer to EDTA: ^{1}H NMR spectroscopy

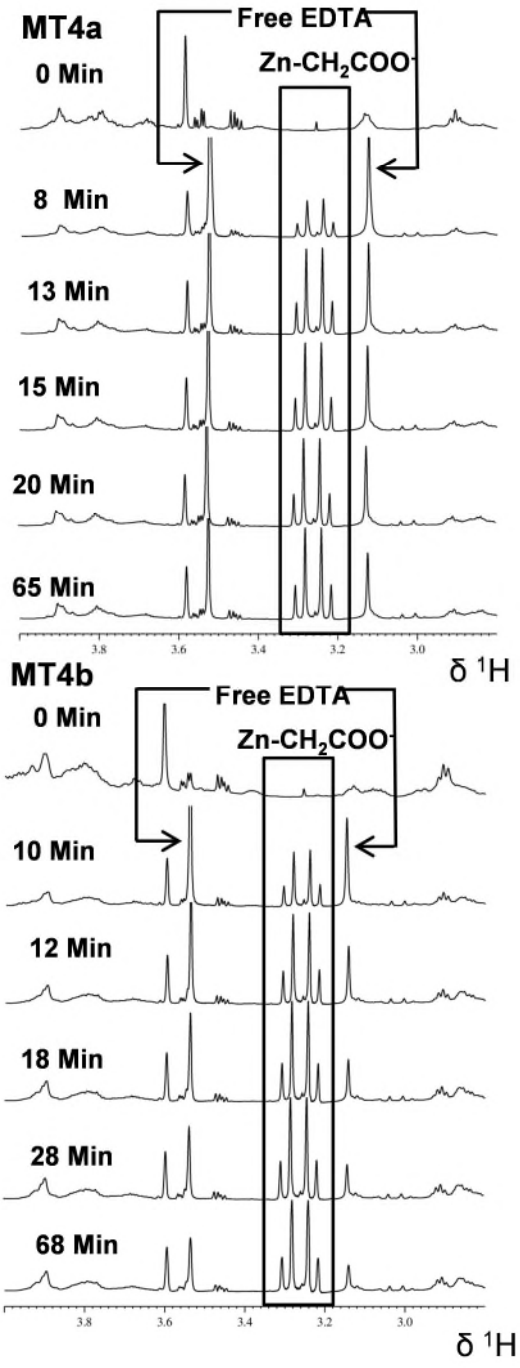

Figure A5 Aliphatic region of ^{1}H NMR spectra of MT4a and MT4b reaction with EDTA. Zn bound EDTA and free EDTA have shown.

A6

Thesis reference: Chapter 5, Section 5.3

Zinc transfer to EDTA: ^{15}N HSQC

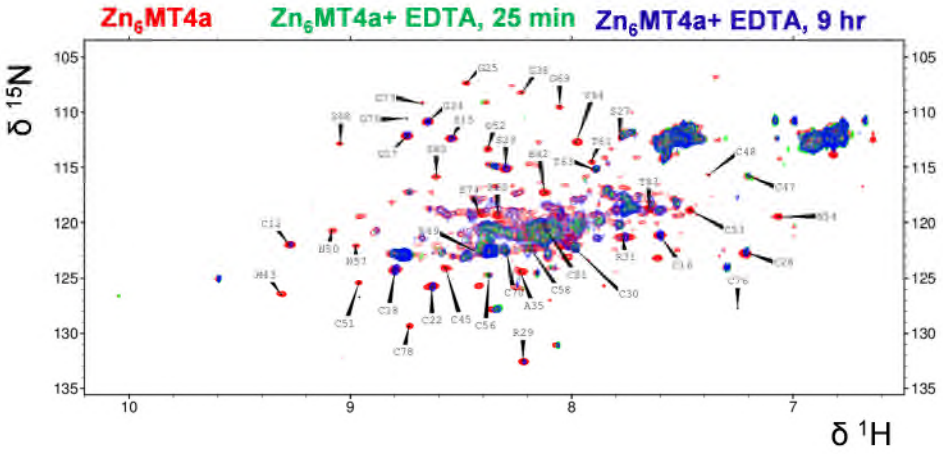

Figure A6 Zinc transfer to EDTA from MT4a. After 9 hr, refolded domain I was observed.

A7

Thesis reference: Chapter 5, Section 5.5

Effect of phytate: ^{1}H NMR spectroscopy

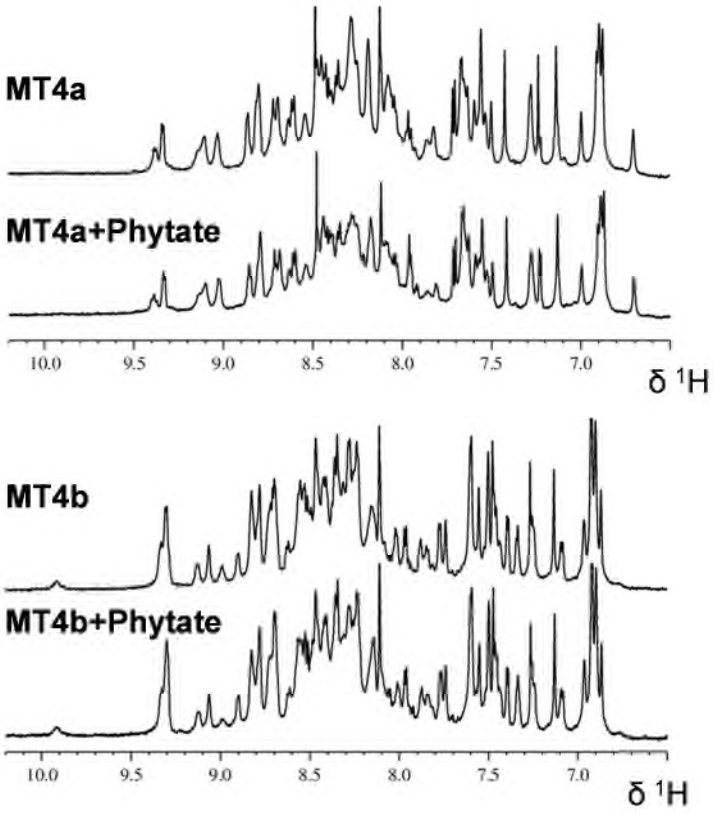

Figure A7 Fingerprint region of MT4a and MT4b with and without reaction with phytate. No significant change was observed after reaction with phytate.

A8

Thesis reference: Chapter 6, Section 6.3

MT4a reaction with DTNB: Mass spectrometry

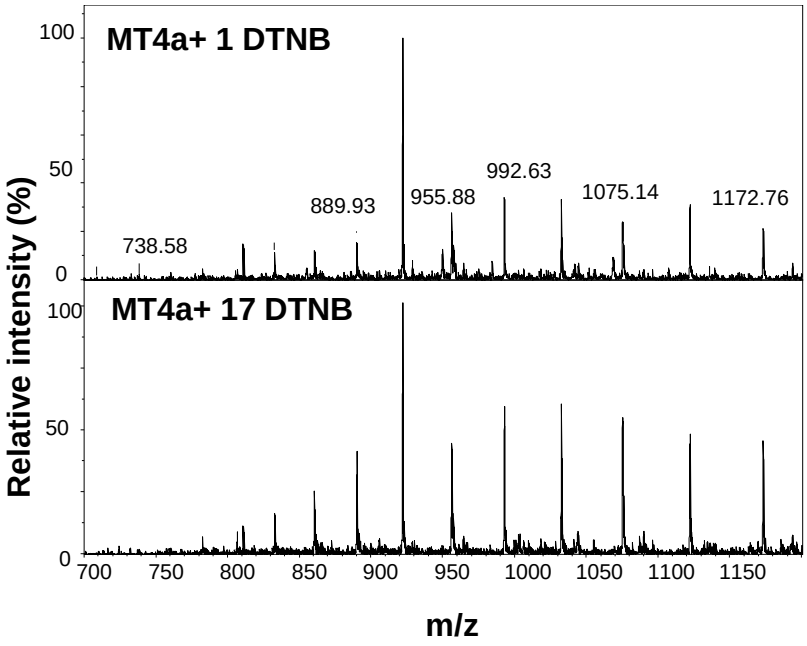

Observed Mass	Matched mass	ΔMass	Cleaved Peptide	position
732.960	733.221	0.261	(E)HCGCNPC(N)	50-56
738.580	738.262	-0.318	(H)MVCPCGE(H)	43-49
738.580	738.313	-0.266	(G)NSCRCR(M)	26-31
889.900	890.361	0.460	(S)PCPGGNSCR(C)	21-29
889.900	890.386	0.485	(N)PCNCPKTQ(T)	55-62
889.900	890.396	0.496	(M)REASAGDQG(H)	33-41
955.800	955.397	-0.402	(T)QTSAKGCTCG(E)	64-73
992.630	992.458	-0.172	(C)RMREASAGD(Q)	31-39
992.630	992.537	-0.092	(P)KTQTQTSAK(G)	60-68
1075.140	1075.430	0.289	(E)ASAGDQGHMVC(P)	35-45
1172.760	1172.410	-0.349	(Q)GHMVCPCGEHC(G)	41-51
1172.760	1172.410	-0.349	(G)HMVCPCGEHCG(C)	42-52
1172.760	1172.482	-0.277	(E)ASAGDQGHMVCP(C)	35-46

Figure A8 Raw spectra of MT4a reaction with DTNB results in low molecular weight cleaved peptides. Resulting cleaved peptides were identified by using Findpept tools (ExPASy).

A9

Thesis reference: Chapter 6, Section 6.3

MT4b reaction with DTNB: Mass spectrometry

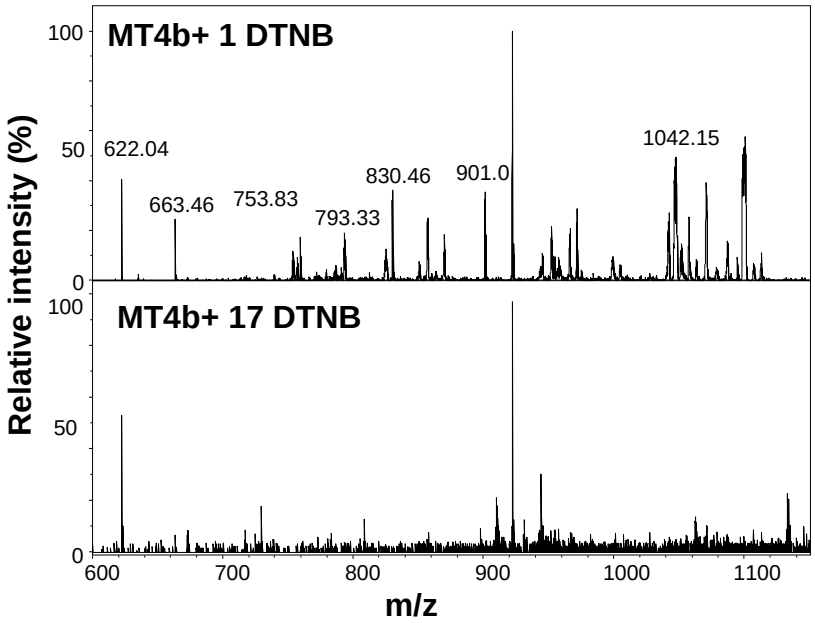

Observed Mass	Matched mass	ΔMass	Cleaved Peptide	position
622.040	622.231	0.191	(M)SEASGGD(Q)	34-40
634.890	635.336	0.445	(Q)TQTSAK(G)	64-69
663.400	663.258	-0.142	(S)EASGGDQ(E)	35-41
726.330	726.291	-0.039	(T)SAKGCTCG(E)	67-74
753.830	754.261	0.430	(A)SCNDRCG(C)	11-17
759.440	759.255	-0.185	(G)EHCGCNP(C)	50-56
771.590	771.313	-0.276	(S)CRCKMM(S)	28-33
786.820	787.242	0.421	(G)EGCTCATC(A)	75-82
793.330	793.405	0.075	(P)KTQTQTS(A)	61-67
825.060	825.298	0.237	(S)ASCNDRCG(C)	10-17
830.400	830.335	-0.065	(C)PSPCPGGES(C)	19-27
855.000	855.308	0.308	(A)SASCNDRC(G)	9-16
910.010	910.368	0.358	(G)SASASCNDR(C)	7-15
930.980	931.340	0.359	(D)QEHNTCPC(G)	41-48
1004.770	1004.429	-0.341	(C)NPCNCPKTQ(T)	55-63
1042.150	1042.448	0.297	(C)RCKMMSEAS(G)	29-37

Figure A9 Raw spectra of MT4b reaction with DTNB results in low molecular weight cleaved peptides. Resulting cleaved peptides were identified by using Findpept tools (ExPASy).